For my grandparents Peter George Sharpe
and Margaret Kathleen Sharpe for their
unconditional love, support and belief.

This is for you. 

Characterisation of HER2 binding Affimer drug conjugates in 2D and 3D cell culture

Sophie Elizabeth Roberts

Submitted in accordance with the requirements for the degree of

Doctor of Philosophy

The University of Leeds

Faculty of Biological Sciences and Faculty of Medicine and Health

School of Molecular and Cellular Biology

Leeds Institute of Cancer and Pathology

July 2020

The candidate confirms that the work submitted is her own and that appropriate credit has been given where reference has been made to the work of others.

This copy has been supplied on the understanding that it is copyright material and that no quotation from the thesis may be published without prior acknowledgement.

The right of Sophie Elizabeth Roberts to be identified as Author of this work has been asserted by her in accordance with the Copyright, Designs and Patent Act 1988.

© 2020 The University of Leeds and Sophie Elizabeth Roberts

Acknowledgements

Whilst the name on the front is solely mine, this thesis is attributed to so many more. Firstly I would like to thank my original primary supervisor Prof. Valerie Speirs for her guidance and encouragement throughout the beginning of my PhD and thereafter. Also, to Dr. Darren Tomlinson for taking me into his lab halfway through and putting up with the numerous questions I had on a daily basis. To my co-supervisor Dr. Sally Peyman, thank you for always having your office door open to me just to keep me sane. I am also immensely grateful to the NC3R's for funding this project.

Thank you to those who have provided me with valuable reagents. Prof. Michelle Peckham for an antibody against Tubulin, Prof. Margaret Knowles for the DSH-1 bladder cancer cell line, Prof. Eric Lam from University College London for providing resistant breast cancer cell lines and Dr. Thomas Hughes for breast cancer cell lines. To Mr. Ikram Ali for kindly keeping remnants of Herceptin® vials received by patients treated at St. James' University Hospital.

I will be forever grateful to Dr. Jelena Vukasinovik and JT Shoemaker for welcoming me into their lab and making me feel so welcome whilst visiting Atlanta. The experience and everyone I met during my time there will stay with me forever.

Thank you also to the breast group past and present, in particular Dr. Matthew Humphries for his endless patience in checking my calculations one hundred times in my first year. Thank you also to the Tomlinson lab for taking me in as their own and teaching me everything I needed to know about a protein lab entering as a final year! To Danah and Tom particularly for giving me so much of their time (and reagents). To Sam who joined the lab as a masters student about the same time I did, our friendship grew from our shared gift of procrastination and I know it will last a lifetime. Thank you all for the endless banter, support, shared tears of happiness and sadness and for always being there after work for 'one' drink.

I don't believe I could have got through the last few months without the friendship of the PPF. Laura Wilkinson Hewitt, for staying up until 2 am to talk me through setting up the

ÄKTA and Dr. Brian Jackson for booking a holiday through the busiest week of my PhD. I appreciate everything you both have done immensely and know that whilst I won't be the source of constant entertainment in your lab now, we will always remain friends!!

I would like to give a special mention to Julie Roberts and Suzanne Nicholson, who sadly passed away due to breast cancer. Also, to Dee Statham who fought and won her battle. The strength you all showed along with the pain experienced by your individual battles gave me the drive to continue with the PhD when it would have been so much easier to give up. Thank you.

Thank you to our cat Harvey for supporting me going to uni for a second time and to our puppy, Copper, for reminding me I have to take breaks from writing to play. To Pig, for following me everywhere and being that home comfort we all need. Last, but by no means least, thank you to my family. To my Mum and Dad who have been there through the many highs and lows at the end of the phone (and facetime- Mum) always and for believing in me when I struggled to myself. To my siblings Abi and Ben, partners Ange and Annabelle, children Abbey Cat and William for all being there and believing in me. Finally. To my grandparents, thank you for always being my own personal cheer squad, for believing I am the best and for always supporting me. Nothing I do can express my gratitude to the both of you but this thesis is dedicated to you.

Achievements

Publications that arose through my PhD

Roberts S and Speirs V. Advances in the development of improved animal-free models for use in breast cancer biomedical research. Biophysical Reviews 2015 9(4) p.321.

Roberts S, Peyman S and Speirs V. Current and Emerging 3D Models to Study Breast Cancer. 2019. ISBN 978-3-030-20300-9. P. 413-427.

Conferences in attendance through my PhD

2019	Faculty of Biological Sciences Postgraduate Symposium. Leeds, UK. Oral presentation.
2019	Astbury centre for structural and molecular science retreat. Manchester, UK. Poster presentation and invited 2 minute flash talk.
2018	Cancer cell signalling conference. Leeds, UK. Invited oral presentation.
2018	British Association for Cancer Research Student Conference. London, UK. Organising committee.
2018	Building Capacity in 3D Tissue Modelling and its Application in Cancer Research. Leeds, UK. Run a 3D modelling stand demonstrating spheroid growth and talked about my experience with PerfusionPal.
2018	Interdisciplinary Breast Cancer Symposium. Manchester, UK. Poster presentation.
2018	Leeds Institute of Molecular Medicine Postgraduate Symposium. Leeds, UK. Poster presentation.
2017	NC3Rs Workshop: Human tissue models for cancer research. London, UK. Poster presentation.
2017	19th IUPAB congress and 11th EBSA congress. Edinburgh, UK. Poster presentation and invited finalist platform presenter for a 3 minute thesis.
2017	Leeds Institute of Molecular Medicine Postgraduate Symposium. Leeds, UK. Poster presentation.

2016 Goodbye Flat Biology: models, mechanisms and microenvironment. Berlin, Germany.

Other achievements

Young scientist travel award to attend the 19th IUPAB congress and 11th EBSA congress.

Student elect member of the British Association for Cancer Research (BACR) executive committee from 2017-2019.

Successful grant application to CRUK to help fund the BACR student lead conference.

Abstract

The human epidermal receptor 2 (HER2) receptor tyrosine kinase (RTK) is overexpressed in approximately ~12 % of breast cancer. Currently, patients exhibiting this phenotype are predominantly treated with the monoclonal antibody Trastuzumab alongside chemotherapy. Whilst this stratified approach is successful in some patients there are drawbacks such as high production costs, intrinsic and acquired resistance and evidence of cardiotoxocity in a subset of patients. Therefore, the development of a therapeutic alternative is preferable.

Affimers are an example of a non-immunoglobulin scaffold. HER2 binding Affimers were previously isolated. Two HER2 binding Affimers, Affimers D11 and H7, bound with nM affinity to HER2 with no cross-reactivity to HER3, despite a high level of structural homology. Both Affimers were successfully internalised by HER2 overexpressing breast cancer cell lines specifically. When conjugated to the cytotoxic moiety monomethyl auristatin E (MMAE) they reduced the metabolic activity of HER2 overexpressing breast cancer cell lines in a dose dependent manner whilst having little off target effect on HER2 negative cell lines.

Often preclinical drug models do not translate to what is observed clinically. Analysis of Affimer drug conjugates in a fully humanised cell culture system would allow a more reflective representation of the drug effect *in vivo*. Affimer D11 MMAE (AfD11M) was cultured with breast cancer cell lines and primary breast cancer cells in the novel 3D cell culture model PerfusionPal. Further optimisation could lead to a high-throughput drug platform that could reduce the need for animals in preclinical drug testing in the future.

Abbreviations

AfD11M	Affimer D11-MMAE
AfH7M	Affimer H7-MMAE
AfCM	Affimer control-MMAE
AKT	Protein kinase B
APS	ammonium persulfate
BSA	Bovine serum albumin
BSTG	Bioscreening Technology Group
CHO	Chinese hamster ovary
DAPI	4′,6-diamidino-2-phenylindole
DARPin	Designed Ankyrin Repeat proteins
DMSO	Dimethyl sulfoxide
DMEM	Dulbecco's modified eagle medium
DNA	Deoxyribonucleic acid
DPBS	Dulbecco's phosphate buffered saline
E.coli	Escherichia coli
EDC	(N-(3-dimethylaminopropyl)-N'-ethylcarbodiimide
EDTA	Ethylenediaminetetraacetic acid
EEA1	Early endosome antigen 1
EGFR	Endothelial growth factor receptor
ELISA	Enzyme-linked immunosorbent assay
epiFL	Fibrolife medium optimised for epithelial growth
ER	Oestrogen receptor
ERK	Extracellular signal-regulated kinase
FBS	Fetal bovine serum
FGF	Fibroblast growth factor
HEPES	4-(2-hydroxyethyl)-1-piperazineethanesulfonic acid
HER	Human epidermal receptor
HRP	Horseradish peroxidase
IPTG	Isopropyl B-D-1 thiogalactopyranoside
Kb	Kilobase
LAMP2	Lysomal associated membrane protein 2

LB	Luria broth
LC-MS	Liquid chromatography mass spectrometry
mAb	Monoclonal antibody
MAPK	Mitogen activated protein kinase
MMAE	Monomethyl auristatin E
Mops	M 3-(N-morpholino)propanesulfonic acid
MWCO	Molecular weight cut off
MTA	Material transfer agreement
NHS	N-hydroxysuccinamide
Ni-NTA	Nickel-nitrilotriacetic acid
NP-40	nonyl phenoxypolyethoxylethanol
OD	Optical density
PBS	Phosphate buffered saline
PCR	Polymerase chain reaction
PDB	Protein data bank
PDMS	Poly-di-methyl-siloxane
PDTC	Patient derived tumour cells
PDX	Patient derived xenograft
PEG	Polyethylene glycol
PFA	Paraformaldehyde
PFC	Perfluorocarbon
PgR	Progesterone receptor
PIP3	Phosphatidylinositol-3,4,5-trisphosphate
PI3K	Phosphatidylinositol-3-Kinase
PNGase F	Peptide: N-glycosidase F
POI	Protein of interest
PPF	Protein production facility
PTEN	Phosphatase and tensin homolog
RMSD	Root-mean-square deviation
RNA	Ribonucleic acid
R.P.M	Rotations per minute
RPMI	Rosewell park memorial institute medium
RT	Room temperature

RTK	Receptor tyrosine kinase
RU	Reaction units
SDS-PAGE	sodium dodecyl sulphate polyacrylamide gel electrophoresis.
SEC	Size exclusion chromatography
SELEX	Systematic evolution of ligands by exponential enrichment
SOC	Super optimal broth with catabolite repression
SPR	Surface plasmon resonance
STR	Short tandem repeat
SUMO	Small ubiquitin-like modifier
TBS	Tris-buffered saline
TBST	Tris-buffered saline with tween
TEMED	N N N’ N’ tetramethyl-ethylenediamine
TEV	Tobacco etch virus
TGFB	Transforming growth factor beta
TGS	Tris glycine SDS
UPLC	Ultra-performance liquid chromatography
VR	Variable region
WT	Wild-type
2TY	2x tryptone and yeast

Characterisation of HER2 binding Affimer drug conjugates in 2D and 3D cell culture

TABLE OF CONTENTS

1 CHAPTER 1 3

1.1 INTRODUCTION 3

1.2 FEMALE BREAST CANCER 4

1.2.1 The Genetic basis of breast cancer 4

1.2.2 Diagnosis, staging and grade 4

1.2.3 Therapeutic intervention for breast cancer patients 6

1.3 THE HER FAMILY OF RECEPTOR TYROSINE KINASES 6

1.3.1 Role of the HER family in normal development 7

1.3.2 Attenuation of HER signalling 8

1.3.3 Aberrant signalling from the HER receptors and their transforming abilities 9

1.3.4 Discovery of HER2 and its role in breast cancer pathogenesis 9

1.4 SIGNALLING THROUGH THE HER FAMILY 10

1.4.1 Activation of receptors through binding of ligands 10

1.4.2 Ligand induced receptor dimerisation 11

1.4.3 Downstream signalling from the HER2/HER3 heterodimer 12

1.4.4 PI3K pathway through HER3 containing heterodimers and its role in breast cancer pathogenesis 13

1.4.5 Ligand independent firing of HER2 induces transforming phenotype in cells 13

1.4.6 Induction of the MAPK pathway following phosphorylation of HER2 cytosolic domain 14

1.5 DIAGNOSING HER2+ BREAST CANCER 15

1.5.1 Current treatments for primary and metastatic HER2+ breast cancer 16

1.5.2 Monoclonal antibodies as therapeutic entities 16

1.5.3 Trastuzumab therapy targeting HER2 on breast cancer cells 17

1.6 NEXT GENERATION OF HER2 TARGETING DRUGS 20

1.6.1 Synergistic effects of Trastuzumab and Pertuzumab combination therapy 21

1.6.2 Development of antibody-drug-conjugate Ado-Trastuzumab emtansine 21
1.6.3 Using small molecule inhibitors of the receptor tyrosine kinase domain of HER2 22
1.7 THERAPEUTIC ALTERNATIVES FOR THE POTENTIAL TREATMENT OF HER2+ BREAST CANCER 22
1.7.1 1.7.1 Antibody fragments svFc 23
1.7.2 Non-immunoglobulin scaffolds in the context of HER2+ breast cancer 23
1.8 MODELLING BREAST CANCER 26
1.8.1 2D cell culture and its contributions to breast cancer research 27
1.8.2 Spheroid models for studying cancer 29
1.8.3 Advantages of using primary patient samples over cell lines 29
1.8.4 Organoids derived from primary breast cancer patient samples 30
1.8.5 Microfluidic modelling of cancer 30
1.9 USING MOUSE MODELS TO STUDY HUMAN DISEASE 30
1.9.1 Early mouse models to study human disease 30
1.9.2 Patient-derived xenograft models 31
1.10 HYPOTHESIS 32
1.11 AIMS OF THE PROJECT 32
2 MATERIALS FOR LABORATORY 35
2.1 COMMONLY USED REAGENTS 35
2.2 LABORATORY STOCK SOLUTIONS 35
2.3 BACTERIAL CELL LINES 35
2.3.1 BL21 Star™ (DE3) 36
2.3.2 XL 1-Blue supercompetent cells 36
2.3.3 Lemo21(DE3) 36
2.3.4 SHuffle T7 Express 36
2.3.5 Rosetta-Gami2(DE3)PLysS 37
2.4 PLASMID VECTORS 37
2.5 ANTIBIOTICS 37

2.6 GROWTH MEDIA 38
2.7 PROTEIN PRODUCTION AND PURIFICATION 38
2.7.1 Bacterial transformation 38
2.7.2 Protein production by isopropyl β-D-1-thiogalactopyranoside induction 39
2.7.3 Purification of 6 x His-tagged Affimer by Ni-NTA affinity chromatography 40
2.8 PROTEIN ANALYSIS 41
2.8.1 Determination of protein concentration 41
2.8.2 SDS-PAGE 42
2.8.3 Western blot analysis 44
2.8.4 DNA sub-cloning 45
2.9 AFFINITY PRECIPITATION OF ENDOGENOUS HER2 48
2.9.1 Conjugating of Affimer via maleimide link 49
2.9.2 Conjugating HER2 specific Affimers to monomethyl auristatin E (MMAE) for use in cell culture. 49
2.9.3 Liquid chromatography mass spectrometry 50
2.10 MATERIALS AND METHODS FOR CELL CULTURE 50
2.10.1 Cells and common reagents used in cell culture 51
2.10.2 Methods for culture of mammalian cell lines 52
2.11 IMMUNOFLUORESCENCE USING AFFIMERS 54
2.11.1 Immunofluorescence using unconjugated Affimers 54
2.11.2 Immunofluorescence using Affimers conjugated to AlexaFluor 488 55
2.12 DOSE RESPONSE USING AFFIMER-MMAE CONJUGATES 56
2.13 3D CELL CULTURE 57
2.13.1 3D cell culture using FibroLife 57
2.13.2 3D cell culture in SeedEZ and PerfusionPal 57
2.13.3 Primary cell culture using SeedEZ and PerfusionPal 60
2.14 PURIFICATION OF HER2/ AFFIMER D11 COMPLEX AND CRYSTALLISATION TRIALS UNDERTAKEN IN THE PROTEIN PRODUCTION FACILITY 62
2.14.1 Production of HER2 extracellular domain by mammalian cell culture 62

2.14.2 Production of D11 Affimer with Strep Tag® II 62
2.14.3 Formation of HER2 extracellular domain in complex with Affimer D11 ..63
2.14.4 Deglycosylation of HER2 ECD/ Affimer D11 complex by PNGase F 64
2.14.5 Deglycosylation of HER2 extracellular domain in complex with Affimer D11 65
2.14.6 Size exclusion chromatography 66
2.14.7 Concentration of proteins 66
2.14.8 Crystallisation trials 66
2.15 HER2 SUBDOMAIN PRODUCTION IN *E. COLI* 66
2.15.1 Cloning HER2 subdomains into pOPIN vectors 66
2.15.2 Cloning HER2 subdomains into pOPIN vectors 68
2.15.3 Automated minipreps using the Hamilton Robot and Promega MagneSil kit 69
2.15.4 Small scale expression screening 70
2.15.5 Larger scale expression screen in 1 L cultures 71
2.15.6 Pull down protocol using StrepTactin 72
2.16 BIACORE SURFACE PLASMON RESONANCE (SPR) BINDING ASSAY 72
2.17 STATISTICAL ANALYSIS 73
3 CHARACTERISATION OF HER2 BINDING AFFIMERS 76
3.1 INTRODUCTION 76
3.1.1 Affimer Reagents 76
3.1.2 Type II Affimers raised against HER2 extracellular domain 78
3.1.3 Aims 79
3.2 RESULTS 80
3.2.1 Testing the ability of Affimers to bind endogenous HER2 from cell lysate 80
3.2.2 Investigating the ability of HER2 specific Affimers to be internalised by HER2 overexpressing cell lines 84
3.2.3 Comparing effects of HER2 binding Affimers to Trastuzumab on HER2+ cell lines 86
3.2.4 Affimer internalisation observed using confocal microscopy 91

3.2.5 Affimer internalisation following conjugation to Alexa Fluor™ 488.....96
3.2.6 Internalisation by receptor mediated endocytosis 109
3.3 CHAPTER SUMMARY AND FUTURE PERSPECTIVES.....114
3.3.1 HER2 binding Affimers are not effective in breast cancer cell lines compared to Trastuzumab.....114
3.3.2 Internalisation of HER2 binding Affimers.....114
3.3.3 Internalisation of non-immunoglobulin scaffolds 115
3.3.4 Chapter conclusion 115
4 DEVELOPMENT OF HER2 SPECIFIC AFFIMER DRUG CONJUGATES.....119
4.1 ANTIBODY DRUG CONJUGATES.....119
4.1.1 Ado-trastuzumab emtansine (Kadcyla™) for the treatment of HER2+ metastatic breast cancer.....120
4.1.2 Emergence of antibody alternative molecules for therapeutic intervention 121
4.1.3 Aim.....122
4.2 RESULTS 123
4.2.1 Conjugation of Affimer to antineoplastic warhead.....123
4.2.2 Conjugation of Affimer to antineoplastic warhead.....124
4.2.3 Analysing HER2 expression in cell lines by western blot 128
4.2.4 Dose responses using Affimer drug conjugates 130
4.2.5 Monomethyl Auristatin E modulation of Tubulin in HER2+ cells 137
4.2.4 Determination of affinities and specificity of Affimer drug conjugates 142
4.2.6 Targeting cell lines resistant to current therapies with AfD11M and AfH7M 150
4.3 CHAPTER SUMMARY AND FUTURE DIRECTION.....152
4.3.1 Dose response.....154
4.3.2 Effect of MMAE of Tubulin 155
4.3.3 Binding affinity of Affimer drug conjugates.....156
4.3.4 Chapter summary.....156
CHAPTER 5 160

5 CREATING A NOVEL 3D CELL CULTURE MODEL FOR HER2+ BREAST CANCER 160

5.1 INTRODUCTION 160

5.1.1 Recapitulating the extracellular matrix *in vitro* 160

5.1.2 Growing mammary epithelial cells in 3D cell culture *in vitro* 161

5.1.3 Aims 162

5.2 RESULTS 163

5.2.1 Using modified FibroLife medium to culture cells in 3D 163

5.2.2 Establishment of a novel cell culture system 164

5.2.3 Culturing breast cancer cell lines in PerfusionPal and SeedEZ in standard culture media 169

5.2.4 Culturing breast cancer cell lines in PerfusionPal with epiFL media 178

5.2.5 Dose response of breast cancer cell lines with Trastuzumab in PerfusionPal 181

5.2.6 Growing primary HER2+ cells in PerfusionPal 182

5.3 DISCUSSION AND FUTURE DIRECTION 190

5.3.1 Using epiFL as a matrix free medium to culture cells in 3D 190

5.3.2 Dynamic perfused culture results in higher metabolic activity compared to static culture 190

5.3.3 Primary cell culture in 3D 191

5.3.4 Limitations of culturing SeedEZ scaffolds in the PerfusionPal system 192

5.3.5 Conclusion and future work 193

6 INVESTIGATING THE INTERACTION BETWEEN AFFIMERS AND HER2 EXTRACELLULAR DOMAIN 196

6.1 INTRODUCTION 196

6.1.1 X-ray Crystallography 197

6.1.2 Aim 197

6.2 RESULTS 199

6.2.1 Affimer D11 complex with full length HER2 in mammalian cell culture 199

6.2.2 Production of Peptide: N-glycosidase F (PNGase) 204

6.2.3 Larger scale production of Affimer D11 in complex with full length HER2 206
6.2.4 Expressing the HER2 extracellular subdomains in *E. coli* 212
6.3 CHAPTER SUMMARY AND FUTURE WORK 226
6.3.1 Producing HER2 subdomain II in *E.coli* 227
6.3.2 Affimer D11 binding to subdomain II of the HER2 extracellular domain 227
6.3.3 Chapter conclusion 228
7 DISCUSSION AND FUTURE PERSPECTIVES 231
7.1 DISCUSSION AND CONCLUSION 231
7.2 AFFIMER D11 AND H7 AS VEHICLES FOR THE SPECIFIC DELIVERY OF CYTOTOXIC MOLECULES 231
7.3 CONTINUATION OF THE PROJECT AND FUTURE PERSPECTIVE 232
7.3.1 Further investigation of Affimer drug conjugates 232
7.3.2 Determination of the structure of Affimer D11 in complex with the HER2 extracellular domain 233
7.3.3 Optimisation of PerfusionPal for the culture of primary breast cancer cells 234
7.3.4 Overcoming resistance to first line therapy in breast cancer cell lines .235
7.3.5 Addressing the 3Rs 235
7.4 CONCLUSION 235
8 APPENDIX 237
BIBLIOGRAPHY 239

List of Figures

Figure 1.1 Original hallmarks, emerging hallmarks and enabling characteristics of cancer. 3
Figure 1.2 Schematic diagram of female breast anatomy with malignant tumour. 5
Figure 1.3 Diagram representing stages 1 to IV of breast cancer. 5
Figure 1.4 Diagram to show the four members of the HER family of receptor tyrosine kinases. 7
Figure 1.5 Extracellular domain of EGFR (HER1) in bound and unbound state. 12
Figure 1.6 HER2:HER3 heterodimer downstream signalling. 15
Figure 1.7 Antibody and antibody fragments. 17
Figure 1.8 Binding sites of approved HER2 targeted therapies. 21
Figure 1.9 Ribbon diagrams to show structures of various non-immunoglobulin scaffold. 24
Figure 1.10 Example models used for preclinical drug testing. 27
Figure 1.11 Heterogeneity in solid tumour compared to 2D cell culture. 29
Figure 2.1 Mechanism of the lac operon. 40
Figure 2.2 Beer Lambert equation used to quanity protein concentration when using the NanoDrop Lite. 42
Figure 2.3 Set up of western blot using the Bio-Rad Turbo blot system. 44
Figure 2.4 Chemical reaction of Affimer and Alexa Fluor™ 488 maleimide. 49
Figure 2.5 SeedEZ scaffold. 58
Figure 2.6 PerfusionPal cell culture plate. 59
Figure 2.7 Work flow of production of the HER2 extracellular domain/ Affimer D11 complex. 64
Figure 2.8 Chip derivatisation by amine coupling. 73
Figure 3.1 Ribbon diagram of type I and type II Affimer scaffolds. 77
Figure 3.2 Phage display. 78
Figure 3.3 SDS-PAGE of His-tagged Affimer reagents purified by Ni-NTA chromatography. 81
Figure 3.4 Optimisation of anti-HER2 antibody for western blot analysis. 82
Figure 3.5 Affinity purification of endogenous HER2 using Affimer reagents. 83
Figure 3.6 Immunofluorescence using HER2 binding Affimers on breast cancer cell lines. 85

FIGURE 3.7 DOSE RESPONSE USING TRASTUZUMAB MONOCLONAL ANTIBODY ON BREAST CANCER CELL LINES. 87
FIGURE 3.8 AGAROSE GEL ELECTROPHORESIS OF VECTOR AND INSERT DNA. 88
FIGURE 3.9 SDS-PAGE TO CONFIRM PURITY OF AFFIMER REAGENTS CONTRAINING C-TERMINAL CYSTEINE RESIDUES. 89
FIGURE 3.10 DOSE RESPONSE OF UNCONJUGATED AFFIMER ON BREAST CANCER CELL LINES. 90
FIGURE 3.11 CONFOCAL MICROSCOPY USING HIS-TAGGED AFFIMERS ON BREAST CANCER CELL LINES. .. 95
FIGURE 3.12 SKELETAL FORMULAR OF HISTIDINE AND METHIONINE AMINO ACID RESIDUES. 97
FIGURE 3.13 TRACE OF MASS SPECTROMETRY ANALYSING AFFIMER WITH C-TERMINAL CYSTEINE RESIDUES. 98
FIGURE 3.14 MASS SPECTROMETRY TRACE ANALYSING AFFIMER ALEXA FLUOR™ 488 CONJUGATES. ... 99
FIGURE 3.15 CO-LOCALISATION OF AFFIMER ALEXA FLUOR™ 488 CONJUGATES WITH HER2 USING CONFOCAL MICROSCOPY. 104
FIGURE 3.16 CO-LOCALISATION OF AFFIMER ALEXA FLUOR™ 488 CONJUGATES WITH HER2 OBSERVED BY CONFOCAL MICROSCOPY. 107
FIGURE 3.17 AFFIMER ALEXA FLUOR™ 488 CONJUGATE CO-LOCALISATION WITH ANTI-HIS ZOOMED IN. 108
FIGURE 3.18 CO-LOCALISATION OF AFFIMER ALEXA FLUOR™ 488 CONJUGATE WITH EEA1 OBSERVED BY CONFOCAL MICROSCOPY. 111
FIGURE 3.19 CO-LOCALISATION OF AFFIMER ALEXA FLUOR™ WITH LAMP2 OBSERVED BY CONFOCAL MICROSCOPY..... 113
FIGURE 4.1 ANTIBODY DRUG CONJUGATE. 119
FIGURE 4.2 HYPOTHETICAL IMAGE DEMONSTRATING CONJUGATION OF AFFIMER TO MMAE..... 124
FIGURE 4.3 SDS-PAGE ANALYSIS TO CONFIRM THE PURITY OF AFFIMER MMAE CONJUGATES. 125
FIGURE 4.4 CONFIRMING CONJUGATION OF AFFIMER TO MMAE BY LC-MS..... 127
FIGURE 4.5 ANALYSIS OF HER2 EXPRESSION BY WESTERN BLOT AND DENSITOMETRY. 129
FIGURE 4.6 DOSE RESPONSE USING AFFIMER-MMAE CONJUGATES ON A RANGE OF BREAST CANCER CELL LINES. 131
FIGURE 4.7 NUCLEAR CELL COUNT OF VARIOUS CELL LINES TREATED WITH DIFFERENT CONCENTRATIONS OF AFFIMER MMAE CONJUGATE..... 133
FIGURE 4.8 EXAMPLE PICO IMAGES FOLLOWING INCUBATION OF AFFIMER MMAE CONJUGATES ON BREAST CANCER CELL LINES. 136
FIGURE 4.9 IMMUNOFLUORESCENCE TO SHOW MODULATION OF TUBULIN BY MMAE. 142

FIGURE 4.10 SEQUENCE ALIGNMENT OF HER2 AND HER3 EXTRACELLULAR DOMAIN AMINO ACID SEQUENCES. 145
FIGURE 4.11 SUPERIMPOSITION OF HUMAN HER2 AND HER3 EXRACELLULAR DOMAINS..... 146
FIGURE 4.12 SENSORGRAM TO TEST BINDING AFFINITY OF AFFIMER MMAE CONJUGATES TO RECOMBINANT HER2 AND HER3 USING SPR. 148
FIGURE 4.13 ESTIMATE OF KINETIC PARAMETERS OF AFFIMER MMAE CONJUGATES TO RECOMBINANT HER2 USING SPR. 149
FIGURE 4.14 EXAMPLE FIT USING 1:1 LANGMUIR BINDING MODEL. 150
FIGURE 4.15 WESTERN BLOT OF HER2 EXPRESSION IN WILDTYPE AND RESISTANT CELL LINES. 151
FIGURE 4.16 STAGES OF MITOSIS IN EUKARYOTIC HUMAN CELLS. 153
FIGURE 5.1 BT-474 CELLS SEQUENTIALLY TRANSFERRED FROM RPMI TO EPIFL MEDIA. 164
FIGURE 5.2 SEEDEZ SCAFFOLD..... 165
FIGURE 5.3 3D CELL CULTURE SYSTEM PERFUSIONPAL..... 166
FIGURE 5.4 COMPARING PROPERTIES OF BT-474 CELLS GROWN IN SEEDEZ UNDER DIFFERENT CONDITIONS. 168
FIGURE 5.5 BT-474 CELLS CULTURED IN SEEDEZ SCAFFOLDS ± PERFUSIONPAL IN RPMI MEDIA..... 170
FIGURE 5.6 BT-474 CELLS GROWN IN SEEDEZ SCAFFOLD STAINED WITH CALCEIN AM. 171
FIGURE 5.7 CULTURING MDA-MB-231 CELLS IN SEEDEZ SCAFFOLD ± PERFUSION. 173
FIGURE 5.8 CULTURING AU-565 CELLS IN RPMI MEDIUM IN SEEDEZ SCAFFOLDS WITH AND WITHOUT PERFUSIONPAL..... 175
FIGURE 5.9 NORMALISATION OF PERFUSIONPAL DATA FOR AU-565, BT-474 AND MDA-MB-231 IN STANDARD CULTURE MEDIA. 177
FIGURE 5.10 BT-474 CELLS CULTURED IN EPIFL MEDIA IN SEEDEZ ± PERFUSIONPAL..... 179
FIGURE 5.11 CULTURING MDA-MB-231 CELLS IN SEEDEZ ± PERFUSIONPAL IN EPIFL MEDIA..... 180
FIGURE 5.12 AU-565 CELLS CULTURED IN SEEDEZ SCAFFOLDS ± PERFUSIONPAL IN EPIFL MEDIA. 181
FIGURE 5.13 BT-474 AND MDA-MB-231 DOSE RESPONSE WITH TRASTUZUMAB IN PERFUSIONPAL. 182
FIGURE 5.14 AU-565 CELLS INCUBATION WITH AFD11M COMPARED TO AFCM AND TRASTUZUMAB IN PERFUSIONPAL. 184
FIGURE 5.15 PRIMARY BREAST CANCER CELL LINES CULTURED IN PERFUSIONPAL..... 186
FIGURE 5.16 CONFOCAL MICROSCOPY OF HER2 IN PRIMARY PATIENT SAMPLES CULTURED IN PERFUSIONPAL..... 189
FIGURE 5.17 MIDIFLUIDIC MODEL DESIGN. 193

FIGURE 6.1 RIBBON DIAGRAM OF THE HER2 EXTRACELLULAR DOMAIN WITH TRASTUZUMAB AND PERTUZUMAB FAB REGIONS..... 196
FIGURE 6.2 PHASE DIAGRAM FOR PROTEIN CRYSTALLISATION. 197
FIGURE 6.3COMPONENTS OF AFFIMER D11 STREP TAG II..... 199
FIGURE 6.4 AFFIMER D11 INSERT DNA AND AFFIMER D11 STREP TAG® II ANALYSIS. 200
FIGURE 6.5 COMPONENTS OF HER2 FUSION PROTEIN..... 201
FIGURE 6.6 PURIFICATION OF AFFIMER D11 IN COMPLEX WITH HER2 FUSION PROTEIN. 202
FIGURE 6.7 SDS-PAGE ANALYSIS OF AFFIMER D11 HER2 EXTRACELLULAR DOMAIN COMPLEX FOLLOWING SEC..... 203
FIGURE 6.8 PNGASE F PURIFICATION USING C-TERMINAL 6X HIS TAG..... 205
FIGURE 6.9 ANALYSIS OF HER2 FUSION PROTEIN BY SDS-PAGE AND WESTERN BLOT..... 207
FIGURE 6.10 LARGER SCALE PRODUCTION OF AFFIMER D11 AND HER2 EXTRACELLULAR DOMAIN COMPLEX. 209
FIGURE 6.11 SDS-PAGE ANALYSIS OF VARIOUS FRACTIONS DURING THE PURIFICATION OF AFFIMER D11/HER2 COMPLEX. 210
FIGURE 6.12 SEPARATION OF AFFIMER D11/HER2 COMPLEX BY SEC AND ANALYSIS BY SDS-PAGE.211
FIGURE 6.13 ANALYSIS OF UNBOUND HER2 CONDITIONED MEDIA BY SDS-PAGE AND WESTERN BLOT. 212
FIGURE 6.14 RIBBON DIAGRAM OF TEN POSSIBLE HER2 SUBDOMAIN STRUCTURES..... 214
FIGURE 6.15 PCR AMPLIFICATION OF HER2 SUBDOMAIN ANALYSIS BY AGAROSE GEL ELECTROPHORESIS. 215
FIGURE 6.16 COMPOSISION OF HER2 SUBDOMAIN FUSION PROTEINS..... 216
FIGURE 6.17 EXPRESSION TRIAL OF HER2 SUBDOMAINS IN DIFFERENT E.COLI STRAINS..... 218
FIGURE 6.18 LARGER SCALE EXPRESSION TRIAL OF HER2 SUBDOMAIN FUSION PROTEINS IN LEMO21(DE3) CELLS. 219
FIGURE 6.19 PULL-DOWN OF AFFIMER D11/HER2 SUBDOMAIN COMPLEX USING STREPTACTIN BEADS. 220
FIGURE 6.20 PURIFICATION OF HER2 SUBDOMAIN II MBP FUSION PROTEIN..... 222
FIGURE 6.21 PURIFICATION OF AFFIMER D11 STREP-TAG® II USING STREP TRAP HP COLUMN ON AN AKTA. 223
FIGURE 6.22 ANALYSIS OF MBP TAG REMOVAL BY SDS-PAGE..... 224
FIGURE 6.23 SEC OF AFFIMER D11 HER2 SUBDOMAIN II COMPLEX. 226
FIGURE 8.1 PLASMID VECTOR MAPS..... 238

LIST OF TABLES

TABLE 1.1 CURRENT TARGETED THERAPIES USED TO TREAT HER2+ BREAST CANCER. 20
TABLE 2.1 TABLE OF COMMON REAGENTS. 35
TABLE 2.2 STOCK AND WORKING CONCENTRATIONS OF ANTIBIOTICS. 38
TABLE 2.3 DETAILS OF ANTIBODIES USED FOR WESTERN BLOTS. 45
TABLE 2.4 DNA SEQUENCES OF AFFIMER PRIMERS. 46
TABLE 2.5 THERMOCYCLING CONDITIONS USED FOR PCR AMPLIFICATION 46
TABLE 2.6 PRIMERS USED FOR SEQUENCING PET11A PLASMIDS. 47
TABLE 2.7 MAMMALIAN CELL LINES AND CULTURE CONDITIONS. 52
TABLE 2.8 SEEDING DENSITITES OF CELL LINES USED FOR DOSE RESPONSE ASSAYS. 53
TABLE 2.9 CELL SEEDING DENSITITES FOR SEEDING CELLS IN 24 WELL TISSUE CULTURE PLATE. 54
TABLE 2.10 ANTIBODIES USED FOR IMMUNOFLUORESCENCE EXPERIMENTS. 56
TABLE 2.11 LIST OF REAGENTS USED FOR CULTURE OF PRIMARY BREAST CANCER CELLS. 61
TABLE 2.12 PRIMERS AGAINST HER2 SUBDOMAINS FOR CLONING INTO POPIN VECTORS. 67
TABLE 2.13 PCR CONDITIONS USED FOR AMPLIFICATION OF HER2 SUBDOMAIN DNA. 67
TABLE 2.14 PCR THERMOCYCLING CONDITIONS 68
TABLE 2.15 POPIN SEQUENCING PRIMERS. 70
TABLE 2.16 ANTIBIOTIC RESISTANCE OF E.COLI STRAINS USED FOR SMALL SCALE PROTEIN EXPRESSION. . 70
TABLE 3.1 SEQUENCES OF EIGHT HER2 BINDING AFFIMER VARIABLE REGIONS. 79
TABLE 3.2 COMPARING THE EXPECTED AND ACTUAL MASS VALUES DETERMINED BY LC-MS. 100
TABLE 4.1 FDA APPROVED ANTIBODY-DRUG-CONJUGATES FOR TREATMENT OF CANCER. 120
TABLE 4.2 EXPECTED AND PREDICTED MASSES OF AFFIMER MMAE CONJUGATES ANALYSED BY LC-MS. 126
TABLE 4.3 EXPRESSION AND PROFILING OF BREAST CANCER CELL LINES. 155
TABLE 5.1 TABLE TO SHOW CHARACTERISTICS OF PRIMARY PATIENT TUMOUR CELLS. 185
TABLE 6.1 MOLECULAR WEIGHT OF HER2 EXTRACELLULAR DOMAIN SUBDOMAINS 217

Chapter 1

Introduction



'Everybody is a genius. But if you judge a fish by its ability to climb a tree, it will live its whole life believing that it is stupid.'

-Albert Einstein

1 Chapter 1

1.1 Introduction

'Cancer' is a broad term used to describe a group of diseases characterised by the hyperproliferation of cells with metastatic potential. Malignant tumours define those capable of invasion and metastasis opposed to benign tumours that are isolated lesions. A complex plethora of events and conditions need to be met in order for a malignant tumour to arise, these were defined as the 'Hallmarks of Cancer' (Figure 1.1) originally by Hanahan and Weinberg in 2000 (1) and later updated in 2011 to include further hallmarks and enabling characteristics (Figure 1.1) (2). Breast cancer, despite improvements in early detection and targeted therapy, is still the largest cause of cancer related death amongst women in the U.K.

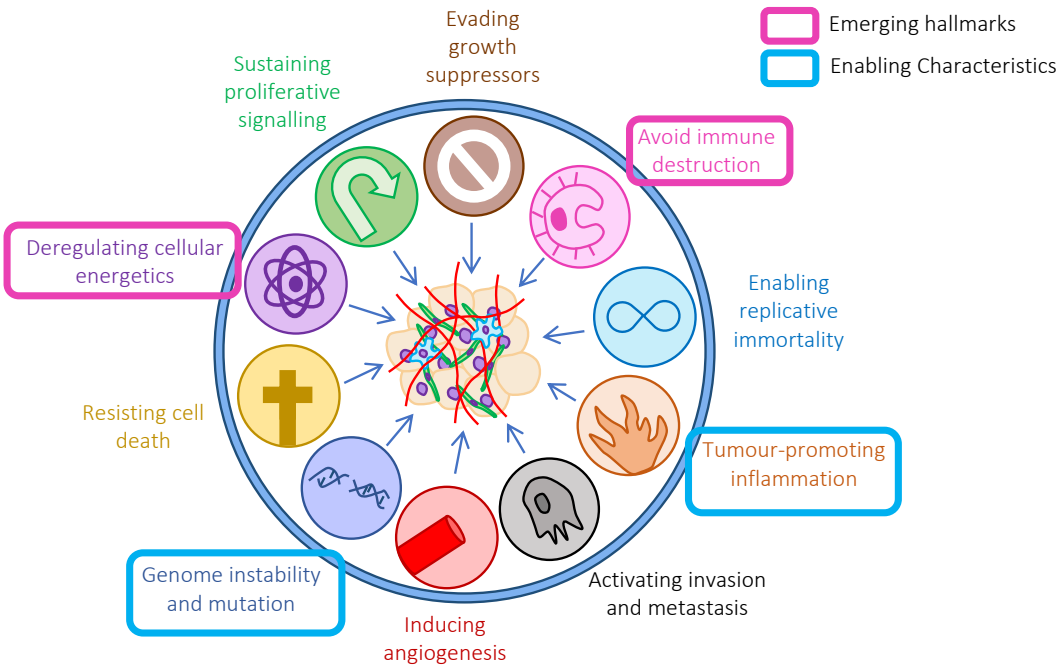


Figure 1.1 Original hallmarks, emerging hallmarks and enabling characteristics of cancer.
The six original hallmarks and the now recognised emerging hallmarks and enabling characteristics as published by Douglas Hanahan and Robert Weinberg.

1.2 Female breast cancer

1.2.1 The Genetic basis of breast cancer

Breast cancers exhibit a number of, if not all, of the characteristics described above. These arise following genetic aberrations leading to the disregulation of pathways critical in controlling normal cellular processes such as cell division and apoptosis. It has long been recognised that some breast cancers are a result of a germline mutation in genes such as BRCA1 and BRCA2 that lead to an increased lifetime risk (reviewed in (3, 4)). However, the majority of breast cancers arise due to sporadic mutations. Analysis of 173 genes in over 2000 primary breast tumours by the Caldas group highlighted a number of genes that were more commonly mutated in breast cancers. The most common somatic mutations were observed in PIK3CA and the tumour suppressor gene TP53 followed by other genes including MUC16, GATA3 and SYNE1 (5). Not all breast cancers arise through mutation, however. The HER2 positive subtype is most commonly caused by gene amplification leading to an increased volume of HER2 on the cell surface. The type of breast cancer is reviewed following diagnosis.

1.2.2 Diagnosis, staging and grade

The human female breast is a modified cutaneous exocrine gland composed of skin, breast parenchyma (ducts and lobules) and supporting stroma including adipose tissue, blood vessels and lymphatic system (Figure 1.2) (6). The majority of breast cancers arise from the luminal epithelial cells lining ducts and milk producing lobules (7). Cancerous epithelial cells lose their apical-basal polarity allowing them to undergo epithelial to mesenchymal transition (EMT) or travel in clusters to invade surrounding tissue (7). Breast cancer is generally diagnosed following routine breast screens or general practioner examination following the patient identification of an abnormality, both of which are confirmed with a biopsy (NHS website). Upon diagnosis breast cancer is given a stage from I to IV that considers the size of the cancer, lymphatic presence and metastatic lesions (Figure 1.3) and grade. A grade between 1 and 3 is given considering how abnormal the cells look and how quickly they are proliferating. Grade 1 cells are defined as being mostly normal and slow growing, grade 2 look less normal due to

alterations in nuclear shape and faster growing and grade 3 breast cancer cells have an abnormal phenotype and divide quickly (breast cancer now).

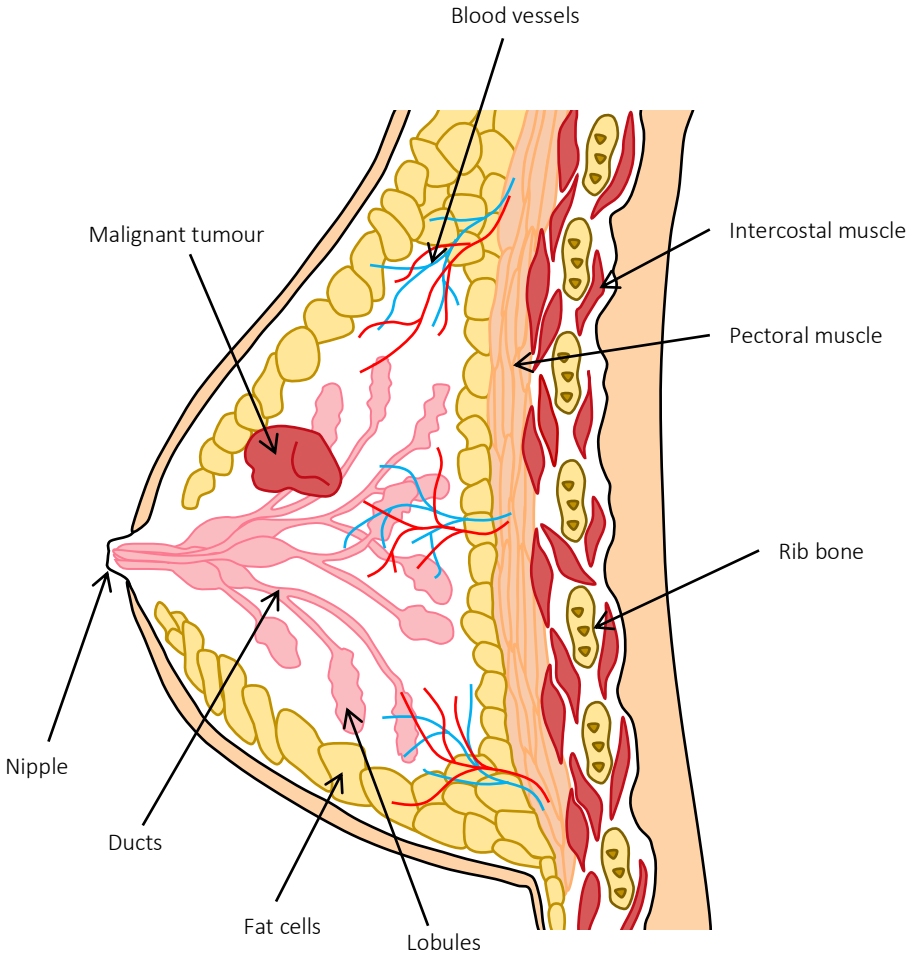


Figure 1.2 Schematic diagram of female breast anatomy with malignant tumour.
The female breast is composed of multiple tissue types (labelled in the diagram).

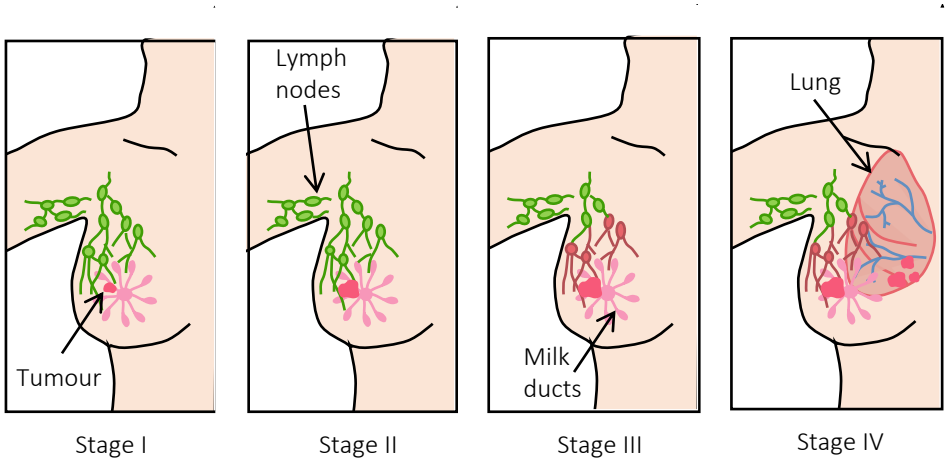


Figure 1.3 Diagram representing stages 1 to IV of breast cancer.
Stage I shows an isolated lesion of < 2 cm in diameter. Stage III is defined by local metastasis to nearby lymph nodes. Stage IV is characteristed by distant metastasis.

A further consideration and potential for stratified cancer treatment is the molecular subtype given to breast cancer. There are four generally accepted molecular subtypes of breast cancer; luminal A, luminal B, HER2+ and basal-like (8, 9). There are three molecular biomarkers that are indicative of molecular subtype; oestrogen receptor (ER), progesterone receptor (PgR) and human epidermal receptor 2 (HER2). ER is expressed in around 80 % of breast cancers diagnosed and is the main marker to predict potential response to endocrine therapies such as Tamoxifen. PgR expression largely correlates with ER expression due to its proposed reliance on the ER pathway, therefore ER+/PgR- tumours are rarely found and somewhat controversial (10). Overexpression of the HER2 receptor tyrosine kinase is observed in ~12 % of breast cancers (cBioPortal for Cancer Genomics). The knowledge of breast cancer size, stage, grade and molecular subtype guides therapeutic intervention strategy.

1.2.3 Therapeutic intervention for breast cancer patients

The majority of patients with breast cancer are treated by surgical resection, chemotherapy, endocrine therapy and radiotherapy. Cancers that express a receptor differentially to 'normal' cells give rise to the opportunity of stratified cancer therapy. The anti-oestrogen therapy drug Tamoxifen (Nolvadex), originally designed as a contraceptive that failed was later identified for its potential in the treatment of ER+ breast cancer by Dr. Arthur L. Walpole (11, 12). HER2 is expressed on the surface of tumour cells and so overexpression of HER2 makes it an ideal target for HER2+ breast cancer. HER2 has been the target of monoclonal antibodies Trastuzumab (Herceptin)(13), Pertuzumab (Perjeta)(14) and small molecule inhibitor Lapatinib (Tykerb)(15). Expression of a specific receptor on the surface provides a targeting moiety to potential novel therapeutics. Herein the focus will be on the HER family of receptor tyrosine kinases, the implication of HER2 overexpression in breast cancer and the shortcomings of current therapies.

1.3 The HER family of receptor tyrosine kinases

Human epidermal receptor 2 (HER2/ERBB2/*neu*) is a receptor tyrosine kinase (RTK) belonging to the human epidermal growth factor receptor (EGFR/HER/ERBB) family. The HER family is conserved across the nematodes *Caenorhabditis elegans* (16, 17), fruit fly

Drosophila melanogaster (18), that each contain one single receptor, and vertebrate that contain four; HER1 (EGFR, HER1, ERBB1), HER2 (*neu*, HER2, ERBB2), HER3 (ERBB3) and HER4 (ERBB4). The term 'ERBB' comes from the similarity of EGFR to the v-Erb-b gene responsible for causing avian erythroblastosis virus (AEV) (19). The annotation ERBB is accepted across all mammals whereas HER2 refers to the human gene and *neu* the mouse homologue. Despite small differences in receptors across different organisms all contain an extracellular ligand binding domain, single transmembrane domain and a cytosolic tyrosine kinase domain (18, 20)(Figure 1.4). The extracellular domain consists of four subdomains (21) I, II, III and IV that are responsible for the activation of downstream signalling pathways.

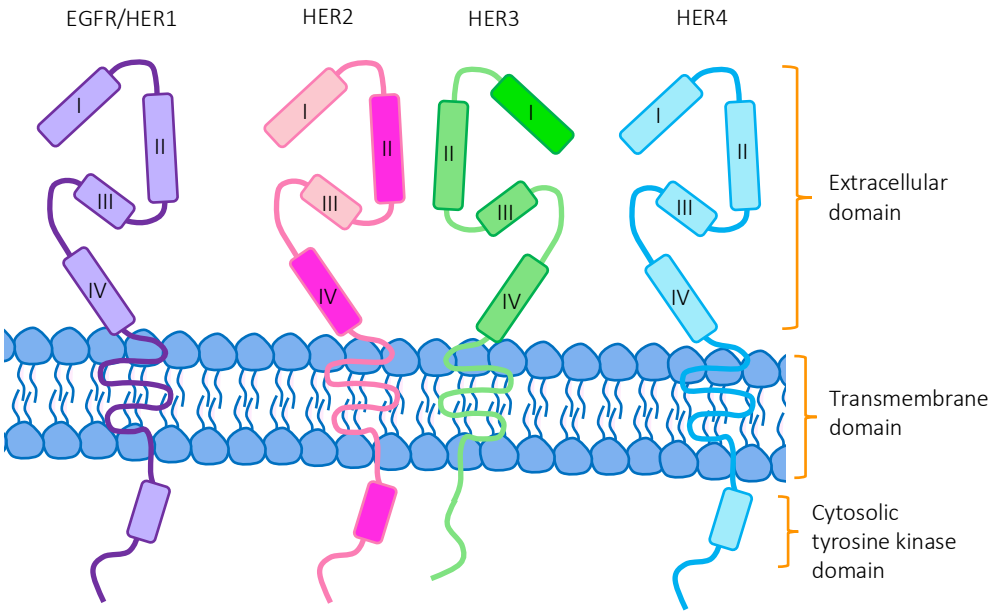


Figure 1.4 Diagram to show the four members of the HER family of receptor tyrosine kinases.
There are four members of the HER family of receptor tyrosine kinases; EGFR (HER1), HER2, HER3 and HER4. Each of these receptors contains an extracellular domain, a transmembrane domain and a cytosolic tyrosine kinase domain (with the exception of HER3).

1.3.1 Role of the HER family in normal development

There are around 60 RTKs encoded by the human genome (22). The function of these receptors is to facilitate the transfer of an extracellular signal to elicit an intracellular signalling response. RTKs are responsible for a range of roles involving proliferation, differentiation and cell survival (23). The roles of different members of the HER family have been demonstrated using an array of mouse models (24-29). Particularly, through null mutations, the importance of *ErbB2*, *ErbB3* and *ErbB4* and their ligands neuregulins

(NRGs) in neural and cardiac development has been highlighted. Both *ErbB2*$^{-/-}$ and *ErbB4*$^{-/-}$ homozygous deficient mice died *in utero* demonstrating that they are paramount in normal development of such tissue (25, 27). As well as being important to the development of cardiac tissue there is also evidence to show their importance in adult cardiac tissue. Downstream signalling from HER receptors can lead to activation of phosphatidylinositol 3-kinase (PI3K) and subsequently protein kinase B (AKT), these pathways have proven important for the survival and function of cardiomyocytes (30, 31). Together, this evidence demonstrates crucial roles of the HER family in both the development and maintenance of neural and cardiac tissue. Insufficient control of such pathways can lead to the development of a malignant phenotype. Therefore, signalling through these pathways needs to be stringently controlled.

1.3.2 Attenuation of HER signalling

Attenuation of signalling occurs through different mechanisms with different levels of success between receptors of the HER family. The role of phosphatases in signal attenuation is evidently important. It has been suggested that dephosphorylation of EGFR can occur through the action of protein-tyrosine phosphatases (32) and HER2 by proline, glutamic acid, serine and threonine-type protein-tyrosine phosphatase brain derived phosphatase 1 (33). One mechanism of control specific to HER2 is through the 68 kDa alternate transcript of HER2 deemed Herstatin that is identical to regions I and II of the HER2 ECD (34). Herstatin is hypothesised to attenuate signalling through inhibitory binding to HER2 preventing dimerisation and signal transduction (34). Attenuation of signalling is not restricted to the receptors themselves but can be through modulators downstream. Phosphatase and tensin homologue (PTEN) is a tumour suppressor protein that suppresses the PI3K pathway regulating cell signalling and thus can control signalling downstream of the receptors themselves (35).

Another mechanism thought to be important for the downregulation of RTKs is through receptor endocytosis (36). Upon endocytosis receptors can undergo degradation through different pathways. Leucine rich repeats and immunoglobulin like domain 1 (LRIG1) is upregulated following EGF stimulation and is reported to target EGF bound EGFR for ubiquitination by E3 ubiquitin ligase leading to its inevitable degradation and attenuation

of signalling (37). However, with the exception of EGFR all other members of the HER family do not appear to undergo ligand-induced endocytosis (38). Furthermore, when HER2 is overexpressed it reduces targeting of endocytosed EGFR to lysosomes for degradation but promotes recycling of the ligand bound receptor back to the cell surface therefore enhancing signalling (39). Dysregulation of signalling through the HER family of receptor tyrosine kinases can lead to phenotypes consistent with cancer including hyperproliferation and resisting cell death (2).

1.3.3 Aberrant signalling from the HER receptors and their transforming abilities

The implication of aberrant expression through the HER family of RTKs has long been recognised (40, 41). The HER family of receptors have been implicated in multiple types of cancer including breast, lung, stomach and bladder. Both EGFR and HER2 were found to have transforming abilities in NIH-3T3 cells when overexpressed either alone (HER2) or alongside EGF expression (EGFR) (42, 43). HER2 is thought to be the most oncogenic of the four receptors and is overexpressed in ~12 % of female breast cancers (44).

1.3.4 Discovery of HER2 and its role in breast cancer pathogenesis

Aberrant signalling from members of the HER family of receptors has been linked to a multitude of diseases but cancer is most heavily studied. Early studies linked the transforming ability of rat neuroblastoma to a 185 kDa protein in 1982 (45). This protein was later named *neu* and found to be homologous to ERBB2 (HER2) and related to retrovirus associated oncogene *v-erb-B* (19, 46). Rodent models have since elucidated the importance of HER2 and its role in oncogenesis.

Oncogenic activation is generally believed to be a multi-step process. Transgenic mice have been used to investigate the role of oncogenes in breast cancer pathogenesis under the influence of mouse mammary tumour virus (MMTV) (47). Transgenic mice carrying either *v-Ha-ras* or *c-myc* gene under the influence of MMTV promotor/enhancer were unable to induce full malignant transformation but showed synergistic effects in mice containing both, leading to full transformation in a tissue specific manner (48). Unlike myc and Ras, expression of activated *c-neu* under the control of the MMTV was enough

to induce tumourigenesis without the need for further genetic aberrations (47). This led to the understanding that the mouse homologue of HER2, *ErbB2/neu,* played an important role in malignant transformation. However, although mouse models contributed to our understanding of the role HER2 plays in the pathogenesis of cancer there are distinct differences. A single point mutation of valine to glutamic acid is responsible for activation of the *neu* proto-oncogene in mice (49). Whereas HER2 overexpression is found to be a driver in a subset of human cancers with mutations rarely being found. Whilst HER2 can induce transforming abilities alone it often works alongside other members of the HER family.

1.4 Signalling through the HER family

1.4.1 Activation of receptors through binding of ligands

The ligands for the HER family of receptors are synthesised as membrane precursors that undergo proteolysis (50). The ADAMs family is particularly important for ectodomain shedding of ligands for the HER family (51). Such ligands contain at least one EGF-like domain consisting of a conserved cysteine-containing motif that confers specificity to the HER family of receptors (EGF-like domain) (52). The nematode *Caenorhabditis elegans* has just a single ligand (lin-3)(53), *Drosophila melanogaster* have four ligands (spitz, vein, gurken and keren) (54, 55) while vertebrates have at least ten known ligands (56, 57). Mammalian ligands for EGFR (Erb-B1, HER1) alone or alongside other members of the HER family include endothelial growth factor (EGF), transforming growth factor alpha (TGF-α), heparin-binding EGF-like growth factor (HB-EGF), amphiregulin (AR), betacullulin (BTC), epiregulin (EPR) and epigen and schwannoma derived growth factor (SDGF) (58-63), recently reviewed (64). Another set of ligands are the Neuregulins (NRGs), sometimes referred to as heregulins (HRGs), that bind to HER3 and HER4. The NRGs are encoded for by four genes NRG1 (65), NRG2 (66) and the HER4 specific ligands NRG3 (67) and later discovered NRG4 (68) that produce a number of spliced variants that each contain the conserved EGF-like motif (69). HER2 is singled out from the other receptors and is referred to as an 'orphan receptor' as there is no known ligand that binds to the HER2 extracellular domain. Despite this, however, HER2 is the preferential

dimerisation partner following the binding of a ligand to another member of the HER family.

1.4.2 Ligand induced receptor dimerisation

RTKs dimerise as either homo- or heterodimers to induce their downstream signalling pathways. Whilst most dimerise at the ligand interface with one ligand per dimer, each HER family member bind to a ligand that induces a conformational change allowing subsequent receptor dimerisation of two ligand:receptor complexes (70). The extracellular domain of the HER receptors consist of four subdomains; I (L1), II (CR1), III (L2) and IV (CR2) (71). Homologous regions I and III are separated by cysteine rich regions II and IV (72). When in an unbound state HER1 and HER3 exhibit tethering of the β-hairpin loop of subdomain II to subdomain IV (70, 73) (Figure 1.5). This tethering prevents receptor dimerisation and consequent downstream signalling. Retrospective ligands bind through interactions with subdomains I and III (71, 74). Ligand binding induces a conformational change that releases the β-hairpin loop of domain II allowing the receptor to dimerise with another receptor also in its active state (74)(Figure 1.5). Receptors EGFR, HER2 and HER4 either form homodimers with themselves or heterodimers consisting of themselves and another receptor of the HER family. As previously mentioned, HER2 is an 'orphan receptor' with no known ligand. HER2 is found in a constitutively active conformation that mirrors that of activated EGFR, with interactions between subdomains I and III being present and the interaction between subdomains II and IV missing due to residue changes (75). There is a hierarchy when it comes to dimerisation with HER2 being the preferred dimerisation partner for other receptors with its greatest preference to the HER2:HER3 heterodimer (76). It is the HER2:HER3 heterodimer that can have transforming abilities that can lead to breast cancer pathogenesis.

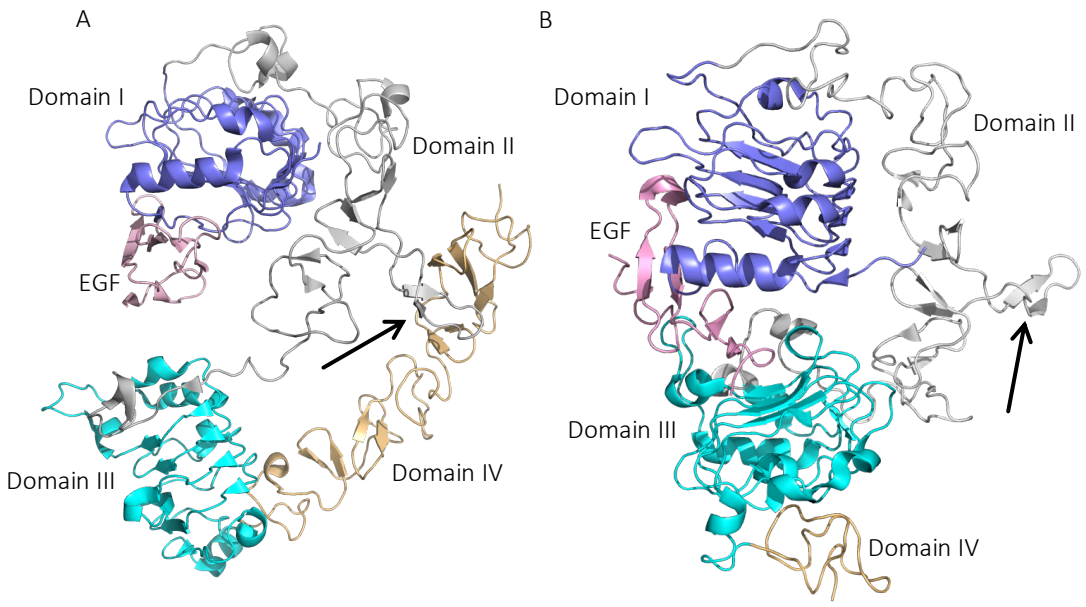


Figure 1.5 Extracellular domain of EGFR (HER1) in bound and unbound state.
EGFR extracellular domain displaying regions I, II, III and IV in purple, grey, cyan and orange respectively. EGF ligand is shown in pink. EGFR contains a β-hairpin in domain II (indicated by a black arrow) that **(A)** forms a tether with domain IV in its unbound state (when EGF is bound at low pH leading it to be in its inactive form) or **(B)** protrudes to bind to a second active receptor upon binding of EGF ligand. Respective PDB files are 1NQL **(A)** and 1IVO **(B)**.

1.4.3 Downstream signalling from the HER2/HER3 heterodimer

Ligand binding to the extracellular domain induces receptor dimerisation that brings the cytosolic tyrosine kinase domains in close proximity to each other. With the tyrosine kinase domains in close proximity to each other it allows trans- or autophosphorylation of tyrosine residues and subsequent activation of downstream signalling pathways such as PI3K and MAPK. The downstream signalling pathway that is triggered depends on the receptor heterodimer that is formed with HER2 influencing the signalling pathway activated (77).

The most preferential heterodimer to form is HER2:HER3. HER2, as previously stated, is an orphan receptor lacking a known ligand and being in a constitutively active conformation (75). HER3 lacks intrinsic tyrosine kinase ability (78) and thus is unable to activate downstream signalling pathways alone and relies on its heterodimer to phosphorylate its tyrosine residues. Most preferentially HER3 binds to HER2 bringing its kinase domain into close proximity of the HER2 cytosolic domain leading to signalling

through HER3 (79). HER3 has been found to play an important role in the progression of HER2+ breast cancer. It was initially found that co-expression of the activated form of *neu* and *ErbB3* was found in mouse mammary tumours (80). Since this the role of HER3 has been elucidated as a potent activator of the PI3K pathway following heterodimerisation with HER2.

1.4.4 PI3K pathway through HER3 containing heterodimers and its role in breast cancer pathogenesis

Upon transphosphorylation of the HER3 cytosolic tyrosine kinase domain the PI3K pathway is activated. PI3K is a heterodimer formed from 85 kDa and 110 kDa proteins (81). The 85 kDa subunit binds phosphorylated tyrosine residues through its SH2 domains (82) allowing activation of the 110 kDa catalytic subunit (83). HER3 contains six Tyr-Xaa-Xaa-Met (YXXM) consensus binding sites at its C-terminus capable of binding the SH2 domains of PI3K (84, 85). The catalytic subunit of PI3K goes on to phosphorylate the 3'-hydroxyl group of the inositol ring of phosphatidylinositol-4,5-bisphosphate (PI-4,5-P2) to form phosphatidylinositol-3,4,5-trisphosphate (PIP_3) (86, 87). PIP3 recruits both pyruvate dehyrodrogenase kinase 1 (PDK1) and AKT to the plasma membrane via their pleckstrin homology (PH) domains. Here, AKT is phosphorylated by PDK1. AKT then has a number of downstream substrates including Bad, CREB, the fork-head family of transcription factors (FOX) and Raf. These transcription factors influence processes such as proliferation, differentiation and apoptosis and so aberrant signalling can lead to tumorigenesis.

1.4.5 Ligand independent firing of HER2 induces transforming phenotype in cells

Whilst HER2 is the preferential dimerisation partner for other HER family members it has been found in breast cancer to also initiate downstream signalling as a monomer or homodimer when overexpressed, independent of ligand binding (88). HER2 can activate itself through autophosphorylation sites isolated to the carboxyl-terminal tail (89). HER2 homodimer signalling leads to activation of the extracellular-signal-regulated kinase (Erk)1/2 but not the AKT pathway (88).

1.4.6 Induction of the MAPK pathway following phosphorylation of HER2 cytosolic domain

The PI3K pathway is the most widely accepted pathway to have pathogenic significance in relation to HER2+ breast cancer, whereas the role of the MAPK pathway is unclear (Figure 1.6). One study has shown that HER2+ breast malignancies are more reliant on the PI3K pathway whilst other HER2+ tumours in other organs such as lung and ovarian show a higher dependence on the MAPK pathway (90) suggesting it could be tissue type dependent. Another study showed MAPK to be important in breast cancer expressing ER (91). Whilst its role in HER2+ breast cancer is unclear it will briefly be discussed.

Three MAPK families have been clearly identified in mammalian cells; MAPK (ERK), c-Jun N-terminal kinase/ stress-activated protein kinase (JNK/SAPK) and p38 kinase. Each pathway is composed of a cascade of protein kinases; a MAPK kinase kinase (MAPKKK), a MAPK kinase (MAPKK) and a MAP kinase (MAPK) (92). The pathway that is focussed on and potentially has a role in HER2+ breast cancer pathogenesis is the MAPK (ERK) pathway. Phosphorylation of the cytosolic tyrosine kinase domain of HER2 as well as phosphorylation of SHC occurs (93). Both of these events act as a docking site for the SH2 domains of adaptor protein Grb2 (94). Grb2 also binds, through two SH3 domains, to the Ras guanylnucleotide exchange factor sons of sevens (SOS) locating SOS to the plasma membrane where Ras is found (95). When in its guanosine-5'-triphosphate (GTP) bound state Ras binds to the serine/threonine kinase Raf (96). Raf then goes on to phosphorylate MEK that in turn phosphorylates ERK1/2 (92). ERK can regulate a range of downstream signalling targets that are involved in critical cellular processes such as proliferation, differentiation, cell cycle progression and apoptosis (97). As such if these signalling pathways are not controlled they can lead to the development of a malignant phenotype.

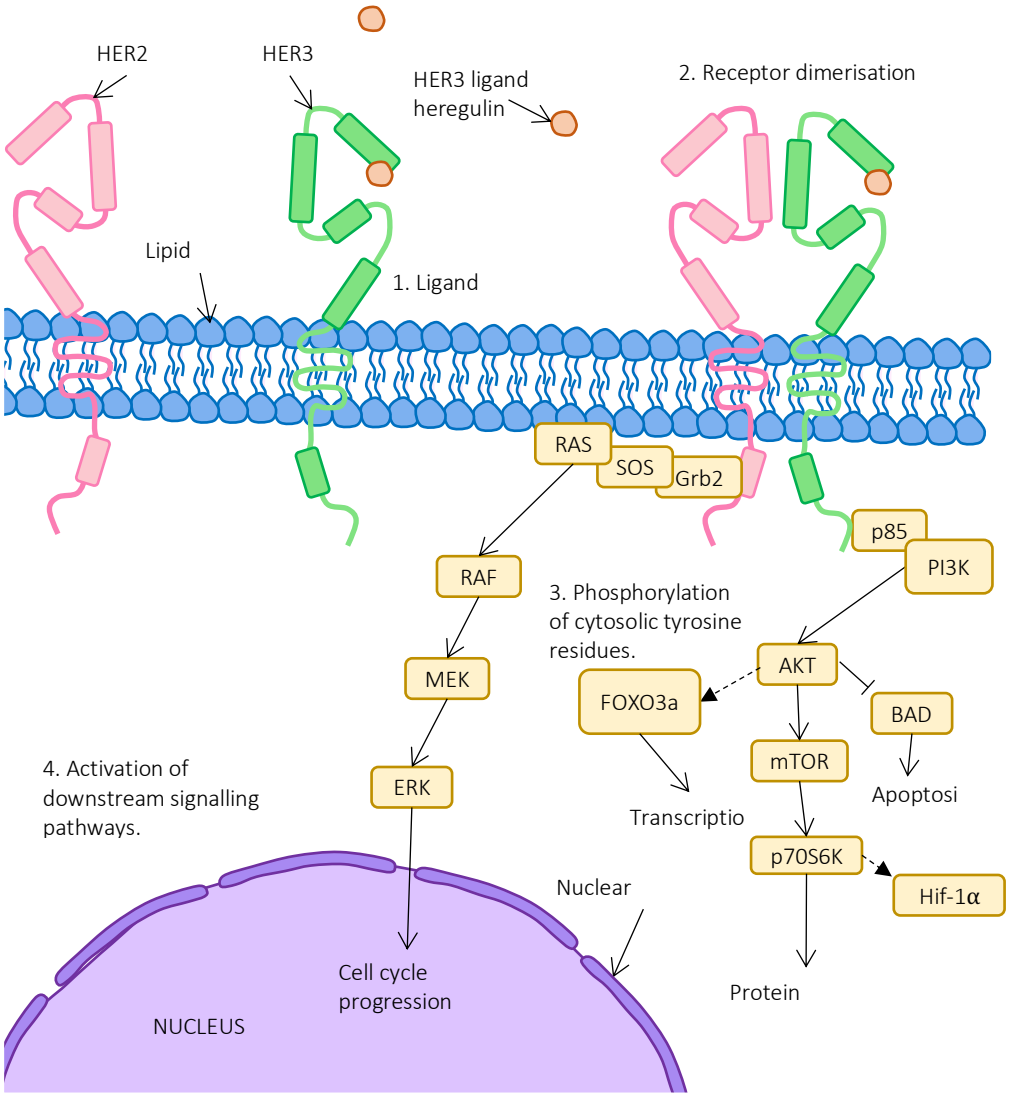


Figure 1.6 HER2:HER3 heterodimer downstream signalling.
Diagram to show downstream signalling pathways that are activated by both HER2 and HER3 and are often found to be dysregulated in multiple types of human cancer. Sons of Sevenless (SOS), growth factor receptor-bound protein 2 (Grb2), protein kinase B (AKT), mammalian target of rapamycin (mTOR), phosphatidylinositol-3-kinase (PI3K), extracellular signal-regulated kinase (ERK), hypoxia-inducible-factor 1 alpha (Hif-1α), mitogen-activated protein kinase kinase (MEK), BCL2 associated agonist of cell death (BAD), Foxohead box O (FOXO).

1.5 Diagnosing HER2+ breast cancer

HER2+ breast cancer is diagnosed by immunohistochemistry. Tumours are given a score (1+, 2+ or 3+) corresponding to HER2 expression. If a patient receives a score of 3+ the tumour is deemed positive for HER2 overexpression. A score of 1 + is HER2 negative and 2+ is followed up with further analysis such as fluorescent in situ hybridisation. A number

of commercial assays are also available to identify HER2 overexpression such as the HercepTest, Ventenna PATHWAY assay and PathVysion assay. As well as HER2 being a biomarker for breast cancer pathogenesis, it also has an important role in 'normal' cells along with other members of the HER family of RTK both in humans and other organisms.

1.5.1 Current treatments for primary and metastatic HER2+ breast cancer

Breast cancer is most often treated by surgical resection and chemotherapy. Unpleasant side effects result from systemic delivery of chemotherapeutic agents due to their lack of specificity. Chemotherapeutics target all dividing cells, so whilst the cancer is targeted due to its high proliferative ability, so are a multitude of other cell types. Targeting cancer specifically would lead to a reduction in side effects and potentially improve patient survival.

1.5.2 Monoclonal antibodies as therapeutic entities

Monoclonal antibodies were first produced in 1975 by Köhler and Milstein (98) and have proven indispensable for research, diagnostics and particularly therapeutic applications (99). Antibodies contain both heavy and light chains with the heavy chain regions CH2 connected by a disulphide bridge (Figure 1.7)(100). The variable regions (Fv) are crucial for the specificity of the antibody to its target whereas the constant regions (Fc) are utilised in eliciting an immune response through binding to Fc receptors on the surface of natural killer (NK) cells (100). Early monoclonal antibodies were mouse lineage and as such elicited strong immune responses against them when used therapeutically in humans, this led to the development of fully humanised monoclonal antibodies. There are now around 60 therapeutic antibodies that received FDA approval for evaluation in clinical trials treating a range of disease types including respiratory, autoimmune and cancer (101). Included in these are Trastuzumab (Herceptin) and Pertuzumab (Perjeta) that target HER2.

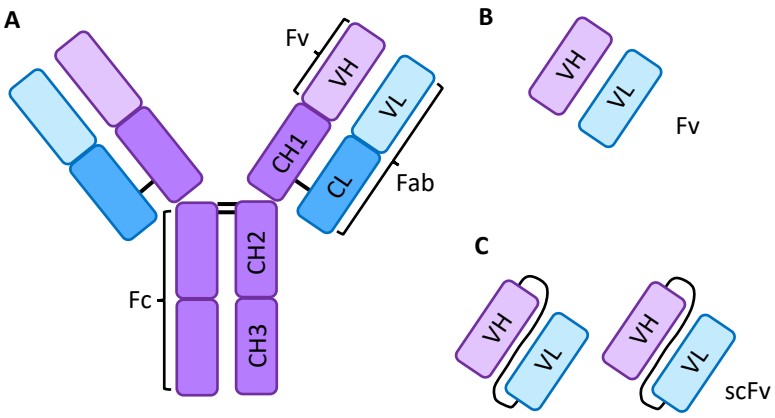


Figure 1.7 Antibody and antibody fragments.
Antibodies and antibody fragments have been utilised in both a clinical and laboratory setting. Monoclonal antibodies **(A)** have a fork-like structure with heavy (purple) and light (blue) chains. Both chains contain variable regions (VH- variable heavy, VL- variable light) that determine specificity and constant regions (CH1-4- constant heavy 1-4, CL- constant light). Fragments can be used individually as either single FV regions **(B)** or scFV **(C)** consisting of the variable regions connected by a linker.

1.5.3 Trastuzumab therapy targeting HER2 on breast cancer cells

The overexpression of HER2 on the cell surface of some types of breast cancer make it an attractive target for therapeutic antibodies. The first indication that it could be utilised for targeted therapy was when a monoclonal antibody, 4D5, against HER2 selectively inhibited the growth of NIH 3T3 cells transformed with the rodent homologue of HER2, *neu* (102, 103). The humanised version of mouse 4D5 monoclonal antibody was developed to reduce the risk of immune destruction (104). Trastuzumab (Herceptin®, Genentech Corporation, United States/Hoffman-Roche, Switzerland) is an IgG1 class humanised monoclonal antibody that binds to subdomain IV of the extracellular domain of HER2 (75). Trastuzumab was shown to be effective when given as a single agent or alongside cytotoxic chemotherapy (105-107). Trastuzumab was FDA approved for the treatment of HER2+ metastatic breast cancer in 1998 and primary HER2+ breast cancer in 2007. It is unclear exactly how Trastuzumab elicits its therapeutic response although several hypotheses have been made including enhanced ubiquitination of HER2 (108), prevention of HER2 ectodomain cleavage (109) and inhibition of angiogenesis (110) although limited data supports these hypotheses.

1.5.3.1 Targeted killing by natural killer cells through antibody dependent cellular cytotoxicity

Perhaps the most accepted mode of action is the ability of Trastuzumab to initiate antibody dependent cellular cytotoxicity (ADCC) in tumour cells (111, 112). As Trastuzumab binds to HER2 on the cell surface it forms a coat of Fc fragments being displayed on the cell. These fragments are then recognised by NK cells, that are lymphocytes part of the innate immune response. Fcγ receptor III (FcγRIII) is found on the cell surface of natural NK cells. This receptor binds to the Fc fragment of the antibody. NK cause apoptosis in target cells through the release of cytolytic granules containing perforin and granzyme that lead to decreased membrane integrity and, in turn, apoptosis (113). Whilst Trastuzumab has undeniably had a positive impact on HER2+ breast cancer treatments it does not come without drawbacks.

1.5.3.2 Negative side-effects associated with Trastuzumab treatment in breast cancer patients

All drugs that have been approved for the treatment of different diseases come with their own side effects, it has just been denoted that the positives largely outweigh the negatives of not taking them. With this, Trastuzumab is no different. The development of cardiotoxicity is the most serious side-effect noted in some patients following Trastuzumab treatment (107). It has been suggested that cardiotoxicity is observed in patients that have underlying cardiac conditions (114) and that function improves following termination of Trastuzumab treatment (115). HER2 has a role in normal cardiac development that may explain the association of Trastuzumab treatment with cardiotoxicity in some patients.

1.5.3.3 Mechanisms of resistance to monoclonal antibody therapy Herceptin

Patients treated with Trastuzumab have exhibited both intrinsic and acquired resistance to the drug. Around 20 % of primary and over 50 % of metastatic patients with HER2 overexpressing tumours experience intrinsic resistance to Trastuzumab (116, 117). Patients expressing higher levels of HER2, particularly HER2:HER2 homodimers respond

more favourably to Trastuzumab to those with lower expression (118). Whilst this may seem obvious, HER2 expression alone is not responsible for the efficacy of the drug across patients.

1.5.3.3.1 Expression of truncated p95HER2 lacking Trastuzumab binding site

Resistance can be conferred through multiple mechanisms. The expression of truncated p95HER2 lacks the extracellular domain that contains the Trastuzumab binding site, however, ligand independent firing maintains downstream signalling thereby acting as a mechanism of resistance (119). High levels of truncated p95HER2 in HER2+ breast cancer patients has been correlated with a shorter progression-free-survival when treated with Trastuzumab in multiple independent studies (119, 120).

1.5.3.3.2 Loss of PTEN expression confers resistance to Trastuzumab

PTEN is a tumour suppressor protein that negatively regulates AKT by dephosphorylation thereby acting to modulate downstream processes such as proliferation and apoptosis. Loss of PTEN function is a marker for resistance to HER2 targeted therapies (121, 122). HER3 is the main mediator of PI3K and subsequent AKT signalling as it contains multiple SH2 binding sites at its cytosolic carboxy-terminus. Therefore, loss of PTEN and HER3 expression lead to signalling independent of HER2.

1.5.3.3.3 Overexpression of HER3

Trastuzumab is thought to inhibit HER2 homodimer signalling (88) but not heterodimer signalling, hence, overexpression of HER3 can confer resistance to Trastuzumab (123). HER3 expression combined with loss of PTEN function conferred resistance to Trastuzumab (124) as HER3 is a potent activator of the PI3K pathway and PTEN acting as a negative regulator.

It can be concluded that there is no one mechanism for Trastuzumab resistance and that it is often a combination of multiple that results in such a phenotype. However, this resistance is one reason why new therapeutics that target HER2 need to be developed.

1.6 Next generation of HER2 targeting drugs

HER2 is now a highly targeted protein due to its expression and ease of access at the cell surface. Following the success of Trastuzumab multiple drugs were then developed including Pertuzumab, Ado-Trastuzumab emtansine (T-DM1) and Lapatinib (Table 1.1). The HER2 targeting monoclonal antibodies Trastuzumab and Pertuzumab bind to different subdomains within the extracellular region of HER2 whilst Lapatinib binds to the cytosolic domain (Figure 1.8).

Drug	Chemical name	Type of molecule	Mode of action
Herceptin®	Trastuzumab	Monoclonal antibody	Antibody dependent cellular cytotoxicity
Kadcyla	Ado-trastuzumab emtansine (T-DM1)	Antibody drug conjugate	Delivery of cytotoxic agent leading to apoptosis
Perjeta	Pertuzumab	Monoclonal antibody	Prevents HER2/3 receptor dimerisation
Tykerb	Lapatinib	Small molecule inhibitor	Inhibits tyrosine kinase activity

Table 1.1 Current targeted therapies used to treat HER2+ breast cancer.
A table to show the drunks currently FDA approved and used in the treatment of some HER2 overexpressing breast cancers.

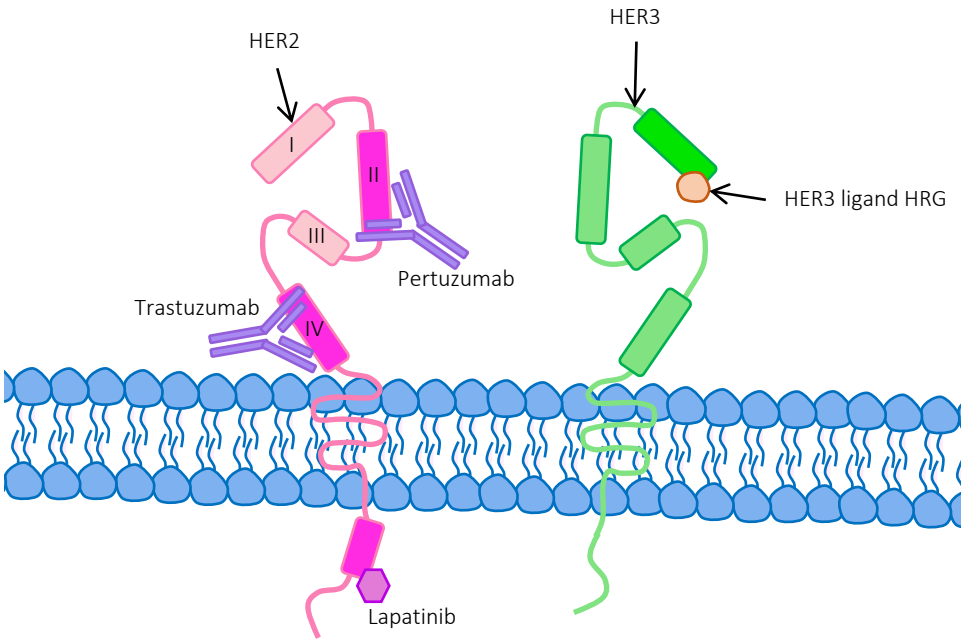


Figure 1.8 Binding sites of approved HER2 targeted therapies.
Interactions that HER2 specific drugs Trastuzumab, Pertuzumab and Lapatinib have on the HER2 receptor in relation to the HER2/HER3 heterodimer. Pertuzumab binds to subdomain II, Trastuzumab binds to subdomain IV and Lapatinib binds to the intracellular tyrosine kinase domain. HER3 ligand HRG binds to HER3 subdomain I.

1.6.1 Synergistic effects of Trastuzumab and Pertuzumab combination therapy

Pertuzumab is a monoclonal antibody that was FDA approved for the treatment of HER2 overexpressing metastatic breast cancer in 2013 and early breast cancer in 2017 (125). It was determined by X-ray crystallography to bind to subdomain II of the HER2 extracellular domain (126). Unlike Trastuzumab, Pertuzumab has a clear mechanism of action as it binds to the dimerisation arm of subdomain II thereby preventing the formation of a heterodimer involving HER2 preventing the activation of downstream signalling pathways (126). As Trastuzumab and Pertuzumab bind to unique sites on the extracellular domain of HER2 they have since been found to have synergistic effects (14, 127). Again there are adverse effects including diarrhoea, fatigue and peripheral neuropathy but the benefits are thought to outweigh the side effects (125).

1.6.2 Development of antibody-drug-conjugate Ado-Trastuzumab emtansine

Following the success of targeted monoclonal antibody Trastuzumab the antibody-drug-conjugate (ADC) Ado-Trastuzumab emtansine (T-DM1) was developed. T-DM1 combines the anti-HER2 monoclonal antibody Trastuzumab with the potent cytotoxic maytansinoid

derivative DM1. ADCs allow for the targeted delivery of a cytotoxic payload that is otherwise too toxic to deliver systemically (128). T-DM1 received FDA approval as a second line treatment for advanced breast cancer previously treated with Trastuzumab and Lapatinib. T-DM1 maintains Trastuzumab mechanisms of action (129) whilst having the added mechanism of inducing apoptosis through cytotoxic means. DM1 is an anti-mitotic agent so it was no surprise that a mechanism of T-DM1 action is to induce mitotic catastrophe in HER2 overexpressing cells leading to apoptosis (130).

Innate resistance to T-DM1 is rare, however, most patients still develop acquired resistance following treatment (130). Mechanisms of resistance aren't completely understood, however, some methods are thought to include defective lysosomal degradation of T-DM1, poor internalisation of the ADC and mechanisms mirrored from Trastuzumab resistance including HER3 signalling and high p95HER2 expression.

1.6.3 Using small molecule inhibitors of the receptor tyrosine kinase domain of HER2

As well as targeting the extracellular domain of HER2 efforts have undergone to target the cytosolic tyrosine kinase domain. Small molecule inhibitors Lapatinib and Neratinib both bind to the cytosolic tyrosine kinase domain of HER2. Neratinib is an irreversible inhibitor of HER1, HER2 and HER4 that binds to the intracellular kinase domain usually given as adjuvant therapy following Trastuzumab therapy (reviewed in. (131)). Lapatinib is another example of a small molecule that has dual targets EGFR (HER1) and HER2 autophosphorylation (reviewed in. (132)). Unsurprisingly the overexpression of the HER3 ligand heregulin has been correlated to resistance to lapatinib and trastuzumab *in vitro* and *in vivo* but not T-DM1 (133). Whilst there have been multiple attempts to target HER2 in the treatment of HER2+ breast cancer with unarguable success, resistance is largely inevitable. Therefore, there is still need for further development of novel therapeutics for the targeting of the HER2 receptor tyrosine kinase in the context of breast cancer.

1.7 Therapeutic alternatives for the potential treatment of HER2+ breast cancer

Both Trastuzumab and Pertuzumab are monoclonal antibodies and whilst these amongst many others have been utilised in a therapeutic context they do have drawbacks.

Antibodies have demonstrated limitations regarding their large size (~ 150 kDa) restricting their efficacy in penetrating solid tumours, immunogenicity, high production costs, complex structures, need for post-translational modifications and instability (134). To overcome some of these shortcomings the use of antibody fragments such as Fab fragments or single-chain Fv (scFvs) was developed (Figure 1.7)(135).

1.7.1 1.7.1 Antibody fragments svFc

Whilst antibodies rely on mammalian systems for their production due to the high number of disulphide bonds and complex post-translational modifications svFvs and Fab segments contain 2-6 disulphide bonds respectively and no N-glycosylation so have successfully been produced in *E.coli* (136). These single-chain antigen-binding proteins (svFc) were first described in 1988 to contain a variable light chain sequence (VL) to a variable heavy chain sequence (VH) connected by a flexible linker Figure 1.7(137). A Fab fragment comprises an antibody light chain (VL and CL) linked to antibody heavy chain VH and CH1 by a disulphide bond (Figure 1.7).

One of the most advantageous points for the use of antibody fragments in the treatment of solid tumours is their superior ability to penetrate a solid mass compared to monoclonal antibodies (138). As such, scFvs have been generated against the EGFR family (139, 140). Their therapeutic potential was highlighted in the context of HER2 with an scFV 'cocktail' of scFVs that bind to different domains of the HER2 extracellular domain that proved effective in the downregulation of HER2 signalling in HER2+ cell line (141, 142)

Both antibody fragments suffer a reduced half-life compared to full length antibodies. To overcome this they can be produced in complex with larger molecules such as polyethylene glycol (PEG) that in turn extends their half-life whilst maintaining specificity (143). However, issues can arise from increasing molecule size such as reduced ability to penetrate solid tumours.

1.7.2 Non-immunoglobulin scaffolds in the context of HER2+ breast cancer

A number of non-immunoglobulin scaffolds have also been developed in recent years (Figure 1.8). The scaffolds share common properties including their small size, ease of production and low production cost. Three of these proteins in particular; designed ankyrin repeat proteins (DARPins), Affibodies and Aptamers have been developed against HER2 for use in laboratory and clinical settings and will be discussed further below.

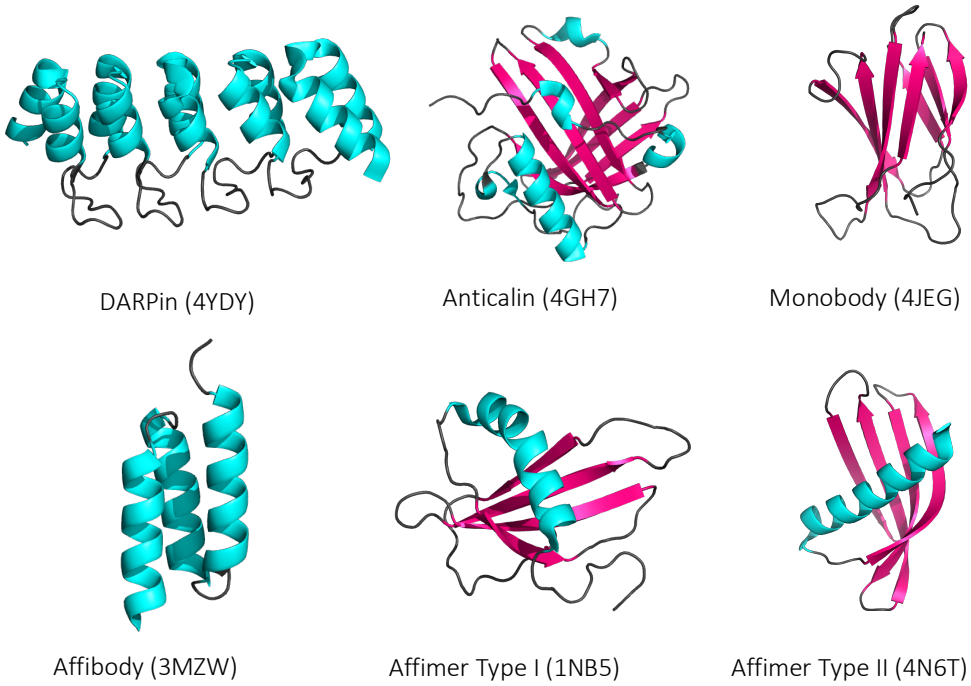


Figure 1.9 Ribbon diagrams to show structures of various non-immunoglobulin scaffold.
Crystal structures of antibody alternative molecules were taken from the PDB website (accession numbers displayed next to the protein name). Alpha helices are shown in cyan whilst beta sheets are in magenta.

1.7.2.1 Designed ankyrin repeat proteins (DARPins)

DARPins are one example of an antibody alternative molecule (144). Their size ranges from 14 to 21 kDa and their structure comprises repeats of a β-turn, two antiparallel helices and a loop to reach the β-turn of the next repeat (144). DARPins have shown to be beneficial in vast areas of science including as biosensors, in diagnostics and tumour targeting (145). DARPins that bind to HER2 with nanomolar affinity and high specificity shown through immunohistochemical staining were isolated (146). Improved picomolar binding affinity was achieved through error-prone PCR later by the same group (147). DARPins have been shown to have therapeutic potential against HER2 overexpressing

breast cancer. A bispecific DARPin against region I and IV of the extracellular domain exhibited cytotoxic effects on HER2+ cell lines (148). They have been used for the targeted delivery of lentiviral vectors using HER2 specific DARPins (149). HER2 specific DARPin-miniSOG fusion protein combined the specificity of the HER2 specific DARPin and the cytotoxic effect of phototoxin to target HER2+ cells (150). This demonstrates their possible use for the therapeutic intervention of HER2+ breast cancer.

1.7.2.2 Affibodies

Affibodies are based on a single 58 residue immunoglobulin binding staphylococcal protein A analogue Z (151). A phage display library was generated through randomisation of 13 amino acid surface residues located on two α-helices involved in binding of the wildtype protein (151). Along with their small size, thermostability and reproduceability to produce this makes them attractive for scientific and therapeutic use. Affibody named His_6-Z_{HER2} was demonstrated to bind to the HER2 extracellular domain with nanomolar affinity at a site independent of monoclonal antibody Trastuzumab (152). They have also been used to target liposomes containing cisplatin to HER2+ cells (153). A bi-valent HER2 specific Affibody was developed, $(Z_{HER2:4})_2$ with nanomolar affinity for HER2 that, when fused to a radionuclide showed promising efficacy as a tumour imaging agent (154, 155). In 2008 it was found that the dimeric form of HER2 specific affibodies, but not the monomeric, could inhibit the growth of HER2 overexpressing SKBR3 cells with similar efficacy to currently used monoclonal antibody Trastuzumab (156). It was determined by X-ray crystallography that the HER2 specific affibody investigated bound to a site unique from currently used therapeutic antibodies Trastuzumab and Pertuzumab involving domains III and IV of the HER2 extracellular domain (157).

More recently the use of HER2 specific affibodies as vehicles for the specific delivery of cytotoxic compounds for targeted delivery has been investigated, much like currently used ADCs. Conjugation of HER2 specific affibody molecule to cytotoxic moiety Auristatin E was shown to specifically deliver a drug to HER2 overexpressing cells (158). Affitoxins were developed by combining HER2 specific Affibody to Pseudomonas exotoxin A and showed to inhibit protein synthesis in HER2 overexpressing cell lines (159). Together this demonstrates the large range of evidence for the use of Affibodies in a clinical setting.

1.7.2.3 Aptamers

Aptamer molecules are DNA or RNA oligonucleotide ligands that are isolated through systematic evolution of ligands by exponential enrichment (SELEX). The first RNA Aptamers were identified through this technique in 1990 (160). Aptamers alone are quickly filtered out by the kidneys so most Aptamers are modified to increase their half-lives. Aptamers are also at risk of degradation by exo- and endonucleases, to overcome this 'locked nucleic acids' have been used at the 3' and 5' ends of the Aptamer to improve *in vivo* stability (161)

Aptamers show promise as therapeutic alternatives to monoclonal antibodies due to the usual small size, low immunogenicity, low toxicity and that they are inexpensive to produce. The first aptamer to be FDA approved for the treatment of human disease was an RNA aptamer (Macugen; Eyetech Pharmaceuticals/Pfizer) raised against vascular endothelial growth factor (VEGF) for the treatment of macular degeneration (162). The potential ability of targeting an Aptamer against HER2 has been studied. Novel DNA Aptamers raised against endogenous HER2 of the HER2 overexpressing cell line SKBR3 (whole cell-SELEX) were developed and found to have an inhibitory effect on HER2+ cells (163). HER2 specific RNA Aptamers were also isolated using cell-SELEX showing high affinity to HER2+ cells (164). Cell-SELEX allows selection by proteins in their native conformation and also from a heterogeneous population of proteins on the cell surface (165).

1.8 Modelling breast cancer

Improvements are needed in preclinical drug models as well as the drug itself. Oncology drugs have one of the lowest probabilities of receiving FDA approval when entering clinical trials (166). This is, in part, due to poor translation of preclinical drug studies to patients. Over the years the way in which we model human breast cancer has advanced greatly from 2D cell culture to mouse models and now complex multicellular 3D humanised organoids and patient derived organoid models. With each method comes its own benefits and shortfalls, some of which will be discussed in the following sections.

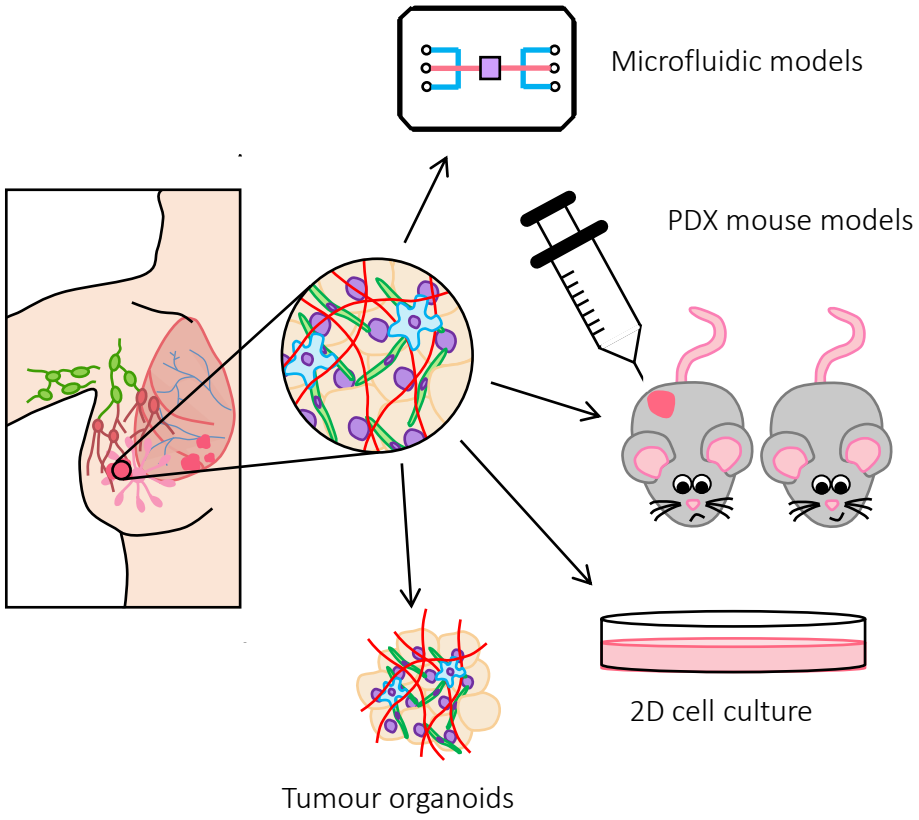


Figure 1.10 Example models used for preclinical drug testing.
Multiple models have been developed for preclinical drug testing each with their advantages and disadvantages. The figure highlights the main current models available.

1.8.1 2D cell culture and its contributions to breast cancer research

Cell culture methods have advanced greatly over the last decade. Perhaps the simplest of methods to model human breast cancer is 2D cell culture of spontaneously immortalised cells- resulting in cell lines- from patient tumours. The first breast cancer cell line, BT20, was developed in 1958 from an invasive ductal carcinoma (167). There are now many cell lines available that have been derived from multiple different breast cancers (168). Since this development scientists have been able to use cell lines for *in vitro* modelling of human disease where they have contributed to the development of novel therapeutics such as Tamoxifen for the treatment of ER+ breast cancer and Trastuzumab for the treatment of HER2+ breast cancer (169). However, whilst cell lines have contributed to the advancing knowledge surrounding breast cancer, limitations to their use have been highlighted in recent years. Breast cancer is a highly heterogeneous disease and there has been an increasing acceptance that the tumour microenvironment

contributes a large part to cancer pathogenesis (170). A tumour comprises multiple cell types such as epithelial cells, fibroblasts, immune cells and the extracellular matrix (Figure 1.11). Therefore, it is no surprise that a monolayer of a single cell type, whilst useful in many contexts, does not provide an accurate representation of a tumour *in vivo* (Figure 1.11). In recent years there have been many efforts to improve the translation from bench to bedside. An editorial published in Nature in 2003 was perhaps a turning point for the acceptance of 3D cell culture and from this stemmed an incline in research adopting 3D cell culturing techniques (171). The tumour microenvironment is vital to tumour growth and progression, now being one of the hallmarks of cancer, and is therefore needed to be considered when undertaking *in vitro* drug studies. This new era of cell culture began to emerge after the 'Goodbye Flat Biology' editorial was published in 2003 captivating the importance of 3D cell culture and reiterated by Bissell 15 years later (172).

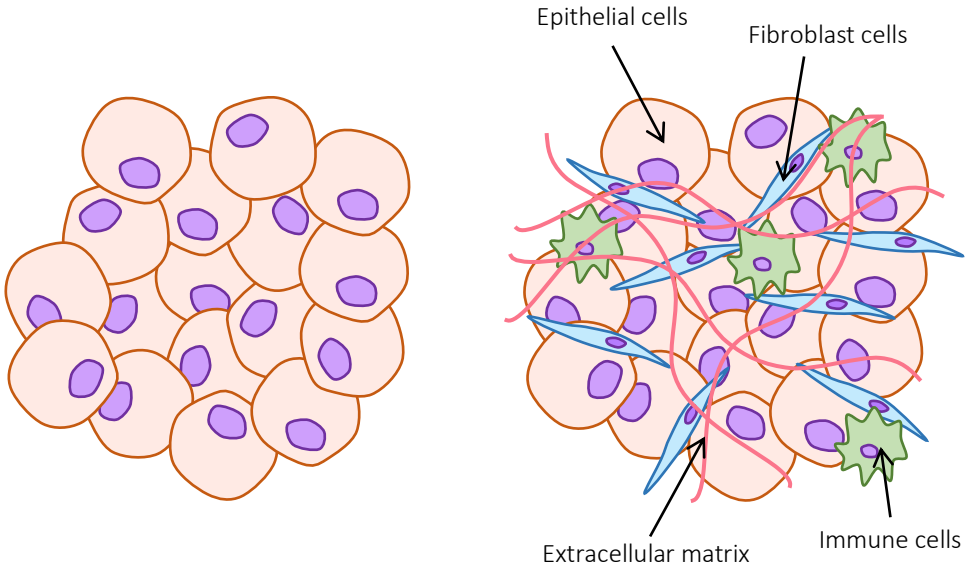


Figure 1.11 Heterogeneity in solid tumour compared to 2D cell culture.
(A) shows cell culture of cell line monolayers **(B)** shows the complexity of a human breast tumour with the multiple cell types and extracellular matrix.

1.8.2 Spheroid models for studying cancer

Spheroid culture is one method of culturing cells in 3D. This was first used to observe the effects of irradiation of tumours cells (173). Spheroids can be cultured in a number of ways including the hanging drop technique (174), magnetic levitation (175), 3D collagen culture or in matrix-free medium called epiFL (176). Spheroids recapitulate characteristics of human tumours such as necrotic centres and proliferating surface cells (177). Initially, spheroid models were generated using single cell lines (178), however, availability of patient derived cells from the Breast Cancer Now Tissue Bank (BCNTB)(179) has made co and tri-culture models with patient samples possible (180, 181).

1.8.3 Advantages of using primary patient samples over cell lines

Breast cancer is a highly heterogeneous disease and as such cell lines are homogeneous in nature so do not accurately recapitulate this *in vitro* (182). Breast cancer heterogeneity is observed on many levels with different gene signatures being observed between primary, metastatic and disseminated tumour cells (183). Using primary cells has advantages as they more closely mimic the tumour in its native environment (182). But with using primary cells challenges are also posed as they require much more stringent

conditions in order to grow *ex vivo.* Different models have been generated with an effort to increase success in maintaining patient tumours outside of the body.

1.8.4 Organoids derived from primary breast cancer patient samples

The study of organoids derived from breast cancer patients opens the possibility of testing novel therapeutics in a clinically relevant model (184). A biobank of breast cancer organoids that reflect heterogeneity of the respective patient has recently been generated for use in experimental research and provides methodology for the maintenance of such organoids (185, 186). Publications like this pave the way to the next generation of human disease models that better reflect what is observed in patients.

1.8.5 Microfluidic modelling of cancer

The field of microfluidics is an emerging model system that could prove to be revolutionary in the modelling of human disease (187, 188). One advantage of modelling disease at such a small scale is the limited cost of reagents and small sample volume that is needed. The use of 'organ-on-chip' models could advance the way in which cancer is being studied by allowing the inter-relationships of different organ systems to be analysed on a micron scale to study metastasis and drug effects on a whole organ system (188). Microfluidics is also arguably the only non-animal model to incorporate the influence of mechanical stresses on tumours into its model (189). Microfluidic chips have been used to increase our understanding of breast cancer including the effect of changing the extracellular matrix composition (190), factors that affect the migration capability of the cells (191) and to mimic the tumour microenvironment (192).

1.9 Using mouse models to study human disease

1.9.1 Early mouse models to study human disease

The potential use of mice to model human disease was a concept accepted long ago. Initial studies concentrated on transgenic mice. These studies, aforementioned, contributed to our understanding of oncogenes such as *neu*, MYC and Ras and their roles in cancer initiation and progression. Then came the development of genetically

engineered mouse models (GEMM). GEMM models provide a huge advantage over other murine models in that develop *de novo* tumours in an immune-proficient environment that provide hope for the future of investigating drug responses in a clinically relevant model (193). Possibly the most widely used mouse model for preclinical drug studies to date is patient derived tumour xenograft (PDTX) models.

1.9.2 Patient-derived xenograft models

The simplest form of xenograft model involved the engraftment of human cell lines (194) into an immunocompromised mouse (195, 196). Such engraftment is termed a cell derived xenograft (CDX) model. However, CDX models exhibit the same limitations of 2D cell culture in that they do not recapitulate the heterogeneity of breast tumours *in vivo* and are also infiltrated with mouse, not human, stroma. This led to the development and use of patient derived xenograft models (PDX). In brief, PDX models are generated by the transplantation of patient tumour biopsy or tumour cells into an immunocompromised mouse (197). A major advantage of using PDX models is that the graft maintains phenotypical and molecular characteristics observed in the parent tumour including histopathology, clinical markers, DNA copy number and oestrogen dependence in ER+ tumours (198). Whilst other subtypes of breast cancer appear to be more successful in generating PDX models some HER2+ xenografts have been successfully implanted into mice (199, 200). The Caldas group published in 2016 that they had successfully generated a Biobank of patient derived tumour xenograft derived tumour cells (PDTC) that held high potential for pharmacogenomic studies to predict response of patients. PDX models are now recognised as a reliable indication of preclinical efficacy of new therapeutics supported by the decision of the US National Cancer Institute to retire the panel of human cancer cell lines (NCI-60) to use a library of PDX derived patient samples (201).

However, as with all model systems there are drawbacks to PDX models. Whilst PDX models are thought to maintain a higher level of heterogeneity than other mouse models there is still evidence that clonal selection does occur in some samples (202). Also, this first line of PDX mouse models is unable to model the role that the human immune system plays in tumorigenesis that has been recognised to be an important factor in the development of cancer (1, 2). Whilst mouse models have and continue to provide invaluable contribution to the field of therapeutic efficacy trials of developing drugs they

are still not ideal. With many researchers driven by the 3R's attempting to reduce, refine and replace the number of animals used in research the field of 3D cell culture is rapidly advancing. The generation of complex 3D multicellular models that recapitulate tumour heterogeneity are, for the first time, opening the possibility for complete replacement of the use of animals in preclinical modelling of human disease.

1.10 Hypothesis

The development of non-immunoglobulin Affimers specific for HER2 that are capable of site specific conjugation to a cytotoxic payload could potentially overcome some of the shortcomings associated with monoclonal antibodies. In addition the development of a fully humanised model system would contribute to reducing the gap between 2D cell culture and animal models in preclinical drug studies.

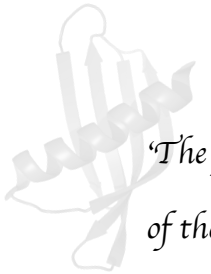
1.11 Aims of the project

The aims of the current project are as follows;

1. Characterise the ability of HER2 binding Affimers to be internalised by HER2 overexpressing cell lines.
2. Generate Affimer drug conjugates with high affinity for HER2 that cause cell death in cell lines overexpressing HER2 specifically.
3. Develop the novel 3D cell culture system PerfusionPal as a preclinical drug testing platform.
4. Investigate the binding site of HER2 binding Affimers through X-ray crystallography.

Chapter 2

Materials and Methods



'The future belongs to those who believe in the beauty of their dreams'

-Eleanor Roosevelt



2 Materials for laboratory

2.1 Commonly used reagents

Reagents that are commonly used to make buffers are shown in table 2.1.

Reagent	Supplier (Cat. No)
NaH_2PO_4	MP Biomedicals , LLC (195500)
NaCl	Fisher Scientific (S/3160/63)
Imidazole	VWR (286874D)
Glycerol	Fisher Scientific (G/0600/17)
Tris	Bio Basic (TB0194)
Tween-20	ChemCruz® (BC-29113)
Tryptone	OXOID (LP0042)
SDS	Fischer Chemicals (1281-1680)
Methanol	Fisher Scientific (M/4000/17)
Acetic Acid	Fisher Scientific (A/0360/PB17)
Glucose	Fisher Scientific (G/0500/61)
Glycine	Fisher BioReagents (BP381-1)
Yeast Extract	OXOID (LP0021)

Table 2.1 Table of common reagents.
Reagents are shown on the left with suppliers and catalogue numbers on the right (Cat. No).

2.2 Laboratory stock solutions

Ammonium Persulphate (APS) (Fisher Scientific, A/P470/46) APS was dissolved at 10 % (w/v) in double distilled water (ddH_2O) and stored at -20 °C.

Isopropyl b-D-1-thiogalactopyranoside (IPTG) 1 M IPTG stock solution was made up in ddH_2O and stored at -20 °C.

Nuclease free water (Sigma) Water was treated with UV prior to aliquoting and storage at -20 °C.

10 x Orange G loading dye 30 (v/v) % glycerol, 0.2 % (w/v) Orange G

SDS-PAGE running buffer: 25 mM Tris, 200 mM glycine, 0.1 % (w/v) SDS, pH 8.3

Coomassie Blue Stain 45 % methanol; 7 % acetic acid; 0.25 % Coomassie Brilliant Blue R-250 (Fluka) made up with H_2O.

Destain 25 % methanol; 7.5 % acetic acid made up with ddH_2O

2.3 Bacterial cell lines

2.3.1 BL21 Star™ (DE3)

Genotype: F⁻*omp*T *hsd*S_B (r_B^-, m_B^-) *galdcmrne*131 (DE3)

The BL21 Star™ (DE3) chemically competent cells (Invitrogen™, C601003) encoding T7 RNA polymerase and carbenicillin resistance were used for high-level protein expression. The DE3 lysogen carries the gene for the T7 polymerase under the control of the lacUV5 promoter enabling IPTG induced protein expression. The strain also allows for increased mRNA stability due to a mutation in the RNase E gene (*rne 131*) that reduces mRNA degradation and reduced levels of endogenous RNases.

2.3.2 XL 1-Blue supercompetent cells

Genotype: *recA1 endA1 gyrA96 thi-1 hsdR17 supE44 relA1 lac* [F′ *proAB lacI*^{q}*ZΔM15* Tn*10* (Tet^r)]. (Genes listed are mutant).

XL1 (supercompetent, Agilent) cells were used for DNA preparation.

2.3.3 Lemo21(DE3)

Genotype: *fhuA2 [lon] ompT gal (λ DE3) [dcm] ΔhsdS/ pLemo*(Cam^R) *λ DE3 = λ sBamHIo ΔEcoRI-B int::(lacI::PlacUV5::T7 gene1) i21 Δnin5* pLemo = pACYC184-*PrhaBAD-lysY*

Lemo21(DE3) chemically competent *E.coli* cells (New England Biolabs, stocks made by the protein production facility) were used for enhanced expression of mammalian highly glycosylated protein. Protein expression is tuneable utilising the control of T7 lysozyme by L-rhamnose.

2.3.4 SHuffle T7 Express

Genotype: *fhuA2 lacZ::T7 gene1* [lon] *ompT ahpC gal λatt::*pNEB3-r1-*cDsbC* (Spec^R, *lacI*^{q}) Δ*trxB sulA11 R(mcr-73::miniTn10*-Tet^S)2 [dcm] *R(zgb-210::Tn10* --Tet^S) *endA1 Δgor Δ(mcrC-mrr)114::IS10*

Shuffle T7 Express strain (New England Biolabs, in house stocks made by the protein production facility) has an enhanced ability to currently fold proteins containing disulphide bonds. The strain utilised the T7 expression system.

2.3.5 Rosetta-Gami2(DE3)PLysS

Genotype: Δ(*ara-leu*)*7697* Δ*lacX74* Δ*phoA Pvu*II *phoR araD139 ahpC galE galK rpsL*(DE3) F′[*lac*$^{+}$ *lacI*^{q} *pro*] *gor522*::Tn*10 trxB* pLysSRARE2 (Cam^{R}, Str^{R}, Tet^{R}).

Rosetta-Garmi2(DE3)PLysS strain (Merck, in house stocks made by the protein production facility) used for enhanced mammalian protein expression and correct folding of disulphide bonds.

2.4 Plasmid vectors

pET11a (Novagen) bacterial expression vector was used. This vector contains a T7 promotor region, *lac* repressor gene and ampicillin resistance gene.

pDHisII (203) phagemid vector encoding dsbA secretion signal, Affimer coding sequence and a C-terminal coding sequence for domain II and III from bacteriophage M13 gene III and ampicillin resistance.

pETLECTRA bacterial expression vector used for initial Affimer production containing T7 promotor region, *lac* repressor gene and kanamycin resistance gene.

pOPIN (204) bacterial expression vectors based on pTriEx2 (Novagen). pOPIN vectors encode N-His$_{6}$ and 3C cleavage site, T7 promotor region and CMV enhancer and ampicillin resistance gene.

2.5 Antibiotics

Stock solutions of antibiotics were made up in deionised water and filter sterilised through a 0.2 μm filter (Millipore). Antibiotic was aliquoted into 1 mL microcentrifuge tubes and stored at -20 °C. Stock and working concentrations are as shown in Table 2.2.

Antibiotic	Stock concentration	Working concentration
Carbenicillin	50 mg/mL	100 mg/mL
Kanamycin	25 mg/mL	50 mg/mL
Chloromphenicol	34 mg/mL	34 mg/mL
Spectomycin	50 mg/mL	50 mg/mL
Streptomycin	50 mg/mL	50 mg/mL
Ampicillin	50 mg/mL	100 mg/mL

Table 2.2 Stock and working concentrations of antibiotics.

2.6 Growth media

LB agar (Invitrogen, 22700025). 32 g LB agar was dissolved in 1 L ddH_2O and autoclaved at 121 °C 15 p.s.i. for 21 minutes. Solution was allowed to cool until it was able to be held before the addition of appropriate antibiotic.

LB broth base (Invitrogen, 12780052). 20 g LB broth was dissolved in 1 L ddH_2O and autoclaved at 121 °C 15 p.s.i. for 21 minutes. Solution was allowed to cool until able to be held before the addition of appropriate antibiotic.

2TY. 16 g Tryptone (Oxoid), 10 g Yeast Extract (Oxoid) and 0.5 g NaCl (Fisher Scientific) were dissolved in 1 L ddH_2O. Solution was autoclaved at 121 °C 15 p.s.i. for 21 minutes.

2.7 Protein production and purification

2.7.1 Bacterial transformation

DNA was transformed into either BL21 Star™ (DE3) or XL-1 supercompetent cells depending on whether protein or DNA production was desired. 1 μL DNA was added to 10 μL competent cells and incubated on ice for 30 mins prior to heat shocking at 42 °C

for 45 seconds. 100 μL SOC medium (New England BioLabs®, B9020S) was added and tubes were incubated at 37 °C, 230 rpm for 1 hour prior to plating on LB agar plates made with appropriate antibiotic. The following day colonies were picked and cultured overnight in 2/7 mL 2TY + 1 % glucose for protein production (depending on whether 50 mL or 400 mL cultures were planned) or 5 mL LB for plasmid preparation with appropriate antibiotics in 50 mL falcon tubes (Stratech). Tubes were incubated at 37 °C with shaking at 230 rpm.

2.7.2 Protein production by isopropyl β-D-1-thiogalactopyranoside induction

50/400 mL LB with appropriate antibiotic was prewarmed to 37 °C in 250 mL or 2 L conical flasks accordingly. Flasks were inoculated with 1/5 mL of overnight culture and grown at 37 °C, 230 rpm. until they reach an OD_{600} of ~0.7. At this point they were induced with IPTG to a final concentration of 0.1 mM and incubated overnight at 25 °C, 150 rpm. Induction with IPTG utilises the *lac* operon (Figure 2.1). Cells were harvested by centrifugation at 4,816 x g for 20 mins. Supernatant was discarded and pellets were stored at -20 °C, if not used immediately.

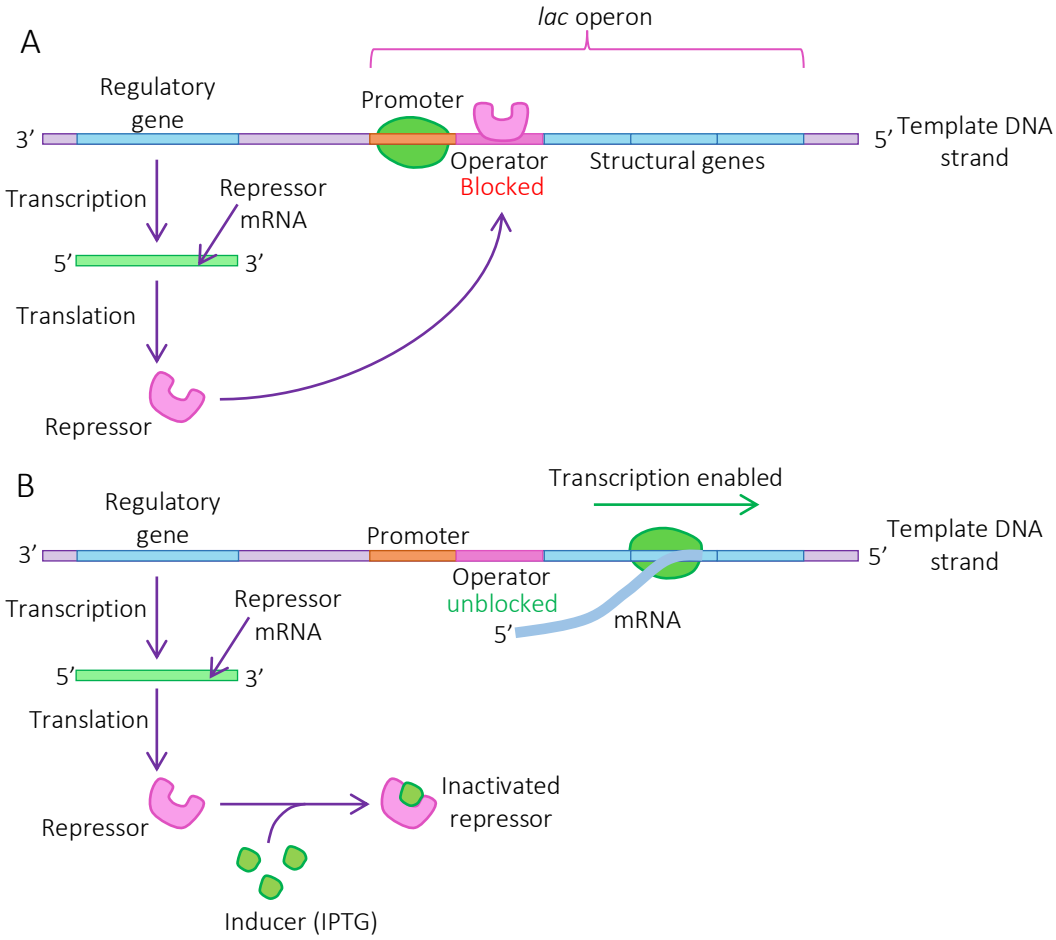


Figure 2.1 Mechanism of the lac operon.
IPTG is a mimic of allolactose and is used to enable protein production in systems that utilise the lac operon. **(A)** Without IPTG the operator is blocked by the repressor preventing the DNA polymerase from moving thus inhibiting transcription. **(B)** Upon IPTG induction this binds to the repressor preventing it from binding to the operator. Therefore, transcription can now take place and protein production is enabled.

2.7.3 Purification of 6 x His-tagged Affimer by Ni-NTA affinity chromatography

2.7.3.1 Buffers used during Affimer purification

Elution buffer: 50 mM NaH_2PO_4 (across organics), 500 mM NaCl, 300 mM Imidazole (VWR), 10 % glycerol (Fisher Scientific), pH 7.4.

Lysis buffer: 50 mM NaH_2PO_4, 300 mM NaCl, 30 mM Imidazole, 10 % glycerol, pH 7.4.

Wash buffer: 50 mM NaH_2PO_4, 500 mM NaCl, 20 mM Imidazole, 10 % glycerol, pH 7.4.

2.7.3.2 Affimer protein purification

Pellets from 50/400 mL cultures were resuspended in 1/50 volume of lysis buffer supplemented with lysozyme® (Sigma-aldrich, L6876-1G)(0.1 mg/mL), Triton™ X-100 (Sigma-aldrich, X100-100 mL)(1%), Benzonase Nuclease, purity > 99% (Novagen®, 70664) (25 U/mL), Halt Protease Inhibitor Cocktail (100X, Thermo Scientific, 78439)(1x). Suspension was transferred to a 2/14 mL microcentrifuge tube/ falcon tube and incubated for 1 hour at room temperature (Stuart fixed speed rotator). Tubes were incubated in a 50 °C heat block/ waterbath for 20 mins to denature non-specific proteins. Tubes were centrifuged at 16,000 x g for 20 mins/ 4,816 x g for 20 mins. During this time 300/800 μL Amintra Ni-NTA slurry (Expedeon, ANN0100) was resuspended in 1/5 mL wash buffer and centrifuged at 1,000 x g for 1 min. Wash buffer was aspirated off and supernatant was added to the washed resin and incubated for 1-2 hours at room temperature on the rotator. Tubes were centrifuged at 1,000 x g for 1 min and the supernatant containing unbound protein was removed. Resin was washed several times using 2 mL polystyrene columns (ThermoScientific, 29920) with wash buffer until the A280 of the wash buffer was < 0.09. At this point Affimers were incubated with elution buffer (1 mL for first elution, 500 mL thereafter) for 5 mins prior to elution from the column. Affimers were stored at either 4 °C or -20 °C depending on experiment.

2.8 Protein analysis

2.8.1 Determination of protein concentration

Protein concentrations were determined using different methods depending on what the protein was or to compare across methods.

2.8.1.1 Nanodrop-lite

Concentration of Affimer protein was determined using a Nanodrop-lite spectrophotometer (Thermo Fisher Scientific). The system was blanked using the protein storage buffer. 1.5 mL sample was loaded onto the pedestal and the A_{280} was measured. The extinction coefficient and absorbance at 0.1 % of the protein was determined using the ExPASY ProtParam tool. The protein concentration was estimated using the Beer Lambert law (Figure 2.2).

$$A. \quad \varepsilon = (nW * 5500) + (nY * 1490) + (nC * 125)$$

$$B. \quad A = \varepsilon * b * c$$

$$C. \quad c = A/\varepsilon b$$

Figure 2.2 Beer Lambert equation used to quanity protein concentration when using the NanoDrop Lite. **(A)** Extinction coefficient at 280 nm is determined by tryptophan (Trp, W), tyrosine (Tyr, Y) and cysteine (Cys, C) residues. This value is determined by multiplying the number of these residues by there weight. **(B)** shows the Beer Lambert equation in its original form whereby absorbance (A) is equal to the extinction coefficient (ε) multiplied by the path length in cm (b) multiplied by molarity M (c). **(C)** rearranged Beer Lambert equation used to determine the concentration when absorbance, extinction coefficient and path length are known.

2.8.1.2 BCA assay

Protein concentration could also be determined using the Pierce™ BCA assay (23225). Concentrations were determined following the manufacturers protocol. Protein standards were set up in a 96 well plate (ThermoScientific) using BSA diluted in the protein storage buffer. Absorbance was read at 562 nm and a standard curve was plotted to interpolate unknown concentrations from using GraphPad prism.

2.8.1.3 Bradford assay

Bradford assays for the determination of protein concentration were undertaken using the Quick Start™ Bradford Protein Assay (Bio-Rad) as per the manufacturers instructions. Protein standards were set up in a 96 well plate (ThermoScientific) using BSA diluted in protein storage buffer. Absorbance was measured at 595 nm. Standard curves were plotted using GraphPad prism where unknown protein concentrations were interpolated.

2.8.2 SDS-PAGE

Protein samples were separated according to their size by SDS-PAGE. Samples were mixed with 4 x loading buffer (200 mM Tris-HCl, pH 6.8, 20 % (v/v) glycerol, 8 % (w/v) SDS, 0.4 % (w/v) bromophenol blue, 20 % (v/v) β-mercaptoethanol (Fisher Scientific, M/P200/05)) prior to heat denaturing of proteins at 95 °C for 5 mins. Gels were prepared

using a Bio-Rad mini-PROTEAN casting system. Depending on the size of the protein to be analysed either a 15 % resolving gel (15 % (v/v) acrylamide (Severn Biotech Ltd), 375 mM Tris, pH 8.8, 0.1 % (w/v) SDS, 0.15 % (w/v) ammonium persulfate (APS), 0.04 % (v/v) N N N' N' tetramethyl-ethylenediamine (TEMED)) or 8 % resolving gel (8 % (v/v) acrylamide (Severn Biotech Ltd), 375 mM Tris, pH 8.8, 0.1 % (w/v) SDS, 0.15 % (w/v) ammonium persulfate (APS), 0.04 % (v/v) TEMED) was made. Solution was poured between two casting plates and ~200 μL isopropanol was used to create a level surface. Gels were left to set for ~45 mins. Isopropanol was removed and the stacking gel (5 % (v/v) acrylamide, 125 mM Tris pH 6.8, 0.1 % (w/v) SDS, 0.1 % (w/v) APS, 0.1 % (v/v) TEMED) was dispensed in between the two casting plates with either a 10 or 15 well comb and left for 1 hour to polymerise. Protein samples and either PageRuler™ or PageRuler™ Plus pre-stained protein ladder (ThermoFisher Scientific, 26616/26620) were loaded and gels were run at 150 V in SDS-PAGE running buffer for 1 hour.

For visualisation of the protein, gels were stained with Coomassie blue. Gels were incubated for 1 hour prior to washing with destain to remove background. Gels were imaged using an Amersham Imager 600 (GE Healthcare).

2.8.2.1 SDS-PAGE in the Protein Production Facility

2.8.2.1.1 Buffers used for SDS-PAGE in the Protein Production Facility

Laemmli protein loading buffer: 125 mM Tris pH 6.8, 4 % (w/v) SDS, 40 % (v/v) glycerol, 0.2 % (w/v) bromophenol blue, 10 mM DTT.

TGS SDS-PAGE running buffer: 250 mM Tris, 1920 mM glycine, 1 % (w/v) SDS.

2.8.2.1.2 SDS-PAGE in the Protein Production Facility

When using the protein production facility a slight variation of SDS-PAGE was used. Samples were mixed with 2 x Laemmli protein loading buffer prior to boiling at 95 °C for 3 minutes. Samples were loaded into 4-20 % Mini-PROTEAN® TGX™ Precast Protein Gels, 15-well (BIO-RAD, 4561096). Gels were placed in a Bio-Rad mini PROTEAN casting system

with TGS SDS-PAGE running buffer. Gels were ran at 150 V for ~1 hour. Bands were visualised using InstantBlue® (Expedeon) and imaged on a G:Box.

2.8.3 Western blot analysis

For western blot analysis following SDS-PAGE (2.8.2), proteins were transferred to nitrocellulose blotting membrane (GE healthcare Life science, 10600016) using a BIORAD turbo-blot. Membrane and filter paper (ThermoFisher Scientific, 88610) were submerged in transfer buffer (0.1 M tris, 0.192 M glycine, 20 % methanol in water) and placed in the BIORAD turbo-blot tray (Figure 2.3). After transfer, membranes were blocked in 5 % (w/v) milk (Sigma) in TBST and incubated for at least 1 hour room temperature with movement. After blocking, primary antibody was diluted in 10 mL of 5 % (w/v) milk in TBST and added (Table 2.3). Membranes were washed in TBST 2 x for 1 min and 3 x for 10 min. If primary antibody was not conjugated to horseradish peroxidase (HRP) an anti-primary secondary HRP-conjugated antibody was diluted in 5 % (w/v) milk in TBST and incubated with the membrane (Table 2.3). 1 mL Immobilon® Forte Western HRP Substrate (Millipore, WBLUF0500) was incubated on the membrane for 1 min at room temperature prior to chemiluminescence imaging on a Amersham Imager 600 (GE Healthcare).

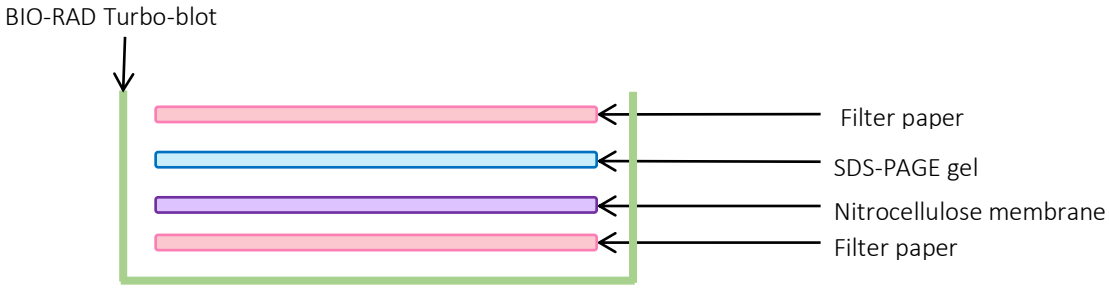


Figure 2.3 Set up of western blot using the Bio-Rad Turbo blot system.
Gels were sandwiched between two pieces of filter paper alongside the gel and placed in a Bio-Rad Turbo blot tray. Gels are transferred to nitrocellulose membrane by incubation in the turbo blot system for 30 mins.

Antibody	Manufacturer (Cat. No)	Western Blot Dilution	Incubation
Rb anti-HER2	Cell signalling (2165S)	1:10,000	4 °C overnight
Rat anti tubulin alpha	BioRad (MCA77G)	1:3000	4 °C overnight
Rb pAb to 6X His tag® (HRP)	Abcam® (ab1187)	1:10,000	1 h RT
Goat pAb to Rb IgG (HRP)	Abcam® (ab97051)	1:10,000	1 h RT
Goat pAb to Ms IgG (HRP)	Abcam® (ab97040)	1:10,000	1 h RT
Goat pAb to Rt IgG (HRP)	Abcam® (ab97057)	1:10,000	1 h RT
Strep mAb-classic (HRP)	Iba (2-1509-001)	1:5000	1 h RT

Table 2.3 Details of antibodies used for western blots.
Antibodies used during western blot analysis alongside manufacturer details and catalogue numbers are displayed in the table. Antibody dilutions were either recommendations or optimised. 'h' = hour and 'RT' = room temperature.

2.8.4 DNA sub-cloning

Affimers were sub-cloned into appropriate vectors for use in different experiments by the following methodology.

2.8.4.1 PCR amplification of insert DNA

Affimer DNA sequences were PCR amplified. Stock primers (
Table ***2.4***) were diluted 1:10 in ddH_2O. Reactions were set up in 0.2 mL PCR tubes (Sarstedt) as 25 μL reaction mixtures (13.8 μL sterile H_2O, 5 μL 5 x Phusion HF buffer, 0.2 μL dNTP mix (25 mM)(MP Biomedicals, Cat. No. NTPMX255), 0.75 μL DMSO, 2 μL each forward and reverse primer (10 mM), 0.02 units/mL Phusion high-fidelity DNA polymerase (Thermo Scientific, Cat. No. F-530) and 1 μL template DNA). Thermal cycling PCR conditions are shown in
Table ***2.4***. PCR was carried out using a G-Storm GS2 thermal cycler.

Primer	Primer sequence
Forward shorter	5' – ATGGCTAGCAACTCCCTGGAAATCGAAG
pDHis-C-reverse	5'-TTACTAATGCGGCCGCACAAGCGTCACCAACCGGTTTG
Strep Tag-reverse	GCGGCCGCGCCCTGAAAATACAGGTTTTCGTCACCAACCGGTTTGAAC

Table 2.4 DNA sequences of Affimer primers.
DNA sequences from 5' to 3' of primers used during PCR amplification of Affimer sequences from pDHis vector.

Cycle step	Temperature (°C)	Time (seconds)	Cycles
Initial Denaturation	98	30	1
Denaturation	98	20	30
Annealing	54	20	
Extension	72	20	
Final extension	72	20	1
Hold	4	10 min hold	

Table 2.5 Thermocycling conditions used for PCR amplification.
PCR reactions followed an initial denaturation step (pink) followed by 30 denaturing, annealing and extension cycle (blue) until a final extension step (purple).

2.8.4.2 DNA digest

0.5 μL *DpnI* (NEB, R0176) was incubated with PCR amplified DNA at 37 °C for 1 hour to digest methylated DNA. DNA was purified using the Nippon Gel and PCR clean-up kit and eluted in 50 μL ddH_2O. Amplified DNA was digested with *NheI-HF*™ (NEB, R3131S) and *NotI-HF*™ (NEB, R3189S). To the 50 μL PCR product 3 μL sterile H_2O, 6 μL CutSmart™ Buffer (supplied with NEB restriction enzymes), 0.5 μL *NheI-HF* and 0.5 μL *Not-I* were added and incubated at 37 °C for 4 hours.

2.8.4.3 Analysis of DNA by Agarose gel electrophoresis

DNA samples were mixed with 1x DNA loading dye. 5 μL sample was loaded onto a 0.8 or 2 % agarose gel. Agarose was melted into 1 x TAE buffer (1 mM EDTA, 20 mM glacial acetic acid, 40 mM Tris base). Once cooled slightly 1 x SYBRsafe DNA gel stain (Invitrogen) was added and mixed. 5 μL of Quick-Load Purple 2-Log DNA Ladder (NEB) was used. Gels

were run in a RunOne electrophoresis cell (EmbiTec) at 50 V for ~30 mins. Bands were visualised under UV using an Amersham Imager 600 (GE Healthcare).

2.8.4.4 DNA Ligation

Ligations of DNA inserts and pET11a vector were carried out in 1.5 mL microcentrifuge tubes containing 2 μL 10 x T4 DNA ligase buffer, 55 ng vector DNA (55ng/mL), 10 ng insert DNA (10 ng/mL) and 1 μL T4 DNA ligase (NEB, M0202). Ligations were incubated at 4 °C for 5 hours before being transformed into XL-1 supercompetant cells (as per section 3.2.2). Colonies were picked from plates for overnight culture in 2 TY with carbenicillin (100 mg/mL). For purification of plasmid DNA a QIAprep Spin Miniprep Kit (Qiagen) was used following the manufacturers protocol.

2.8.4.5 Measuring DNA concentration

DNA concentration was determined using a Nanodrop-lite spectrophotometer. The Nanodrop was blanked using the DNA storage buffer (ddH_2O). A 1.5 μL aliquot of DNA solution was added to the pedestal and the concentration was determined by measuring the A_{260} reading considering the Beer-Lambert equation; $c = A/(\varepsilon * b)$ where A= UV absorbance in absorbance units (AU), ε = extinction coefficient in L/mol-cm, b= pathlength in cm and c= analyte concentration, molarity (M).

2.8.4.6 DNA sequencing

Purified DNA was diluted to ~80 ng/μL and sequencing was carried out by GeneWiz using the primer shown in Table 2.6. Affimer loops were compared to previously sequenced Affimer.

Plasmid	Name	Primer position	Sequence
pET11a	T7F	Forward	5' TAATACGACTCACTATAGGG 3'

Table 2.6 Primers used for sequencing pET11a plasmids.

2.9 Affinity precipitation of endogenous HER2

Mammalian cell lysis buffer: 25 mM Tris-HCl, 150 mM NaCl, 5 % glycerol, pH 7.0

Mammalian cell lines were expanded to 80 % confluency (2.10.2.1) and pelleted by centrifugation at 1000 x g for 5 mins. The supernatant was discarded and cell pellets were stored at -80 °C until used. Cell lysates were prepared by lysing cell pellets with 1 mL mammalian cell lysis buffer (for a T-75 flask). To 980 μL filter sterilised (0.2 mM) mammalian cell lysis buffer 10 μL NP-40 (Sigma) and 10 μL 100 x halt protease inhibitor cocktail. Resuspended cells were transferred to 2 mL microcentrifuge tubes and incubated at 4 °C with rotation for 35 mins. Cells were pelleted by centrifugation at 12,000 x g for 20 mins. Supernatant was removed and transferred to a clean 1.5 mL microcentrifuge tube. Cell lysate concentration was determined using a Pierce™ BCA Protein Assay Kit BCA assay (2.8.1.2). Lysates were diluted in mammalian cell lysis buffer to concentrations of either 1.5 or 2 mg/mL. Affimers in the pETLECTRA vector were produced and purified (2.7). Affimers were diluted to a concentration of 0.65 mg/mL in lysis buffer and desalted using 7 MWCO 0.5 mL zeba spin columns (ThermoFisher Scientific, 89882) as per the manufacturers protocol. 100 μL Affimer was mixed 100 μL cell lysate and incubated at 4°C, rotating overnight.

The following day Ni-NTA slurry was washed in 2 x volume wash buffer (Affimer wash buffer) with 0.1 % tween-20 (ChemCruz), and centrifuged at 1,000 x g for 1 min. Wash buffer was discarded and resin was re-suspended in equal volume of wash buffer. 30 μL slurry was pipetted into clean 1.5 mL microcentrifuge tubes with frequent vortexing to prevent Ni-NTA resin settling. The overnight mixture of Affimer and cell lysate was added to the slurry and incubated for 90 mins at 4 °C with rotation. After the incubation slurry was pelleted by centrifugation at 1000 x g for 1 min and the supernatant was discarded. Saturated slurry was then washed 5 x using wash buffer with 0.1 % tween. After the fifth wash the supernatant was discarded and 50 μL elution buffer was added and incubated for 15 mins at 4 °C with rotation. Slurry was then centrifuged at 1000 x g for 1 min and supernatant was transferred to clean tubes for separation by SDS-PAGE (2.8.2) and western blot (2.8.3).

2.9.1 Conjugating of Affimer via maleimide link

Affimer reagents were conjugated to AlexaFluor 488 via a maleimide linker (Figure 2.4). AlexaFluor 488 maleimide (Thermofischer Scientific, A10254) was made up to 2 mM stock solution in DMSO (Sigma) and stored in 15 μL aliquots at -20°C. Affimers were diluted in 1 x PBS to achieve 150 μL at a concentration of 0.5 mg/mL. 150 μL immobilised TCEP disulphide-reducing gel (Thermo Scientific, 77712) was washed three times with 300 μL 1 x PBS containing 1 mM EDTA (VWR International Ltd., 443885J), spinning down at 1,000 x g for 1 min between washes. To washed resin, 4 μL 1 x PBS containing 50 mM EDTA was added along with 150 mL 0.5 mg/mL Affimers. Tubes were incubated on the Stuart SB2 fixed speed rotator (20 rpm) for 1 hour at room temperature. Solutions were centrifuged at 1,000 x g for 1 min and 130 μL supernatant was transferred to a new tube containing 6 μL AlexaFluor 488-maleimide stock, mixed and incubated at room temperature for 2 hours. Conjugation occurred via a maleimide link between the cysteine on the Affimer (Figure 2.4). Affimer conjugates were desalted to remove remaining AlexaFluor 488 using zeba spin desalting columns, 7K MWCO (Thermo Scientific) according to manufacturer's instructions. Tubes were equilibrated with 1 x PBS. Final concentrations were measured via a BCA assay (2.8.1.2). Conjugates were stored at 4°C until used.

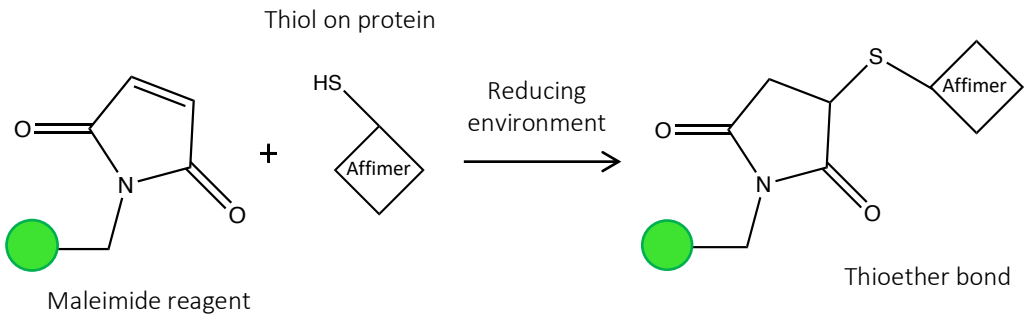


Figure 2.4 Chemical reaction of Affimer and Alexa Fluor™ 488 maleimide.
The maleimide group of the AlexaFluor 488 reacts with the thiol group of the reduced cysteine in the Affimer reagent. As there is only one cysteine residue in the Affimers structure this allows for site specific conjugation of Affimer:AlexaFluor 488 at a ratio of 1:1.

2.9.2 Conjugating HER2 specific Affimers to monomethyl auristatin E (MMAE) for use in cell culture.

Affimers were conjugated to monomethyl auristatin E (MMAE) via a maleimide link. Ab-Val-Cit-PAB-MMAE (Broadpharm Therapuetics) was dissolved in DMSO to a concentration of 1 mg/mL and stored at -20 °C in 15 μL aliquots. The protocol was adapted from section 2.9.1 to link the Affimer to MMAE opposed to AlexaFluor 488. Affimer was incubated as a 1:3 ratio with Ab-Val-Cit-PAB-MMAE for 2 hours at room temperature followed by quenching with 2:1 ratio of β-mercaptoethanol (Fisher Scientific):Affimer prior to desalting. Conjugates were stored at 4 °C.

2.9.3 Liquid chromatography mass spectrometry

Conjugation was confirmed by mass spectrometry carried out by Rachel George of the Mass Spectrometry Facility at the University of Leeds, who provided these methods. Protein desalting and mass analysis was performed by liquid chromatography mass spectrometry (LC-MS) using an M-class ACQUITY UPLC (Waters UK, Manchester, UK) interfaced to a Xevo QToF G2-XS mass spectrometer (Waters UK, Manchester, UK). Samples were diluted to 5μM using 0.1% TFA. 1 μL of the 5 μM sample was loaded onto a MassPREP protein desalting column (Waters UK, Manchester, UK) washed with 10% solvent B in A for 5 min at 25 μL min^{-1}. After valve switching, the bound protein was eluted by a gradient of 2-40% solvent B in A over 1 min at 25 μL min^{-1}. The column was subsequently washed with 95 % solvent B in A for 6 min before re-equilibration at 5% solvent B in A ready for the next injection. Solvent A was 0.1% formic acid in water, solvent B was 0.1% formic acid in acetonitrile.

The column eluant was directed in to the mass spectrometer via a Z-spray electrospray source. The MS was operated in positive TOF mode using a capillary voltage of 3.0 kV, sample cone of 20 V and source offset of 80 V. The source temperature was 100°C and desolvation was 250 °C. Masscalibration was performed by a separate injection of [Glu]-fibrinopeptide b at a concentration of 250 fmol $μl^{-1}$. Data processing was performed using the MassLynx v4.1 suite of software supplied with the mass spectrometer.

2.10 Materials and methods for cell culture

2.10.1 Cells and common reagents used in cell culture

2.10.1.1 Cell lines

AU-565 breast cancer cell line (CRL-2351, ATCC®) were purchased from ATCC. BT-474, MCF-7 and MDA-MB-231 breast cancer cell lines were provided by Prof. Valerie Speirs (University of Leeds). These cell lines were verified to be correct by short-tandem repeat (STR) profiling carried out by Dr. Claire Taylor. SKBR3, MDA-MB-453 and ZR-75-1 breast cancer cell lines were provided by Prof. Valerie Speirs (University of Leeds). Bladder cancer cell line DSH-1 were gifted by Prof. Margaret Knowles (University of Leeds). Lapatinib resistant BT-474 cells and wild-type (WT) along with Capatinib resistant SKBR3 cells and WT were gifted by Prof. Eric Lam (University College London).

2.10.1.2 Primary breast cancer cells

Primary breast cancer cells were provided by Breast Cancer Now Tissue Bank via material transfer agreement (MTA) application by Mr. Iain Goulding and Dr. Jenny Gomm from Barts Cancer Institute, London. Primary cells from four patients with HER2- breast cancer and four HER2+ breast cancer were provided.

2.10.1.3 Reagents used for culture of mammalian cells

Dulbecco's Modified Eagle Medium (DMEM) 1 x + GlutaMAX™ (Gibco™, 61965026) 4.5 g/L D-Glucose; pH 6.8-7.2.

RPMI-1640 medium (Gibco™, 21875-034,) 300 mg/L L-glutamine; 2g/L D-Glucose pH; 7.0-7.4.

RPMI-1640 + GlutaMAX™ (Gibco™, 61870010) RPMI 1640 medium modified to contain GlutaMAX™.

Minimum essential medium (MEM)-Alpha (Gibco™, 11590606) widely used for mammalian cell culture.

DMEM-F12 (Gibco™, 11320033) Media is a 1:1 mixture of DMEM and Ham's F-21. Combines DMEM characteristics such as high glucose and amino acids with F-12's components.

Advanced DMEM F12 (Gibco™, 12634028) allows the culture of mammalian cells with reduced FBS supplementation.

Dulbecco's Phosphate Buffered Saline (DPBS) (Corning, 21-031-CVR)

Opti-MEM® (Gibco™, 31985-070)

Dimethyl sulfoxide (DMSO) (Sigma-Aldrich, 276855-100ML)

2.10.2 Methods for culture of mammalian cell lines

2.10.2.1 2D cell culture of mammalian cell lines

Cell lines were cultured according to Table 2.7. Media details are referenced in section 2.10.1.3. To dissociate cells from the flask TrypLE Express Enzyme (1x) (Thermo Fisher Scientific (Life Technologies), 12604013) was added and incubated at 37 °C with 5 % CO_2 until cells detached. Cells were split at around 80 % confluency with the exception of AU-565 that are recommended to not be grown above 60 % confluency.

Cell line	HER2 expression	Origin	Media
BT-474	HER2 overexpressing	Breast	RPMI + 10 % FCS
AU-565	HER2 overexpressing	Breast	RPMI + 10 % FCS
SKBR3	HER2 overexpressing	Breast	DMEM + 10 % FCS
MCF-7	Moderate HER2 expression	Breast	RPMI + 10 % FCS
MDA-MB-453	Moderate HER2 expression	Breast	RPMI + 10 % FCS
DSH-1	HER2 expressing	Bladder	RPMI GlutaMax™ + 10 % FCS
MDA-MB-231	HER2 negative	Breast	DMEM + 10 % FCS
ZR-75-1	HER2 negative	Breast	RPMI + 10 % FCS

Table 2.7 Mammalian cell lines and culture conditions.

2.10.2.2 Dose response with mammalian cell lines

Dose responses were performed on a range of cell lines in 96 well tissue culture plates (Sarstedt). Cells were seeded on day 0 at a density that would lead to ~40 % coverage of

the plate bottom on day 1. Seeding densities for different cell lines is presented in Table 2.8. The following day Affimer/drug/Affimer drug conjugate were diluted to twice the intended concentration in cell culture media and added to 96 well plates as a half-media change. Plates were then incubated for 72 hours at 37 °C, 5 % CO_2 with humidity.

Cell line	Seeding density
AU-565	3 x 10^4 cells/mL
SKBR3	3 x 10^4 cells/mL
BT-474	5 x 10^4 cells/mL
MDA-MB-453	3 x 10^4 cells/mL
MCF-7	3 x 10^4 cells/mL
ZR-75-1	3 x 10^4 cells/mL
MDA-MB-231	3 x 10^4 cells/mL

Table 2.8 Seeding densitites of cell lines used for dose response assays.

2.10.2.2.1 AlamarBlue assay

The AlamarBlue assay was used as a measure of metabolic activity following dose response. Media was removed and pre-warmed media containing 10 % AlamarBlue was added and incubated on cells at 37 °C, 5 % CO_2 with humidity until a colour change was visible. Colour change was measured with an excitation of 570 nm and emission 590 nm on a Tecan Spark® microplate reader (Tecan Trading AG). Colour change correlates to metabolic activity of the cells. Background was accounted for by deducing a media only control from all values. Graphs were created using GraphPad Prism.

2.10.2.2.2 Cell count using ImageXpress Pico Automated Cell Imaging System

As the AlamarBlue assay is non-toxic to cells it allows for further analysis. Cells were washed 3 x in PBS followed by fixation in 4 % PFA for 20 mins. Cells were incubated with hoescht diluted in PBS (1:1000) for 1 hour at room temperature protected from light. Cells were washed a further 3x in PBS and either stored at 4 °C until imaged or imaged immediately. Plates were imaged using an ImageXpress Pico Automated Cell Imaging System (Molecular Devices). The automated method for cell counts was used where

nuclei were manually defined. Images were taken and data regarding cell counts was plotted in GraphPad prism.

2.11 Immunofluorescence using Affimers

2.11.1 Immunofluorescence using unconjugated Affimers

Cells were seeded onto glass coverslips in a 24 tissue culture plate on day 0 at densities shown in Table 2.9. The following day culture medium was removed and cells were washed gently with 1 x DPBS for 5 minutes. Affimers were diluted to 25 mg/mL in optiMEM and 500 μL was added to respective wells. Controls were carried out using control Affimer and optiMEM only. After incubation for varying lengths of time at 37 °C. Cells were washed 3 x in PBS prior to fixing in 4 % PFA (VWR)(15 mins) followed by 5 minutes in PBS with 0.1 % Triton-X. Cells were washed in PBS and blocked with 1 % milk (Sigma Aldrich) overnight at 4 °C. Cells were incubated with 200 μL primary mouse MAb to 6 x His-tag® (AbCam, Cat. No. ab18184) diluted in 1 % milk (1:3500) for 1 hour at room temperature followed by 3 x PBS washes and 1 hour incubation with AlexaFluor™ 488 goat anti-mouse (Invitrogen, Cat. No. A11001) (1:1000) in 1 % milk for 1 hour at room temperature. Cells were washed 3 x PBS and mounted using ProLong™ Gold antifade reagent and DAPI (Invitrogen, Cat. No. P36935). Images were taken using the Nikon fluorescent microscope or Zeiss confocal LSM880 Inverted/ LSM880 Upright microscope.

Further immunofluorescent experiments were carried out to investigate co-localisation. Experiments were undertaken using the same protocol but with additional antibodies from Table 2.10.

Cell line	Seeding density
AU-565	1.2 x 10^6 cells/mL
BT-474	5 x 10^5 cells/mL
MDA-MB-231	5 x 10^5 cells/mL

Table 2.9 Cell seeding densitites for seeding cells in 24 well tissue culture plate.

2.11.2 Immunofluorescence using Affimers conjugated to AlexaFluor 488

Cells were seeded onto coverslips in a 24 well plate. The following day coverslips were washed once in 1 x DPBS and incubated with 500 μL of Affimer conjugated to AlexaFluor 488 maleimide (2.9.1) diluted to a concentration of 25 μg/mL in optiMEM for 1 hour. OptiMEM was removed and 500 μL of DPBS containing wheatgerm (1:250) and hoescht (1:1000) was added and incubated at 37 °C for 30 mins. Coverslips were washed 3 x in PBS and fixed in 4 % PFA for 20 mins. Coverslips were washed once in DPBS and mounted onto slides using ProLong™ Diamond mounting media (ThermoFischer Scientific, P36961). Slides were left to set overnight prior to sealing and storing at 4°C in the dark until imaged.

Antibody	Supplier (Cat. No.)	Dilution	Condition
HER2	Cell Signalling technology (2165S)	1:2000	4 °C, overnight
Mouse monoclonal 6 x His tag® antibody	Abcam (ab18184)	1:3500	1 h, RT, protected from light
Tubulin alpha	Gift from Peckham laboratory	1:1000	1 h RT, protected from light
Rabbit polyclonal IgG Anti-LAMP2	GeneTex (GTX103214)	1:200	1 h, RT, protected from light
Purified Mouse Anti-EEA1	BD Trasnduction Laboratories™ (610456)	1:200	1 h, RT, protected from light
Goat anti-Mouse IgG (H+L) cross-adsorbed secondary antibody, Alexa Fluor™ 488	Invitrogen (A-11001)	1:1000	1 h, RT, protected from light
Goat anti-Rabbit IgG (H+L) cross-adsorbed secondary antibody, Alexa Fluor™ 488	Invitrogen (A-11034)	1:1000	1 h, RT, protected from light
Anti Rat Alexa Fluor™ 647	Gift from Peckham laboratory	1:1000	1 h, RT, protected from light
Goat anti-mouse IgG (H+L) highly cross-adsorbed Alexa Fluor™ 594	Invitrogen (A-11032)	1:1000	1 h, RT, protected from light
Alexa Fluor™ 488 AffiniPure Donkey Anti-Rat IgG (H+L)	Jackson Immunoresearch (712-545-153)	1:500	1 h, RT, protected from light
Wheat germ Agglutinin, Alexa Fluor™ 633	Invitrogen (1155081)	1:250	1 h, RT, protected from light
Hoescht 33342	Invitrogen (H3570)	1:1000	1 h, RT, protected from light

Table 2.10 Antibodies used for immunofluorescence experiments.
Immunofluorescence was carried out on mammalian breast cancer cell lines. Various antibodies were used and are displayed in the table alongside the suppler and Cat. No. (catalogue number), dilution used at and incubation conditions used.

2.12 Dose response using Affimer-MMAE conjugates

Affimers specific to HER2 and Affimer control were conjugated to MMAE following the protocol in section 2.9.1. Mammalian cell lines were seeded at densities shown in table 2.3 on day 0. On day 1 Affimer MMAE conjugates were diluted to concentrations ranging from 1 mg/mL to 0.05 mg/mL in cell culture media. Affimer MMAE conjugates were added as a half media change to cells leading to final concentrations ranging from 0.5 mg/mL to 0.025 mg/mL. Cells were incubated at 37 °C, 5 % CO_2 for 72 hours. Metabolic activity was analysed using the AlamarBlue assay (2.10.2.2.1).

2.13 3D cell culture

2.13.1 3D cell culture using FibroLife

Cells were sequentially transferred from their standard culture medium to FibroLife medium (Cell Technology, LM-0001) adapted for epithelial cell growth by omitting fibroblast growth factor (FGF) and transforming growth factor beta (TGF-β) supplements. This media will be referred to as epiFL from now on. Cells aggregated gradually as media was changed to 100 % epiFL. To change media flasks were held at an angle to allow spheroids to settle to the corner. At this point half the total media volume was aspirated using a stripette and replaced with fresh media. Media changes were carried out approximately twice weekly.

2.13.2 3D cell culture in SeedEZ and PerfusionPal

2.13.2.1 3D cell culture in SeedEZ scaffolds

SeedEZ (Gifted by LenaBioscience) is a clear, hydrophilic scaffold that consists of randomly arranged glass fibers (Figure 2.5). The aim of the scaffold is for cells to be seeded into it and to assist the formation of 3D cellular aggregates in between the glass fibers. SeedEZ scaffolds were placed in 24 well plates and 100 μL cell suspension was added and incubated for 20 mins at 37 °C with 5 % CO_2. Meanwhile 500 μL was aliquoted into a new 24 well plate and after 20 mins scaffolds were transferred to the fresh plate using forceps. Plates were returned to the incubator and cultured for five days with media changes being carried out as necessary. SeedEZ scaffolds were either cultured under static conditions in a 24 well plate or with perfusion in PerfusionPal.

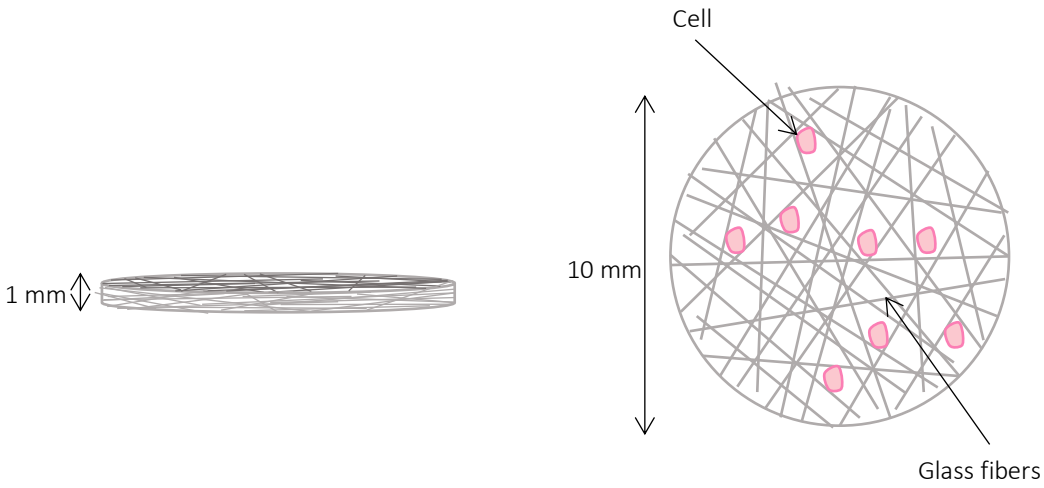


Figure 2.5 SeedEZ scaffold.
SeedEZ scaffold consists of randomly arranged glass fibers. The scaffolds are around 1 mm in diameter and 10 mm in width. Cells are seeded into the scaffold that encourages growth between the fibers.

2.13.2.2 3D cell culture with SeedEZ in PerfusionPal

PerfusionPal (LenaBioscience) is a novel multi-well platform for the culture of cells in 3D with perfusion. PerfusionPal consists of a reservoir that harbours a high-density blood substitute perfluorocarbon (PFC)(Flutec, PP11), a 12 open-bottom well insert and a lid (Figure 2.6A). Plates were sterilised using ethylene oxide in the US and shipped. All components were placed in a cell culture hood prior to opening. The plate was removed from the packaging and placed flat in an incubator safe dish. 55 mL PFC was added to the reservoir and the 12 open-bottom well insert and lid were placed on top. Sterile tubing was attached using a luer lock to the plate and a 60 mL syringe (BD). A syringe pump (chemyx fusion-500) was used to withdraw 20 mL PFC at 1 mL/min. Following this withdrawal the syringe was held upright and flicked to dislodge any small bubbles. The plunger was slowly pushed in to remove air from the syringe and the tubing until the 5 mL mark was reached. The syringe was then placed back in the pump. The set up of PerfusionPal with the syringe pump is explained by the diagram in Figure 2.6.

After the system was primed, 750 μL media was pipetted into each well. SeedEZ scaffolds were seeded with cells and incubated for 20 mins as per section 2.13.2.1. SeedEZ were transferred from the 24 well plate to PerfusionPal using forceps and the static control were transferred from the 24 well plate to a fresh 24 well plate. A seating insert was used to push the scaffolds into the PerfusionPal wells to the correct depth. The whole system

was then placed in a 37 °C incubator with 5 % CO_2 and cultured for as long as desired. Media changes were carried out depending on cell-type and density seeded. The syringe pump was set to infuse and withdraw 10 mL twice over a 24 hour period.

Metabolic activity of cells was by removing SeedEZ scaffolds from PerfusionPal/24 well plate using forceps and placing in 500 μL fresh media containing 10 % AlamarBlue. Samples of 200 μL were taken from media following a colour change and analysed on the Tecan Spark plate reader as described in section 2.10.2.2.1.

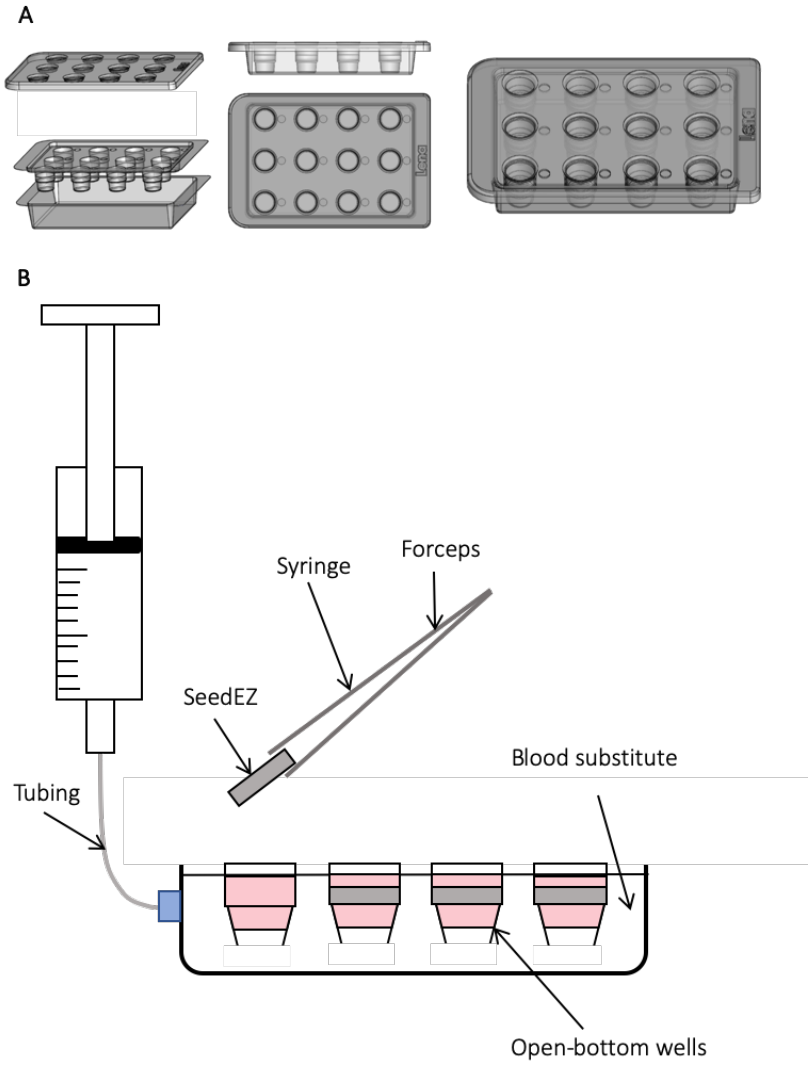


Figure 2.6 PerfusionPal cell culture plate.
The PerfusionPal cell culture system consist of a reservoir that harbours a 12 open-bottom well insert and a lid. **(A)** PerfusionPal plate set up. Image created by Dr. JT Shoemaker. **(B)** Schematic to show how the PerfusionPal system is used alongside SeedEZ scaffolds and syringe pump.

2.13.2.2.1 LIVE/DEAD® cytotoxicity assay

To indicate cell life and death of cells cultured in the SeedEZ scaffold the LIVE/DEAD® Viability/Cytotoxicity Kit for mammalian cells (Invitrogen, MP03224). To make up the assay solution calcein AM and Ethidium homodimer-1 was thawed on ice. As per the manufacturer's instructions 2.5 μL calcein AM and 10 μL ethidium homodimer-1 was added to 5 mL DPBS. Culture medium was removed from seedEZ scaffolds and washed with 1 x DPBS gently. 200 μL Calcein AM/Ethidium homodimer-1 solution was added to each scaffold and incubated for 30 minutes at room temperature. Scaffolds were imaged using an EVOS microscope.

2.13.2.2.2 Calcein AM

Calcein AM (Insight Biotechnology) was frozen in aliquotes of 10 μL. For staining of cells in SeedEZ scaffold Calcein AM was thawed and diluted 1:200 in DPBS. 200 μL Calcein AM in DPBS was incubated on SeedEZ scaffold for 30 mins and imaged using an EVOS fluorescent microscope.

2.13.3 Primary cell culture using SeedEZ and PerfusionPal

Primary cells were kindly provided by BCNTB Cell Culture Programme (2.10.1.2). On arrival cells were stored in liquid nitrogen until use. Cells were thawed and transferred to a 15 mL falcon containing 3 mL of Advanced DMEM-F12 (ThermoFisher Scientific, 12634028) with supplements (Table 2.11) found to enhance primary cell culture based on the published data by Clevers et al. (185). Cells were pelleted at 1000 x g for 5 mins. Cells were resuspended in 1 mL media and immediately 100 μL cells were seeded into SeedEZ scaffold. Scaffolds were then incubated for 20 min at 37 °C incubator with 5 % CO_2 and placed in the PerfusionPal system as per section 2.13.2.2. After 72 hours scaffolds were removed and analysed by AlamarBlue (2.10.2.2.1).

Following AlamarBlue analysis one scaffold from each condition were washed 3 x in DPBS gently prior to fixing in 500 mL 4 % PFA. These scaffolds were blocked in 5 % milk prior to incubation with HER2 antibody at 4 °C overnight. Following HER2 antibody incubation

secondary AlexaFluor 488 was incubated for 1 hour, room temperature. Scaffolds were then imaged on a Zeiss confocal LSM880 Inverted microscope.

Reagent	Supplier (Cat. No)	Diluent	Storage concentration (temperature)	Working concentration
Advanced DMEM-F12	(12634028)	-	- (4 °C)	-
EGF	Peprotech (AF-100-15)	Sterile ddH_2O with 5 % trehalose	10 mg/mL (-20 °C)	5 ng/mL
FGF-7	Peprotech (100-19)	1 x PBS with 0.1 % BSA	5 mg/mL (-80 °C)	5 ng/mL
FGF-10	Peprotech (100-26)	1 x PBS with 0.1 % BSA	20 mg/mL (-80 °C)	20 ng/mL
Noggin	Peprotech (120-10C)	Sterile ddH_2O with 0.1 % BSA	100 mg/mL (-80 °C)	100 ng/mL
Heregulin-1	Peprotech (100-03)	Sterile ddH_2O with 0.1 % BSA	1 mM (-80 °C)	5 nM
Y-27632	Cell guidance systems (SM02)	DMSO	10 mM (-20 °C)	5 mM
A83-01	Tocris Bioscience (2939/10)	ddH_2O	Made fresh	500 nM
SB202190	Sigma (S7067-5MG)	DMSO	5 mM (-80 °C)	500 nM
Nicotinamide	Sigma (N0636-100G)	1 x PBS	1 M (-20 °C)	5 mM
N-acetyl-cysteine	Sigma (A9165-5G)	ddH_2O	250 mM (-20 °C)	1.25 mM
B27 supplement	Thermo Fisher Scientific (Life Technologies) (17504044)	-	50 x (-20 °C)	1 x
Recombinant human R-Spondin 3	R&D Systems, Inc. (3500-RS-025/CF)	1 x PBS	50 mg/mL (-80 °C)	250 ng/mL
HEPES	Thermo Fisher Scientific (Life Technologies)	-	1 M (RT)	15 mM
GlutaMAX™-I (100 x)	Gibco™ (35050-061)	-	100 x (4 °C)	1 x
Antibiotic-Antimycotic (100 x)	Gibco™ (15240062)	-	100 x (-20 °C)	1 x
Gentamicin	Thermo Fisher Scientific (Life Technologies) (15710064)	-	10 mg/mL (RT)	50 μg/mL

Table 2.11 List of reagents used for culture of primary breast cancer cells.
A list of reagents taken from a previously published paper *(185)* were used to culture primary breast cancer cells obtained from BCNTB Cell Culture Programme in the novel 3D cell culture system PerfusionPal. Slight adaptations of the original paper were made on recommendation by BCNTB Cell Culture Programme.

2.14 Purification of HER2/ Affimer D11 complex and crystallisation trials undertaken in the Protein Production Facility

The majority of the following methods were undertaken in the University of Leeds Protein Production Facility.

2.14.1 Production of HER2 extracellular domain by mammalian cell culture

The CHO Lec1 cell line able to secrete the extracellular domain of human HER2 (residues 1-631) as a fusion protein with human growth hormone via a poly-histidine tag and tobacco etch virus (TEV) cleavage site was a kind gift from Dr. Josef Singer (Medical University Vienna, Austria) with permission from Prof. Daniel Leahy (The University of Texas, Austin). Cells were brought up from frozen in Alpha-MEM (Gibco) supplemented with 5 % FBS, 100 nM methotrexate (biobasic, MB0612) and 10 mg/mL gentamicin sulphate (Alfa Aesar, J62834). Following expansion they were transferred to DMEM-F12 with 5 % FBS, 100 nM methotrexate and 10 mg/mL gentamicin sulphate. Cells were grown in either T-175 culture flasks or Corning HyperFlask. Media was collected every 48 hours when cultured in T-75 flasks or 24 hours when cultured in the Corning HyperFlask and replaced with fresh media. The media collected was stored at 4 °C until used.

2.14.1.1 Concentration of HER2 conditioned media using an Amicon® Stirred Cell

A 400 mL Amicon® Stirred Cell (Merck) was used to concentration HER2 conditioned media following large scale collection. The Amicon® Stirred Cell was set up in a 4 °C cold room using 30 kDa cut off Biomax polyethersulfone filters (Merck, PBTK07610). The external compressed gas source used was nitrogen as it would avoid shifts in pH, recommended by the suppliers. Concentrated media was collected in a clean vessel and stored at 4 °C.

2.14.2 Production of D11 Affimer with Strep Tag® II

Affimer D11 was sub-cloned from the pET11a vector to pET11a StrepTag® II vector. The sub-cloning protocol was adapted from section 2.8.4. Affimer D11 DNA was PCR amplified

with the 'forward shorter' primer and reverse Strep Tag® II primer using the same conditions as section 2.8.4.1. The restriction enzymes *NheI* and *NotI* were used to digest the pET11a Strep Tag II plasmid and D11 Affimer DNA inserts. DNA was analysed by agarose gel electrophoresis (2.8.4.3). Insert DNA was purified using the Nippon Gel and PCR clean up kit and sent for sequencing by GeneWiz. Ligation reactions were carried out of vector and insert DNA following the previously described protocol (2.8.4.4).

2.14.3 Formation of HER2 extracellular domain in complex with Affimer D11

The Affimer pellet was resuspended in binding buffer (100 mM Tris-HCl, 150 mM NaCl, 1 mM EDTA, pH 8.0) and lysed by sonication or using the cell disrupter. The insoluble fraction was pelleted by centrifugation at 30,000 x g for 45 mins. A 1 mL StrepTrap™ High Performance column (GE Healthcare, GE29-0486-53) was washed with de-gassed pure water to remove storage solution. The Affimer D11 Strep Tag® II supernatant was immobilised to the column using an AKTA pure in a 4 °C cold cabinet at a flow rate of 1 mL/min. The column was washed with binding buffer until the UV at 280 nM was steady. HER2 conditioned media was flowed over the column containing immobilised Affimer D11 Strep Tag® II with a flow rate of 1 mL/min (fig. 2.8). Following this the column was washed with binding buffer until the UV at 280 nM was steady. The column was then either incubated with TEV protease (2 mg/mL) for 12 hours followed by elution with elution buffer (2.5 mM desthiobiotin in binding buffer) or eluted in a single step with just elution buffer. Fractions were collected and analysed by SDS-PAGE (2.8.2).

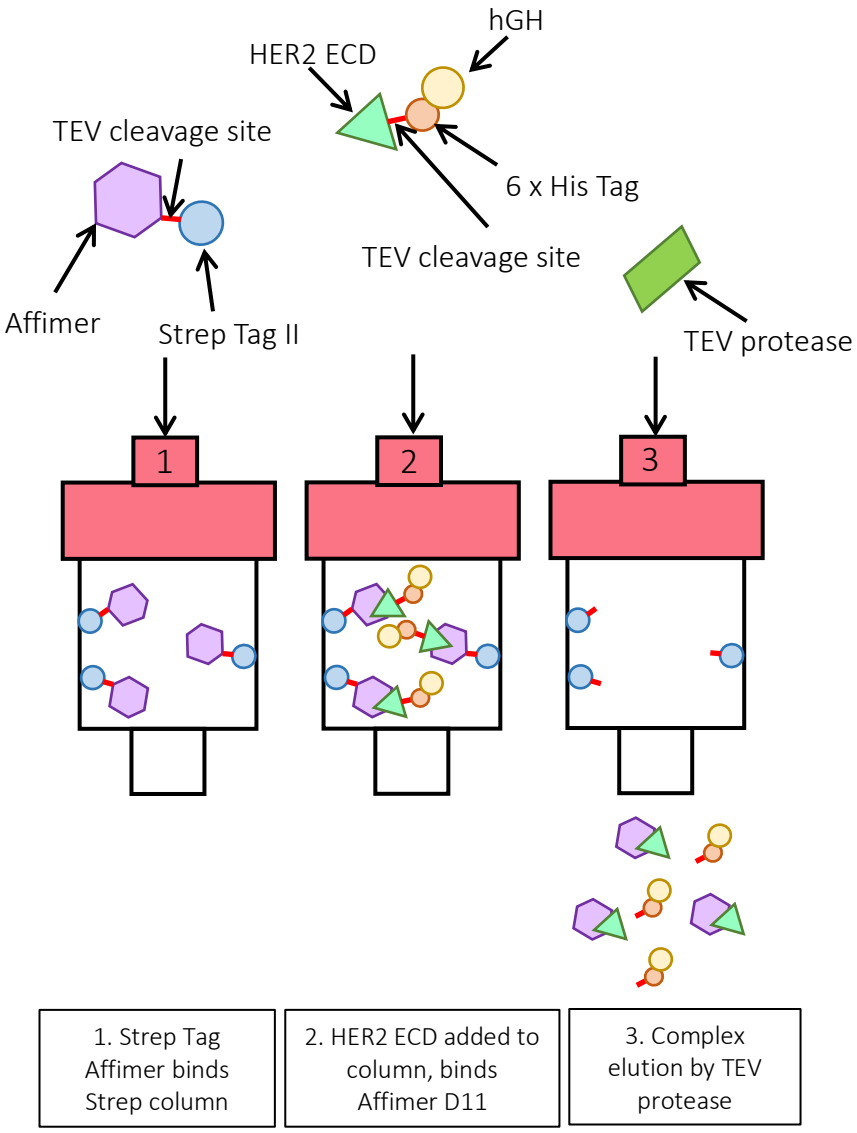


Figure 2.7 Work flow of production of the HER2 extracellular domain/ Affimer D11 complex.
1) Affimer D11 with Strep Tag separated by a TEV cleavage site was loaded onto a Streptactin column. 2) HER2 ECD fusion protein with 6 x His tag and human growth hormone (hGH) separated by TEV cleavage site was loaded onto the column and bound to Affimer D11. 3) TEV protease was added to the column and cleaved the TEV cleavage sites leading to elution of the complex and 6 x His tag with hGH.

2.14.4 Deglycosylation of HER2 ECD/ Affimer D11 complex by PNGase F

2.7.4.1 Buffers used during PNGase F production

2.14.4.1 Production of PNGase F by IPTG induced protein expression

The pOPH6 plasmid was a gift from Shaun Lott (Addgene plasmid #40315 ; http://n2t.net/addgene:40315 ; RRID:Addgene_40315). The plasmid contained the gene of interest Peptide:N-glycosidase F (PNGase F)(GeneBank ID AF165910) from the species *Flavobacterium meningosepticum* with a C-terminal hexa-histidine tag under the control of T7 promoter. Initially a sample of the stab culture was streaked onto an LB agar plate with carbenicillin (100 mg/mL) and incubated overnight at 37 °C. Colonies were picked for overnight culture in 5 mL LB broth with carbenicillin (100 mg/mL). The following day DNA minipreps were carried out using the QIAprep Spin Miniprep Kit as per the manufacturer's instruction. DNA was transformed into BL21 Star (DE3) cells as described in section 2.7.1. Protein was produced by IPTG induction as previously explained (2.7.2). Two 400 mL cultures were pooled and stored at -20 °C following centrifugation at 4816 x g.

2.14.4.2 Purification of PNGase F by Ni^{2+} affinity chromatography

Pellets were resuspended in 5 % of the original culture volume (40 mL) of ice-cold resuspension buffer (0.5 M sucrose in 0.1 mM Tris-HCl, 1 mM EDTA, pH 8). Cells were pelleted by centrifugation at 3000 x g for 20 mins. Pellets were resuspended in ice cold ddH_2O and incubated on ice for 10 mins. $MgCl_2$ (1 M stock in ddH_2O) was added to a final concentration of 1 mM and stored on ice for a further 10 mins. Cells were pelleted by centrifugation at 4816 x g for 20 mins. The supernatant containing the periplasmic proteins was adjusted to pH 7 using 1 M 3-(N-morpholino) propanesulfonic acid)(Mops). The periplasmic protein containing supernatant was purified on an AKTA pure using a His Trap column. Column was washed with wash buffer (20 mM Mops, 0.5 M NaCl, 20 mM imidazole, pH 8) and eluted in elution buffer (20 mM Mops, 0.5 M NaCl, 500 mM imidazole, pH 8) with an increasing gradient concentration of Imidazole. Eluted fractions were analysed by SDS-PAGE (2.8.2) and dialysed using a 12-30 mL 10 MWCO SlideAlize dialysis cassette (Pierce) against 1 x PBS, 4 °C, overnight. Protein was concentrated to 1.5 mg/mL and stored at -20 °C until used.

2.14.5 Deglycosylation of HER2 extracellular domain in complex with Affimer D11

Affimer D11 HER2 extracellular domain complex was incubated with ~ 1 mL PNGase F at 1.5 mg/mL for 48 hours at 37 °C with shaking at 80 rpm.

2.14.6 Size exclusion chromatography

To separate proteins by size exclusion chromatography samples were concentrated down to ~2.5 mL using Millipore concentrators with a MWCO twice the size of the protein. Samples were loaded onto either a HiLoad Superdex 200 or 75 high performance column connected to an AKTA pure system. The column was treated with degassed pure water to elute the storage solution and equilibrated in appropriate buffer. Fractions were collected in volumes of either 1 or 2 mL. Collected samples were analysed by SDS-PAGE to check for purity (2.8.2).

2.14.7 Concentration of proteins

Complex was concentrated using Vivaspin® 5000 MWCO (Satorius) centrifugal concentrators to achieve as high a concentration as possible at 4000 x g. Final concentrations were determined using a Qubit (Thermo Fisher Scientific).

2.14.8 Crystallisation trials

Trials were set up using 96 well 3-drop plates (Molecular dimensions) using an NT8® Drop Setter robotics system (Formulatrix). The protein complex was mixed with buffer in different ratios of either 1:1, 2:1 and 1:2. Plates were sealed using VIEWseal pressure adhesive seals and stored at 20 on a Sonicc RI 1000 Crystal Detector (Formulatrix) for imaging over a 30 day period.

2.15 HER2 subdomain production in *E. coli*

2.15.1 Cloning HER2 subdomains into pOPIN vectors

The pOPIN vector system provides a versatile, ligation independent, mechanism of cloning and was used to create HER2 subdomain fusion constructs (204). The vectors pOPINM (His6-MBP-3C-POI) and pOPINS (His6-SUMO-3C-POI) were used. Primers were ordered through science warehouse as lyophilised samples (Table 2.12). DNA was rehydrated to 100 mM in ddH_2O.

Primer	Sequence
SD1 Forward	AAGTTCTGTTTCAGGGTCCCATGGAGCTGGCGGCCTTG
SD1 Reverse	CTGGTCTAGAAAGCTTTTAACAGGGGTGGCAGGCCC
SD2 Forward	AAGTTCTGTTTCAGGGTCCCTCTCCGATGTGTAAGGG
SD2 Reverse	CTGGTCTAGAAAGCTTTTAGTTGTGCAGGGGGCAGAC
SD3 Forward	AAGTTCTGTTTCAGGGTCCCCAAGAGGTGACAGCAGAGG
SD3 Reverse	CTGGTCTAGAAAGCTTTTAGTTCCGAAAGAGCTGG
SD4 Forward	AAGTTCTGTTTCAGGGTCCCCCGCACCAAGCTCTGC
SD4 Reverse	CTGGTCTAGAAAGCTTTTAGGTGCAGTTGATGGGG

Table 2.12 Primers against HER2 subdomains for cloning into pOPIN vectors.
Primers were designed to clone HER2 DNA subdomains into pOPIN vectors. Red shows plasmid DNA, green HER2 subdomain DNA and blue are stop codons.

2.15.1.1 Manual PCR setup

PCR reaction mix of 25 µL were made up in a freezer block as per Table 2.13. Template DNA was added at a concentration of ~ 1 ng and nuclease-free water volume was adjusted to maintain a 25 µL reaction volume. PCR tubes were capped and placed in a Venti PCR machine. The Q5 polymerase (New England Biolabs) set up was used (Table 2.14).

Reagent	Volume
5 x Q5 reaction buffer	5 mL
10 mM NTPs	0.5 mL
10 mM forward primer	1.25 mL
10 mM reverse primer	1.25 mL
Template DNA	*1 mL
Q5 DNA polymerase	0.25 mL
5 x Q5 high GC enhancer	5 mL
Nuclease-free water	*10.75 mL

Table 2.13 PCR conditions used for amplification of HER2 subdomain DNA.

1 cycle	**Initial denaturation**	**98 °C**	**30 seconds**
30 cycles	Denaturation	98 °C	5 seconds
	Annealing	60 °C	20 seconds
	Elongation	72 °C	20 seconds per kb
	Final extension	72 °C	2 minutes
1 cycle	Hold	4 °C	∞

Table 2.14 PCR thermocycling conditions.

2.15.1.2 PCR analysis by agarose gel electrophoresis in the protein production facility

A small 0.8 % agarose gel was prepared to analyse PCR products. Gels were prepared by melting agarose (Fisher Scientific) in 1 x TBE buffer. Once cooled SYBRSafe (Invitrogen) was added 1:10,000 prior to pouring gel solution into gel plate. To each 5 μL sample 2 μL of 6 x DNA loading dye was added. Samples were loaded onto the gel alongside NEB Quick-Load Purple 2-Log DNA ladder and run for ~40 minutes at 80 V. Gels were imaged on a G:Box.

2.15.1.3 Qiagen PCR purification

For PCR products that only existed as a clean, single band, PCR purification could be carried out immediately with no need for gel extraction. PCR products were incubated with *DpnI* and NEB 10x CutSmart Buffer (2 μL per 20 μL) at 37 °C for 30 minutes. PCR products were then purified using a QIAquick PCR purification kit (Qiagen, 28104) as per the manufacturer's protocol.

2.15.1.4 Qiagen gel extraction and purification

For products that were less pure gel extraction was carried out. Products were run on a 0.8 % agarose gel aforementioned (2.8.4.3). However, gels were not imaged under UV light prior to excising bands. Bands were excised using a scalpel. Gel bands were purified using a QIAquick gel extraction kit (Qiagen, 28704) as per the manufacturer's protocol.

2.15.2 Cloning HER2 subdomains into pOPIN vectors

To perform cloning the NEBuilder HiFi DNA Assembly Master Mix (New England Biolabs, E2621L) for cloning reactions was used. Stocks of linearised pOPIN vectors were supplied by the PPF at 1 mg/mL. Concentration of DNA was calculated using a Qubit prior to cloning reactions. Reactions were set up with a vector:insert ratio of 1:2. A maximum of 0.2 pmol DNA was added to a clean 1.5 mL microcentrifuge tube on ice. After, 10 μL HiFi DNA Assembley Master Mix was added and nuclease-free water to a total volume of 20 μL. Reactions were mixed gently by pipetting up and down. Samples were incubated at 50 °C for 1 hour. Samples were stored at -20 °C prior to transformations.

2.15.2.1 Transformation of pOPIN vectors into DH5α

LB agar plates with 100 mg/mL ampicillin were made prior to transformations. DH5α cells were thawed in a freezer block. 50 μL competent cells were mixed with 2 μL HiFi assembly reaction. Transformations were then carried out as described in section 2.7.1.

2.15.3 Automated minipreps using the Hamilton Robot and Promega MagneSil kit

Using sterile toothpicks individual colonies were picked from transformation plates into 1 mL LB broth containing 100 mg/mL ampicillin in a 2.2 mL deep 96 well plate. Cultures were sealed with a gas-permeable seal and incubated overnight at 37 °C at 220 rpm. The following day cultures were centrifuged at 4,000 x g for 10 mins. Supernatant was removed and the plate was placed on the Hamilton robot. The MagneSil method was set up using Wizard on the Hamilton Robot. Purified plasmid DNA was stored at -20 °C.

2.15.3.1 Sequencing

The Protein Production Facility use Eurofins to perform all sequencing. To prepare samples 15 μL DNA at 50 ng/mL was added to a clean 1.5 mL microcentrifuge tube. DNA was mixed with pOPIN Rev primer. For longer DNA segments the corresponding forward primer was also added- either pOPINS For or pOPINM For. 2 μL primer stock was added to the 15 μL DNA.

Primer	Sequence	Direction
pOPIN	AGCCAGAAGTCAGATGCTCAA	Reverse
pOPINS	GCATCCGTATTCAGGCCG	Forward
pOPINM	GGTATGCCGTGCGTACTGCG	Forward

Table 2.15 pOPIN sequencing primers.

2.15.4 Small scale expression screening

To screen recombinant protein expression and solubility in small scale the protein production facility use Promega's MagneHis purification system.

2.15.4.1 Transformation into three strains of E. coli for small scale expression trial

Each pOPIN vector was transformed into Lemo21(DE3), Shuffle T7 express and Rosetta-Gami2(DE3) pLysS competent cells (Table 2.16). Transformations were carried out using 50 mL competent cells with 1 mL of 1 mg/mL pOPIN plasmid DNA with the transformation protocol previously described (2.7.1).

E.coli strain	Antibiotic resistance
Lemo21(DE3)	Ampicillin, Chloramphenicol
Shuffle T7 express	Ampicillin, Spectinomycin
Rosetta-Gami2(DE3) pLysS	Ampicillin, Chloramphenicol, Streptomycin

Table 2.16 Antibiotic resistance of E.coli strains used for small scale protein expression.

2.15.4.2 Colony picking and growth

Colonies were picked into 1 mL LB in a 2.2 mL 96 deep well block. Plates were sealed with a gas-permeable heat seal and incubated overnight at 37 °C with shaking at 220 rpm. The following morning a clean 96 deep well plate containing 1.8 mL LB broth containing appropriate antibiotic (Table 2.2) was inoculated with 200 μL overnight culture. Plates were incubated at 37 °C with shaking at 220 rpm. until the OD_{600} reached ~0.7. Plates were induced by adding 8 μL of 0.1 M IPTG and grown overnight at 18 °C with shaking at 220 rpm.

2.15.4.3 MagneHis™ purification using the Hamilton Robot

Following overnight growth culture plates were centrifuged at 4,000 x g for 10 minutes. Supernatent was discarded and plate was placed on a plate deck in the Hamilton Robot. The MagneHis™ protocol was set up on the Hamilton Robot using the set-up wizard. Pellets were programmed to be lysed for 5 mins before adding 30 μL beads for 2 minutes. Beads were washed in 125 μL wash buffer three times before eluting in 50 μL elution buffer. Reagents were all from the MagneHis™ kit (Promega). For analysis, 50 μL 2 x protein loading dye was added to elutions and samples were boiled at 95 °C for 3 mins. Samples were analysed by SDS-PAGE (2.8.2).

2.15.5 Larger scale expression screen in 1 L cultures

Clones that were most successfully grown in the small-scale expression screen were grown in 1 L cultures. Colonies were picked from previously transformed plates (2.7.1) into 100 mL LB containing appropriate antibiotic to the *E. coli* strain used. Overnight cultures were used to inoculate 1 L of LB containing antibiotic. Cultures were grown to reach an OD_{600} of ~0.7 at 37 °C with shaking at 180 rpm before being induced with 4 μL 0.1 M IPTG and grown overnight at 18 °C with shaking at 180 rpm. The following day cultures were pelleted by centrifugation at 30,000 x g for 45 minutes.

2.15.5.1 Larger scale protein purification

Proteins were purified on the bench using an adaptation of the Affimer purification protocol (2.7.3.2). Pellets were resuspended in Affimer wash buffer and lysed using the cell disruptor. Lysate was pelleted by centrifugation at 30,000 x g for 45 mins. Meanwhile, ~500 mL Ni-NTA beads were washed once in wash buffer. Supernatent containing soluble protein was loaded onto a Ni-NTA affinity column and purified as per section 2.7.3.

2.15.5.2 Dialysing Affimer D11: HER2 subdomain to remove tags

The Affimer D11 Strep-Tag® II can be removed by incubating with TEV whereas the HER2 subdomains were engineered to contain a 3C protease cleavage site to remove His-tags. Proteins were mixed with ~1 mL 2 mg/mL TEV protease and ~1 mL 5 mg/mL 3C protease respectively where both had been produced by the Protein Production Facility and dialysed into PBS overnight at 4 °C using Slide-A-Lyzer™ dialysis cassettes, 10 K MWCO, 12 mL (ThermoFisher Scientific).

2.15.6 Pull down protocol using StrepTactin

Purified Affimer D11 and purified HER2 subdomains II, III and IV respectively were desalted and buffer exchanged into PBS using ZebaSpin columns. Approximately 100 μL unconcentrated desalted HER2 subdomain was mixed with 100 μL Affimer D11 and incubated at room temperature for 2 hours. Meanwhile, 200 μL Strep-Tactin® Sepharose® 50 % suspension (iba, 2-1201-010) was washed in PBS until the A280 reading, read by a NanoDrop Lite was consistently < 0.09. The Affimer D11: HER2 subdomain mix was incubated on the Strep-Tactin® Sepharose® beads for 1 hour with movement prior to elution in 100 μL 2.5 mM desthiobiotin. Eluted products were analysed by SDS-PAGE and western blot.

2.16 Biacore surface plasmon resonance (SPR) binding assay

SPR experiments were performed on a Biacore T200 instrument (GE healthcare). Recombinant protein encoding the extracellular domains of HER2 (Sino Biological, 10004-HCCH) and HER3 (Sino Biological, 10201-HCCH) were purchased and reconstituted as directed (adding 200 μL nuclease free water to a final concentration of 0.25 mg/mL). Approximately 1000 reaction units (RU) of recombinant HER2 and HER3 were immobilised in 10 mM sodium acetate buffer at pH 5 and pH 5.5 respectively. Appropriate buffer for ligand immobilisation was found by pH scouting to be acetate buffer. Recombinant proteins were immobilised by amine-coupling using an N-hydroxysuccinamide/(N-(3-dimethylaminopropyl)-N'-ethylcarbodiimide-activated CM5 chip (GE Healthcare, 29149603) followed by deactivation with ethanolamine-HCl (1 M solution, pH 8.5)(GE Healthcare)(Figure 2.8). The running buffer for the assays was 1 x

PBS with 0.1 % (v/v) tween-20, pH 7.4. A reference flow cell was generated by activating and deactivating the dextran surface of the CM5 chip without the addition of any protein.

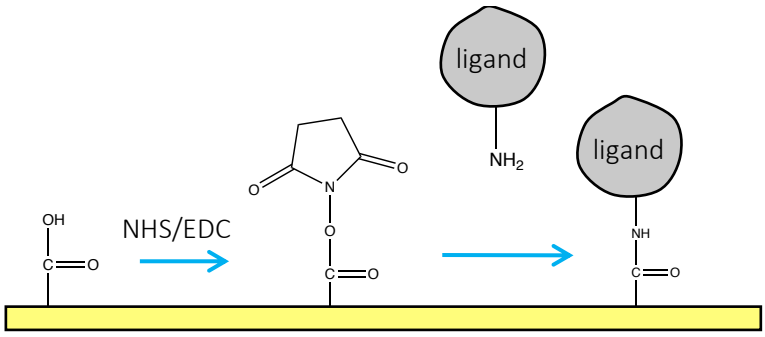


Figure 2.8 Chip derivatisation by amine coupling.
Dextran-based CM5 chop comprising a matrix of carboxymethylated dextran covalently attached to a gold surface **(A)** was activated by N-hydroxysuccinamide/(N-(3-dimethylaminopropyl)-N'-ethylcarbodiimide (NHS/EDC) **(B)** to form reactive succinimide esters **(C)**. Ligands containing amine groups are passed over the chip **(D)** and bind covalently to CM5 chip.

Affimer MMAE conjugates were dialysed into running buffer using a Pur-A-Lyzer™ Mini Dialysis Kit (merck) as per the manufacturers instructions. Conjugates were diluted in running buffer to concentrations ranging from 0.77 to 200 nM and injected over the CM5 chip for 300 seconds. Analyte measurements were carried out at 25°C. After the injection had finished the chip was regenerated by injecting Na_2CO_3 with 0.1 % tween-20. Affinities and rate constants for association and dissociation were analysed using 1:1 Langmuir binding model with BIAevaluation 3.1 software (GE Healthcare).

2.17 Statistical analysis

Where statistical analysis has been undertaken GraphPad prism version 8.0 was used. Data was compared by one-way ANOVA with Tukey's multiple comparisons test.

Chapter 3

Characterisation of HER2 binding Affimers



'Imperfection is beauty, madness is genius and it's better to be absolutely ridiculous than absolutely boring.'



-Marilyn Monroe

Chapter 3

3 Characterisation of HER2 binding Affimers

3.1 Introduction

HER2 is a 185 kDa transmembrane glycoprotein overexpressed in some types of cancer. Due to its location at the cell membrane the HER2 extracellular domain has become an attractive target for stratified therapeutics such as monoclonal antibodies Trastuzumab and Pertuzumab (1.5.3). There are drawbacks to current therapies and a new generation of therapeutic non-immunoglobulin scaffolds are being investigated such as DARPins, Affibodies and Aptamers (1.7.2). Another novel non-immunoglobulin scaffold is the Affimer.

3.1.1 Affimer Reagents

Affimer reagents are another example of an antibody alternative reagent designed to overcome some of the shortcomings of antibodies. Two Affimer scaffolds have been developed based on similar protein conformations containing four β-sheets and one α-helix (Figure 3.1). The two variable regions in the scaffold can be replaced by a nine amino acid randomised sequence to generate large phage display libraries that can be used to screen against a large plethora of targets (Tiede 2013). Affimer technology lends a myriad of advantages over typically used antibodies. Affimer reagents are small versatile proteins potentially allowing the binding of pockets otherwise too small for conventional antibodies to reach. They are also stable in a large range of temperatures and pH, can bind at higher or equal affinity to antibodies and can be identified without the need for animals through means such as phage display. Aforementioned there are two Affimer scaffolds; type I and type II.

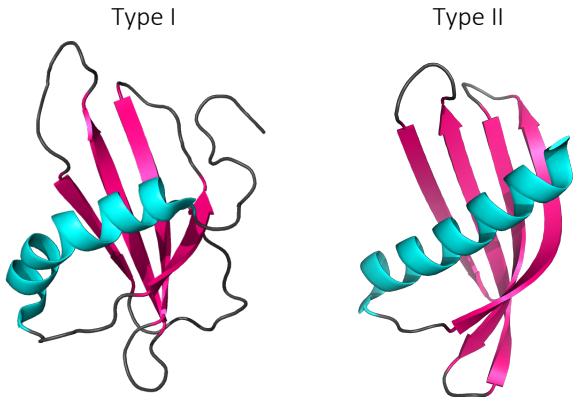


Figure 3.1 Ribbon diagram of type I and type II Affimer scaffolds.
Affimer scaffold containing an alpha helix and four beta strands. Two variable regions are comprised of nine amino acids that can be altered to bind different targets.

3.1.1.1 Type I Affimers

Type I Affimers are based on the naturally occurring human protease inhibitor Stefin A. Stefin A (SteA) is a human protein belonging to the cystatin family of protein inhibitors of the cathepsin family of cysteine proteases (205). SteA is a single domain, single chain protein with no disulphide bonds. It was an attractive choice for a protein scaffold as it contained no posttranslational modifications or disulphide bonds meaning it could be functional in a range of systems. The SteA protein was mutated to produce the stefin A triple mutant (STM) that meant it lost its natural biological activity and allowed it to be used as a tool for analysing protein-protein interactions *in vitro* and *in vivo*.

3.1.1.2 Type II Affimers

Type II Affimers are based on a consensus sequence of plant derived phytocystatins (203) that are small protein inhibitors of cysteine proteases (206). The consensus sequence was derived through the alignment of 57 phytocystatin sequence to give preferable properties. This protein again displayed the desirable traits for a versatile scaffold in that it is small, monomeric, highly stable and lacks disulphide bonds and glycosylation sites (203). By replacing the inhibitory sequence within the variable regions of the

phytocystatin with nine randomised amino acid residues Affimers were produced able to bind to a large plethora of targets and a phage display library was generated. Affimer reagents have been shown to be effective in a large array of scientific applications such as super resolution microscopy, immunohistochemistry and understanding protein-protein interactions (207-209).

3.1.2 Type II Affimers raised against HER2 extracellular domain

The Tomlinson group had previously isolated Affimer reagents that bind to recombinant HER2 (Sino Biological Inc., 10004-H08H) encoding the extracellular domain (Met 1- Thr 652) of the human HER2 protein. In brief, recombinant HER2 was immobilised and incubated with an Affimer phage display library (Figure 3.2). Binders were confirmed using an enzyme-linked immunosorbent assay (ELISA).

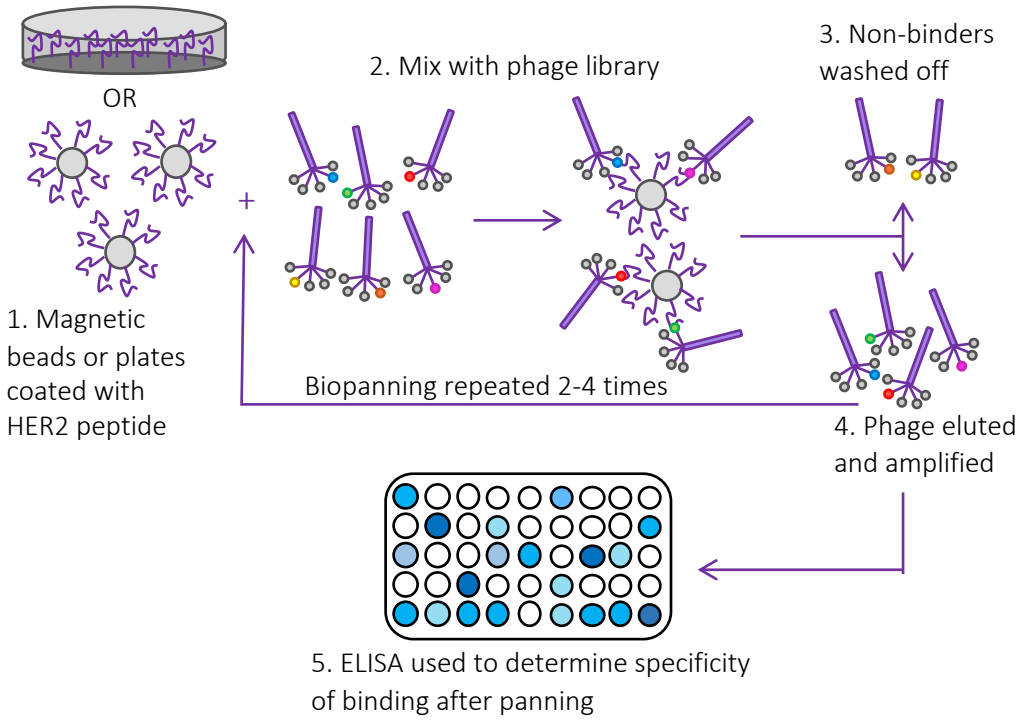


Figure 3.2 Phage display.
Phage display was the technique used to isolate Affimers that bind to their target. In brief, (1) Plates (first and third round) or magnetic beads (second round) were coated in the protein of interest, (2) beads were mixed with a library of phage displaying various Affimer sequences, (3) non-binders are washed off, the process is repeated as necessary, (4) successful phage are eluted and amplified. (5) An ELISA is used to check for specificity.

Affimer	Variable region 1	Variable region 2
D7	WHKSWSPTT	SLINAYYDI
D11	HFVGKFYHN	EFQMGGIWK
E8	YQSQGKPLE	ADGSAAFMF
E12	SWHYQS	VEMLEYQTW
F9	MEPDASWWD	YEELSGQHY
H7	RYEGRGYHN	HYIMKQHWH
H8	RFWDSHYQH	LGGGFYYHY
H9	NWFYNS	TEVYNNKKM

Table 3.1 Sequences of eight HER2 binding Affimer variable regions.
Affimer DNA was sent for sequencing by GeneWiz.

Following isolation of Affimer reagents by phage display, sequencing identified eight unique clones (Table 3.1). All clones contain either a Tyrosine (Y) or Proline (P) residue three positions back from the end of variable region 1 indicating this could be an important region to facilitate binding to the HER2 extracellular domain.

3.1.3 Aims

The aim of this chapter was to characterise eight Affimer reagents that bind to recombinant HER2. This was done by analysing the ability of Affimers to bind endogenous HER2 through a pull-down assay and testing their ability to bind to and potentially be internalised by HER2 overexpressing cell lines by immunofluorecence.

3.2 Results

3.2.1 Testing the ability of Affimers to bind endogenous HER2 from cell lysate

To confirm the ability of HER2 binding Affimers to bind to endogenous HER2 affinity precipitation was carried out from breast cancer cell lysates. Affimers that bind to recombinant HER2 extracellular domain expressed by HEK293T cells were identified by phage display. HEK293 cells are utilised for the production of recombinant protein due to their high transfection efficiency and ability to carry out complex post translational modifications (210). However, the idiosyncratic nature of the protein in its native environment cannot be recapitulated by recombinantly expressed protein.

Eight HER2 binding Affimers sub-cloned in the pETLECTRA vector containing an N-terminal poly-histidine tag (D7, D11, E8, E12, F9, H7, H8 and H9) were provided by Dr. Danah Al'Qallaf. Affimers were produced in BL-21 (DE3) Star *E.coli* cells and purified by Ni-NTA chromatography (2.7.3). Purity was checked using SDS-PAGE (Figure 3.3). Affimers were generally well produced with thick bands ~13 kDa with the exception of Affimer E12 that exhibited low expression and Affimer H8 that was slightly fainter than others (Figure 3.3D). Very little Affimer is present in the 'unbound' fraction (Figure 3.3C) demonstrating effective purification of the Affimer protein. Following purification Affimers were stored at -20 °C until they were used.

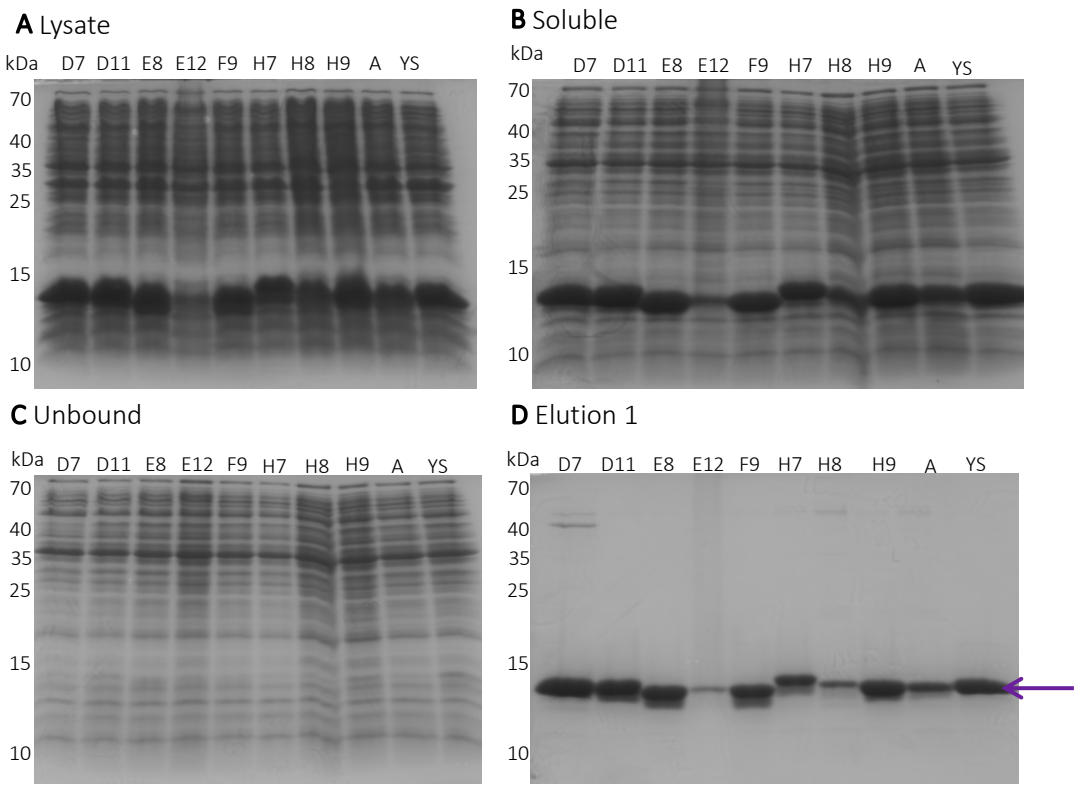


Figure 3.3 SDS-PAGE of His-tagged Affimer reagents purified by Ni-NTA chromatography.
Affimer proteins were purified from bacterial lysate of BL21 Star™ (DE3) competent cells by nickel ion affinity chromatography. Samples were taken from different points of the purification process and analysed by SDS-PAGE and visualised using Coomassie blue to show **(A)** bacterial cell lysate, **(B)** soluble fraction following centrifugation of lysate, **(C)** soluble fraction that did not bind to nickel resin and **(D)** the first elution of purified Affimer proteins (Affimer proteins shown by purple arrow). Gel images were taken using the epillumination setting of an Amersham Imager 600.

Affinity precipitation was used to determine if HER2 specific Affimers could bind to native HER2 from HER2 overexpressing cell lines (2.9). Cells isolated from breast cancer patients overexpressing HER2 (AU-565 and BT-474) and negative for HER2 (MDA-MB-231) were lysed. HER2 specific Affimers were incubated with 0.5 mg/mL cell lysate. The Affimer:lysate solution was incubated with Ni-NTA beads prior to elution and analysis by SDS-PAGE and western blot. An Affimer control containing alanine residues in place of the variable regions (4 in variable region one and 2 in variable region two), herein termed 'Affimer control' was used. Western blot analysis was used to detect the presence of the Affimer and HER2. The optimal dilution factor for the anti-His antibody had been previously identified whilst a range of anti-HER2 concentrations were tested with 1:10,000 being most efficient (Figure 3.4).

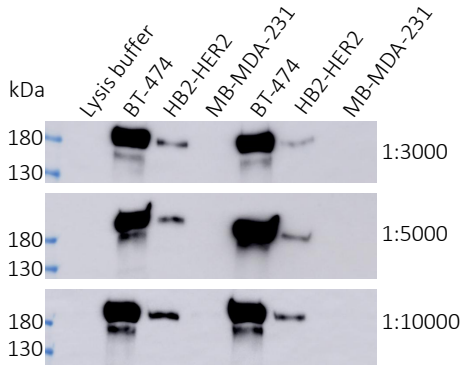


Figure 3.4 Optimisation of anti-HER2 antibody for western blot analysis.
Lysates from the HER2 overexpressing cell lines BT-474 and HB2-HER2 transfected cells alongside the triple negative cell line MDA-MB-231 were separated on an 8 % gel by SDS-PAGE. Gels were transferred to nitrocelluolose membranes prior to blocking in 5 % milk. Membranes were incubated with anti-HER2 antibody at various dilutions (1:3000, 1:5000 and 1:10000) overnight at 4 ºC. Goat anti-Rabbit (HRP) (1:10,000) was incubated for 1 h room temperature. HRP was detected using Luminata substrate and imaged by chemiluminsence on an Amersham Imager 600.

Affimer was present in every fraction at a similar density (Figure 3.5A and 5B). Affimer D7, D11 and E8 successfully precipitated HER2 from lysates at a concentration of 0.5 mg/mL showing potential higher levels of HER2 in AU-565 compared to BT-474 HER2 overexpressing cell lines (Figure 3.5C). Affimer E12 did not precipitate HER2, however, is present as a 'smear' down the gel potentially due to degradation of the protein. For this reason no optimisation of the assay was undertaken to investigate Affimer E12 further. Affimers F9, H7, H8 and H9 showed no successful precipitation of HER2 from lysates at 0.5 mg/mL, however, had previously against lysates of unknown concentration (data not shown). Therefore, affinity precipitation for these Affimers was repeated using cell lysate concentrations of 1 mg/mL (Figure 3.5D). Affimer H7, H8 and H9 successfully precipitated HER2 from lysates at this concentration, again, observing a visually higher level in AU-565 cells compared to BT-474. These results suggest that Affimer H7, H8 and H9 do pull down HER2 but potentially with a lower affinity compared to Affimers D7, D11 and E8. Affimer F9 showed no evidence of precipitating HER2 from cell lysates at this concentration.

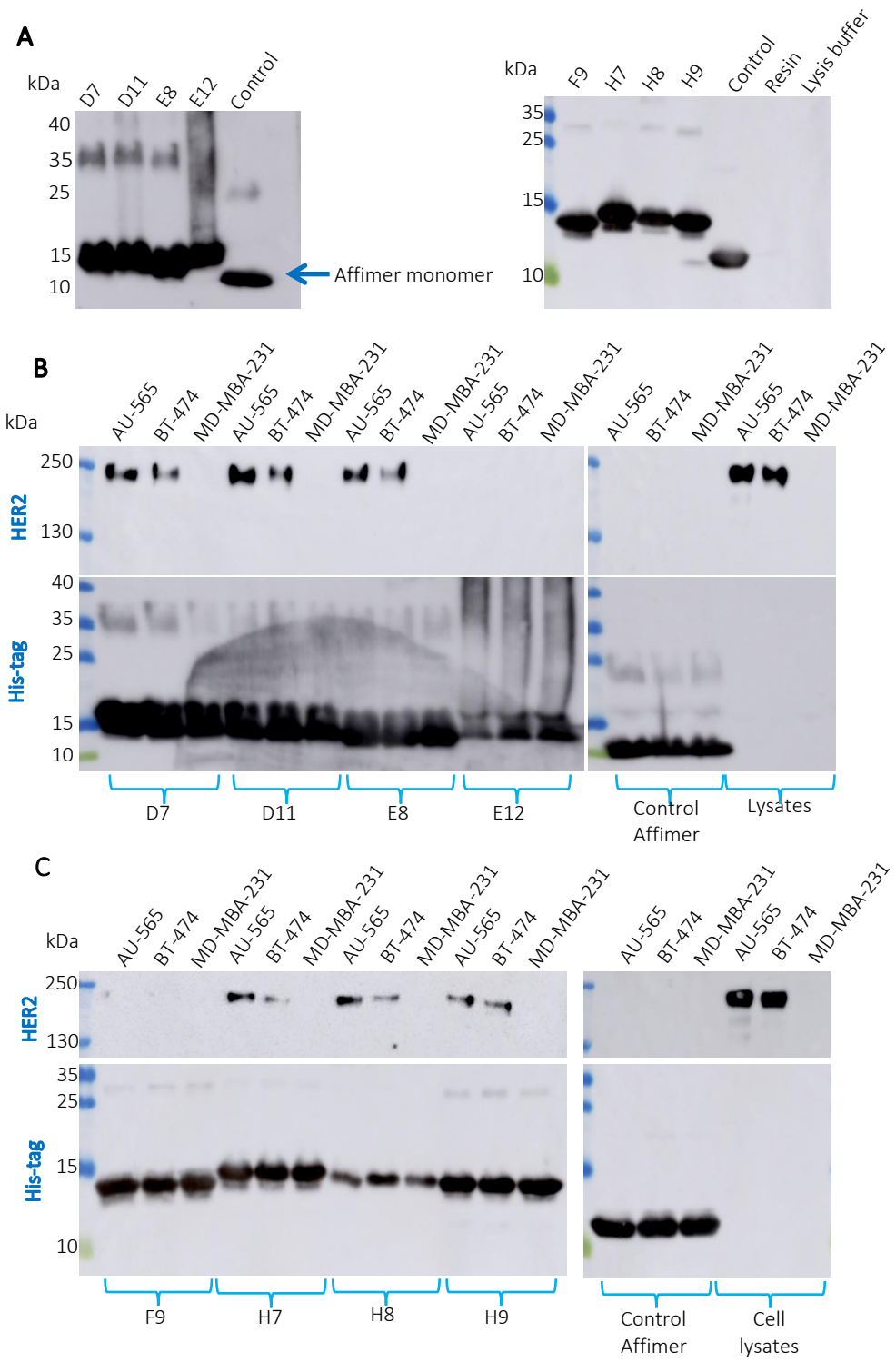
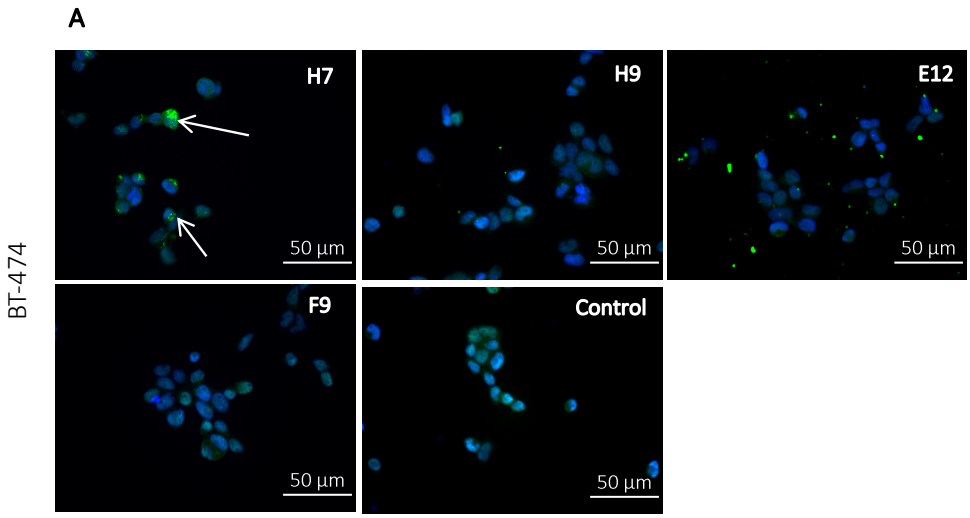


Figure 3.5 Affinity purification of endogenous HER2 using Affimer reagents.
Immunoprecipitation of endogenous HER2 from cell lysates was carried out for HER2 overexpressing cell lines AU-565 and BT-474 and HER2 negative cell line MDA-MB-231. Lysates were incubated with Affimer prior to purification using Ni-NTA beads. Complex was eluted and proteins were separated by SDS-PAGE alongside Affimer straight from purification. Protein was transferred onto nitrocellulose membrane using a Bio-Rad Turbo blot system. Membranes were incubated with **(A)** 6x His tag antibody (HRP) (1:3500) to detect His tagged Affimer reagents **(B and C)** anti-HER2 (1:10000) and HRP secondary (1:10000) to detect HER2 and anti-His (HRP) antibody (1:3500) to detect the 6x His tagged Affimer precipitated from cell lysates. **(B)** used cell lysates of 0.5 mg/mL **(C)** used cell lysates of 1 mg/mL. HRP was detected using Luminata substrate and imaged using the chemiluminescence setting on an Amersham Imager 600.

3.2.2 Investigating the ability of HER2 specific Affimers to be internalised by HER2 overexpressing cell lines

Six of the eight HER2 binding Affimers were able to pull down HER2 from cell lysates. Immunofluorescence was used to further determine Affimer binding and localisation. Initially, the HER2 overexpressing cell line BT-474 and HER2 negative cell lines MCF-7 or MDA-MB-231 cells were used. Following incubation with Affimers at 25 μg/mL for 4 hours cells were fixed in 4 % PFA solution (2.11.1). Aforementioned, Affimers contain a C-terminal 6x His tag that was utilised for the detection of Affimer through anti-His primary and Alexa Fluor™ secondary antibodies. Affimer H7 was present in the cytoplasm of BT-474 cells (Figure 3.6A). Affimer D11 demonstrated the highest level of fluorescence localised both on the periphery and possibly internally of BT-474 cells (Figure 3.6B). Other Affimers exhibited some fluorescence, particularly Affimer E12, however, the staining is random and does not co-localise with the cells themselves. Therefore, from these results combined Affimer D11 and Affimer H7 were the only two taken forward for further characterisation. Also, in subsequent experiments the MDA-MB-231 cell line will be used as a negative control. Whilst MCF-7 is referred to as a HER2 negative cell line in some papers, others suggest evidence for low levels of HER2 so to avoid uncertainty this cell line is not used as a control in future experiments but MDA-MB-231 was consistently used (168, 211, 212).



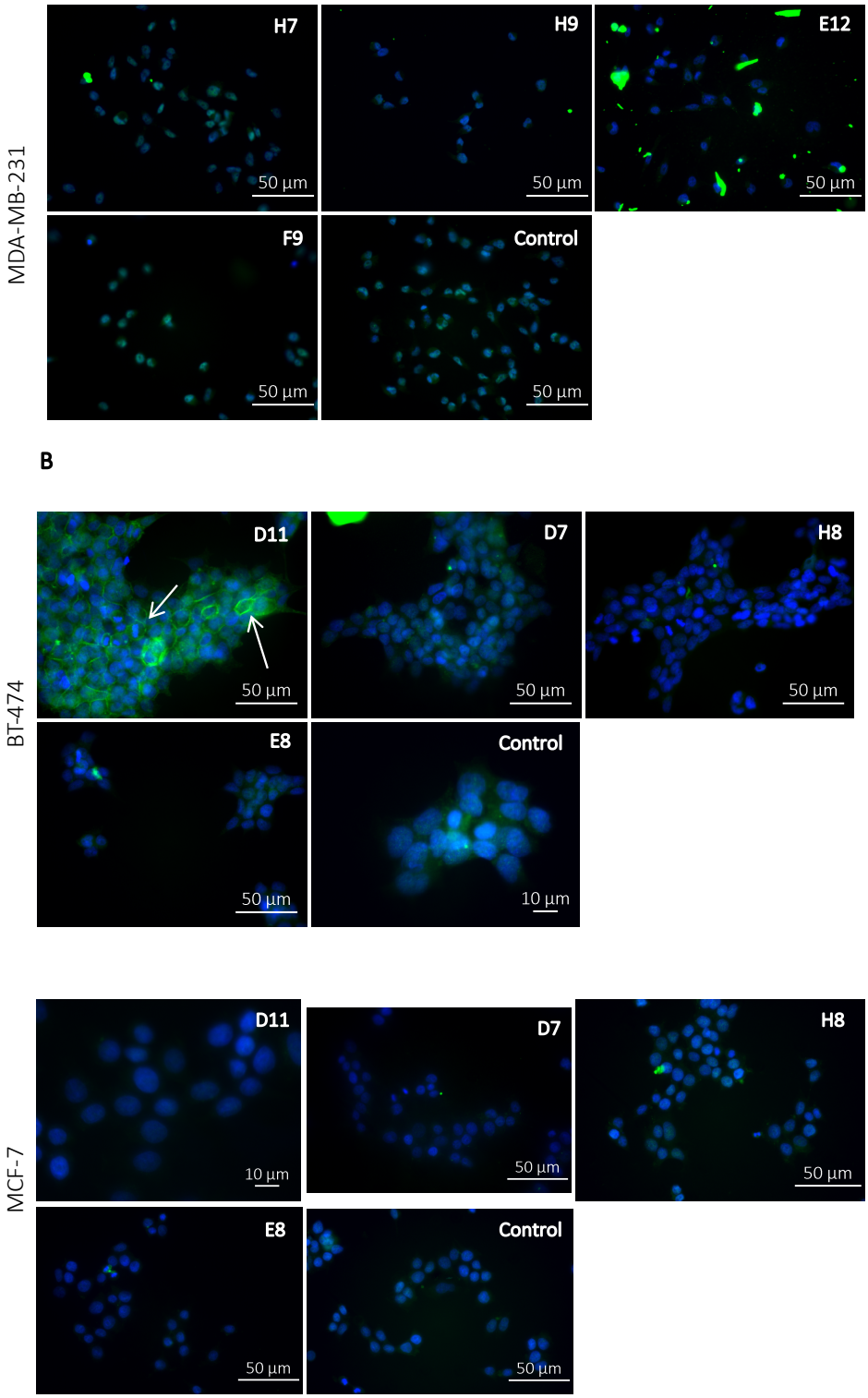


Figure 3.6 Immunofluorescence using HER2 binding Affimers on breast cancer cell lines.
Immunofluorescence was carried out using HER2 overexpressing cell line BT-474 and negative controls **(A)** MD-MBA-231 or **(B)** MCF-7. HER2 specific Affimers were incubated on live cells for 4 hours prior to fixing and permeabilization. Affimer (green) was detected using an anti-His primary antibody and AlexaFluor 488 secondary antibody and the cell nucleus (blue) was detected using DAPI. Coverslips were mounted in mounting media containing DAPI. Images were taken on a Nikon fluorescent microscope. Images are representative of n=1.

3.2.3 Comparing effects of HER2 binding Affimers to Trastuzumab on HER2+ cell lines

Affimers were either expressed from the pETLECTRA (no cysteine) or pET11a vector (C-terminal cysteine). Preliminary experiments found that none of the HER2 binding Affimers, expressed from pETLECTRA, had a detrimental effect on the metabolic activity of BT-474 cells (data not shown). As immunofluorescence showed Affimers D11 and H7 binding to HER2 overexpressing cell lines BT-474 the effects of these Affimers containing a C-terminal cysteine residue was investigated. The inhibitory effect of Affimers D11 and H7 was compared to Trastuzumab in breast cancer cell lines AU-565, BT-474 and MDA-MB-231. Trastuzumab is a monoclonal antibody that has been FDA approved for the treatment of both primary and metastatic breast cancer overexpressing HER2, previously described in in section 1.5.3. To compare the effects of Affimers and Trastuzumab dose responses were undertaken.

3.2.3.1 Trastuzumab dose response against breast cancer cell lines

A dose response with Trastuzumab concentrations ranging from 30 to 0.025 nM was carried out (2.10.2.2). The AlamarBlue assay (2.10.2.2.1) is a non-toxic assay that allows quantification of metabolic activity through the conversion of resazurin to resorufin, a compound red in colour and highly fluorescent, in live cells that is visualised as a colour change from blue to purple and the fluorescence can be read by a microplate reader. As AlamarBlue is non-toxic it allowed for further quantification of results. Cells were stained with hoescht and a nuclear cell count was performed (2.10.2.2.2) to correlate the decrease in metabolic activity to a hypothesised decrease in cell number.

Trastuzumab had the largest effect on BT-474 cells with approximately 40 % inhibition of metabolic activity at concentrations of 6 nM and above (Figure 3.7A). The cell count trend mirrored that of metabolic activity with the exception of a slight decrease in cell number at the highest concentrations (Figure 3.7B). At 15 nM the effects of Trastuzumab in HER2 overexpressing cell lines was evident whilst there was no effect on the HER2 negative cell line. Therefore to more clearly represent the data bar charts were generated to compare results between cell lines incubated with 15 nM Trastuzumab (Figure 3.7B). At 15 nM both metabolic activity and cell count data is reduced by 40 % for BT-474 cells and 20 % for AU-565 cells while MDA-MB-231 remain unaffected (Figure 3.7B).

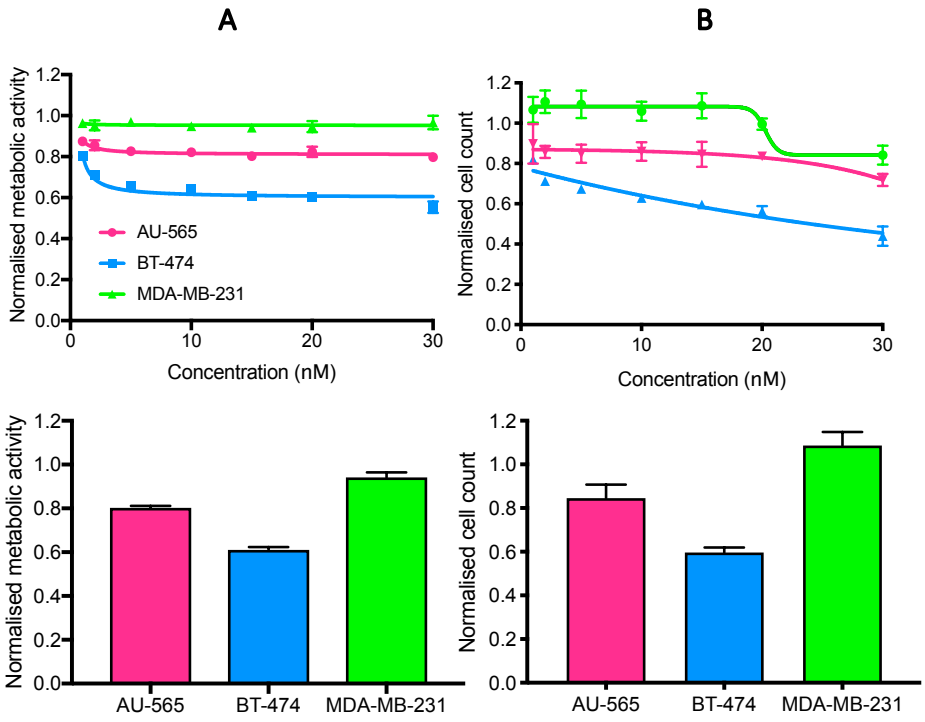


Figure 3.7 Dose response using Trastuzumab monoclonal antibody on breast cancer cell lines.
Cell lines AU-565, BT-474 and MDA-MB-231 were seeded one day prior to addition of Trastuzumab. Cells were incubated for a further 72 hours before analysing **(A)** metabolic activity by the AlamarBlue assay measuring fluorescence at excitation 570 nM and emission 590 nM. Images were taken using a Tecan Spark microplate reader. **(B)** Nuclear cell count following staining with hoescht. Cell counts were carried out using a Pico Imaging express imager. All values were normalised to cells without drug (media only). Graph shows the mean value from three biological replicates each containing three technical replicates. Error bars show standard error of the mean. Bottom graphs are mean values at 15 nM Trastuzumab. Graphs were generated using GraphPad prism.

3.2.3.2 Inhibitory effects of HER2 specific Affimers

It was previously identified that Affimers lacking a C-terminal cysteine residue have no effect on metabolic activity of BT-474 cells (data not shown). The addition of a cysteine residue should not result in any characteristic changes of Affimers, however, to confirm this, dose responses with Affimers containing a C-terminal cysteine residue were carried out to compare their effects to Trastuzumab. Affimer reagents do not naturally contain cysteine residues in their scaffold. Cysteine residues are often utilised for site specific modification. To ensure that the cysteine residue would have no effect on Affimer reagents a dose response was undertaken with unconjugated Affimers containing a C-terminal cysteine residue.

3.2.3.2.1 Cloning Affimer D11 and H7 to contain C-terminal cysteine residue

Affimer reagents were subcloned from the pDHis vector into pET11a plasmid to contain a C-terminal cysteine residue prior to a 6x His-tag (pET11a-C)(2.8.4). Both the pET11a-C vector and Affimer DNA were digested with restriction enzymes *NheI* and *NotI* and analysed by agarose gel electrophoresis (2.8.4.3)(Figure 3.8). Vector and insert DNA were ligated and transformed into XL-1 competent cells (2.7.1). Minipreps were carried out and DNA sequences were confirmed by GeneWiz (2.8.4.6).

Following sequence confirmation ligated plasmids were transformed into BL21 (DE3) Star *E.coli* cells for protein expression as previously described (2.7.1). Fractions from throughout the purification protocol were analysed by SDS-PAGE (Figure 3.9). Whilst all eight HER2 binding Affimers were produced containing a C-terminal cysteine residue only Affimer D11 and H7 were used in subsequent experiments. A high level of purity was achieved for most Affimers with bands at ~ 13 kDa and ~ 26 kDa consistent with Affimer monomer and Affimer dimer sizes. There was some Affimer present in the unbound fraction suggesting the Ni-NTA beads were saturated Figure 3.9B, however, a high enough yield was achieved to continue with Affimer conjugation.

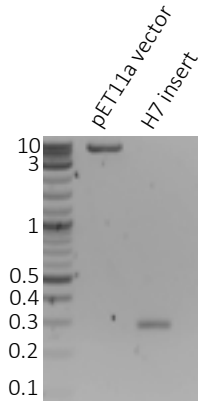


Figure 3.8 Agarose gel electrophoresis of vector and insert DNA.
Samples of pET11a vector and Affimer insert DNA were analysed by gel electrophoresis to determine the correct fragment sizes were achieved.

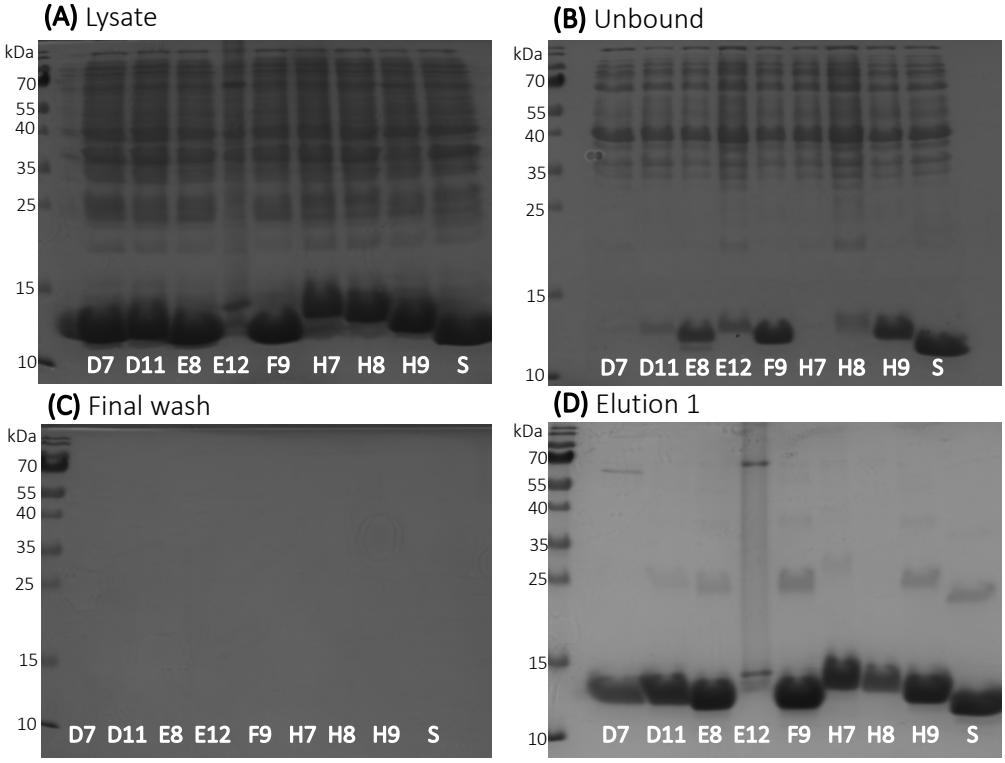


Figure 3.9 SDS-PAGE to confirm purity of Affimer reagents contraining C-terminal cysteine residues. Fractions were taken from each stage of the Affimer purification cycle and analysed by SDS-PAGE to determine purification efficiency and purity of the final product. **(A)** Whole lysate fraction containing all protein lysed from E.coli cells. **(B)** The unbound fraction containing anything that did not bind to the Ni-NTA column. **(C)** Final wash of the Ni-NTA column with wash buffer. **(D)** The first elution from the Ni-NTA column with elution buffer. Gels were stained with Coomassie blue and imaged using an Amersham Imager 600.

3.2.3.2.2 Dose response with Affimers containing C-terminal cysteine residues

Affimer D11, H7 and control containing C-terminal cysteine residues were incubated on cells at concentrations ranging between 0 and ~45 nM (2.10.2.2). Metabolic activity was analysed by the AlamarBlue assay (2.10.2.2.1). Affimer had no observable effect on the metabolic activity of breast cancer cell lines AU-565, BT-474 or MDA-MB-231 (Figure 3.10). In addition, nuclear cell counts were carried out following incubation with AlamarBlue. Cells were washed in PBS and fixed prior to nuclei staining with Hoescht (2.10.2.2.2). Plates were imaged using an ImageXpress Pico Automated Cell Imaging System. Nuclei were identified by the software and confirmed manually to obtain the best representation of cells. Difficulties arose when imaging BT-474 cells as they tend to form clusters of overlapping cells and so nuclei weren't as easy to define computationally. At higher concentrations of Affimer D11, BT-474 showed a decrease in cell count. All cell

lines had decreased cell count at higher concentrations of Affimer H7 and marginal decrease at the highest concentration of Affimer control.

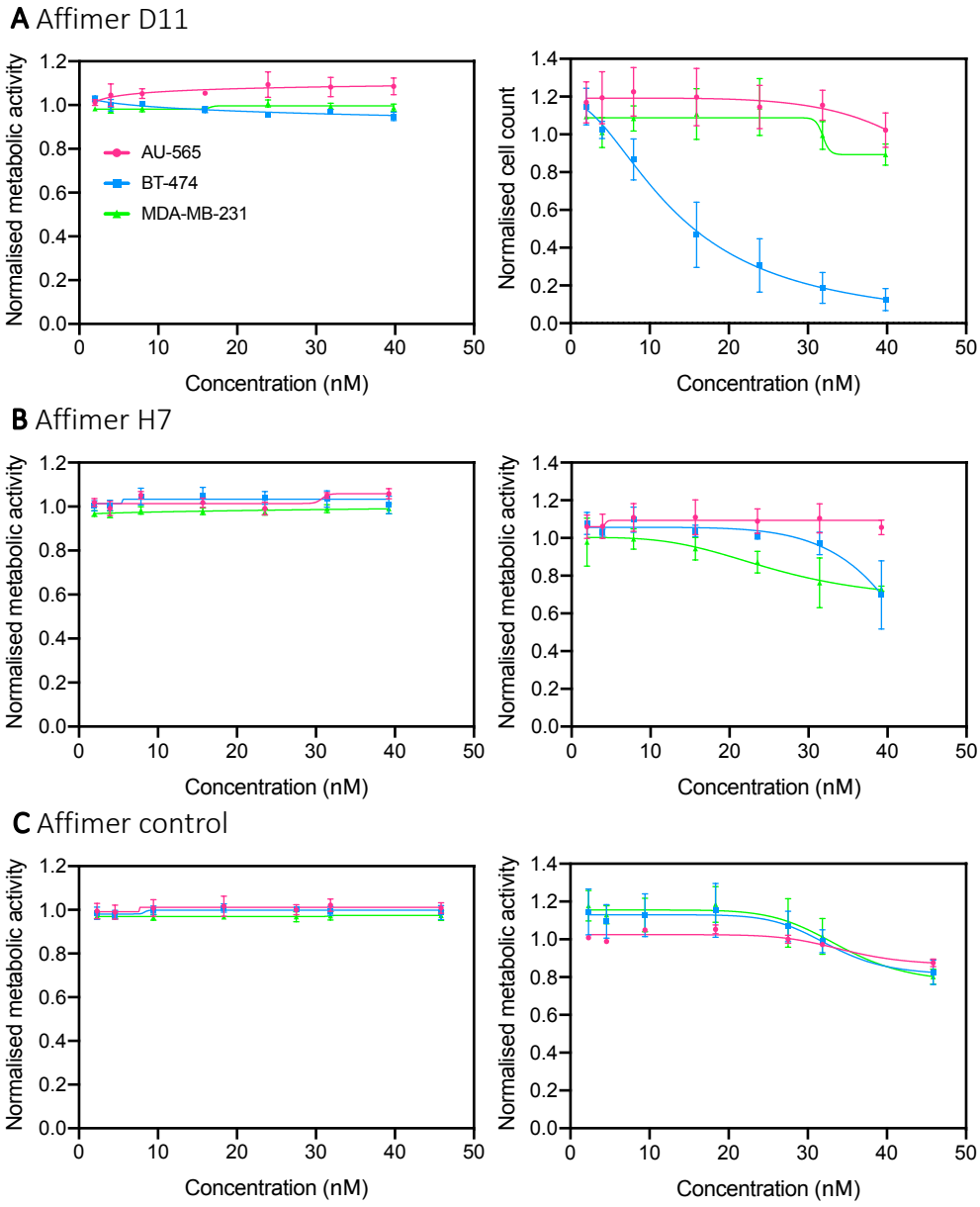


Figure 3.10 Dose response of unconjugated Affimer on breast cancer cell lines.
Cell lines AU-565, BT-474 and MDA-MB-231 were seeded one day prior to the addition of **(A)** Affimer D11 **(B)** Affimer H7 and **(C)** Affimer control. Cells were incubated for 72 hours with Affimer prior to the analysis of metabolic activity **(left)** through the AlamarBlue assay. Fluorescence was measured at excitation 570 nM and emission 590 nM using a Tecan Spark Microplate reader. The final nuclear cell count after staining with hoescht **(right)** was imaged using an ImageXpress Pico Automated Cell Imaging System. All values were normalised to cells without drug (media only). The mean value of three biological repeats were taken together to form a mean value of three experimental repeats where error bars show standard error of the mean. Graphs are representative of n=3 with the exception of MDA-MB-231 Affimer D11 and Affimer H7 cell count data where n=2. Graphs were generated using GraphPad prism 8.

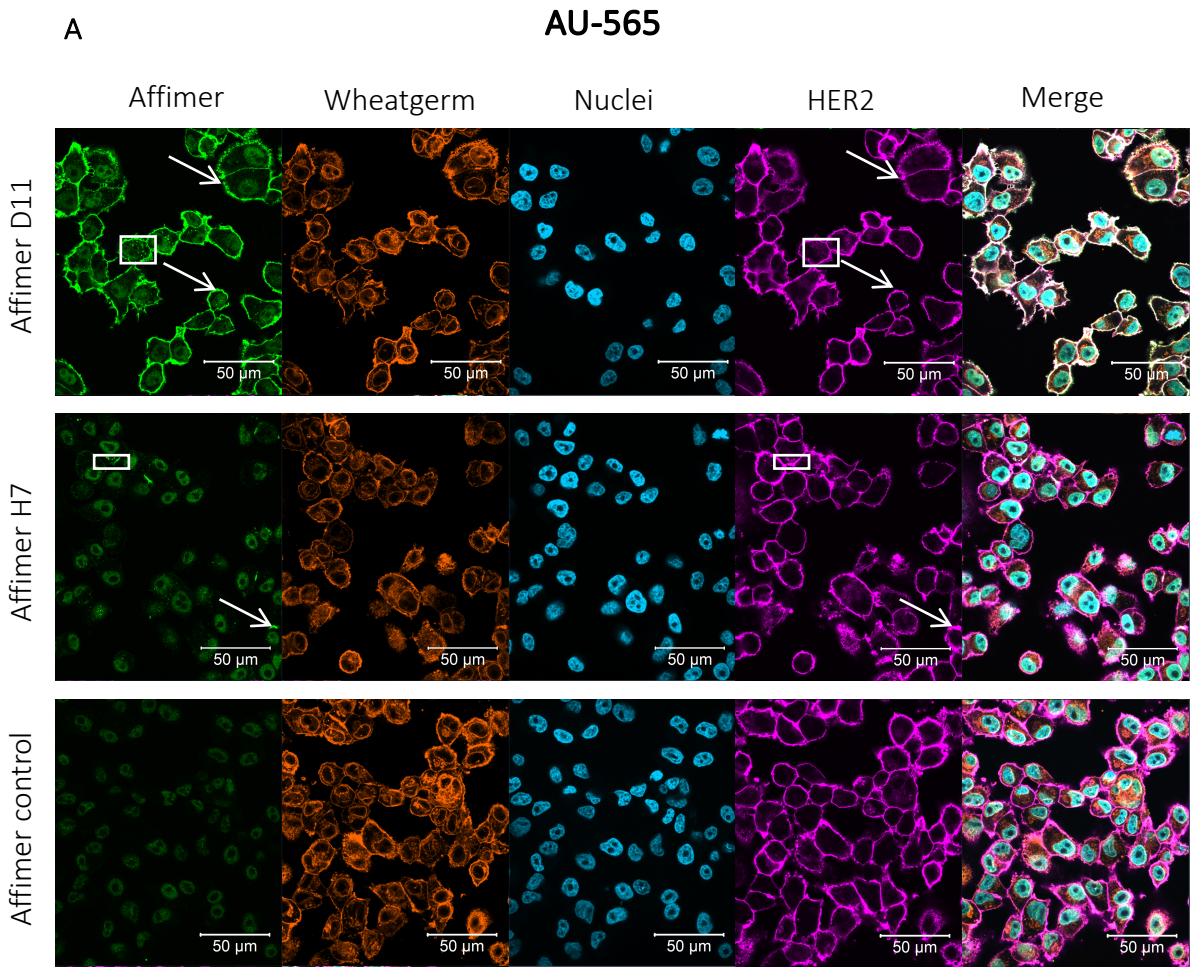
3.2.4 Affimer internalisation observed using confocal microscopy

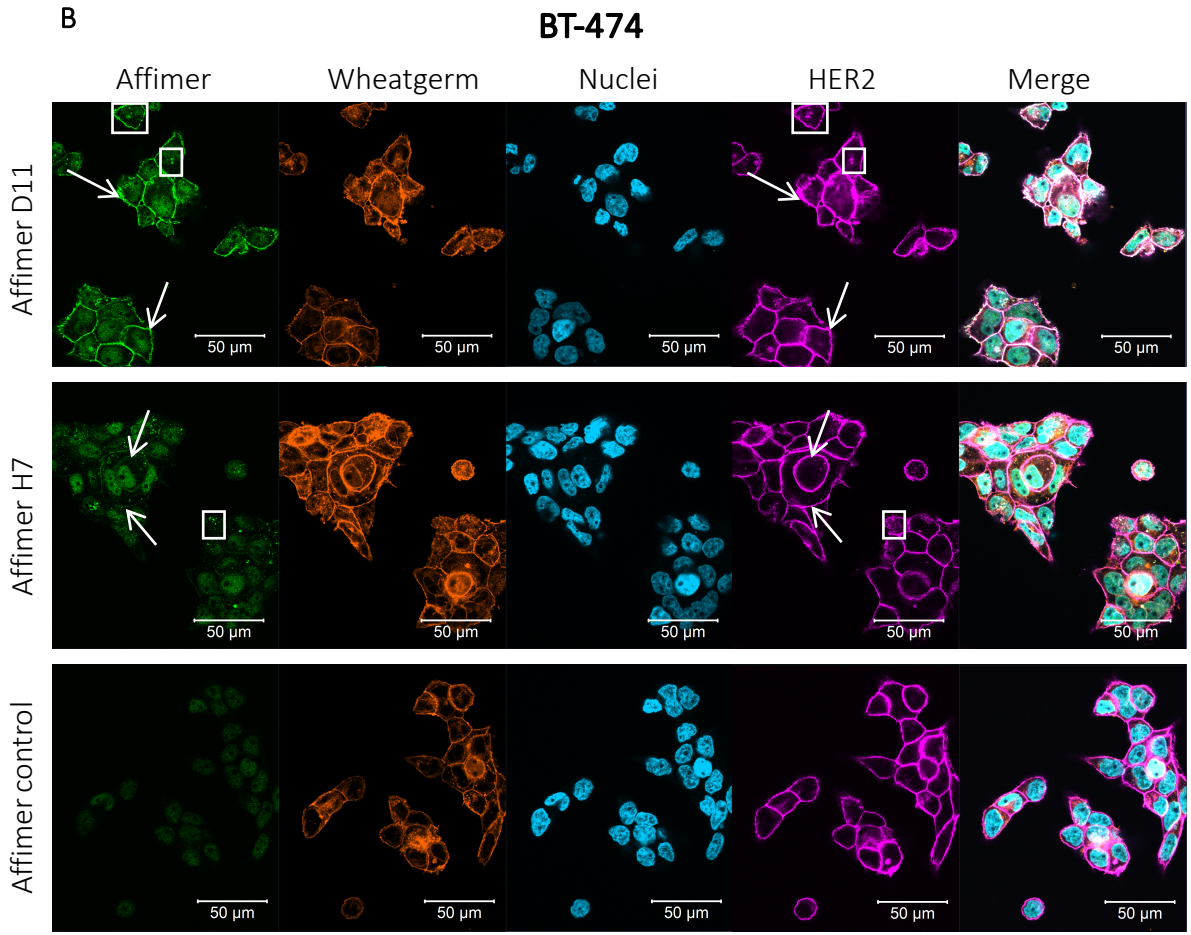
Affimers alone had no detrimental effects on the metabolic activity of HER2 overexpressing cell lines. In recent years non-immunoglobulin scaffolds have been utilised as vehicles for the delivery of cytotoxic compounds to cancer cells (213). Herein we investigated the potential use of Affimers for this application. In order to be used as a vehicle Affimers must first be internalised by HER2 overexpressing cells discriminately of HER2 negative. Confocal microscopy can achieve higher resolution and better contrasting images than widefield fluorescent microscopy. This is due to the use of lasers that can be turned on/ off individually and a spatial pinhole that blocks out-of-focus light from penetrating the image (214). Therefore, to get a more conclusive idea of where Affimers are localising in the cell confocal microscopy was utilised.

Affimers were incubated on the breast cancer cell lines AU-565, BT-474 and MDA-MB-231 for 4 hours following the protocol in section 2.11.1. Proceeding fixation cell membranes were visualised using wheat germ agglutinin. Wheat germ agglutinin is a lectin that is specific for N-acetylglucosamine and N-acetylneuraminic acid (sialic acid) that are oligosaccharides found on cell membranes (215, 216). Conjugated to a fluorophore wheat germ agglutinin provides a method of visualising cellular membranes (217). Cells were then permeabilised to allow anti-His and anti-HER2 antibodies to reach their targets of poly-histidine tagged Affimer and HER2 extracellular domain. Coverslips were mounted in mounting media containing DAPI to visualise the cell nuclei and imaged using a Zeiss confocal microscope.

Membrane co-localisation is depicted by white arrows and intracellular co-localisation by white boxes (Figure 3.11). Affimer D11 co-localised with HER2 at the membranes of AU-565 and BT-474 cell lines. Affimer D11 is also present in the cytosol of AU-565 and BT-474 cell lines and co-localises with HER2, however, this staining is not as obvious as membranous staining. Affimer H7 does not seem to localise to the membrane of AU-565 cells but shows faint staining in BT-474 cells. Affimer H7 does appear in the cytosol of AU-565 and BT-474 cells at a low level. Wheat germ agglutinin is present in all cell lines staining both surface membranes and intercellular membranes. Wheat germ agglutinin co-localises with HER2 in AU-565 and BT-474 cell lines at the cell surface. Affimer

immunofluorescence was repeated a further two times with confocal microscopy after initial experiments with fluorescent microscopy with/ without staining with wheat germ agglutinin and HER2 and demonstrated similar staining each repetition.


A
AU-565
Affimer
Wheatgerm
Nuclei
HER2
Merge
Affimer D11
Affimer H7
Affimer control
50 µm


B
BT-474
Affimer
Wheatgerm
Nuclei
HER2
Merge
Affimer D11
Affimer H7
Affimer control
50 µm

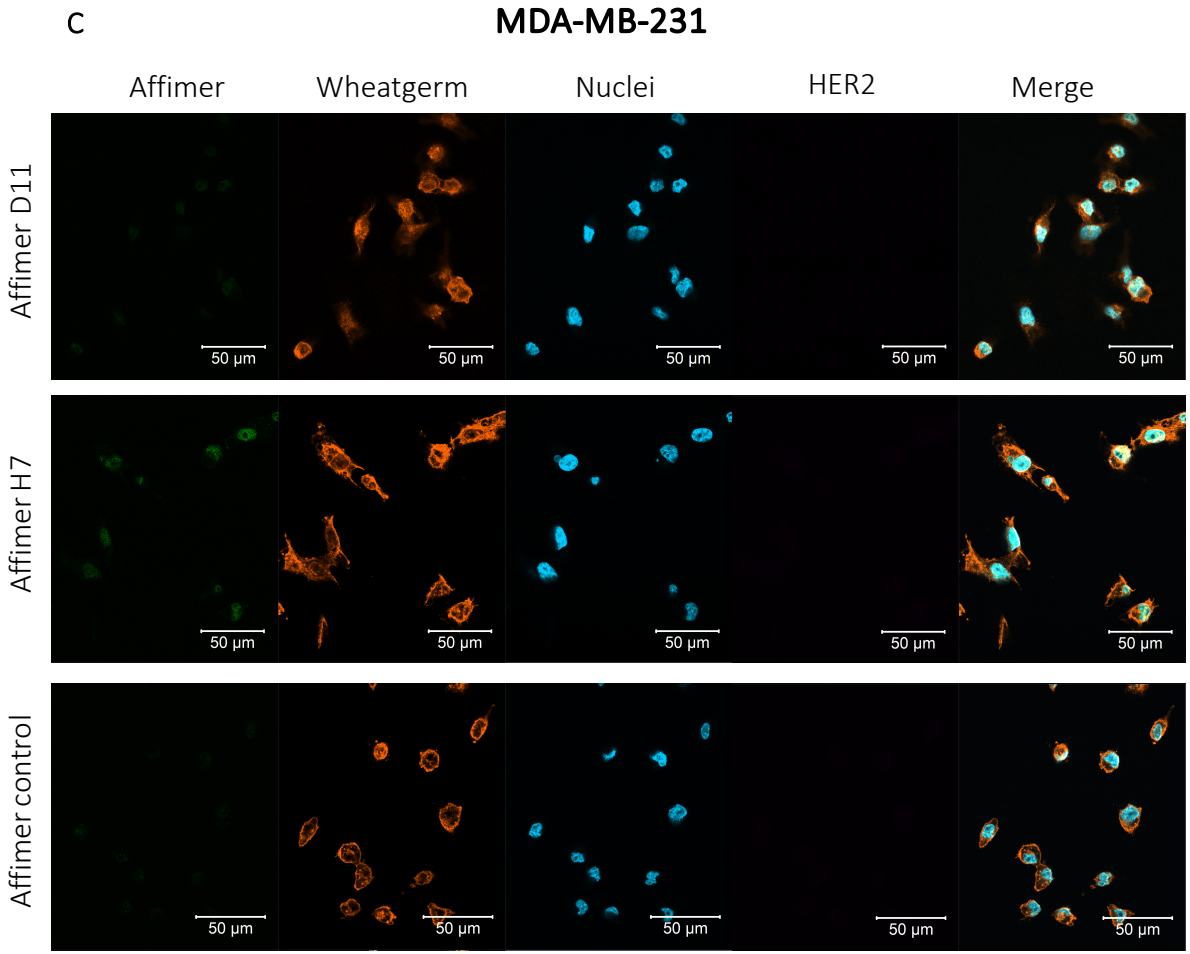


Figure 3.11 Confocal microscopy using His-tagged Affimers on breast cancer cell lines.
Affimers containing a C-terminal 6x His-tag were incubated on cell lines **(A)** AU-565, **(B)** BT-474 and **(C)** MDA-MB-231 for 4 hours prior to fixing. Affimers were detected using anti-His antibody (green), membranes using wheat germ agglutinin (orange), cell nuclei (blue) and HER2 (magenta). Co-localisation of Affimer with membranous HER2 is indicated by white arrows, intracellular co-localisation is indicated by white boxes. Images were taken using an upright Zeiss confocal microscope at a magnification of 40x with oil. n=2.

3.2.5 Affimer internalisation following conjugation to Alexa Fluor™ 488

Non-immunoglobulin scaffolds have been utilised as vehicles for the delivery of cytotoxic warheads to cancer cells. Previously FDA approved ADCs are internalised by receptor mediated endocytosis where the pH alteration in lysosomes facilitates the release of the cytotoxic warhead into the cytosol (218). The ability of Affimer reagents conjugated to Alexa Fluor™ 488 to be internalised by HER2 overexpressing cell lines was analysed by confocal microscopy. These experiments were used as a proof-of-concept that Affimers could potentially be used to deliver cytotoxic warheads.

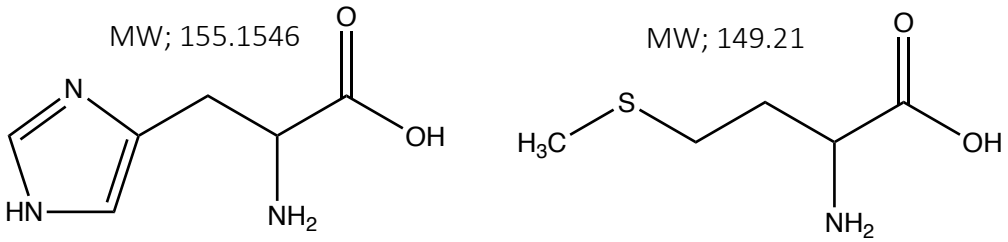
3.2.5.1 Conjugation of Affimer to AlexaFluor 488 maleimide

Affimer D11, H7 and control containing cysteine residues were expressed and purified (2.7). Following purification, Affimers were immediately incubated with TCEP reducing gel to prevent disulphide bond formation between available cysteine residues. Reduced Affimers were conjugated to Alexa Fluor™ 488 maleimide with an Affimer: Alexa Fluor™ 488 ratio of 1:1 (2.9.1). Concentrations of Affimer Alexa Fluor™ 488 conjugates were determined by BCA assay (2.8.1.2).

Liquid chromatography-mass spectrometry (LC-MS) was used to analytically determine the molecular masses of Affimers in their conjugated and unconjugated forms (2.9.3)(Figure 3.13 and Figure 3.14). Samples were separated by ultra-performance liquid chromatography (UPLC) prior to being subjected to mass spectrometry. During mass spectrometry the analyte is ionised prior to entering a quadrant of charged rods. A detector at the end of the quadrant is able to elucidate the charge in which the quadrupole was at the time the analyte hit the detector that enables the exact mass of the analyte to be determined.

During mass spectrometry amino acid residues can be lost from the C- or N-terminus of the protein of interest. The Affimer scaffold contains an N-terminal methionine and C-terminal histidine so these residues are most likely to be lost (Figure 3.12). This can

result in a shift in the expected mass to the calculated mass. The expected mass of the Affimers was calculated using Expasy's Protparam tool and the exact masses were found by LC-MS.



Histidine Methionine

Figure 3.12 Skeletal formular of histidine and methionine amino acid residues.
Amino acid residues are often lost during mass spectrometry. The residues most likely lost from the Affimer scaffold are histidine and methionine. Their skeletal structure and associated masses are shown above.

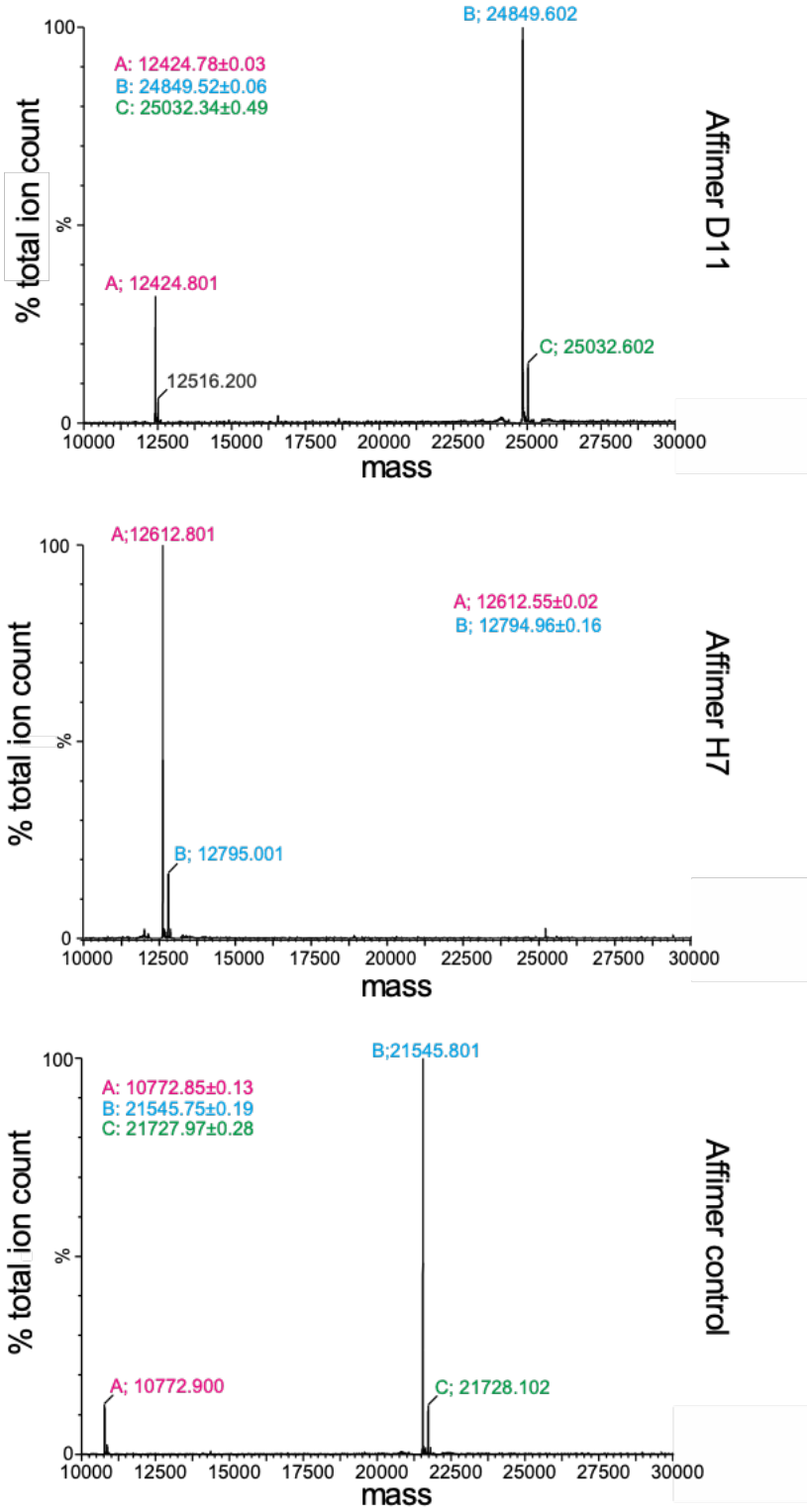


Figure 3.13 Trace of mass spectrometry analysing Affimer with C-terminal cysteine residues.
Denaturing mass spectrometry was undertaken by the Mass Spectrometry facility at the University of Leeds to determine the mass of Affimer D11, H7 and control Affimers. Most abundant peaks are shown in pink, followed by blue and green, if a third main peak was detected. The mass spectrometry facility instrumentation used in this work is supported by the BBSRC (BB/M012573/1) and analysis was carried out by Rachel George.

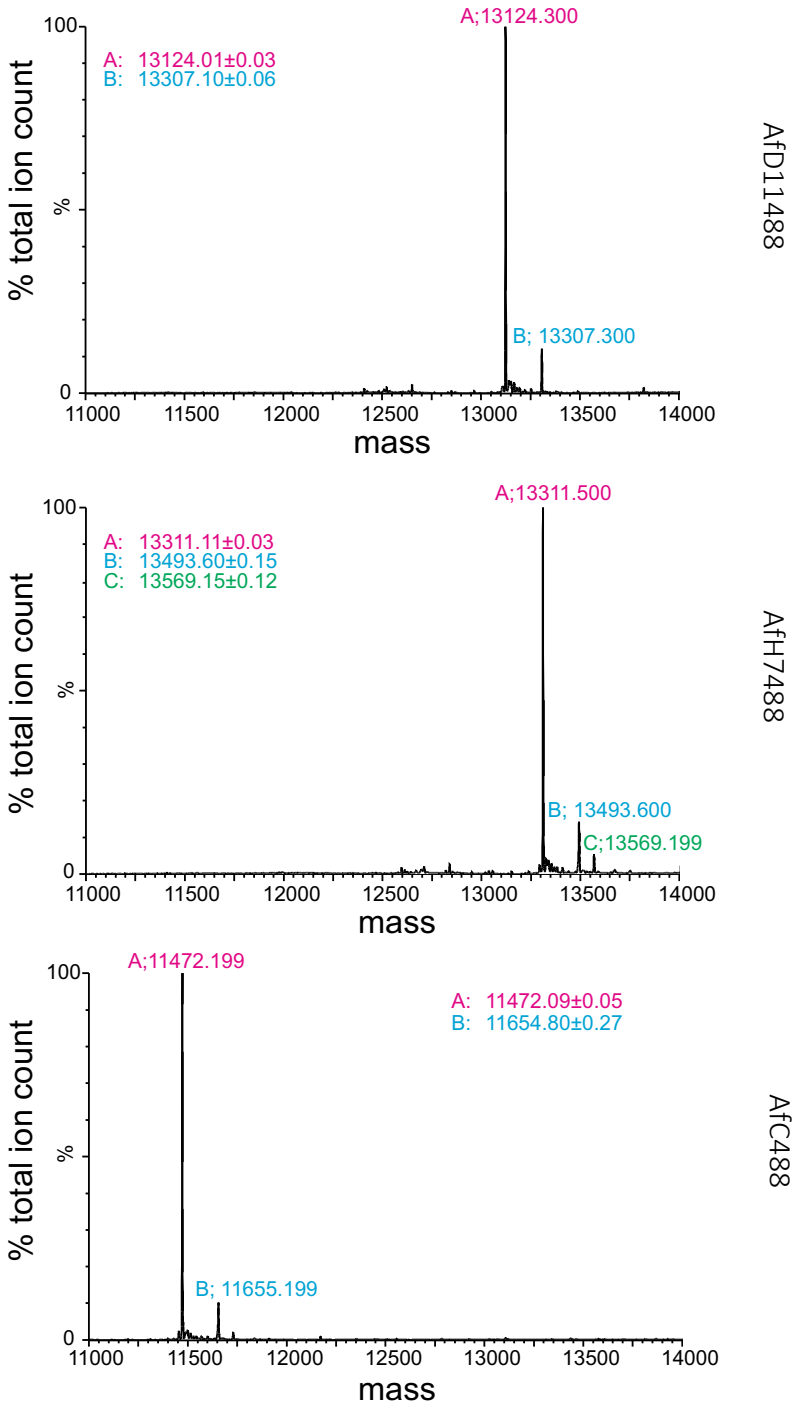


Figure 3.14 Mass spectrometry trace analysing Affimer Alexa Fluor™ 488 conjugates.
Denaturing mass spectrometry was carried out by the Mass Spectrometry facility at the University of Leeds to determine the mass of Affimer D11, H7 and control Alexa Fluor™ 488 conjugates (AfD11488, AfH7488 and AfC488 respectively). Most abundant peaks are shown in pink, followed by blue and green if a third main peak was detected. The mass spectrometry facility instrumentation used in this work is supported by the BBSRC (BB/M012573/1) and analysis was carried out by Rachel George.

	A	B	C	D	E	F	G	H
Affimer	Expected mass	Actual mass	A-B	AlexaFluor 488 mass	B + D	Affimer conjugate actual mass	E-F	Sodium mass
D11	12557.34	12424.80	132.54	720.66	13145.46	13124.30	21.16	22.99
H7	12744.46	12612.80	131.66	720.66	13333.46	13311.50	21.96	22.99
Control	10905.39	10772.90	132.49	720.66	11493.56	11472.20	21.36	22.99

Table 3.2 Comparing the expected and actual mass values determined by LC-MS.
Expected and actual masses were obtained by mass spectrometry and the mass moieties potentially responsible for the mass shifts are shown. **(A)** expected mass of the Affimers calculated using ExPasys ProtParam tool **(B)** actual mass of unconjugated Affimer following mass spectrometry **(C)** difference between expected and actual mass (A-B) **(D)** mass of Alexa Fluor™ 488 maleimide as per manufacturers recommendation **(E)** expected mass of Affimer Alexa Fluor™ 488 conjugate calculated by the actual mass added to the Alexa Fluor™ 488 maleimide mass **(F)** actual mass of conjugates determined by mass spectrometry **(G)** difference in expected mass to actual mass (E-F) **(H)** mass of sodium that could explain the mass shift. All values shown to 2 d.p.

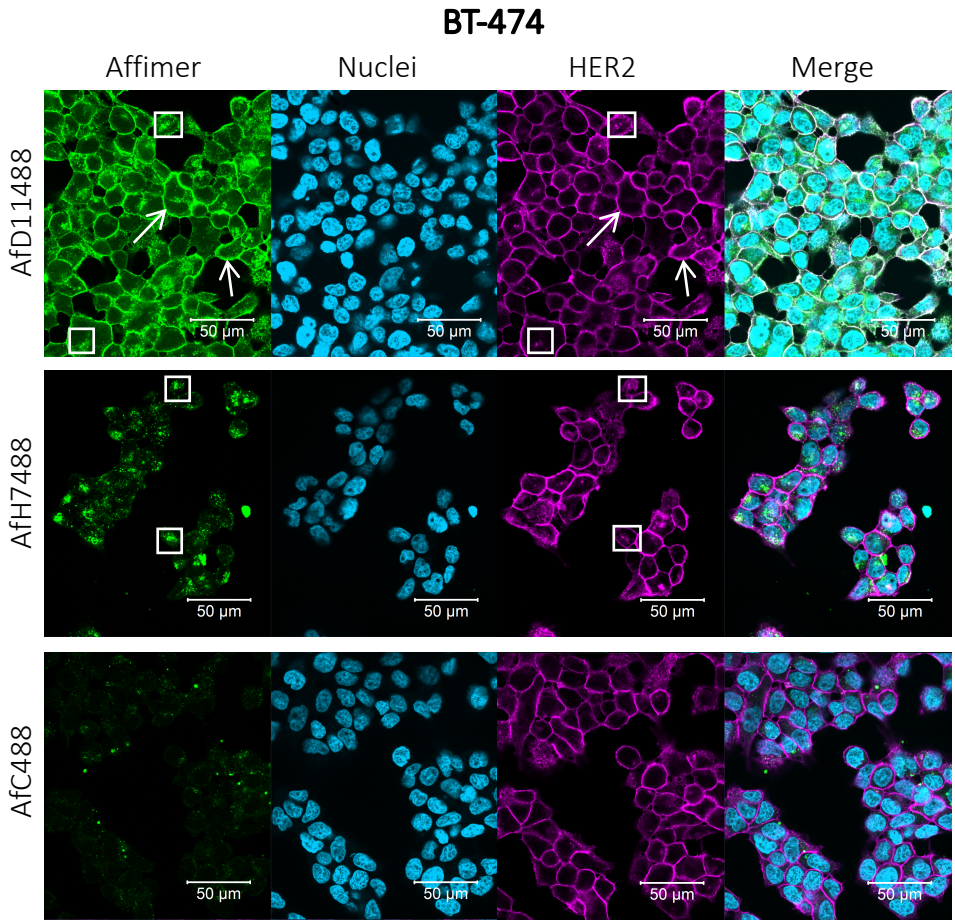
Following LC-MS on conjugated and unconjugated samples a table of expected and actual masses was generated (Table 3.2). The masses of unconjugated Affimer D11, H7 and control were 12424.80, 12612.80 and 10772.90 respectively, deduced by LC-MS. The mass shift between the unconjugated Affimers expected and actual masses were all a loss of ~131 and can be explained by loss of methionine residue from the N-terminus of the Affimer. The expected mass of the Affimer Alexa Fluor™ 488 conjugates was calculated by adding the mass of Alexa Fluor™ 488 (720.66) to the actual mass of unconjugated Affimers identified by LC-MS (Table 3.2, column B). The masses of Affimer conjugates differed from their expected masses by ~21, this can be explained by loss of Na^+ ion in the conjugation reaction as advised by the manufacturer. It was, therefore, concluded that Affimers were successfully conjugated to Alexa Fluor™ 488 by a maleimide link.

3.2.5.2 Investigating Affimer Alexa Fluor 488 conjugate internalisation by HER2+ breast cancer cells

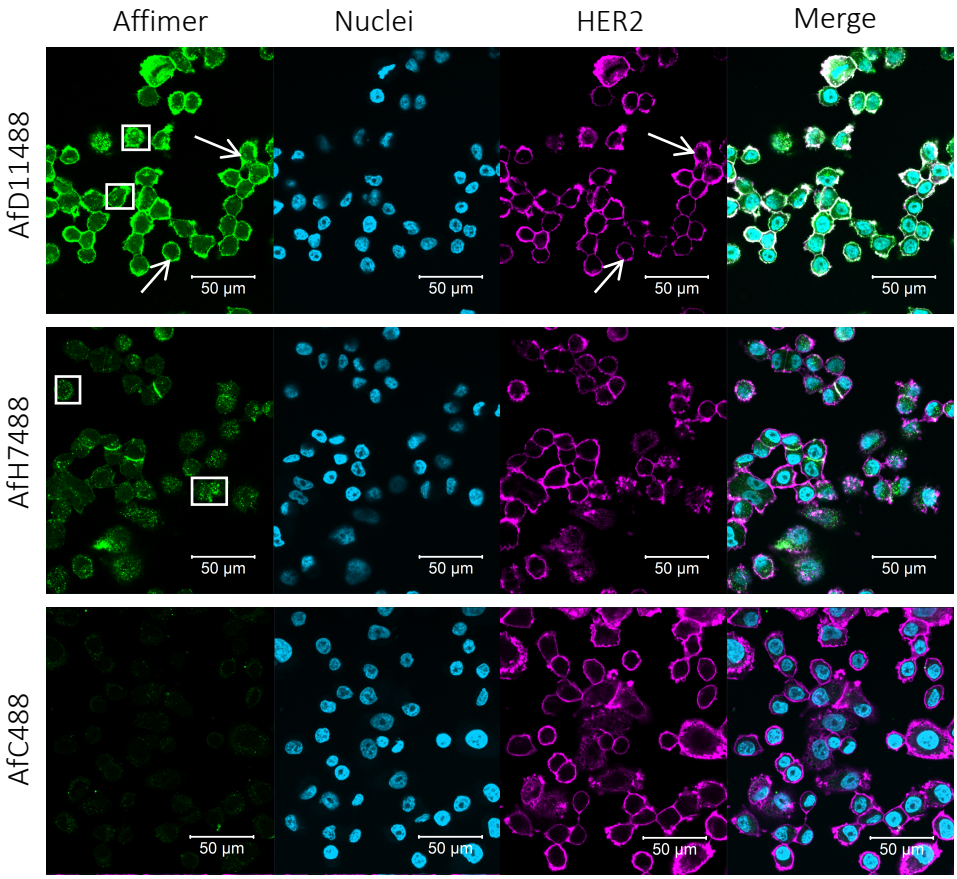
Confocal microscopy was used to analyse Affimer-Alexa Fluor™ 488 internalisation. Previous experiments demonstrated that Affimer D11 and H7 had bound after a 1 hour incubation (data not shown). Concentration of Affimer-Alexa Fluor™ 488 conjugates (in PBS) were low (~100-200 μg/mL). This resulted in a high level of PBS being present when conjugates were diluted in optiMEM for incubation on cell lines.

Therefore, conjugates were incubated on cells for 1 hour to limit the effects of a high PBS concentration on cell growth and morphology.

HER2 binding Affimer Alexa Fluor™ conjugates Affimer D11 Alexa Fluor™ 488 (AfD11488) and Affimer H7 Alexa Fluor™ 488 (AfH7488) were successfully internalised by HER2 overexpressing cell lines AU-565 and BT-474 specifically whilst the Affimer control Alexa Fluor™ 488 (AfC488) was not (data not shown). Initial data demonstrating Affimer Alexa Fluor™ 488 internalisation was repeated twice prior to co-localisation studies. Following confirmation of internalisation, co-localisation of Affimer with anti-HER2 antibody and anti-His antibody were analysed, again, by confocal microscopy. Localisation of both Affimers was similar to what had been identified in previous experiments with unconjugated Affimer (3.2.4). AfD11488 demonstrated a high level of membrane staining and co-localisation with HER2 in both HER2 overexpressing cell lines AU-565 and BT-474 but not the negative cell line MDA-MB-231 (Figure 3.15). There is also evidence of internalisation by AfD11488, although co-localisation with HER2 of internalised AfD11488 is not so obvious in both AU-565 and BT-474 cell lines. AfH7488 did not exhibit high levels of membranous staining. However, AfH7488 shows evidence of internalisation by both HER2 overexpressing cell lines. AfC488 demonstrated little background fluorescence in all cell lines. AfD11488 and AfH7488 showed low levels of fluorescence in the MDA-MB-231 cell line.


BT-474
Affimer
Nuclei
HER2
Merge
AfD11488
AfH7488
AfC488
50 µm

AU-565



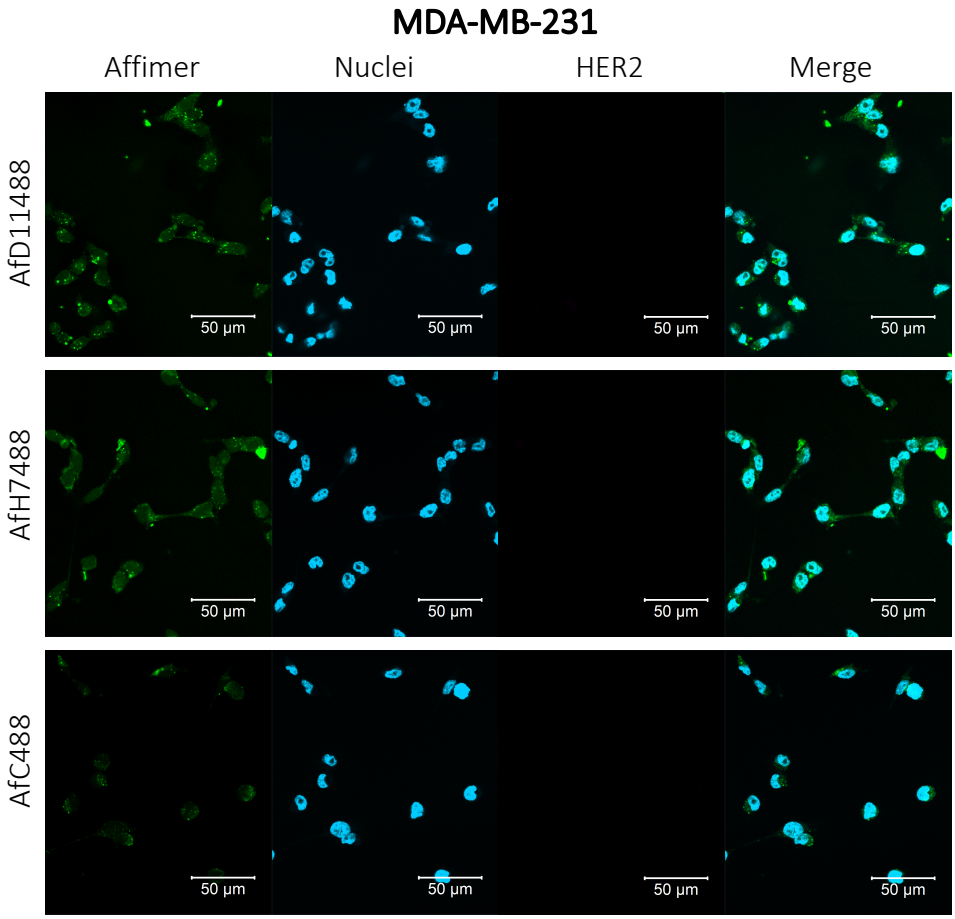
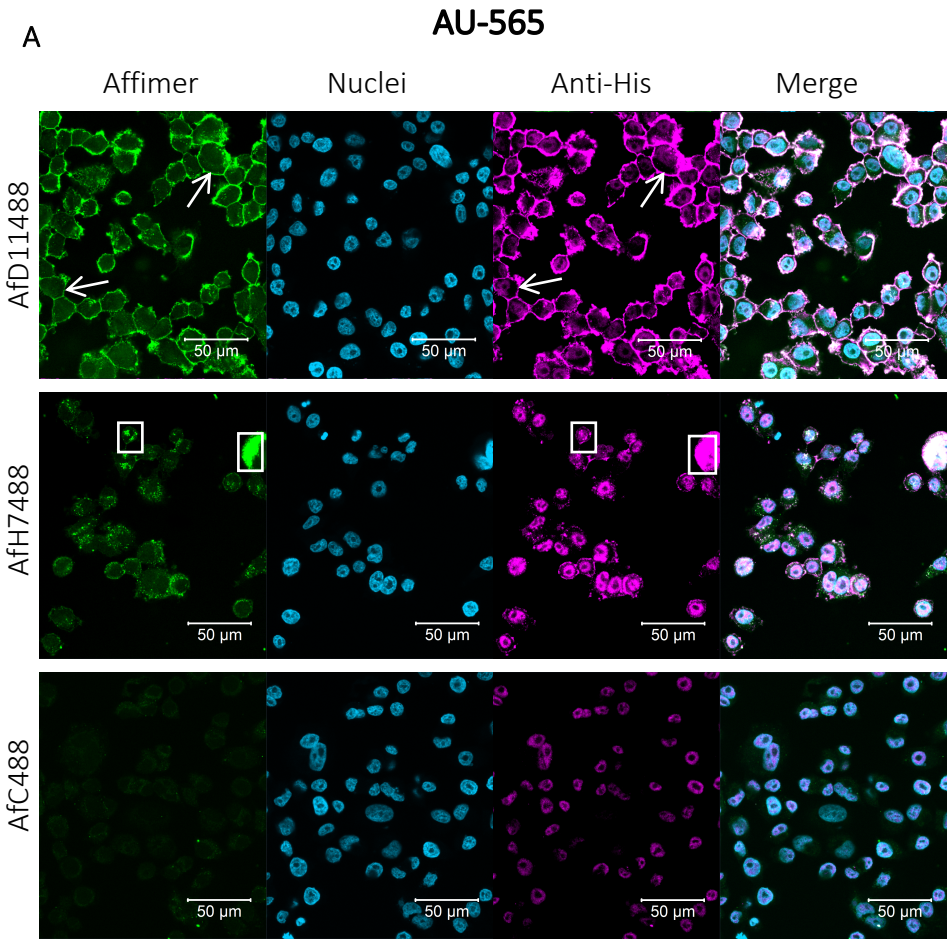


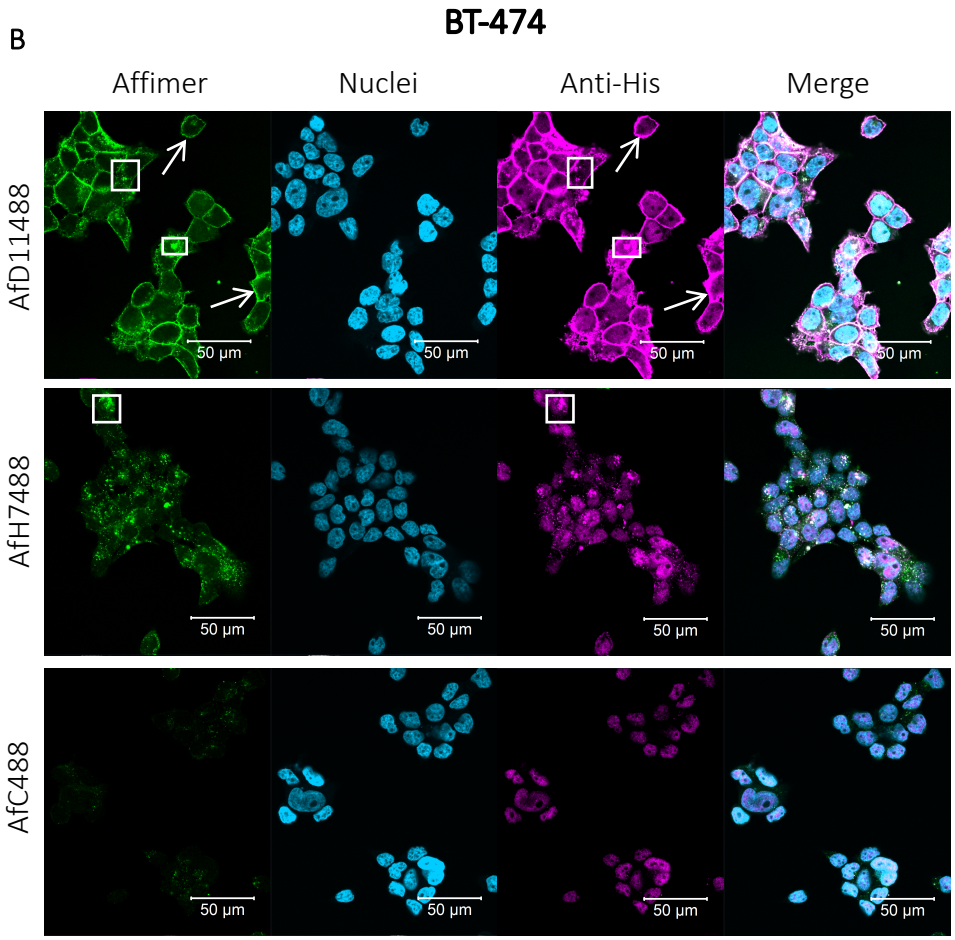
Figure 3.15 Co-localisation of Affimer Alexa Fluor™ 488 conjugates with HER2 using confocal microscopy.
Breast cancer cell lines **(A)** AU-565 **(B)** BT-474 and **(C)** MDA-MB-231 were incubated with Affimer Alexa Fluor™ 488 (green) to observe potential co-localisation with HER2 (pink). Hoescht nuclear stain was also used (blue). Regions of potential membrane co-localisation is indicated by white **ARROWS**. White **BOXES** represent areas of potential internalised Affimer with/without co-localisation with HER2. Images were taken on a Zeiss confocal microscope with a 40x magnification. n=1.

3.2.5.3 HER2 specific Affimer Alexa Fluor™ 488 co-localisation with anti-His antibody

Some background fluorescence is observed in the HER2 negative cell line MDA-MB-231 when incubated with HER2 binding Affimer Alexa Fluor™ 488 conjugates. As Affimers contain a polyhistidine tag, co-localisation with an anti-His antibody using confocal microscopy was used to investigate whether fluorescence was due to unspecific binding of HER2 binding Affimer Alexa Fluor™ 488 conjugates or due to unconjugated Alexa Fluor™ 488.

Co-localisation between membranous AfD11488 staining and anti-His can be observed in both HER2 positive cell lines AU-565 and Bt-474 (Figure 3.16A and B). Internalised AfD11488 showed some evidence of co-localisation with anti-His antibody staining, however this staining is less clear than that observed for BT-474 that had distinguishable co-localisation of internalised Affimer with anti-His. AfH7488, as previously shown, was found at low levels on the cell membrane and was more evident in the cell cytoplasm. AfH7488, again, is more visible in the BT-474 cell line compared to AU-565 in the cytoplasm. Negligible amounts of fluorescence was observed following incubation with AfC488, but of the fluorescence that was detected this did not appear to co-localise with anti-His in any of the three cell lines. AfD11488 and AfH7488 show low level fluorescence in the HER2 negative cell line MDA-MB-231 (Figure 3.16C). Evidence suggests that this background is due to unconjugated Alexa Fluor™ 488 opposed to unspecific binding of Affimers.




B
BT-474
Affimer
Nuclei
Anti-His
Merge
AfD11488
AfH7488
AfC488
50 µm

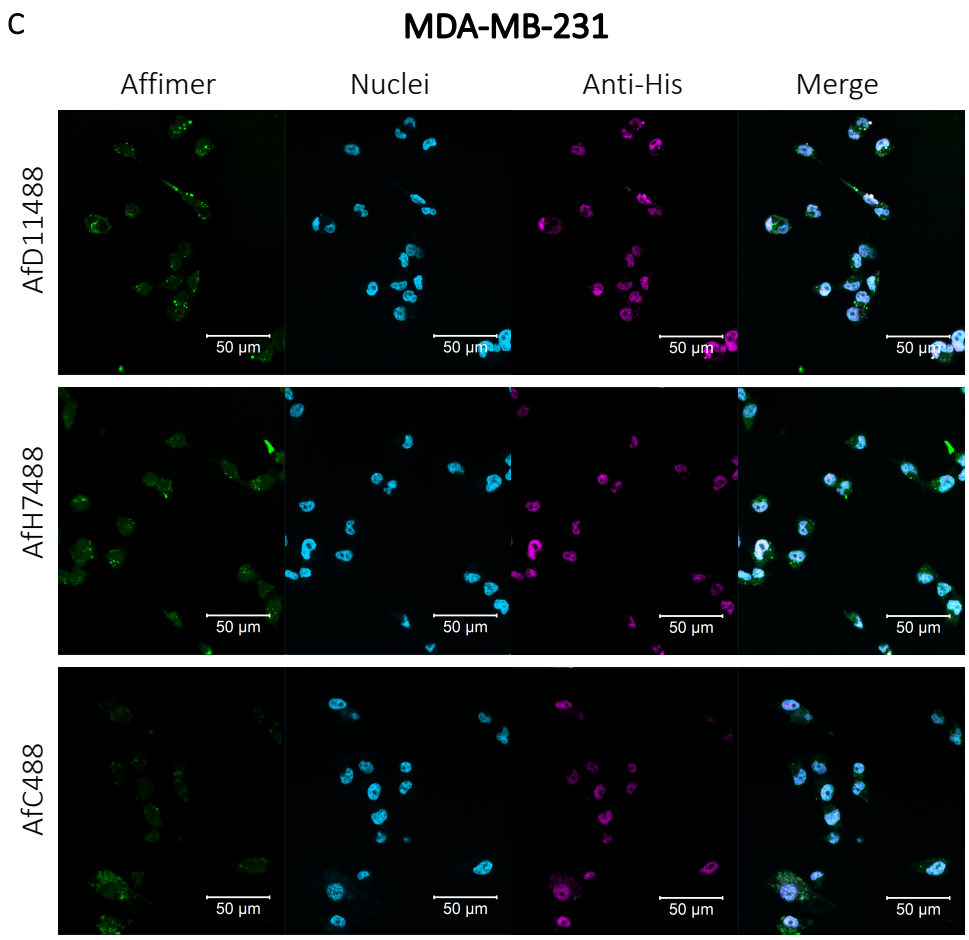


Figure 3.16 Co-localisation of Affimer Alexa Fluor™ 488 conjugates with HER2 observed by confocal microscopy.
Breast cancer cell lines **(A)** AU-565 **(B)** BT-474 and **(C)** MDA-MB-231 were incubated with Affimer Alexa Fluor™ 488 (green) to observe potential co-localisation with anti-His (pink). Hoescht nuclear stain was also used (blue). Regions of potential membrane co-localisation is indicated by white **ARROWS.** White **BOXES** represent areas of potential internalised Affimer with/without co-localisation with anti-His. Images were taken on a Zeiss confocal microscope with a 40x magnification under the same exposure. Images were analysed using ZenLite software. n=2.

To better visualise the cellular location of AfD11488 and AfH7488 in cell lines AU-565 and BT-474 images with higher magnification were generated (Figure 3.17). These images demonstrate the clear intercellular location (white boxes) of both Affimers in BT-474 cells with a high level of co-localisation with anti-his antibody (Figure 3.17B). In AU-565 cells internalisation of AfD11488 is less clear and where Affimer is internalised it is not clearly co-localising with the anti-His antibody (Figure 3.17A).

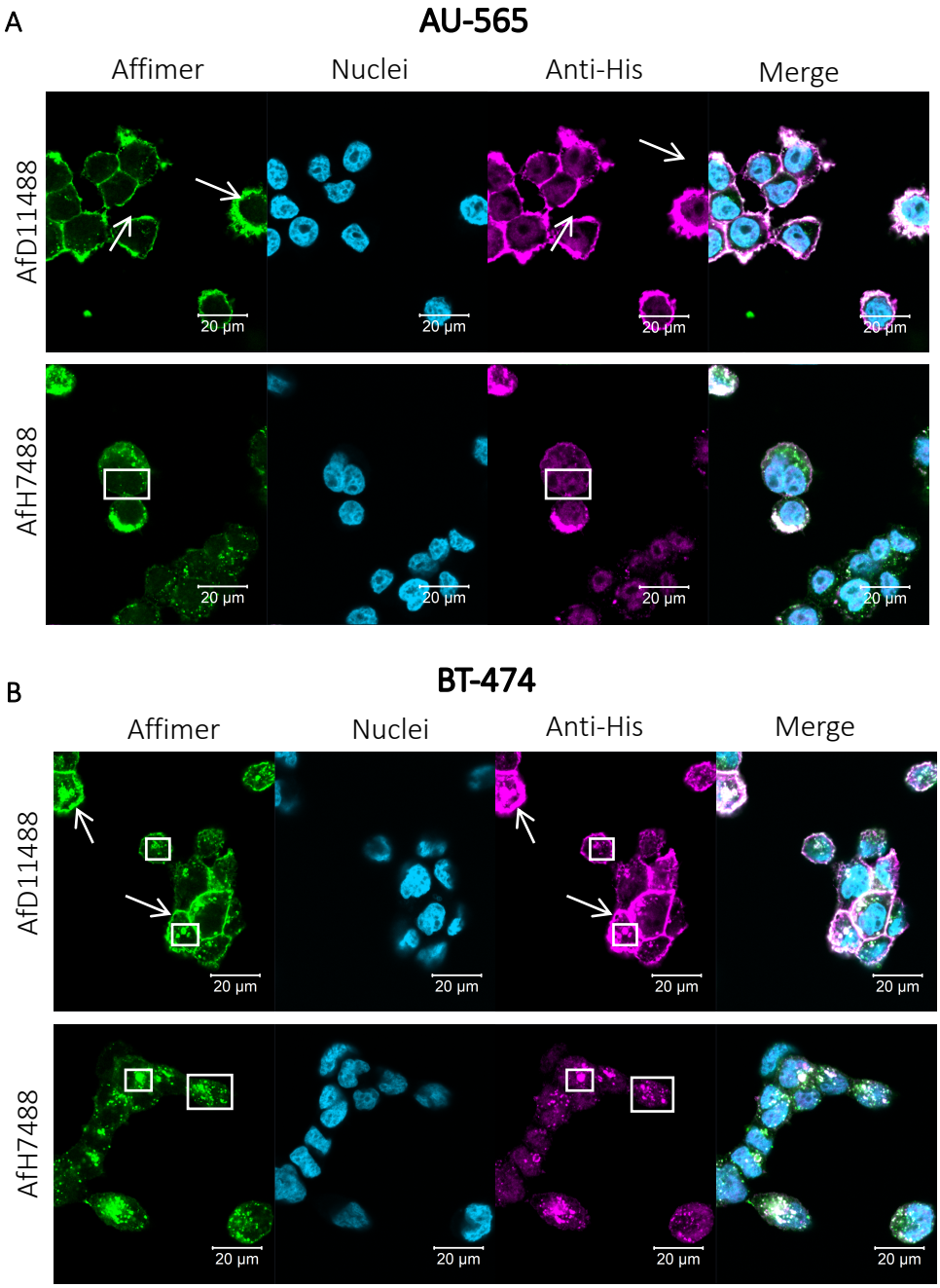


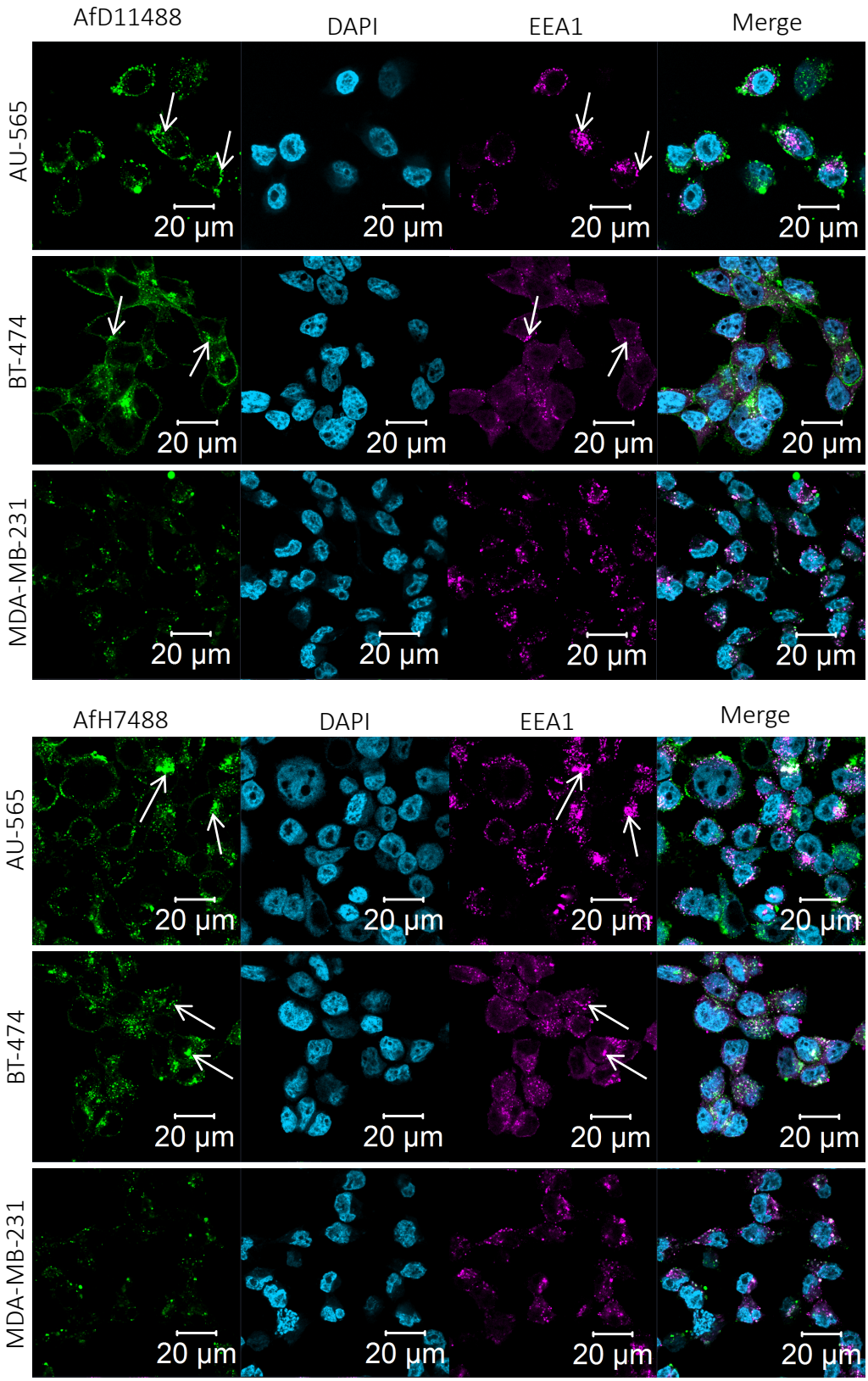
Figure 3.17 Affimer Alexa Fluor™ 488 conjugate co-localisation with anti-His zoomed in.
Breast cancer cell lines **(A)** AU-565 **(B)** BT-47 were incubated with Affimer Alexa Fluor™ 488 (green) to observe potential co-localisation with anti-His (pink). Hoescht nuclear stain was also used (blue). Regions of potential membrane co-localisation is indicated by white **ARROWS.** White **BOXES** represent areas of potential internalised Affimer with/without co-localisation with anti-His. Images were taken on a Zeiss confocal microscope with a 40x magnification under the same exposure. Images were zoomed in when formatting using ZenLite software.

3.2.6 Internalisation by receptor mediated endocytosis

To be used as a vehicle to deliver a cytotoxic warhead that is cleaved from the Affimer in lysosomes, Affimers must enter through receptor-mediated endocytosis. HER2 binding AfD11488 and AfH7488 were monitored for their co-localisation with both endosomal and lysosomal markers; early endosome antigen 1 (EEA1) and lysosomal associated membrane protein 2 (LAMP2) respectively (219, 220). Affimer Alexa Fluor™ 488 conjugates were incubated on cells for one hour prior to fixation and antibody staining as explained previously (2.11.2).

AfD11488 and AfH7488 co-localise with EEA1 in HER2 overexpressing cell lines AU-565 and BT-474 indicated by white arrows (Figure 3.18A and Figure 3.18B). Affimer conjugate staining of HER2 negative cell line MDA-MB-231 is also present at a lower level and shows some co-localisation with endosomal marker EEA1 (Figure 3.18C).

Lysosomes are further along the endocytic pathway and so, as expected, lysosomal staining by LAMP2 appears to be more tightly located to the periphery of the nuclei (Figure 3.19). There is little co-localisation between Affimers and LAMP2 following 1 hour incubation. This may be accounted for as lysosomes are further down the endocytic pathway so Affimer conjugates may, therefore, need a longer incubation period in order to be visualised in these vesicles.


AfD11488
DAPI
EEA1
Merge
AU-565
BT-474
MDA-MB-231
20 µm
AfH7488
DAPI
EEA1
Merge
AU-565
BT-474
MDA-MB-231
20 µm

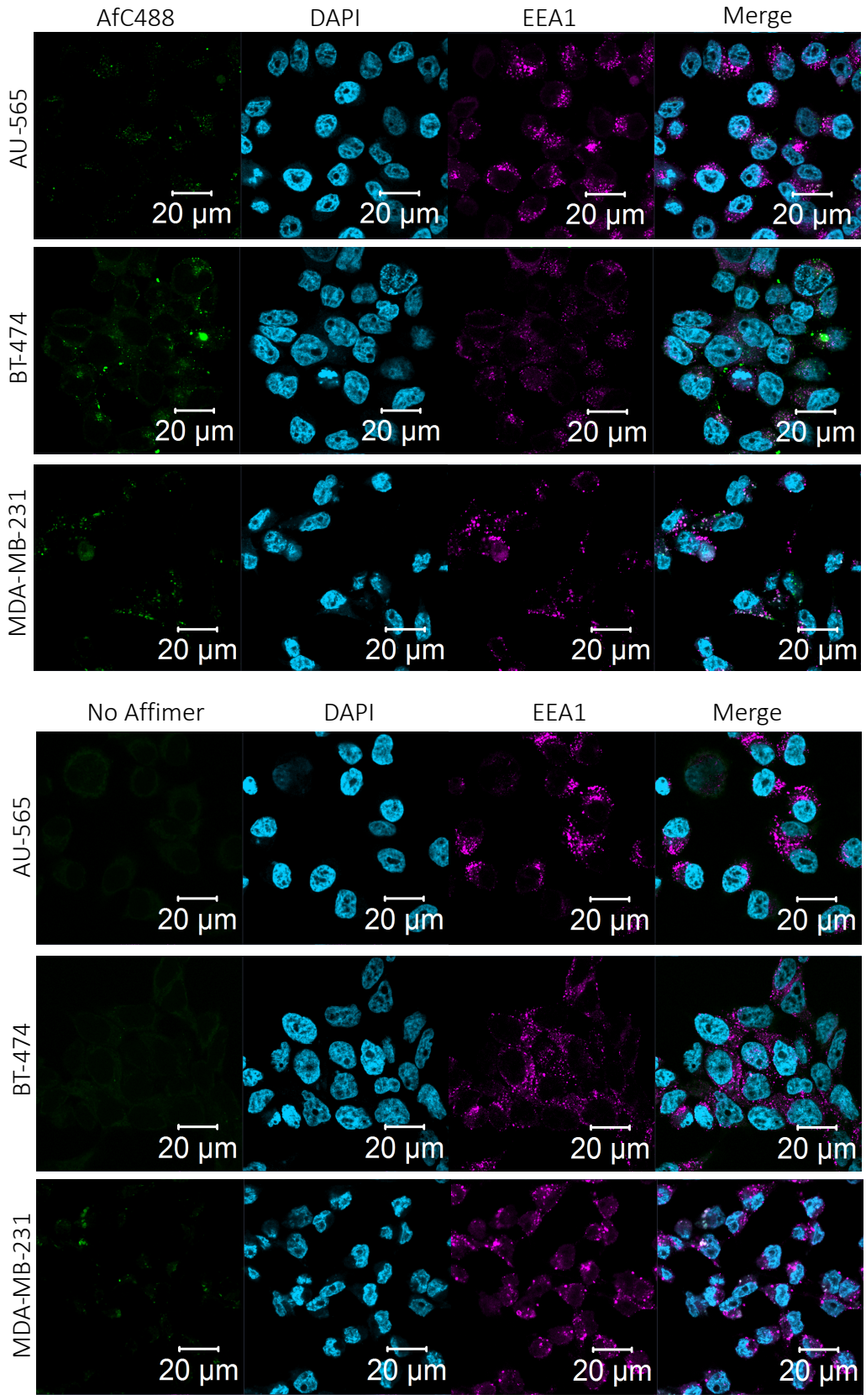
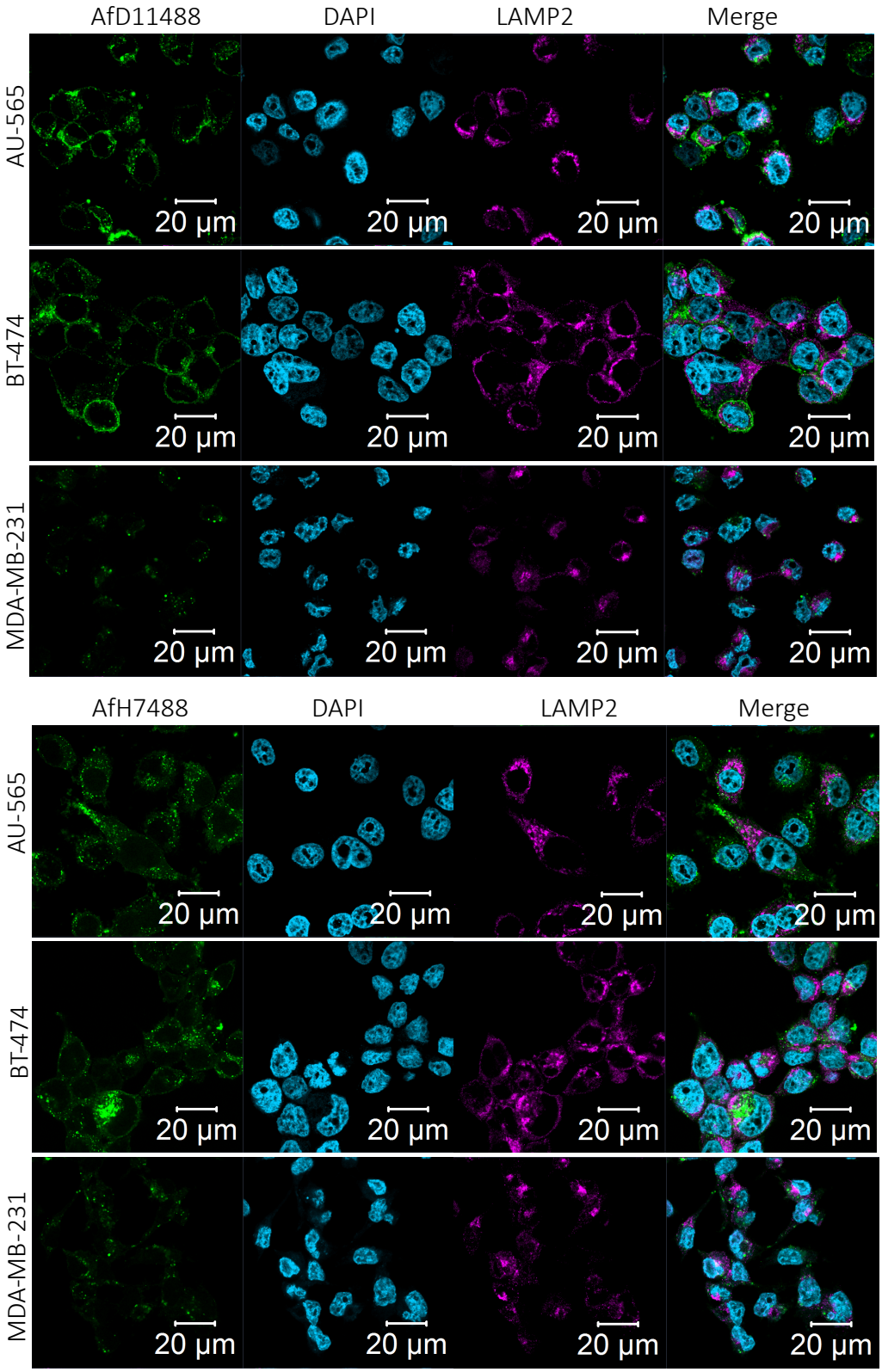


Figure 3.18 Co-localisation of Affimer Alexa Fluor™ 488 conjugate with EEA1 observed by confocal microscopy. Cell lines AU-565, BT-474 and MDA-MB-231 were incubated with **(A)** AfD11488 **(B)** AfH7488**(C)** AfC488 488 and **(D)** no Affimer respectively for 1 hour prior to fixing, permeabilisation and staining of early endosome antigen 1 (EEA1)(magenta). Nuclei were visualised by DAPI present in the mounting media. Images were taken using a Zeiss inverted confocal microscope with 40x magnification. All images were subjected to the same exposure. Images are representative of n=2.


AfD11488
DAPI
LAMP2
Merge
AU-565
BT-474
MDA-MB-231
20 µm
AfH7488
DAPI
LAMP2
Merge
AU-565
BT-474
MDA-MB-231
20 µm

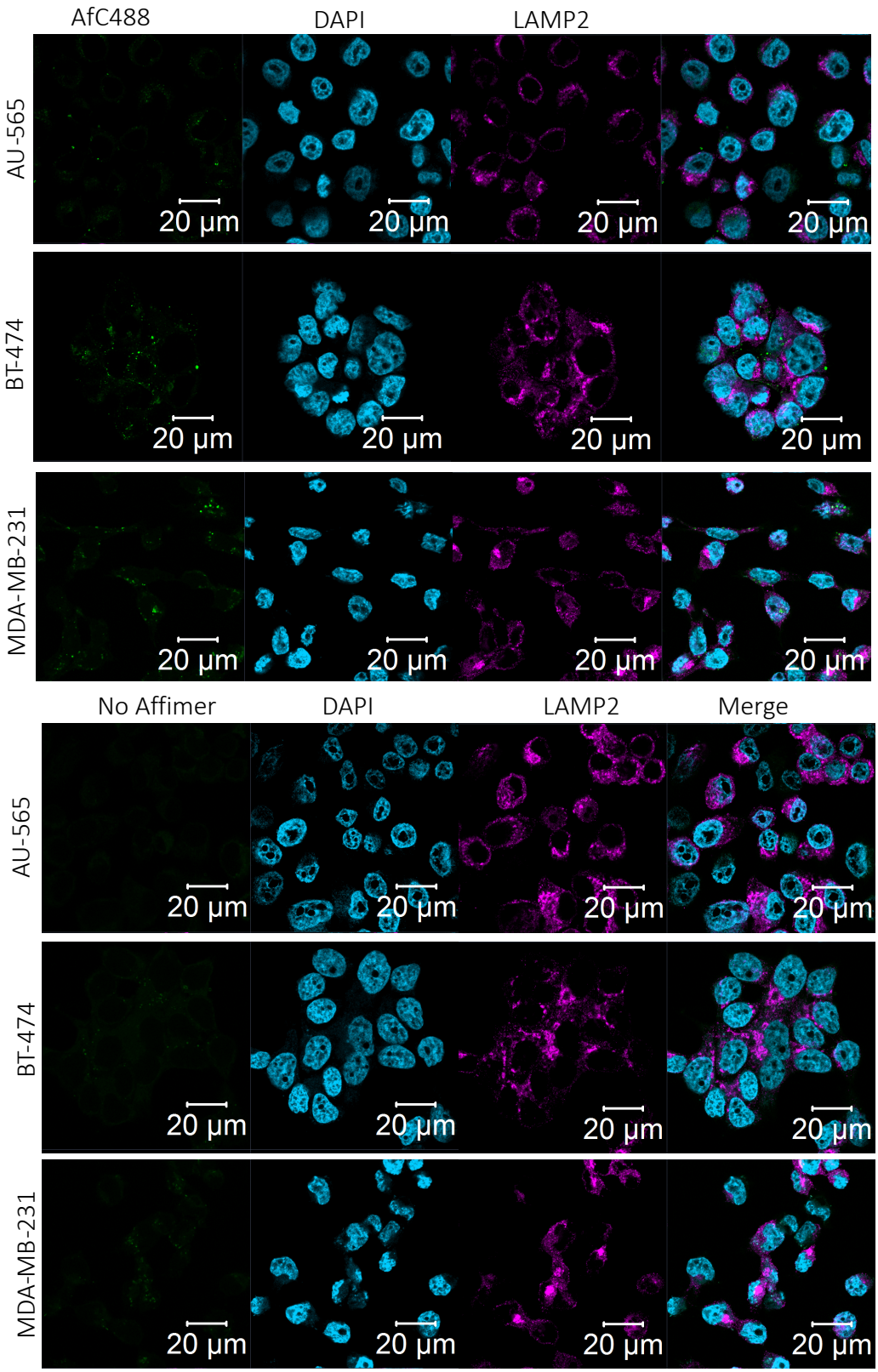


Figure 3.19 Co-localisation of Affimer Alexa Fluor™ with LAMP2 observed by confocal microscopy.
Cell lines AU-565, BT-474 and MDA-MB-231 were incubated with **(A)** AfD11488 **(B)** AfH7488 **(C)** AfC488 and **(D)** no Affimer respectively for 1 hour prior to fixing, permeabilisation and staining of lysosomal associated marker 2 (LAMP2)(magenta). Nuclei were visualised by DAPI present in the mounting media. Images were taken using a Zeiss inverted confocal microscope with 40x magnification. All images were subjected to the same exposure. Images are representative of n=2.

3.3 Chapter summary and future perspectives

In this chapter, eight previously isolated HER2 binding Affimers were characterised. Six of the Affimers successfully precipitated endogenous HER2 from cell lysates whilst Affimer D11 and H7 were also internalised by HER2 overexpressing cell lines when analysed by immunofluorescence.

3.3.1 HER2 binding Affimers are not effective in breast cancer cell lines compared to Trastuzumab

Unconjugated HER2 binding Affimers exerted no inhibitory effects on breast cancer cell lines whilst Trastuzumab did. Studies have suggested that the mechanism of action of Trastuzumab is mainly through antibody dependent cellular cytotoxicity (ADCC) (221). It is possible Trastuzumab would have a greater effect on breast cancer cells in a more physiologically accurate environment where natural killer (NK) cells are present and able to contribute to ADCC. It is clear, however, that neither Affimer D11 or H7 exert the same inhibitory response as Trastuzumab alone in cell lines. Analysis of the literature insinuates that no HER2 binding non-immunoglobulin scaffold has a detrimental effect on cells alone.

3.3.2 Internalisation of HER2 binding Affimers

HER2 binding Affimers did not elicit a response in cell lines, however, they could possibly be used as a vehicle to deliver a cytotoxic element much like ADCs. Following analysis by confocal microscopy it was observed that Affimer reagents conjugated to Alexa Fluor™ 488 were localising to the cytoplasm of HER2 overexpressing cell lines in addition to the membrane. The mechanism of entry for Affimer conjugates was hypothesised to be through the endocytic pathway. Further analysis observing co-localisation with endocytic pathway markers EEA1 and LAMP2 lead to ambiguous results. Immunofluorescence is a qualitative technique and alone does not provide quantitative information about co-localisation. The LysoTracker® dye stains acidic compartments and CellLight™ Late Endosomes-RFP can be used for live cell

immunofluorescence. LysoTracker™ deep red (ThermoFisher Scientific L12492) and CellLight® Late Endosomes-RFP (ThermoFisher Scientific, C10589) could be used to track Affimer AlexaFluor488 conjugate co-localisation in real time allowing better discrimination between suspected and actual co-localisation. Combining the use of these reagents in live cell confocal microscopy with quantitative analysis of co-localisation could provide data that would be less ambiguous to the co-localisation of Affimer conjugates with endosomes and lysosomes (222).

3.3.3 Internalisation of non-immunoglobulin scaffolds

Using non-immunoglobulin scaffolds as vehicles to deliver cytotoxic compounds to cell lines overexpressing HER2 is not a novel idea. HER2 binding Affibodies and DARPins have been internalised via endocytosis following binding to HER2 in previous studies (223, 224). In a similar way to Affimers, the Affibody scaffold contains no cysteine residues and were engineered to contain one for site specific modifications (223). Whilst internalisation of the scaffolds may not be a necessity in the development of a drug conjugate, it is desirable. Currently approved antibody drug conjugates are internalised through receptor mediated endocytosis. Some elicit a bystander effect whereby surrounding cells that do not express the target antigen are also killed due to the drug passing through the cell membrane (225). The linker and drug used in the drug conjugate influences whether the bystander effect occurs. The currently approved antibody drug conjugate for the treatment of HER2 overexpressing breast cancer must be internalised to elicit its therapeutic effect. This is because the cytotoxic moiety DM1 has a positive charge that prevents it being able to pass cell membranes (226). Therefore, going forward these factors should be considered.

3.3.4 Chapter conclusion

The results presented in this chapter demonstrate the potential use of Affimers as a vehicle for drug delivery to HER2 overexpressing cell lines. Previous data using other non-immunoglobulin scaffolds show efficacious results. Preliminary findings

suggesting the internalisation of HER2 binding Affimers D11 and H7 indicate promise for this application.

Chapter 4

Development of HER2 specific Affimer drug conjugates



'Now is no time to think of what you do not have.

Think of what you can do with what there is.'



-Ernest Hemingway

Chapter 4

4 Development of HER2 specific Affimer drug conjugates

4.1 Antibody drug conjugates

HER2 positive breast cancer is primarily treated through chemotherapy alongside targeted therapeutics such as monoclonal antibodies Trastuzumab and Pertuzumab previously described. Trastuzumab has since been conjugated to a cytotoxic moiety to generate an antibody drug conjugate Trastuzumab emtansine (T-DM1, Kadcyla). ADCs utilise a mAb against a cancer specific antigen, such as HER2, for targeted delivery of a cytotoxic payload that is otherwise too toxic to deliver systemically (Figure 4.1). Despite over 60 ADCs being in clinical development only three have received FDA approval (Table 4.1).

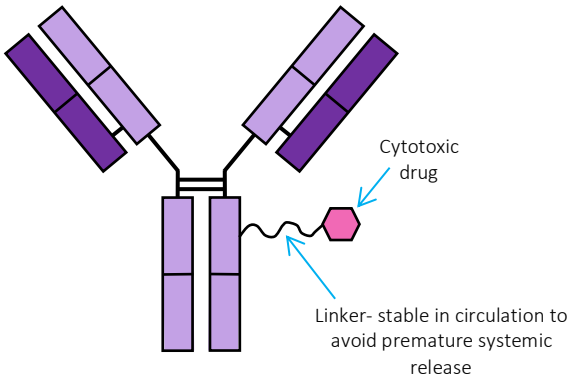


Figure 4.1 Antibody drug conjugate.
Antibodies can be covalently linked to a cytotoxic element via a stable flexible linker attaching the drug covalently to the antibody, which is then released upon internalisation by the cell.

Antibody	Drug	Cytotoxic payload	FDA approved	Company	Target	Disease
Gemtuzumab ozogamicin	Mylotarg®	Ozogamicin	2017	Pfizer	CD33	AML
Ado-tastuzumab emtansine (T-DM1)	Kadcyla™	mertansine	2013	Genentech/Roche	HER2	Metastatic HER2+ breast cancer
Brentuximab vedotin	Adcetris®	MMAE	2011	Seattle Genetics	CD30	Hodgkins Lymphoma and ALCL

Table 4.1 FDA approved antibody-drug-conjugates for treatment of cancer.
Three antibody-drug-conjugates currently have FDA approval for clinical use. Abbreviations; acute myeloid lukaemia (AML), anaplastic large cell lymphoma (ALCL).

4.1.1 Ado-trastuzumab emtansine (Kadcyla™) for the treatment of HER2+ metastatic breast cancer

T-DM1 was FDA approved in 2013 for the treatment of HER2+ metastatic breast cancer previously treated with trastuzumab and a taxane (227). FDA approval followed the randomised phase III trial EMILIA where patients exhibiting advanced breast cancer that had been previously treated with Trastuzumab and a taxane received either T-DM1 or lapatinib alongside capecitabine (228). T-DM1 was found to significantly improve progression free and overall survival of patients (228). Safety was further acknowledged by the larger randomised trial KAMILLA where the most common adverse events were anaemia, thrombocytopaenia and fatigue (229).

Resistance to T-DM1, as with Trastuzumab, can be *de novo* or acquired. Resistance is not fully understood but potential mechanisms include increased lysosomal pH leading to inefficient cleavage of T-DM1 (230), defective cyclin B1 induction (231), reduced cell surface HER2 expression and decreased phosphatase and tensin homolog (PTEN) expression (232). Although showing promise in a subset of patients a large proportion of patients with advanced disease do not respond to T-DM1 so there is still a need for improved therapeutic intervention strategies to replace or complement current therapeutics.

4.1.2 Emergence of antibody alternative molecules for therapeutic intervention

Although ADCs provide a mechanism to deliver targeted chemotherapy there are drawbacks to their use beyond side effects and drug resistance. Other constraints include their large size limiting their ability to penetrate solid tumours, immunogenicity, difficulties in site specific modifications and high expense to make. As a result, alternative scaffolds are being investigated as therapeutics with many in clinical development (reviewed in (233, 234)). Antibody alternative molecules have advantages over monoclonal antibodies as agents for specific drug delivery. These include their smaller size enabling better tissue penetration of solid tumours (235), cost to produce are lower as most alternative molecules are stably expressed in bacteria, high stability and ability to know how many molecules of drug are present on each molecule due to cysteine availability. Alternative scaffold molecules have been investigated for the treatment of HER2+ breast cancer as modes of activating prodrugs such as nucleoside analogs (236) and enhanced delivery of decaying radionuclides (237).

A HER2 binding DARPin conjugated to a fragment of pseudomonas *aeruginose exotoxin A* lead to inhibition of cellular protein synthesis causing an increased apoptotic response in HER2 overexpressing cells (224). DARPins have also been conjugated to phototoxin miniSOG engineered from *Arabidopsis* phototorpin 2 that lead to HER2 specific cell death when exposed to blue light (150).

Affibodies against HER2 have also been raised. Di-affibody molecule conjugated to auristatin E has been designed to selectively target HER2+ cells (238). HER2 specific Affibody $Z_{HER2:2891}$ was conjugated to cytotoxic maytansine derivative to show cytotoxic effects on HER2+ cells with little bystander effect both as a monomer and dimer (223). HER2 specific Affibody conjugated to auristain E shows efficient killing of HER2 overexpressing cell lines (158). This was later improved through conjugating two Affibody molecules to igG1 FC fragment to increase size resulting in a prolonged half-life (239).

4.1.3 Aim

Affimers are another example of a scaffold molecule. The aim of this chapter was to conjugate HER2 specific Affimers D11 and H7, characterised in Chapter 3, to the cytotoxic payload MMAE and test their effects on a range of breast cancer cell lines.

4.2 Results

4.2.1 Conjugation of Affimer to antineoplastic warhead

4.2.1.1 Cytotoxic moiety monomethyl auristatin E (MMAE)

Affimers alone had little effect on metabolic activity and variable effects on cell number of breast cancer cell lines. Affimers D11 and H7 are internalised specifically by HER2 overexpressing cells when conjugated to Alexa Fluor™ 488 and have potential to act as a vehicle for the delivery of a cytotoxic anti-neoplastic warhead. In order to generate a successful Affimer drug conjugate certain criteria have to be met. An appropriate attachment group and linker have to be chosen that is stable in the bloodstream to minimise premature release. The drug monomethyl auristatin E (MMAE) was purchased from BroadPharm therapeutics containing a maleimide group for site specific conjugation, a cathepsin cleavable linker that consists of valine and citrulline amino acid residues and a p-aminobenzyloxycarbonyl (PABC) spacer (Figure 4.2). Cathepsin B is a conserved cysteine protease located in lysosomes of mammalian cells (240). The self immolative PABC spacer provides Cathepsin B enough room to cleave at the citrulline-PABC amide bond (241). Such chemistry has been used in FDA approved ADC brentuximab vedotin (Adcetris) for the treatment of Hodgkin lymphoma and systemic anaplastic large cell lymphoma (242). The conjugation protocol for site specific conjugation of Affimers via a maleimide reacting group has previously been optimised making the VC-PABC-MMAE drug an appropriate choice for conjugation to Affimers (Figure 4.2).

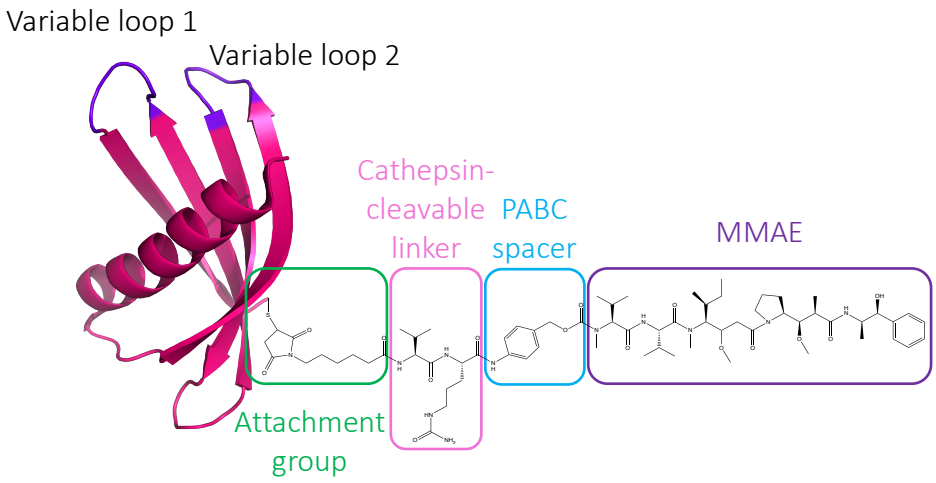


Figure 4.2 Hypothetical image demonstrating conjugation of Affimer to MMAE.
Schematic to show the hypothetical conjugation of Affimer to monomethyl auristatin E. Affimer ribbon diagram (PDB 4N6T) conjugated to MC-VC-PABC-MMAE (skeletal formula) molecule by a thioether bond. Each section of the molecule is labelled.

4.2.2 Conjugation of Affimer to antineoplastic warhead

Whilst HER2 binding Affimers had little effect on cell lines alone, AfD11488 and AfH7488 were internalised by HER2 overexpressing cell lines (3.2.5.2). We therefore wanted to investigate the potential use of these Affimers for the specific delivery of an antineoplastic warhead. Affimer D11, H7 and Affimer control were conjugated to the cytotoxic moiety monomethyl auristatin E (MMAE) (AfD11MMAE, AfH7MMAE and AfCMMAE respectively). MMAE is an antimitotic drug that prevents the polymerisation of tubulin subsequently resulting in apoptosis. The MMAE purchased contained a maleimide attachment group capable of binding to the single N-terminal cysteine residue in the Affimer scaffold to result in a 1:1 drug to Affimer ratio.

4.2.2.1 Confirmation of Affimer drug conjugate purity by SDS-PAGE and mass spectrometry

Affimers were purified as described previously (2.7.3.2) and conjugated to MMAE through a maleimide bond (2.9.2). Purity was analysed by SDS-PAGE (Figure 4.3) that demonstrated a high-level purity. As the molecular weight of MC-VC-PABC-MMAE is 1316.7 the shift in mass is too small to see by SDS-PAGE. To confirm the success of conjugation samples were analysed by LC-MS (2.9.3). There were two main species in

each of the spectra of Affimer drug conjugates (Figure 4.4). In each sample the most prominent peak correlated to the mass of Affimer drug conjugate minus a methionine residue (Table 4.2). All spectra contained a second peak that correlated to the expected mass of the Affimer drug conjugates minus 762 kDa. As all conjugates experienced the same mass shift this could be due to degradation of the MMAE molecule at the same point. However, spectra show a high level of conjugation was achieved.

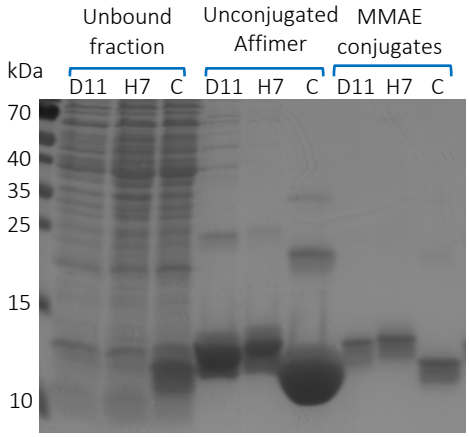


Figure 4.3 SDS-PAGE analysis to confirm the purity of Affimer MMAE conjugates.
Affimer reagents containing a cysteine residue at their C-terminus were purified by Ni-NTA chromatography and reduced by TCEP reducing gel. Reduced Affimers were incubated with monomethyl auristatin E (MMAE) containing a maleimide reactive group. Samples from various fractions were analysed by SDS-PAGE. Fractions show the purity of soluble proteins that did not bind to the nickle beads, the Affimer reagents prior to conjugation and the Affimer reagents following conjugation to MMAE. Gels were stained with Coomassie and destained to remove background. Gels were imaged using an Amersham Imager 600.

	A	B	C	D	E	F
Affimer	Actual mass	MMAE mass	A+B	AfMMAE peak A	AfMMAE peak B	C-D
D11	12424.80	1316.7	13741.5	12979.7	13741.7	761.8
H7	12612.80	1316.7	13929.5	13166.6	13928.8	762.9
Control	10772.90	1316.7	12089.6	11327.9	12089.6	761.7

Table 4.2 Expected and predicted masses of Affimer MMAE conjugates analysed by LC-MS.
Table to demonstrate the expected and actual masses obtained by mass spectrometry of Affimer drug conjugates. **(A)** actual mass of unconjugated previously identified by mass spectrometry that correlated to expected mass minus methionine **(B)** Expected mass of MC-VC-PABC-MMAE **(C)** expected mass of Affimer drug conjugate minus methionine (A+B) **(D)** second most abundant peak following analysis by mass spectrometry **(E)** Most abundant peak following analysis by mass spectrometry **(F)** Difference between expected mass and peak A **(D)**. All values shown to 1 d.p.

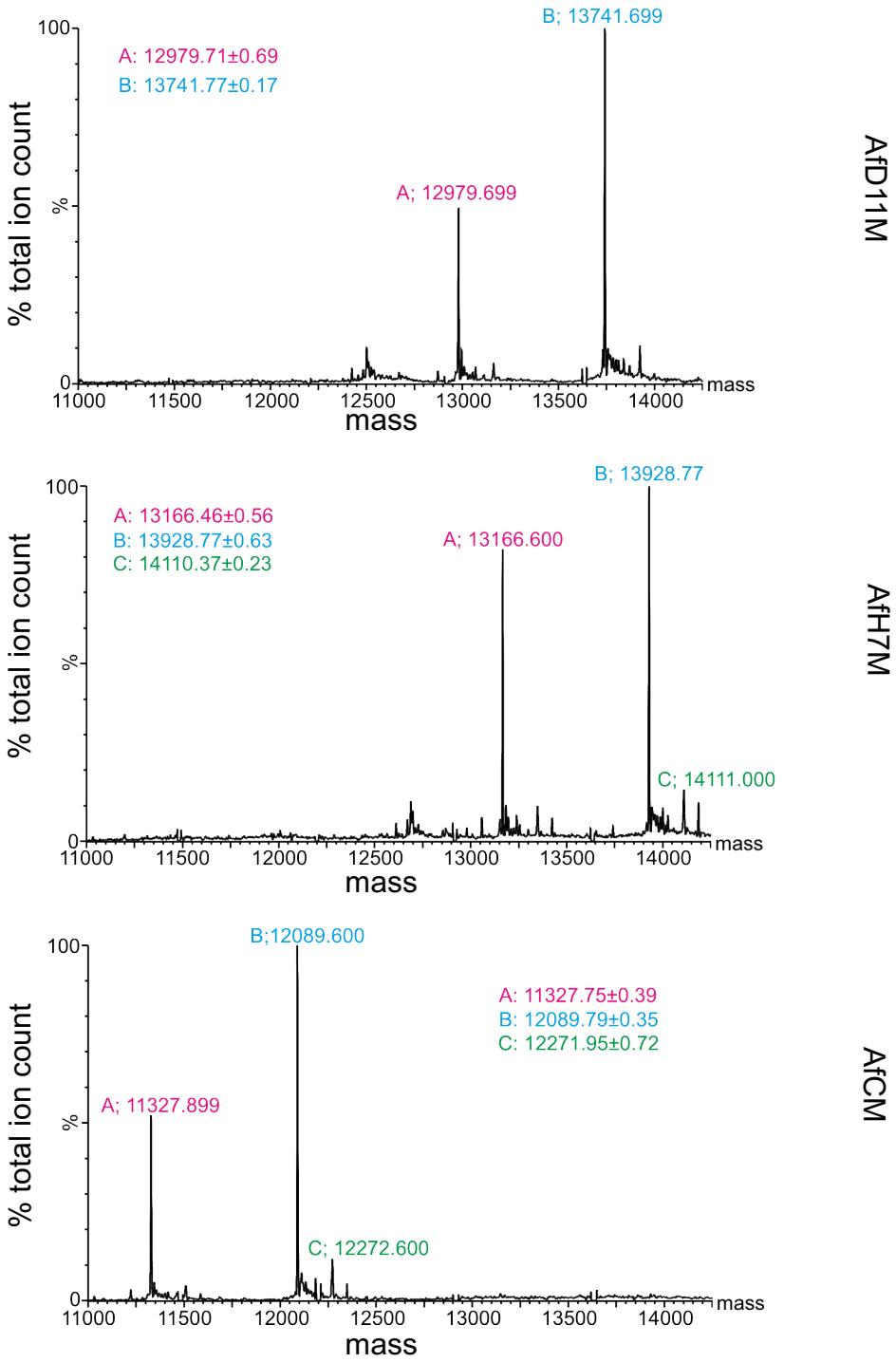


Figure 4.4 Confirming conjugation of Affimer to MMAE by LC-MS.
Denaturing mass spectrometry was carried out by the Mass Spectrometry facility at the University of Leeds to determine the mass of Affimer D11, H7 and control MMAE conjugates (AfD11M, AfH7M and AfCM respectively). Most abundant peaks are shown in pink, followed by blue and green if a third main peak was detected. The mass spectrometry facility instrumentation used in this work is supported by the BBSRC (BB/M012573/1) and analysis was carried out by Rachel George.

4.2.3 Analysing HER2 expression in cell lines by western blot

To confirm HER2 expression levels in cell lines whole cell lysates were subjected to western blot analysis using an antibody against the HER2 extracellular domain. Densitometry was used following western blot to quantify HER2 expression. Cell lines were detached from T-75 flasks using TrypLE Express enzyme, pelleted by centrifugation and stored at -80 °C until used. Cells were lysed and diluted to a concentration of 1.5 mg/ mL prior to SDS-PAGE and western blot (2.8.3).

Eight cell lines were analysed for HER2 expression including three HER2 overexpressing cell lines AU-565, SKBR3 and BT-474, HER2 expressing cell lines MDA-MB-453, MCF-7 and DSH-1 and HER2 negative cell lines MDA-MB-231 and ZR-75-1. Western blot and subsequent densitometry confirmed high levels of HER2 expression in cell lines known to overexpress HER2 (Figure 4.5). MDA-MB-453 expressed moderate levels whilst MCF-7 and DSH-1 expressed low levels. MDA-MB-231 showed no detectable HER2 expression whereas ZR-75-1 had low expression. An additional bladder cancer cell line DSH-1 expressed low levels of HER2.

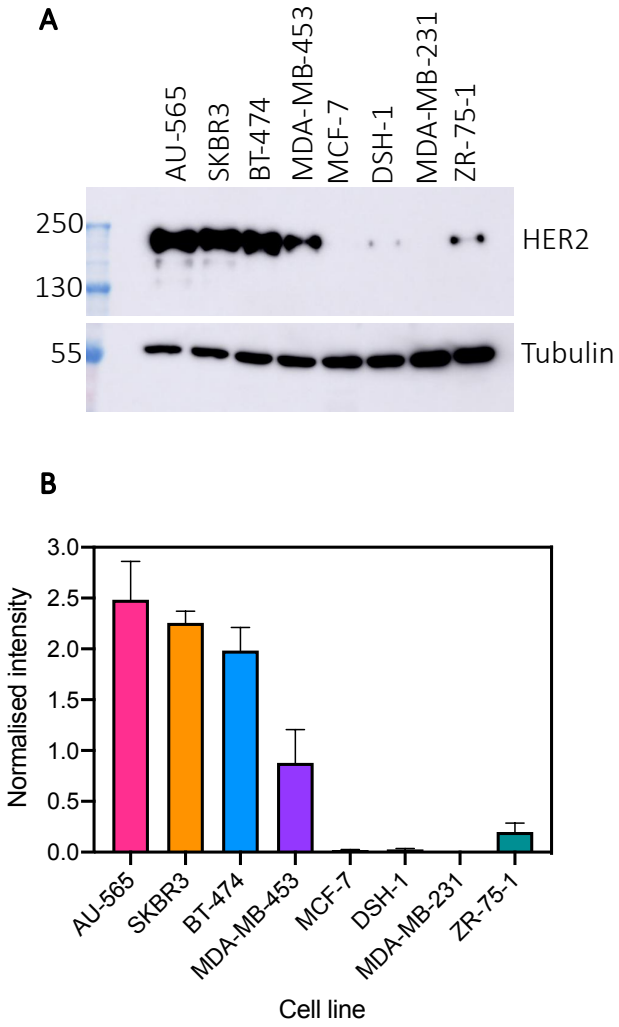


Figure 4.5 Analysis of HER2 expression by western blot and densitometry.
Breast cancer cell lines AU-565 (pink), SKBR3 (orange), BT-474 (blue), MDA-MB-453 (purple), MCF-7 (indigo), MDA-MB-231 (green) and ZR-75-1 (teal) and bladder cancer cell line DSH-1 (red) were analysed for HER2 expression by **(A)** western blot. Tubulin was used as a loading control. **(B)** Bar graphs of HER2 protein densitometry normalised to Tubulin concentrations. Error bars represent standard error of the mean between triplicate repeats. Graph was generated using GraphPad Prism 8. Western blot is representative of n=3, densitometry error bars represent standard error of the mean between repeats where n=3.

4.2.4 Dose responses using Affimer drug conjugates

4.2.4.1 Analysis of metabolic activity using the AlamarBlue assay

Having verified HER2 expression in a panel of cell lines the effect of Affimer drug conjugates was investigated. Cells were seeded into 96 well plates 24 hours before Affimer drug conjugates were added at a range of concentrations from ~1 nM to ~40 nM as per section 2.10.2.2. Following a 72 hour incubation, metabolic activity was analysed by the AlamarBlue assay (2.10.2.2.1). In brief, media was aspirated from 96 well plates and fresh media, containing 10 % AlamarBlue, was added and incubated at 37 °C until a colour change was observed. Colour change was measured using a Tecan Spark microplate reader.

Graphs were plotted initially to include all concentrations tested (Figure 4.6A). From these graphs it was observed that at concentrations of ~15 nM AfD11M and AfH7M had detrimental effects on metabolic activity compared to AfCM. The values at 15 nM were interpolated and plotted as bar graphs to more easily compare the data (Figure 4.6B). At 15 nM both AfD11M and AfH7M exhibit the greatest effect in HER2 overexpressing cell lines AU-565 and SKBR3 reducing metabolic activity to 20 and 30 % respectively at a dose of 15 nM. Metabolic activity of BT-474 cells decreased by around 50 %. Surprisingly cell lines MDA-MB-453 and MCF-7 show a decrease in metabolic activity comparable to each other despite differences in HER2 expression demonstrated by western blot previously (4.2.3). Cell lines MDA-MB-231 and ZR-75-1 are least affected by HER2 specific Affimer drug conjugates experiencing a slight decrease in metabolic activity at higher concentrations. AfCM showed a decrease in metabolic activity at higher concentrations having a greater effect on cell lines that are most responsive to HER2 specific Affimers.

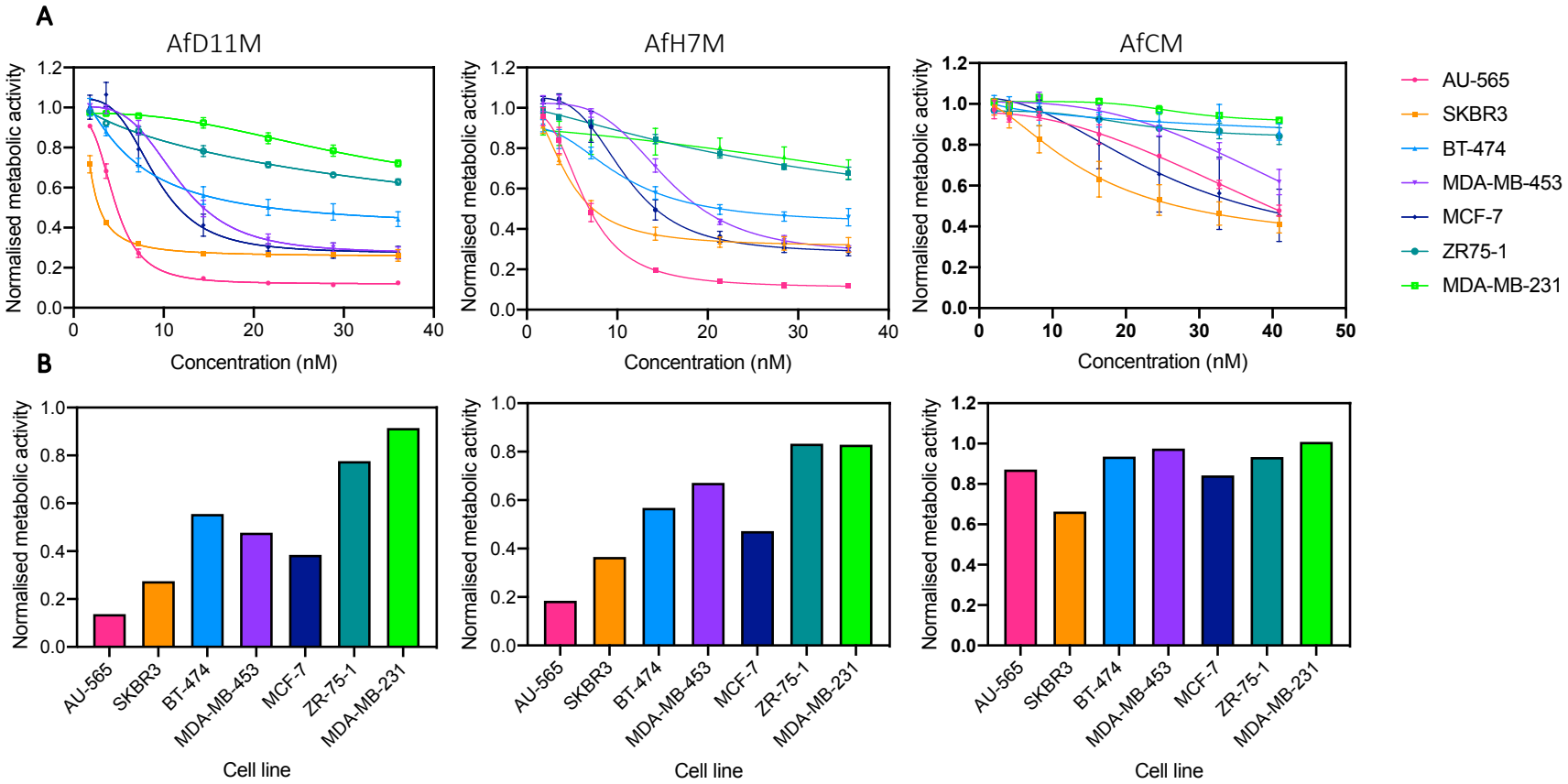


Figure 4.6 Dose response using Affimer-MMAE conjugates on a range of breast cancer cell lines.

A range of breast cancer cell lines AU-565, SKBR3, BT-474, MDA-MB-453, MCF-7, MDA-MB-231 and ZR-75-1 were seeded one day prior to the addition of AfD11M, AfH7M or AfCM. Cells were incubated with Affimer conjugates for a further 72 hours. Metabolic activity was analysed using AlamarBlue that was added to media 10 % v/v. A 100 μL media sample was taken and fluorescence intensity was measured with excitation 560 nm and emission 590 nm using a Tecan Spark Microplate reader. **(A)** Dose response curve with all concentrations of Affimer drug conjugates where error bars represent the standard error of the mean between mean values of three biological replicates. All values were normalised to cells incubated with media alone. **(B)** Values interpolated from **(A)** for 15 nM Affimer drug conjugate.

4.2.4.2 Correlating metabolic activity to cell count data

The AlamarBlue assay demonstrated how the metabolic activity of various cell lines was affected following Affimer drug conjugate incubation. To evaluate if this decrease was due to decreased cell number, nuclear cell counts were performed following the AlamarBlue assay. Such analysis was possible as the AlamarBlue assay is not toxic to cells. Cells were washed with PBS, stained with hoescht and imaged using a ImageXpress Pico Automated Cell Imaging System (2.10.2.2.2).

Cell count data depicted a similar trend to what was observed when analysing metabolic activity showing a decrease in cell count with increasing concentration of Affimer drug conjugate (Figure 4.7A). Increasing concentrations of Affimer drug conjugate seem to have a greater detrimental effect on cell count than what was observed for metabolic activity. The error between biological repeats was larger than that of the AlamarBlue assay. This could be down to error in the software of depicting individual nuclei. Again, cell count values at 15 nM were interpolated and plotted as bar charts to better compare results (Figure 4.7B). The trend at 15 nM mirrored what was observed with metabolic activity.

To visualise data collated by the Pico software sample images were taken at concentrations of 0.2 μg/mL (~ 15 nM) AfD11M and AfCM in cell lines AU-565, BT-474 and MDA-MB-231 (Figure 4.8). Following AfD11M incubation AU-565 have very few cells visible when imaged with large masses of black and disordered morphology when observed by transmitted light consistent with cell death (Figure 4.8A) with a stark difference to when incubated with AfCM or no Affimer. The cell line BT-474, again, have large masses of black cells consistent with cell death with a decrease in cell number when incubated with AfD11M compared to controls (Figure 4.8B). The triple negative cell line MDA-MB-231, however, showed no changes in cell morphology or cell number when observed visually (Figure 4.8C).

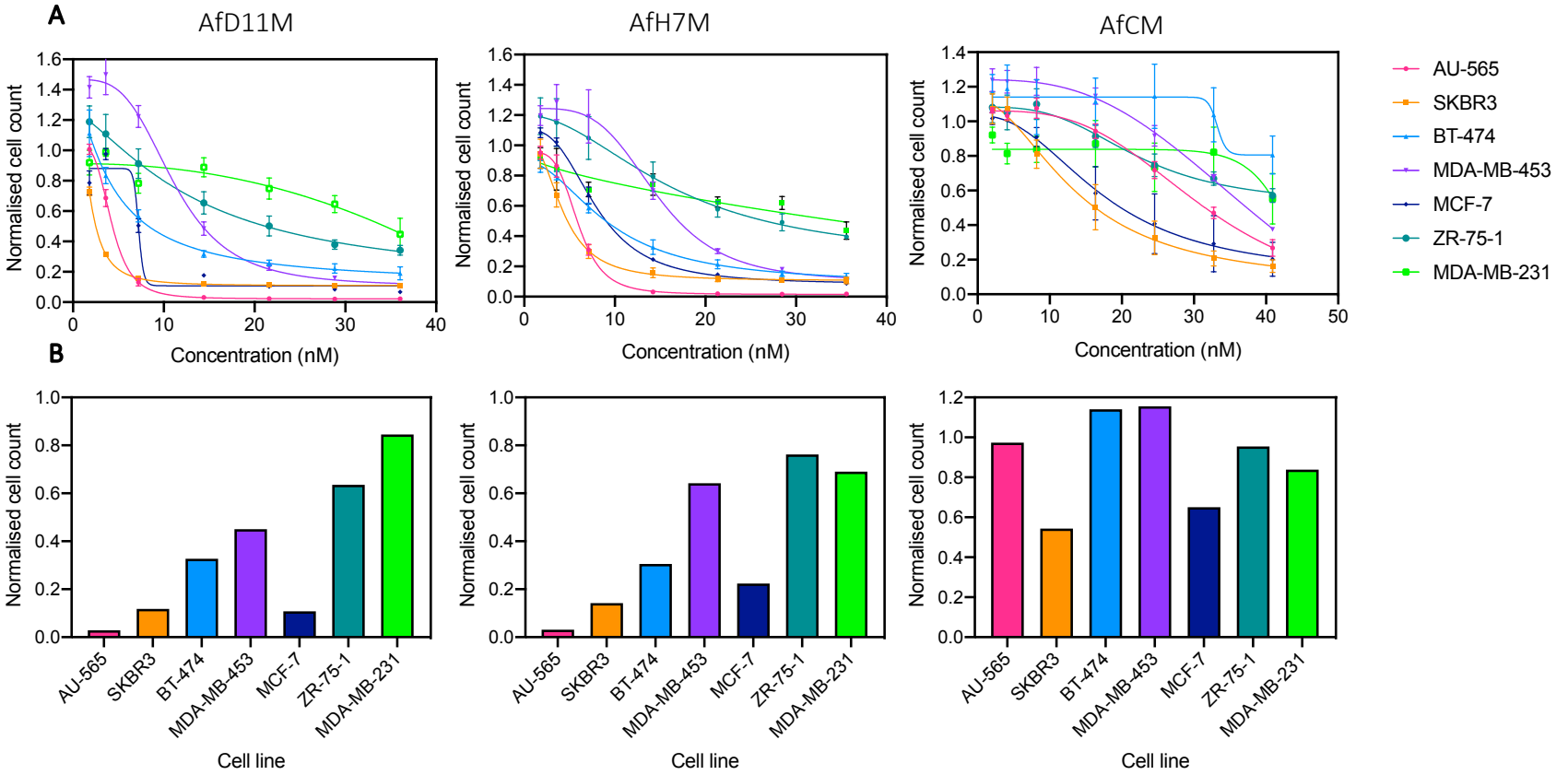
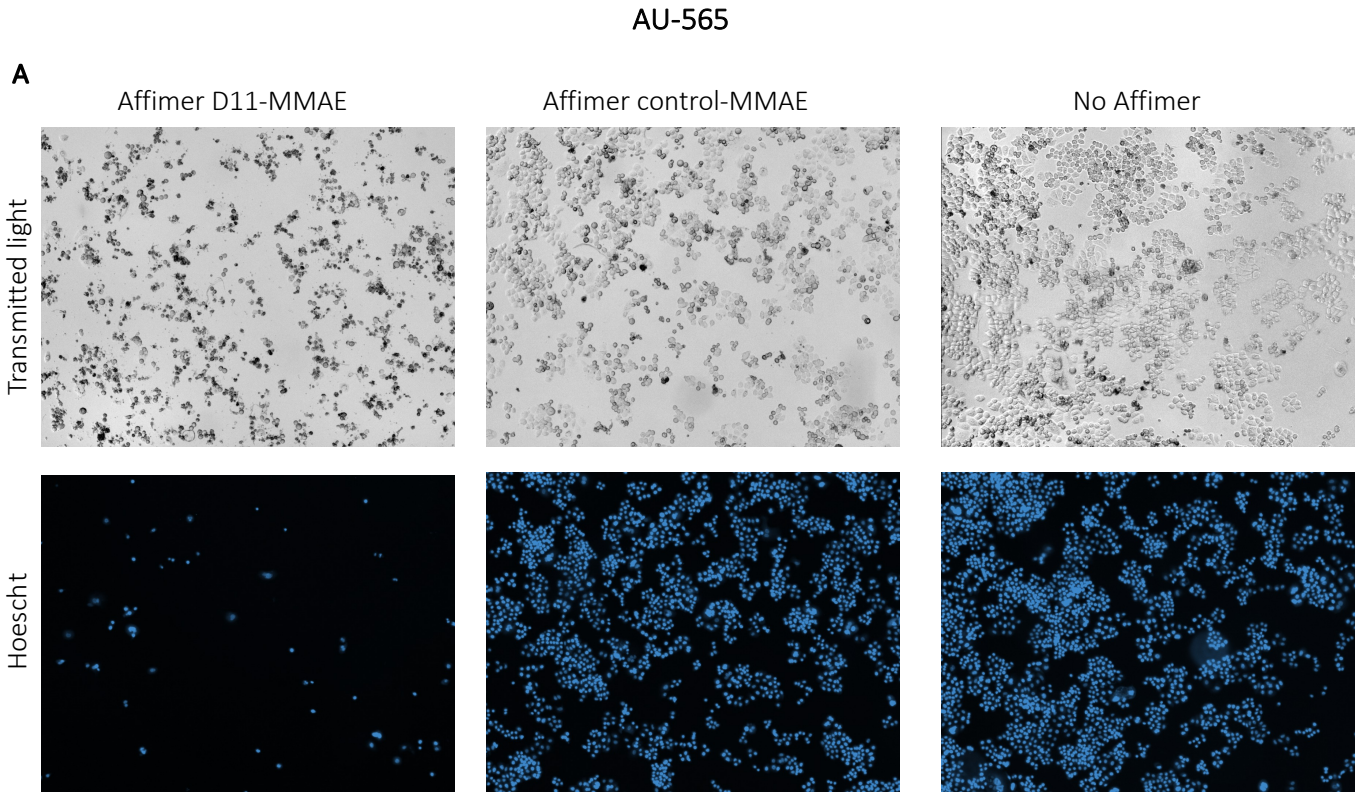
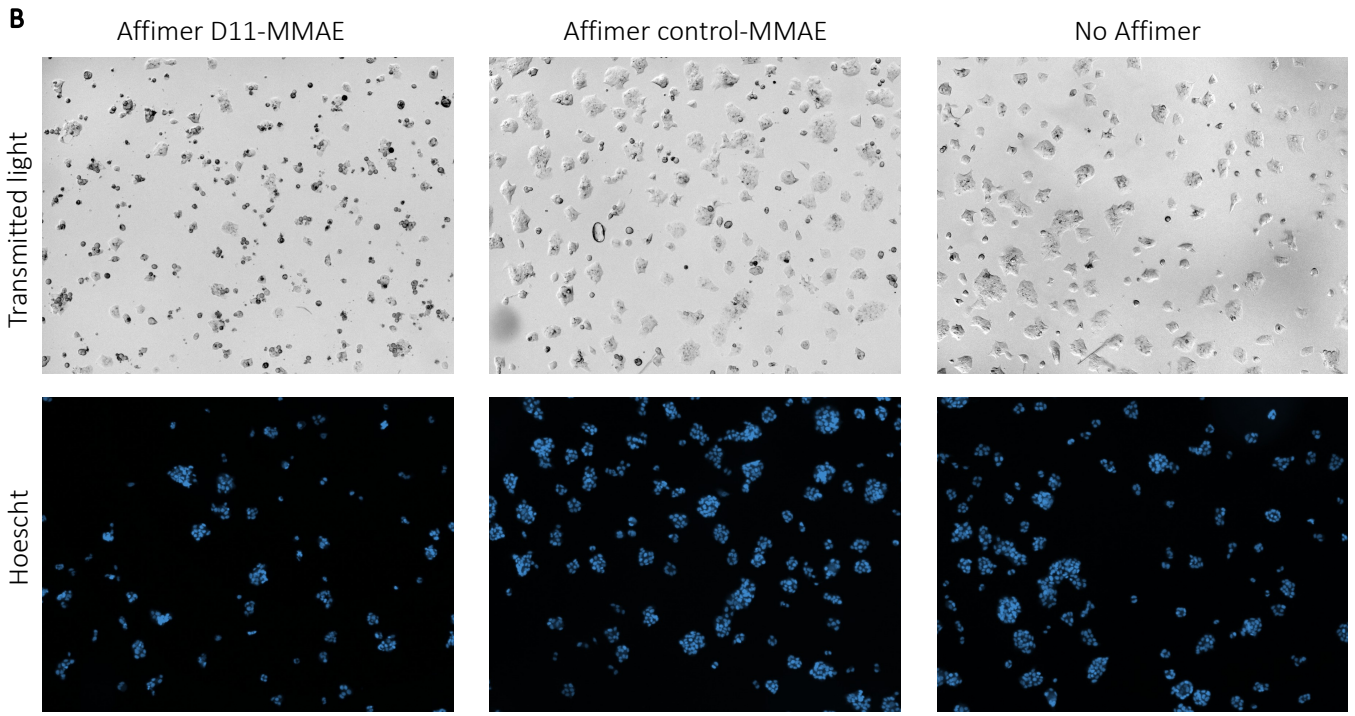


Figure 4.7 Nuclear cell count of various cell lines treated with different concentrations of Affimer MMAE conjugate.

A range of breast cancer cell lines AU-565, SKBR3, BT-474, MDA-MB-453, MCF-7, MDA-MB-231 and ZR-75-1 were seeded one day prior to the addition of AfD11M, AfH7M or AfCM. Cells were incubated with Affimer conjugates for a further 72 hours. Metabolic activity was analysed using AlamarBlue that was added to media 10 % v/v. A 100 µL media sample was taken and fluorescence intensity was measured with excitation 560 nm and emission 590 nm using a Tecan Spark Microplate reader. Following AlamarBlue analysis plates were washed 3 x in 1 x PBS prior to nuclear staining with hoescht. Nuclear cell counts were taken by a Pico Imager. **(A)** Cell count curve with all concentrations of Affimer drug conjugates where error bars represent the standard error of the mean between mean values of three biological replicates. All values were normalised to cells incubated with media alone. **(B)** Values interpolated from **(A)** for 15 nM Affimer drug conjugate.


AU-565
A
Affimer D11-MMAE
Affimer control-MMAE
No Affimer
Transmitted light
Hoescht

BT-474


B
Affimer D11-MMAE
Affimer control-MMAE
No Affimer
Transmitted light
Hoescht

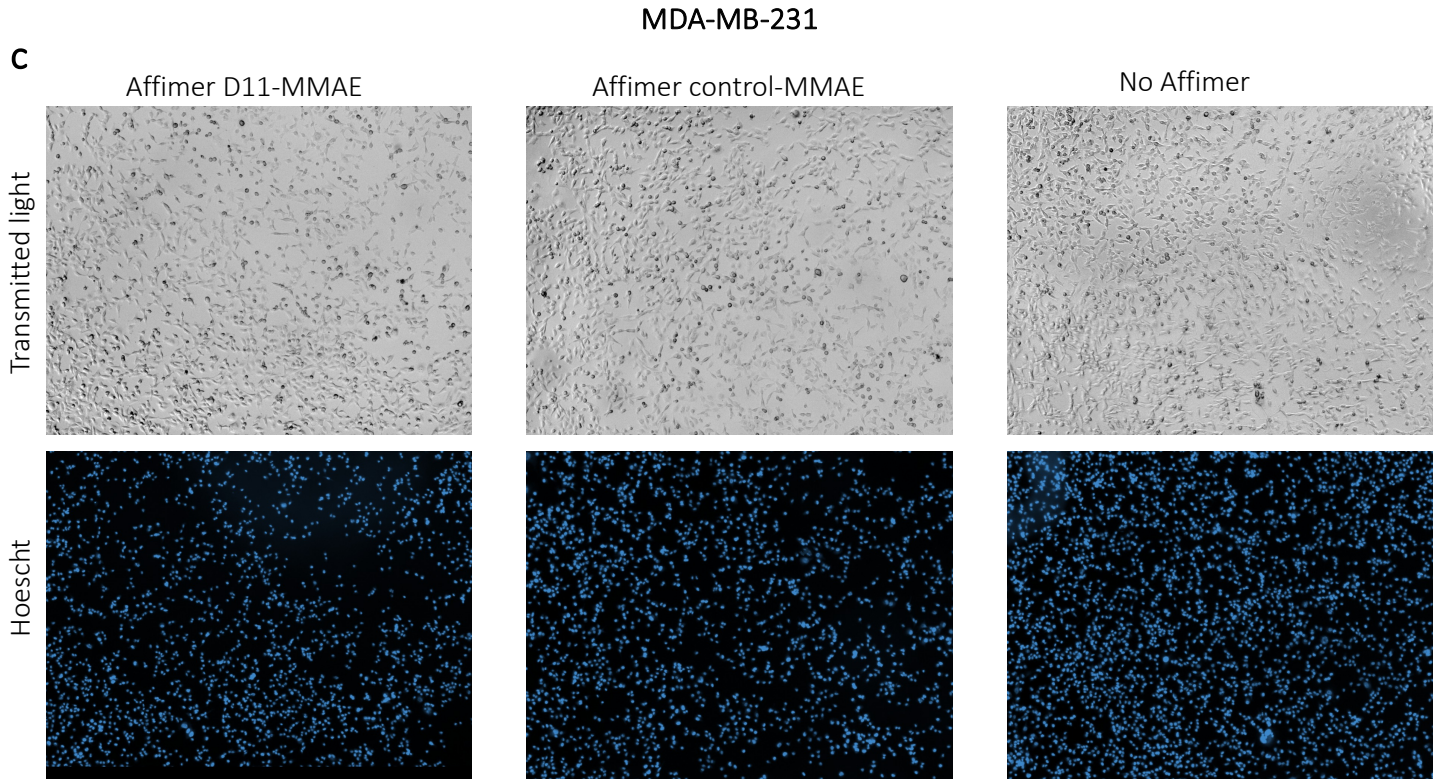
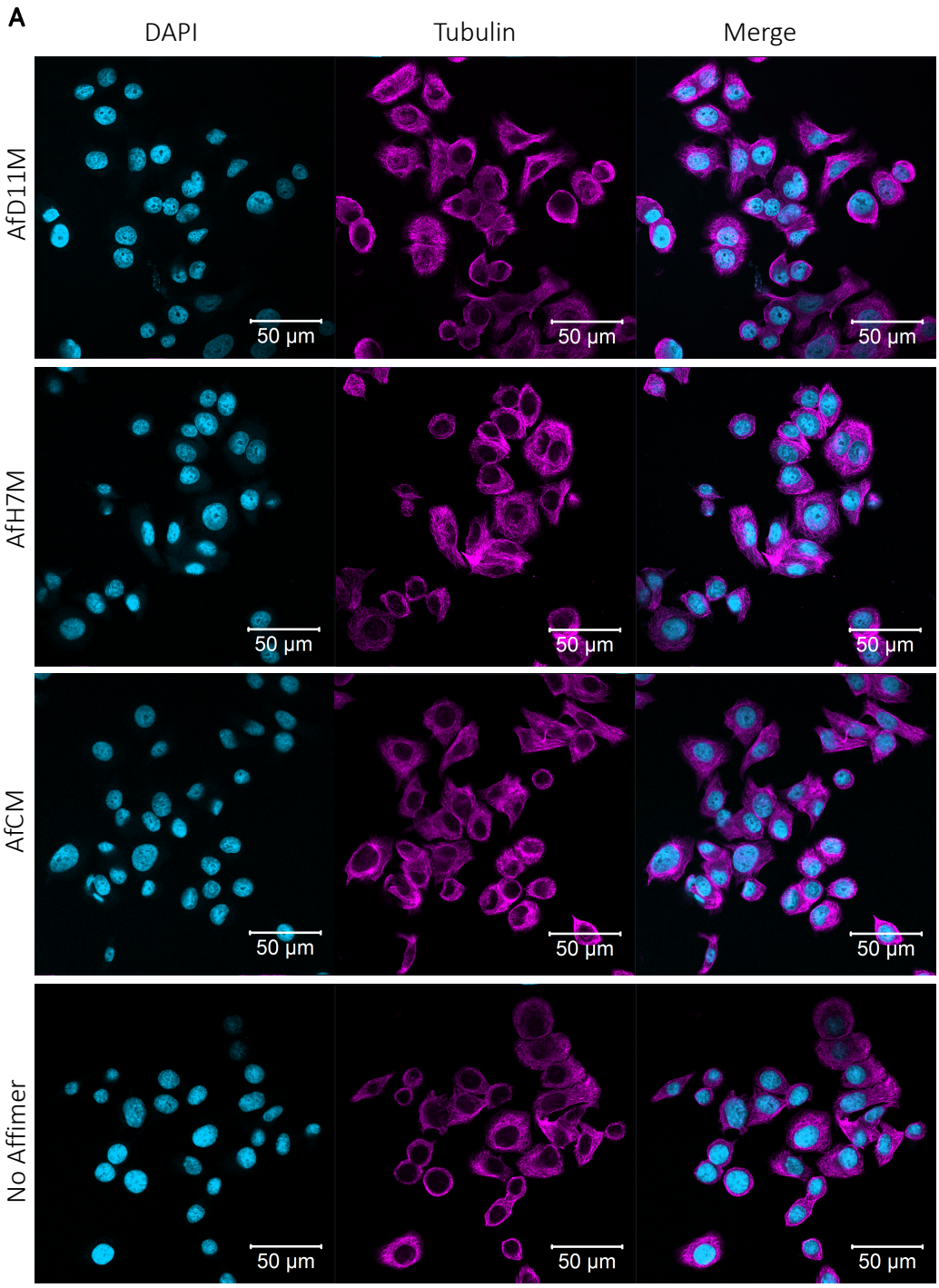


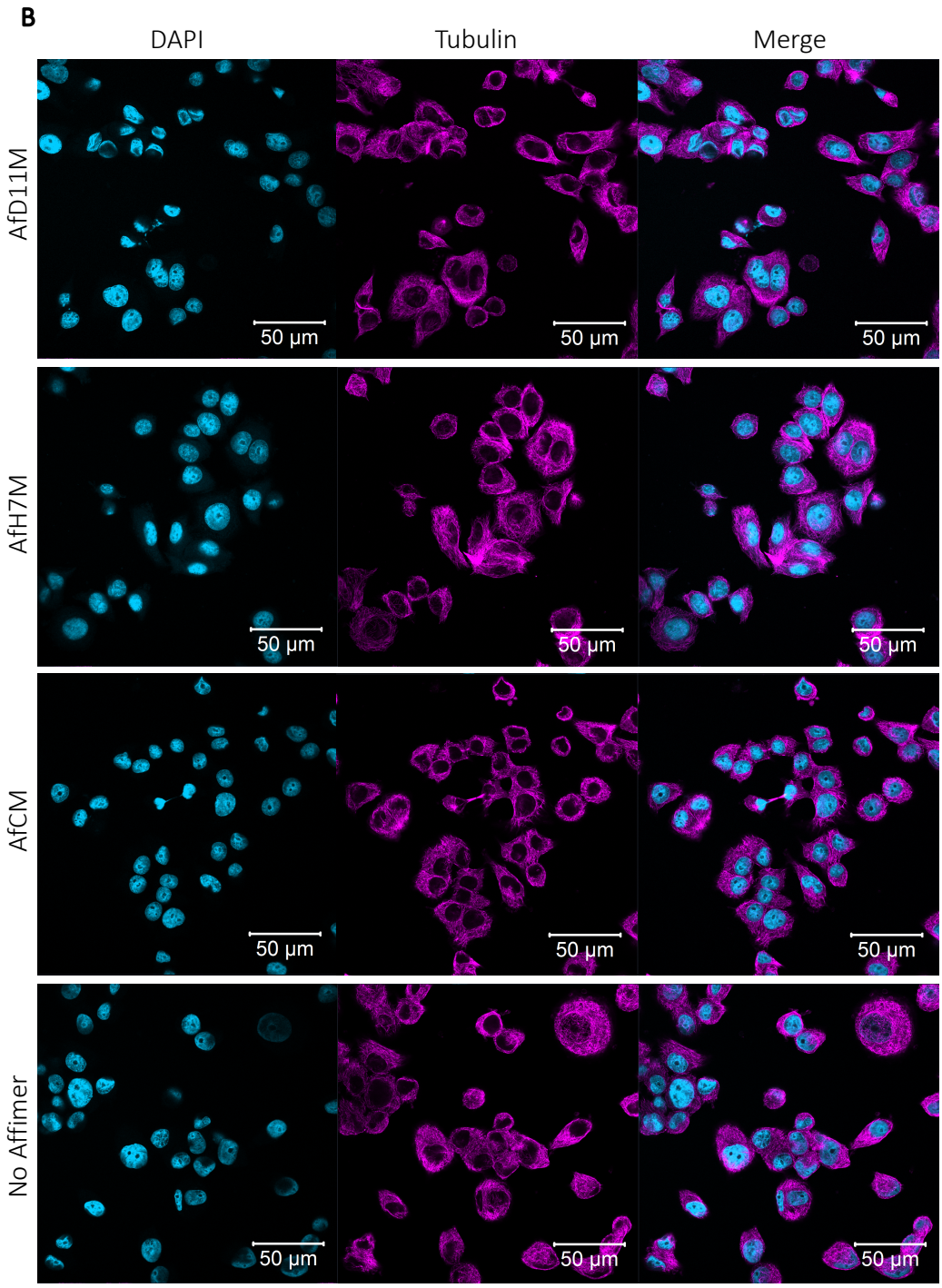
Figure 4.8 Example PICO images following incubation of Affimer MMAE conjugates on breast cancer cell lines.
(A) AU-565 **(B)** BT-474 and **(C)** MDA-MB-231 cell lines following 72 hour incubation with Affimer drug conjugates at a concentration of ~15 nM. Images were taken following staining with hoescht nuclear stain using an ImageXpress Pico Automated Cell Imaging System. Images shown were taken using transmitted light (top) and to visualise nuclear stain (bottom). Images are representative of what was used to undertake the nuclear cell count in Figure 4.7.

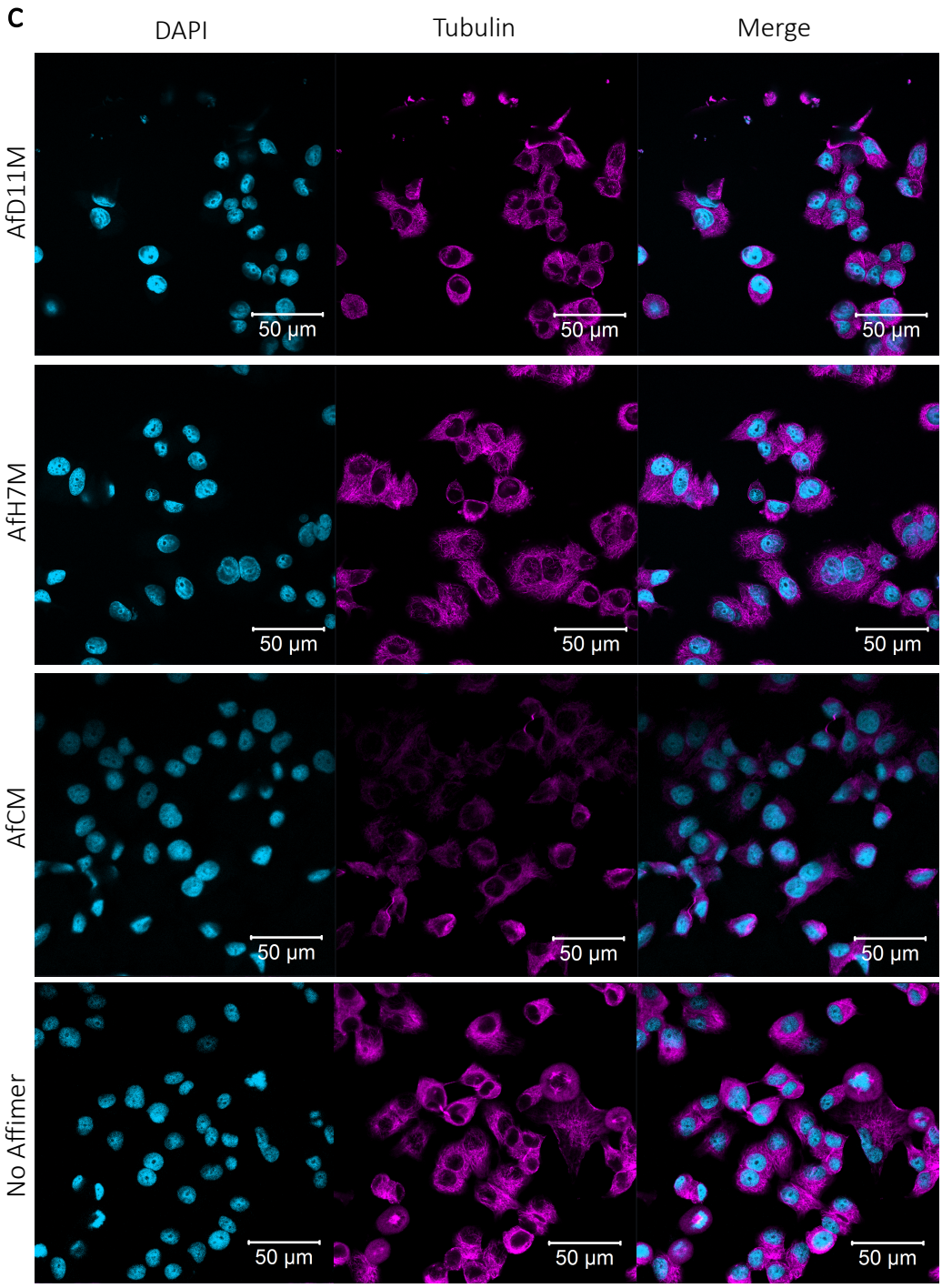
4.2.5 Monomethyl Auristatin E modulation of Tubulin in HER2+ cells

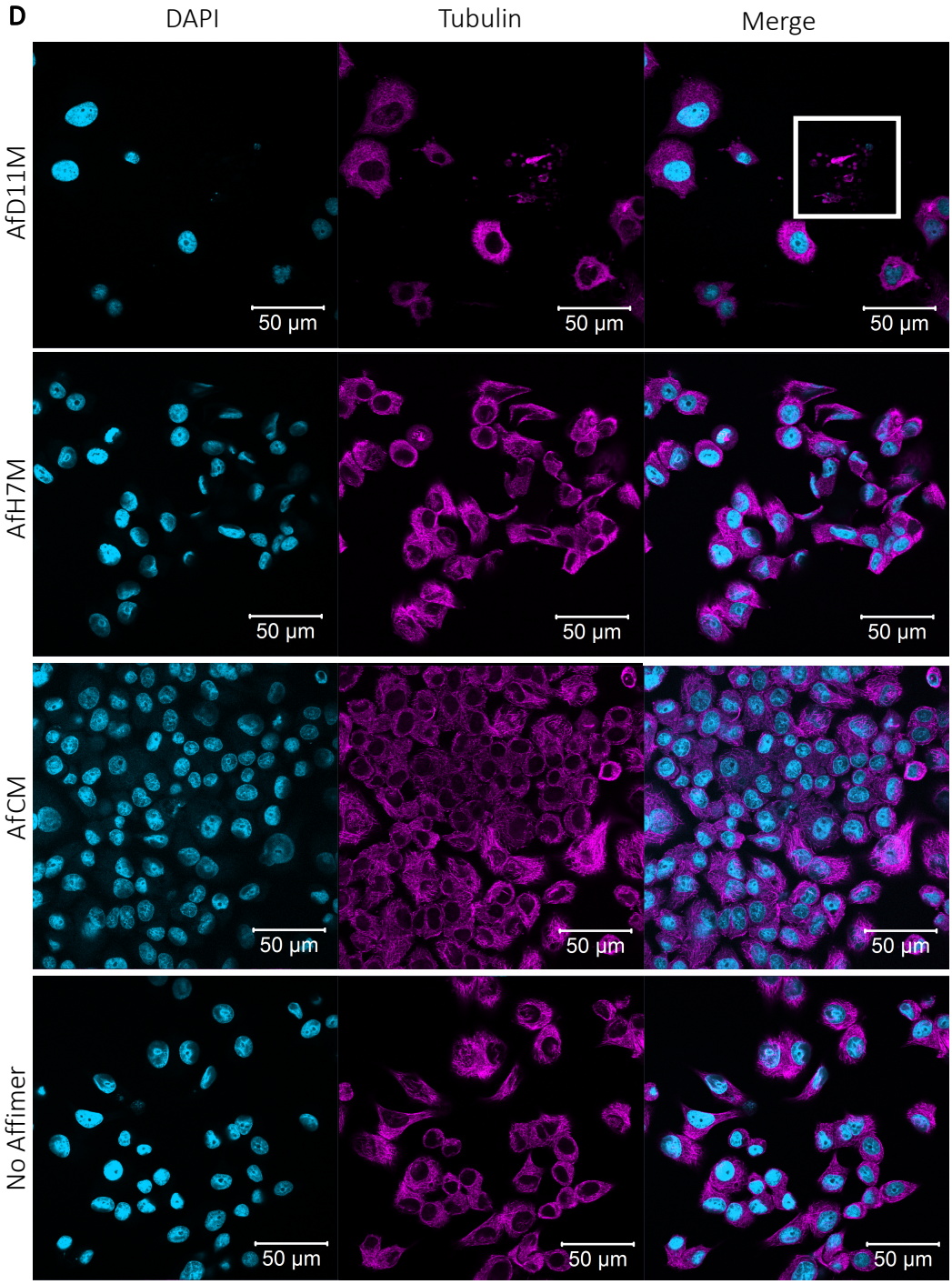
Images from the Pico Imaging express software depicted increased cell debris and death of HER2 overexpressing cell lines following incubation with AfD11M and AfH7M. The antineoplastic moiety MMAE is a potent anti-mitotic agent derived from peptides occurring in marine mollusc *Dolabella auricularia* called dolastatins. It inhibits cell division by blocking tubulin polymerisation leading to apoptosis of affected cells. Confocal microscopy was used to investigate the modulation of tubulin by MMAE. Affimer drug conjugates were diluted in media to a concentration of 0.3 μg/mL and incubated on AU-565 cells for 2, 4, 8, 24 and 48 hours prior to fixing in 4 % PFA and staining with nuclear Hoescht stain and anti-tubulin α followed by secondary antibody as per section 2.11.

There were no obvious differences in cell morphology between HER2 specific Affimer drug conjugates AfD11M and AfH7M and controls (AfCM or no Affimer) following 2 and 4 hour incubation (Figure 4.9A and B). Following 8 hour incubation with AfD11M some distortion in tubulin staining is observed that is not present in other samples (Figure 4.9C). The most distinct changes can be observed following 24 and 48 hour incubations (Figure 4.9D and E). Irregular tubulin morphology is represented by white squares at these later time points (Figure 4.9D and E). There are also less cells present following AfD11M and AfH7M incubation compared to controls at 24 and 48 hours. There were some visual differences in tubulin morphology following incubation with either AfD11M or AfH7M, however, comparison between conjugate would require further analysis as it is difficult to visually identify differences at this magnification.


A
DAPI
Tubulin
Merge
AfD11M
AfH7M
AfCM
No Affimer
50 µm


B
DAPI
Tubulin
Merge
AfD11M
AfH7M
AfCM
No Affimer
50 µm


C
DAPI
Tubulin
Merge
AfD11M
AfH7M
AfCM
No Affimer
50 µm


D
DAPI
Tubulin
Merge
AfD11M
AfH7M
AfCM
No Affimer
50 µm

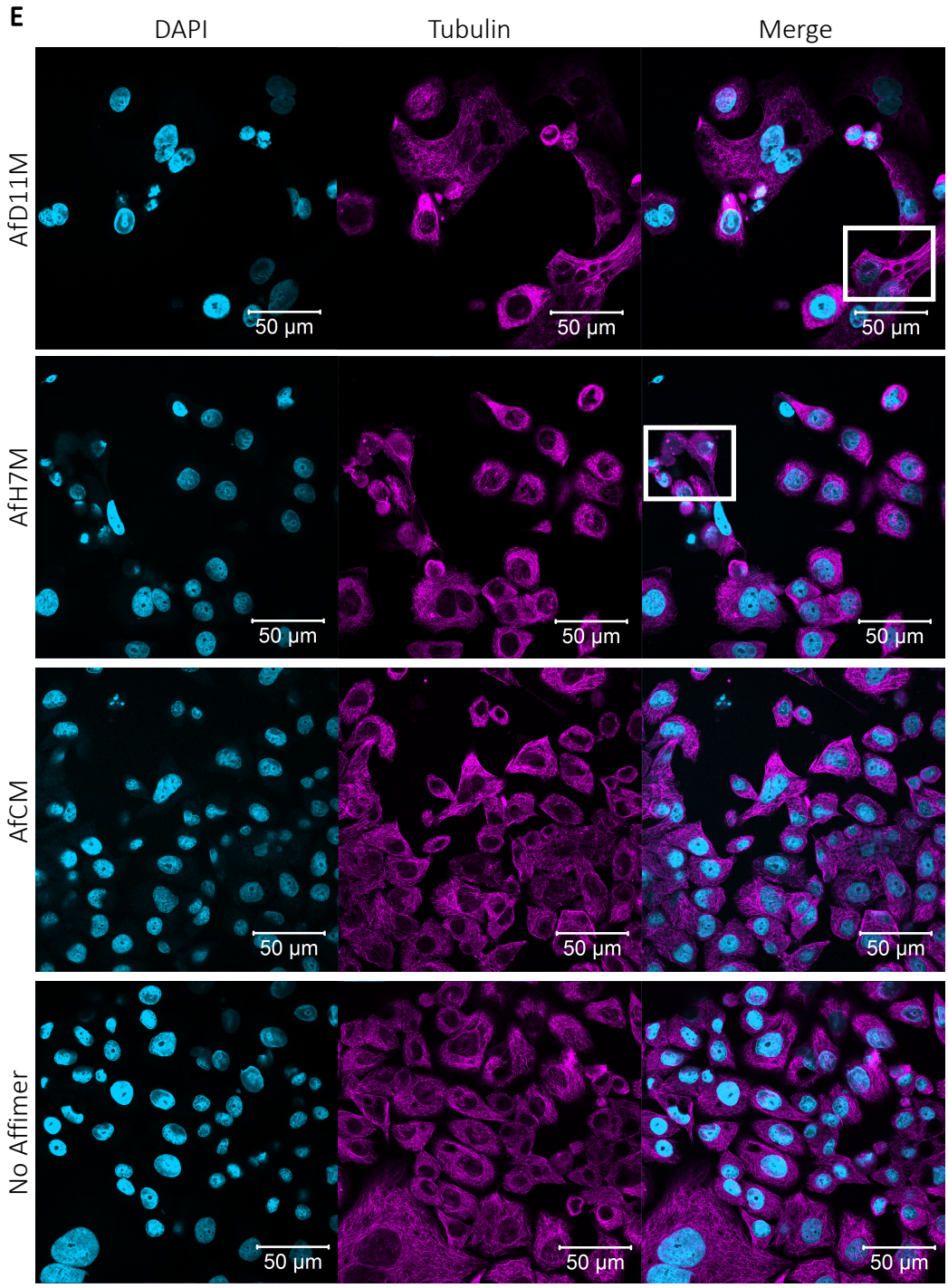


Figure 4.9 Immunofluorescence to show modulation of tubulin by MMAE.
Confocal images of immunofluorescent staining of tubulin (pink) and nuclei (blue) in HER2 overexpressing breast cancer cell line AU-565 following Affimer-MMAE conjugates and no Affimer control incubation for **(A)** 2h **(B)** 4h **(C)** 8h **(D)** 24h and **(E)** 48h prior to fixing in 4 % PFA. Images were taken on a Zeiss LSM880 inverted microscope with a magnification of 40 x oil immersion. Images were analysed using ZenLite software.

4.2.4 Determination of affinities and specificity of Affimer drug conjugates

Both AfD11M and AfH7M cause detrimental effects on HER2 overexpressing cell lines in a dose dependent manner. AfD11M shows slightly increased efficacy and Affimer D11 demonstrated enhanced membrane staining compared to Affimer H7. To determine the affinities of Affimer D11 and H7 for the HER2 extracellular domain surface plasmon resonance (SPR) was used.

4.2.5.1 Sequence and structural homology of HER2 and HER3 extracellular domains

HER2 is one of four members of the HER family of receptor tyrosine kinases. The family is evolutionary conserved with a high level of structural homology. To investigate specificity SPR was performed against both recombinant HER2 and HER3 encoding the extracellular domains. To confer sequence similarity amino acid sequences were aligned using Clustal Omega alignment software (Figure 4.10). Sequence homology by identity was relatively low at 41.406 % (265 amino acids), however, a higher level of similarity is observed when considering amino acids with similar properties (further 177 amino acids). It is known that the family of kinases is structurally conserved that is reinforced by the 100 % homology of cysteine amino acid residues (Figure 4.10). Both the HER2 and HER3 extracellular domains have previously been crystallised (73, 75). The PDB files for retrospective proteins were aligned in MacPyMOL. The full-length extracellular domains do not align due to the HER2 extracellular domain lacking the subdomain II to subdomain IV tether resulting in a constitutively active conformation (Figure 4.11C). However, subdomains I and II and subdomain III and IV from both proteins do superimpose onto one another demonstrating a high level of structural homology (Figure 4.11).

To assign a numerical value to the structural homology between HER2 and HER3 extracellular domain the root-mean-square deviation (RMSD) of atomic positions was calculated using MacPyMOL. The RMSD value of aligned atoms given is, by default, calculated following outlier rejection. The RMSD value for full length HER2 and HER3 extracellular domain was 21.580 Å (3388 atoms). However, the RMSD values for subdomain I and II and subdomains III and IV alignments are much lower at 3.092 Å (1666 atoms) and 1.988 Å (1567 atoms) respectively. The total atom count RMSD values

(without outlier rejection) were 24.639 Å (3598 atoms) for full length, 4.075 Å (1818 atoms) for domains I and II and 2.620 Å (1724 atoms) for domains III and IV. Values closer to 0 Å are indicative of a higher level of structural similarity. RMSD values indicate that the full length extracellular domains have low level structural homology when using the 'align' tool against the whole sequence in MacPyMOL. This was expected due to the difference in conformation of HER2 and HER3. However, RMSD values for subdomain superimposition show there is a high level of structural homology when subdomains are split. This concludes that HER3 is an ideal protein to use to test specificity of Affimer drug conjugates targeting HER2.

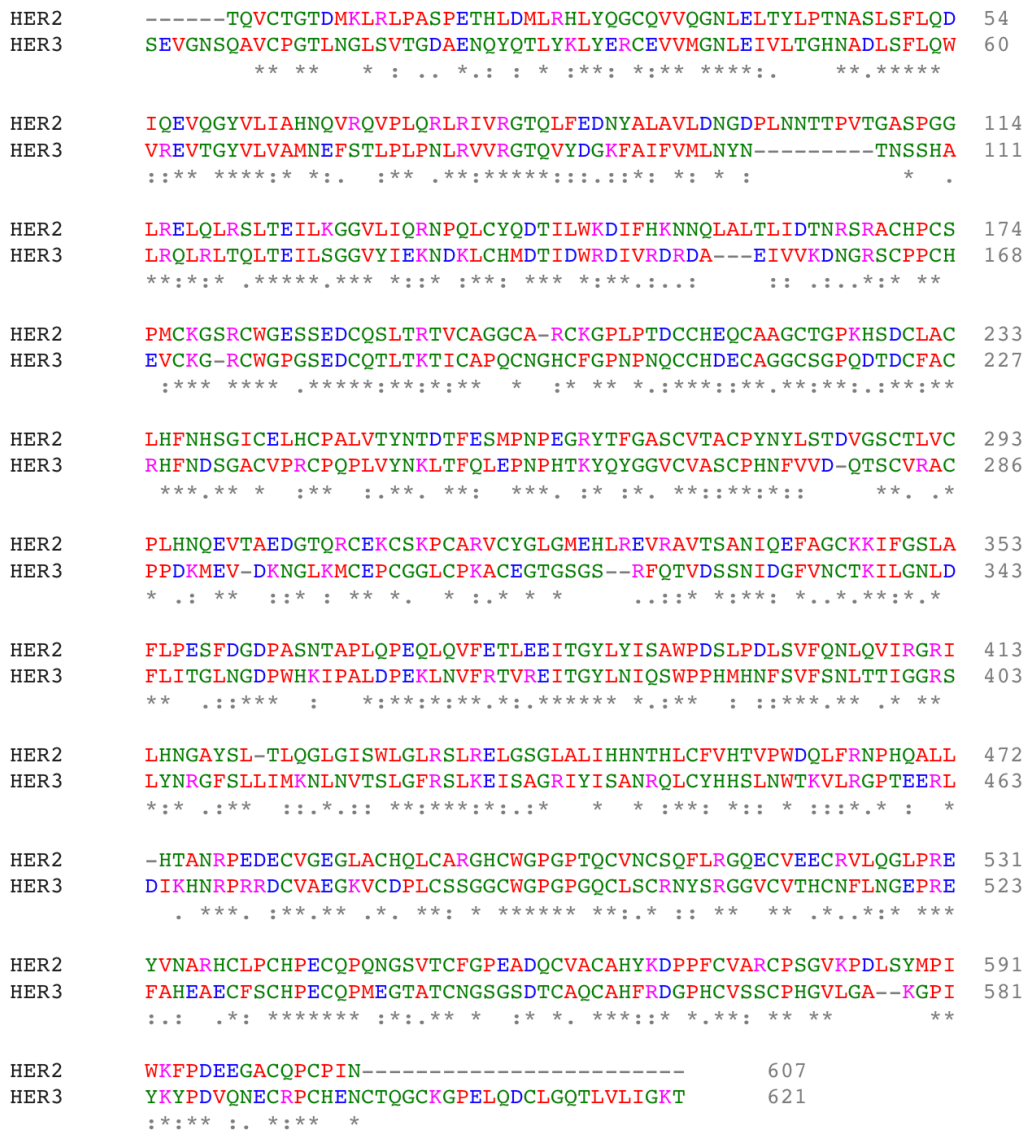


Figure 4.10 Sequence alignment of HER2 and HER3 extracellular domain amino acid sequences.
Sequences of HER2 and HER3 extracellular domains were obtained from PDB files 1N8Z and 1M6B respectively. Sequences were aligned in FASTA format using the Clustal Omega online resource. Identical amino acids are denoted with '*', strongly similar amino acids ':' (Gonnet PAM 250 matrix > 0.5), low similarity '.'(Gonnet PAM 250 matrix ≤ 0.5). Colours represent amino acid properties; small (red), acidic (blue), basic (pink), hydroxyl + sulphydryl + amine (green).

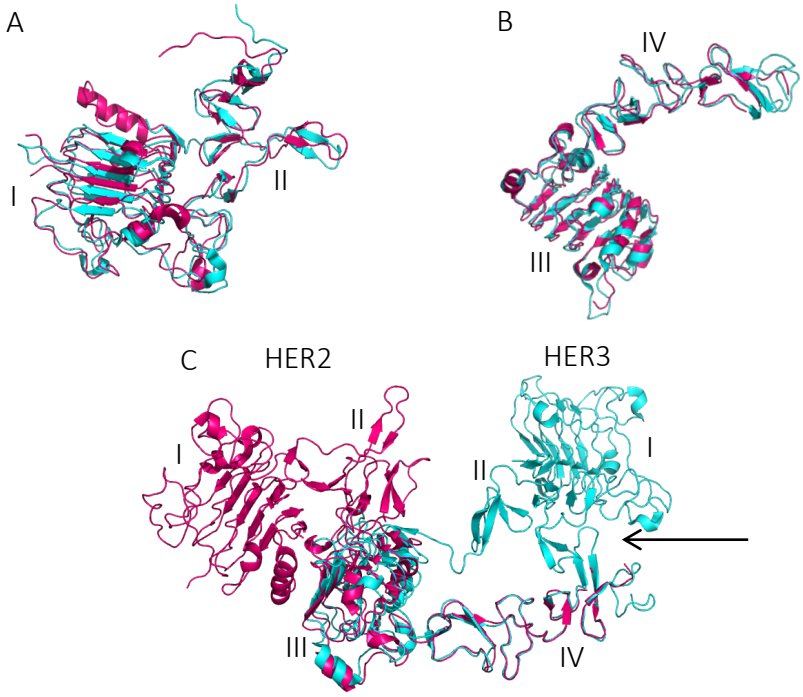


Figure 4.11 Superimposition of human HER2 and HER3 exracellular domains.
HER2 (magenta) and HER3 (cyan) extracellular domain PDB files 1N8Z and 1M6B respectively were superimposed using MacPyMOL 'align' tool. **(A)** Superimposition of sub domains I and II (residues 1-322 for HER2 and 6-310 for HER3) **(B)** superimposition of subdomains III and IV (residues 323-606 for HER2 and 311-610 for HER3) **(C)** superimposition of domain III and IV with the whole structure visible. Individual domains are labelled accordingly and the domain II to IV tether of HER3 is shown by the arrow in **(C)**. Superimpositions were carried out using the 'align' tool in MacPyMOL.

4.2.5.2 Affimer drug conjugates have nM affinities to HER2

Structural alignment demonstrated the high level of structural homology between HER2 and HER3 extracellular subdomains. To test for cross reactivity of the HER2 specific Affimers SPR was performed against recombinant HER2 and HER3. Recombinant HER2 and HER3 extracellular domains were immobilised on neighbouring flow cells of a CM5 chip by amine coupling prior to injection with Affimer drug conjugates at a range of concentrations as described in section 2.16.

There was no significant level of binding from any Affimer drug conjugates on the HER3 derivatised CM5 chip with RU values less than one (Figure 4.12). In contrast, sensorgrams from both AfD11M and AfH7M show evidence of strong binding to recombinant HER2 whereas the AfCM remains minimal (Figure 4.12). Results conclude that HER2 specific conjugates bind to recombinant HER2 extracellular domain with little cross reactivity with HER3.

Sensorgrams were analysed using BIAevaluation software to deduce both the steady state affinity and kinetic values of AfD11M and AfH7M binding to HER2. A graph of steady state affinities for AfD11M and AfH7M was plotted taking values from sensorgrams four seconds prior to the end of the injection (Figure 4.13). The K_D values determined by steady state affinity were 17 and 184 nM for AfD11M and AfH7M respectively.

The kinetics was also analysed using BIAevaluation software. Sensorgrams were cropped to 300 seconds and curves were fitted using the 1:1 Langmuir binding model (Figure 4.14). A good fit was achieved for AfD11M giving an accurate representation of the sensorgram. The best fit achieved for AfH7M misrepresents aspects of the sensorgram and so values obtained from this are given with less confidence. Curves fitted to n=2 AfH7M sensorgram discounted 6.25 nM as this was an outlier so values are n=3 with the exception of this. K_D values were 12 and 77 nM for AfD11M and AfH7M respectively. The association rate for AfD11M was faster at 3.31×10^6 $M^{-1}s^{-1}$ compared to 3.11×10^5 $M^{-1}s^{-1}$ for AfH7M. Dissociation rates of both AfD11M and AfH7M were similar.

Together results show that AfD11M and AfH7M bind to recombinant HER2 with no cross reactivity to recombinant HER3. AfD11M binds with higher affinity and affinities calculated by both steady state affinity and kinetics give similar values whereas AfH7M exhibits a higher level of divergence.

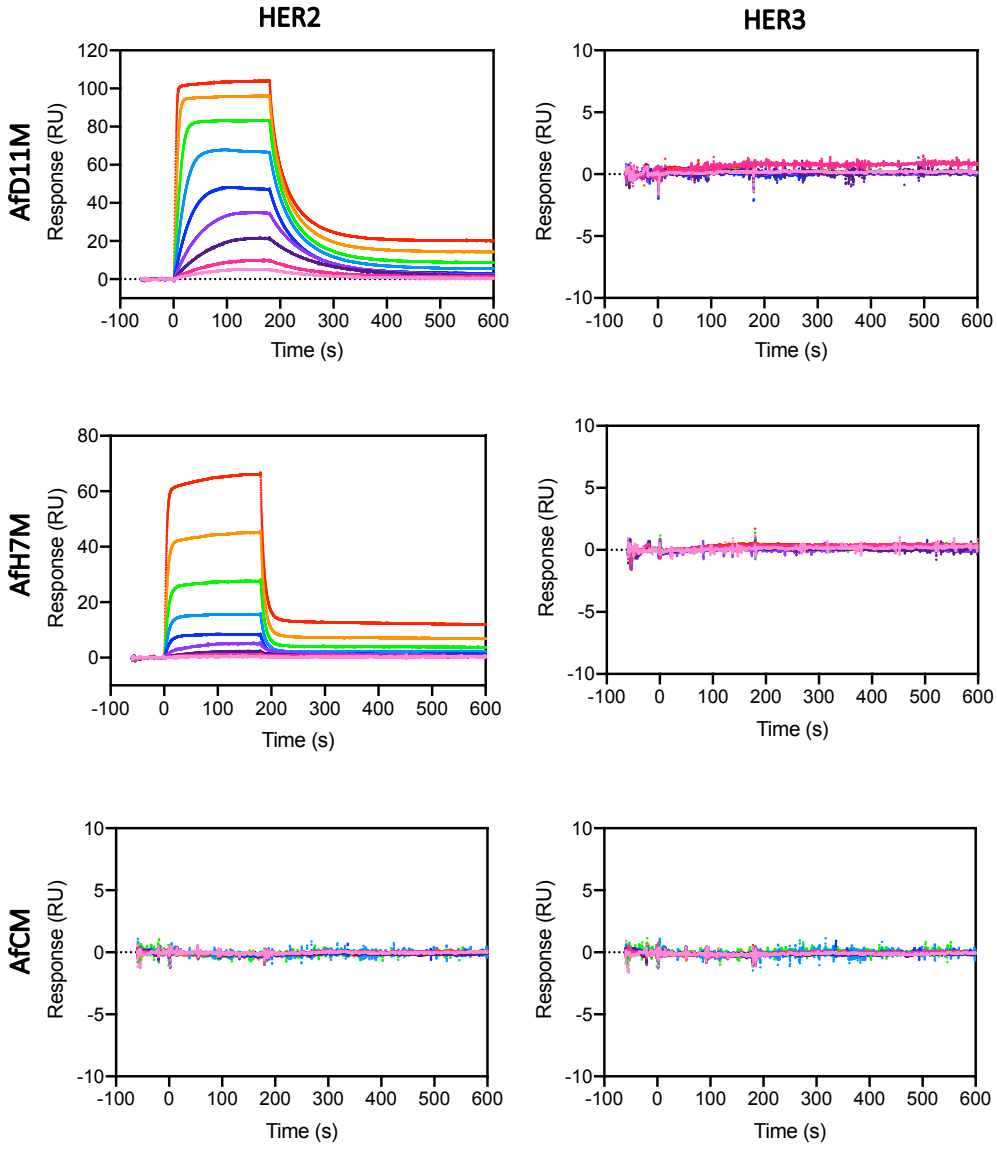
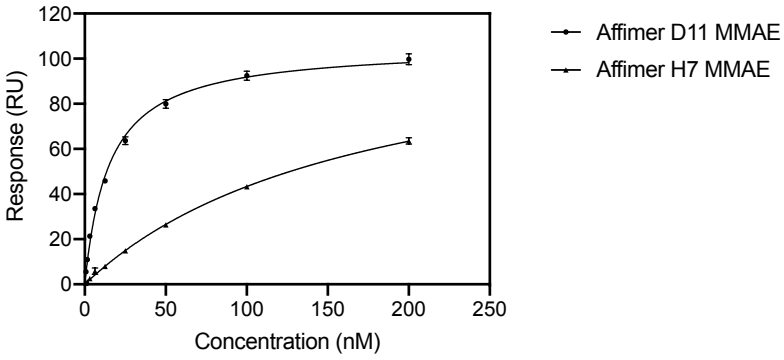


Figure 4.12 Sensorgram to test binding affinity of Affimer MMAE conjugates to recombinant HER2 and HER3 using SPR.

Recombinant HER2 (Met1- Thr652, 1400 RU) and HER3 (Met1-Thr643, 1300 RU) were immobilised on a CM5 chip. Affimer drug conjugates at concentrations of 0.78 (light pink), 1.56 (magenta), 3.13 (dark purple), 6.25 (purple), 12.5 (indigo), 25 (blue), 50 (green), 100 (orange) and 200 (red) nM were injected over the targets at a flow rate of 30 uL/min for 90 s at 25 °C. Sensorgram is shown for 100 s prior to the injection and 600 s thereafter. Injection occurred at time point 0 seconds. Sensorgram is representative of three repeats and has accounted for background through subtraction of blank flow cell. Data was exported from BIAevaluation software into GraphPad Prism version 8.0 to produce graphs. Graph data is representative of individual data values at individual time point, no curves have been fitted.



Affimer	KD SSB K_D ± SD (nM)	Chi^2 ± SD	Kinetics K_D ± SD (nM)	*ka* ± SD ($M^{-1}s^{-1}$)	Kd ± SD (s^{-1})
D11-MMAE	17.0 ± 0.25	3.61 ± 0.40	12.0 ± 0.64	$3.31 \times 10^6 \pm 6.79 \times 10^5$	0.04 ± 0.01
H7-MMAE	184.0 ± 9.32	0.95 ± 1.57	76.5 ± 3.56	$3.11 \times 10^5 \pm 2.21 \times 10^4$	0.02 ± 0.002

Figure 4.13 Estimate of kinetic parameters of Affimer MMAE conjugates to recombinant HER2 using SPR.
K_D single site binding ratio (SSB) were deduced by taking the values 4 s prior to the end of the injection of **(A)** AfD11M and **(B)** AfH7M over a CM5 chip with recombinant HER2 protein immobilised. Points were plotted and K_D values were deduced using Biacore T200 evaluation software. Graphs are representative of triplicate repeat and kinetic values are displayed in the table below ± standard deviation (SD). Three independent experiments were performed to determine K_D values. Representative data is shown above.

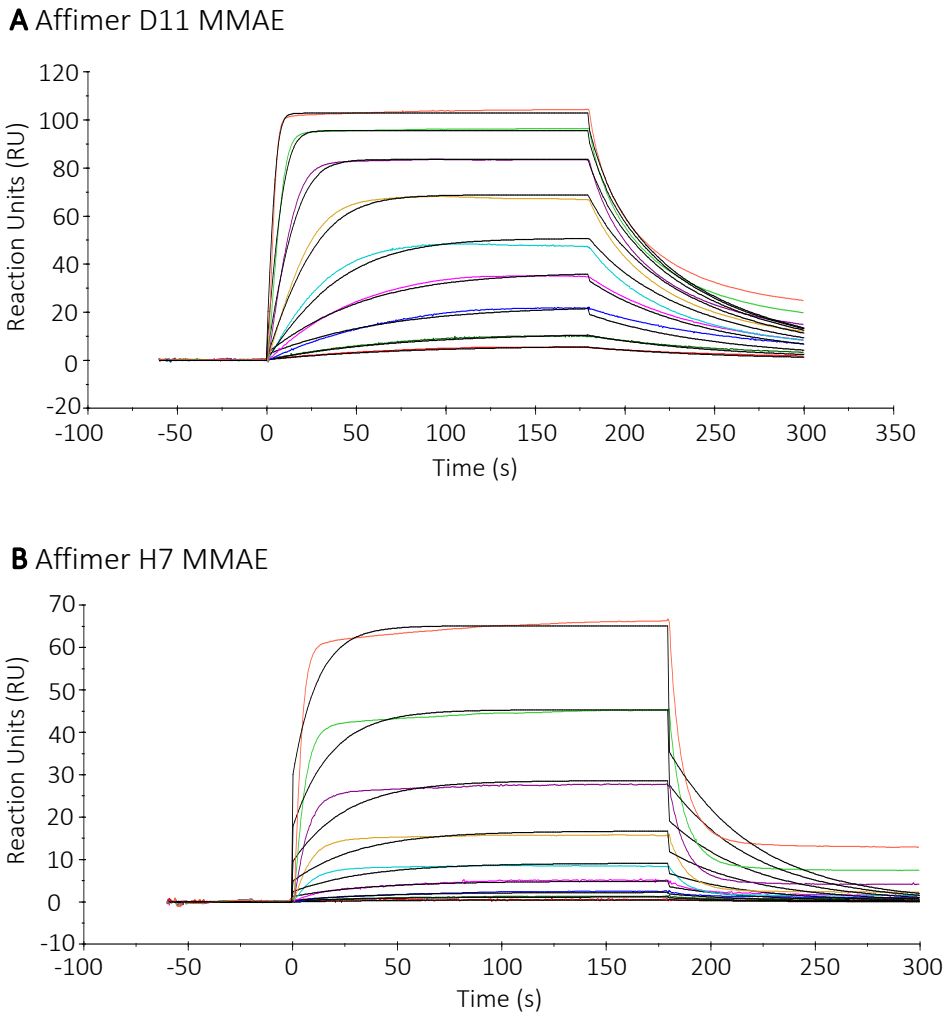


Figure 4.14 Example fit using 1:1 Langmuir binding model.
Sensorgrams for **(A)** AfD11M and **(B)** AfH7M at varying concentrations (200 nM (orange), 100 nM (green), 50 nM (purple), 25 nM (gold), 12.5 nM (cyan), 6.25 nM (magenta), 3.125 nM (indigo), 1.5625 nM (dark green) and 0.78125 (red)) binding to immobilised recombinant HER2 extracellular domains were analysed using BIAevaluation software to determine kinetic values. Curves were fitted (black) to the underlying sensorgram using the 1:1 Langmuir binding model on BIAevalution software. Graphs are one example from n=3 to show curve fits.

4.2.6 Targeting cell lines resistant to current therapies with AfD11M and AfH7M

Two HER2 specific Affimer drug conjugates have been developed that bind with nM affinity to HER2 and have a detrimental effect on breast cancer cell lines expressing HER2 on their surface. Arguably the most challenging problem to overcome with current therapies is acquired and *de novo* resistance. Therefore it is important to test the ability of potential new therapeutics in their ability to overcome resistance and target cell lines previously treated by other drugs.

SKBR3 and BT-474 resistant cell lines were a kind gift from Prof. Eric Lam of University College London. The SKBR3 cell line were resistant to Capatinib whilst BT-474 were resistant to Lapatinib. Both cell lines were shown to be resistant to Trastuzumab in a preliminary experiment by the Lam laboratory (n=1). A dose response using Affimer MMAE drug conjugates would indicate whether AfD11M and AfH7M were able to have a detrimental effect on metabolic activity and cell number of resistant cell lines comparable to wildtype of the same cell line. Prior to a dose response the level of HER2 in both wildtype and resistant cell lines was analysed by western blot (2.8.3). The antibody used to detect HER2 binds to the extracellular domain. Wildtype SKBR3 and BT-474 show high levels of HER2 expression that is omitted in the resistant lines (Figure 4.15). These results suggest that the mechanism of resistance to first line therapy is cleavage of the extracellular domain. Following this result the effect of Affimer drug conjugate treatment on resistant cell lines was not investigated as if the extracellular domain of the HER2 protein is not there then the Affimer will have no means to bind to the cells.

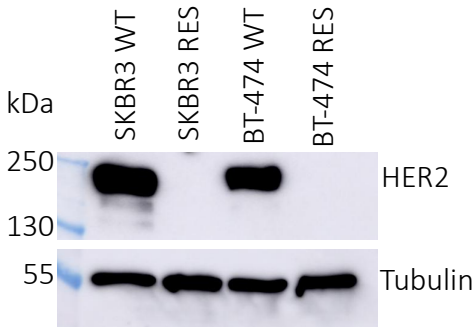


Figure 4.15 Western blot of HER2 expression in wildtype and resistant cell lines.
HER2 overexpressing cell lines SKBR3 and BT-474 were lysed and analysed by western blot to compare HER2 expression between wildtype (WT) and resistant (RES) cell lines. SKBR3 cells were made resistant to Capatinib and BT-474 Lapatinib. HER2 was detected at 185 kDa and Tubulin control at 55 kDa. Secondary HRP antibody was incubated on blots and detected using chemiluminescence. Images were taken on an Amersham imager 600. Results represent repeats of n=2.

4.3 Chapter summary and future direction

The HER2 positive breast cancer subtype is primarily treated by monoclonal antibody Trastuzumab, ADC ado-trastuzumab emtansine, small RTK inhibitor Lapatinib and chemotherapy. To overcome resistance and drawbacks of current therapy non-immunoglobulin scaffolds have been investigated. Affimer reagents that bind to HER2 were previously characterised (chapter 3). Affimer D11 and H7 are internalised by HER2 overexpressing cell lines specifically. Whilst they had little effect on cells unconjugated they had potential to be used as vehicles for the delivery of an anti-neoplastic warhead. In this chapter Affimers D11 and H7 were successfully conjugated to cytotoxic moiety MMAE demonstrating Affimer drug conjugates were able to be used for this application.

4.3.1 Monomethyl Auristatin E (MMAE) as a cytotoxic payload

Affimer D11, H7 and control were conjugated to cytotoxic moiety MMAE. Cytotoxic payloads usually fall into two classes; those that affect DNA synthesis and those that affect mitosis. Two drug classes have been predominantly used in antibody drug conjugates currently on the market, auristatins and maytansinoids (243). Both are anti-neoplastic agents that prevent the polymerisation of tubulin interfering with critical cellular processes such as mitosis (Figure 4.16) resulting in apoptosis. MMAE is an auristatin that has been used therapeutically as the cytotoxic moiety of FDA approved anti-CD40 ADC brentuximab vedotin for the treatment of relapsed Hodgkin lymphoma or relapsed systemic anaplastic large-cell lymphoma (244). It has also been shown to elicit apoptosis in breast cancer cells (245). The payload MMAE was available engineered with a maleimide reactive group; MC-VC-PABC-MMAE. As the conjugation of Affimers to maleimide reactive groups is established this was used to generate Affimer drug conjugates.

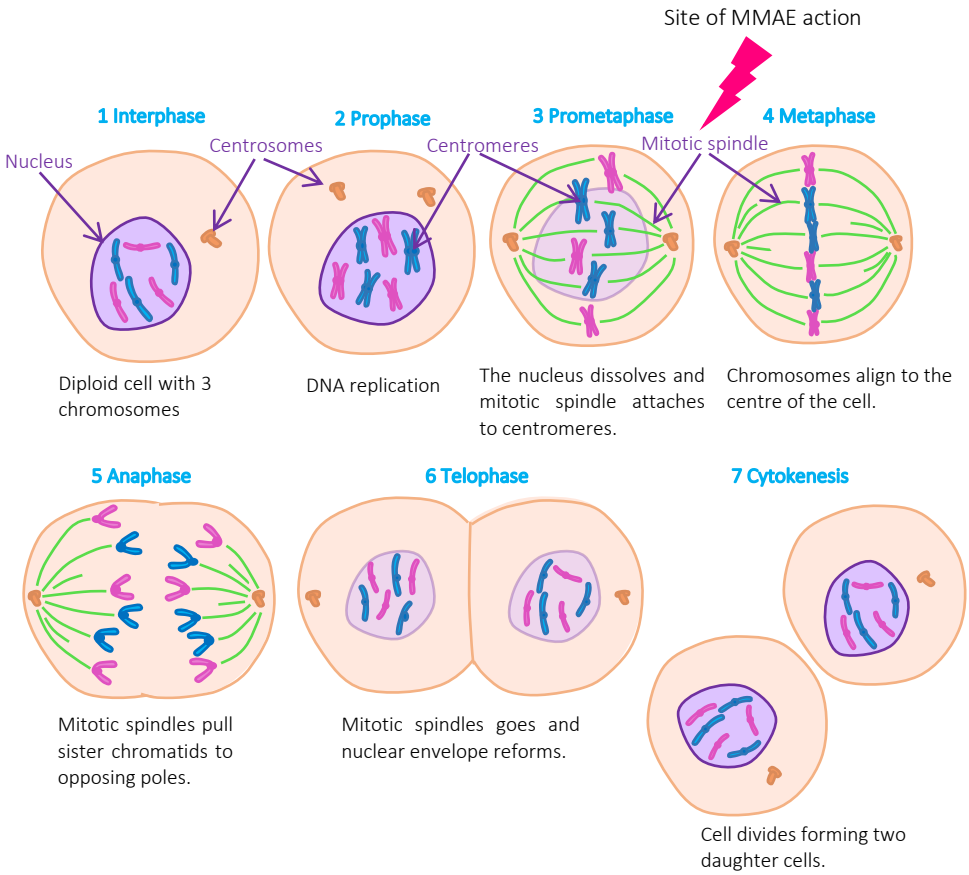


Figure 4.16 Stages of mitosis in eukaryotic human cells.
The cytotoxic payload MMAE is an antimitotic agent that interferes with tubulin polymerisation. The stages of mitosis are depicted in this figure 1) interphase, 2) prophase, 3) prometaphase, 4) metaphase, 5) anaphase, 6) telophase and 7) cytokinesis.

Maleimide chemistry has been the chosen method of conjugation for FDA approved ADCs brentuzimab vedotin and trastuzumab emtansine. This method of conjugation allows for site specific cysteine modification and is one of the most highly used methods for conjugation (246). Clinically approved ADCs comprise a heterogeneous mix of conjugates with different drug to antibody ratios. Ado-trastuzumab emtansine has a drug load distribution of 0 to 8 molecules of DM1 per antibody with an average of ~3.5 (247). Affimers were engineered to contain a single cysteine and so as a result an Affimer to drug ratio of 1:1 as confirmed by LC-MS.

The mass spectra contained two main species corresponding to Affimer drug conjugates and Affimer conjugates minus ~ 762 kDa. The molecular weight of MMAE alone without linkers is 717.98 kDa. It is possible that two species are present; one conjugated to MMAE and one with just the linker. Conjugation of ado-Trastuzumab emtansine by LC-MS demonstrates the presence of multiple variances present that would inevitably lead to batch to batch variability (248). As LC-MS is not a quantitative technique it is challenging

to give a value to the exact levels of conjugation achieved. However, optimisation steps of the conjugation reaction could overcome such problems. Conjugation reactions were carried out in Affimer elution buffer at pH 7.5. Maleimide reactions are most efficient at pH values between 6.5 and 7.5. To improve Affimer conjugation the reaction should be tested at a range of pH values to ensure optimal conjugation is achieved every time. Using SEC following conjugation could be used to achieve a pure solution of Affimer drug conjugate.

4.3.1 Dose response

As Affimer drug conjugates used in dose responses were not from the same batch the ratio of Affimer: Affimer drug conjugate varied. Concentrations deduced by the colourimetric Bradford assay were, therefore, representative of a mixed population of Affimer, Affimer drug conjugate and free drug. Despite this the effects of HER2 specific Affimer drug conjugates were visible in all assays. Both AfD11M and AfH7M have a negative effect on HER2 expressing cell lines in a dose dependent manner. The largest decrease in metabolic activity and cell count was observed in the cell lines AU-565 and SKBR3. These cell lines are both derived from the same patient (white, 43, Caucasian female) that may explain the similarities in their response. The cell line BT-474 is also HER2 overexpressing, however, this cell line was not affected by the HER2 specific Affimer drug conjugates as greatly as AU-565 and SKBR3. It is likely that other factors influence drug response in addition to HER2 expression.

Below is a table showing characteristics of breast cancer cell lines used in this study; biomarker expression, subtype and tumour type (Table 4.3). Of the HER2 overexpressing cell lines, BT-474 are the only ones to express ER and PR. MDA-MB-453 have the same characteristics as AU-565 and SKBR3, this may explain why despite lower HER2 expression the cell line still experiences detrimental effects by HER2 binding Affimer drug conjugates. Differential responses between cell lines have also been observed for T-DM1. Previous data has also shown BT-474 cells to be less affected by Trastuzumab antibody drug conjugates than SKBR3 cells (130, 249). It would be interesting to compare gene expression between cell lines to see if any gene clusters are associated with Affimer drug conjugate response.

Cell Line	ER	PR	HER2	HER3	Subtype	Tumour	Reference
AU-565	-	-	+	+	H	AC	(211, 250)
SKBR3	-	-	+	+	H	AC	(211, 250, 251)
BT-474	+	+	+	+	LB	IDC	(211, 250, 251)
MDA-MB-453	-	-	+	+	H	AC	(211, 250)
MCF-7	+	+	+/-	+/-	LA	IDC	(211, 250, 252)
ZR-75-1	+	+	-	-	LA	IDC	(211, 250)
MDA-MB-231	-	-	-	-	TNB	AC	(211, 250, 251)

Table 4.3 Expression and profiling of breast cancer cell lines.
The expression level of estrogen receptor (ER), progesterone receptor (PR) and HER2 are the primary features that lead to subtyping of breast cancer. HER3 expression can correlate with HER2+ cells responsiveness to HER2 targeting therapies. The 'subtype' column shows breast cancer subtype of the tumour cells were derived from; H (HER2+), LB (Luminal B), LA (Luminal A), TNB (Triple negative breast cancer). The 'Tumour' column denotes the type of tumour cell lines were derived from; AC (adenocarcinoma), IDC (invasive ductal carcinoma).

There is controversial literature for the expression of HER2 and HER3 in MCF-7 cells (Table 4.3). Following western blot analysis MCF-7 was shown to express low levels of HER2. Other groups have also defined them as having low-level expression while some have defined them as HER2 negative (Table 4.3). The literature is suggesting that all cell lines used that express HER2 also express HER3, albeit at varying levels. The involvement of the HER2-HER3 heterodimer in breast cancer pathogenesis is well defined, as previously discussed (1.4.3). It would be interesting to analyse Affimer drug conjugate response in cell lines AU-565, BT-474 and SKBR3 with HER3 knocked down to further analyse the role of HER3 in the therapeutic mechanism of action of Affimer drug conjugates.

4.3.2 Effect of MMAE of Tubulin

Immunofluorescence was used to verify that Affimer MMAE drug conjugates lead to the anticipated destabilisation of tubulin. Whilst characteristics of the staining such as the disorganised tubulin and evidence of multi-nuclearisation were consistent with what has previously been observed, the effects were not as distinct (253, 254). The Affimer drug conjugates display diverse effects across a panel of eight breast cancer cell lines. Such results lead to speculation that the visual effect on tubulin may also vary across cell lines. There seems to be a starked difference in the staining of Tubulin at 8 hours and 24 hours

following incubation with AfD11M, the time at which the destabilisation of Tubulin is most obvious could be in between these two time points in which there is a decrease in cell number. It would, therefore be interesting to perform a live cell time course assay to analyse the effects of Tubulin, in real time, following the addition of Affimer drug conjugates.

4.3.3 Binding affinity of Affimer drug conjugates

K_D is the equilibrium dissociation constant, that is a ratio between the K_{on} and K_{off} value of the ligand and antigen. The K_D value is inversely correlated to affinity, the lower the K_D value the higher the affinity of the ligand. Antibody alternative molecules screened against HER2 have previously been identified. DARPins against the HER2 extracellular domain were found to bind with affinities of 7.3 nM and 28 nM following analysis by SPR (146). Affinities were improved by error prone PCR to produce binders with affinities down to 91 pM (147). Whilst in the literature no DARPins conjugated by maleimide link were found, a HER2 specific DARPin fused to the fragment of *Pseudomonas aeruginosa* endotoxin A was developed (DARPin-PE40) that bound to HER2 with a K_D value of 10.8 nM (224). The affinity of AfD11M is consistent with the affinities of currently developed DARPins. Affibody molecules have also been developed to target HER2 with binding capacities in the nanomolar range. Dimerisation of HER2 specific Affibody improved the affinity from 50 nM to 3 nM (155). The K_D value of AfD11M and AfH7M were found to be in the nM range that correlates with HER2 specific DARPin and Affibody affinities. The dissociation rates of both AfD11M and AfH7M are fast. The dissociation rate of dimeric HER2 specific Affibody ($Z_{HER2:2891}$) conjugated to cytotoxic warhead was slower than the monomeric form, presumably due to an avidity effect (223). Dimerisation of Affimer reagents could, therefore, lead to increased affinity and a slower dissociation rate due to the avidity affect.

4.3.4 Chapter summary

The work in this chapter has demonstrated that two HER2 specific Affimer drug conjugates hold a superior ability to kill HER2 overexpressing breast cancer cell lines compared to controls. Whilst cell lines provide a promising base their similarity to the complexity of cells and tissue found in the human body limits their translatability to the

clinic. It is, therefore, paramount to test the ability of Affimer drug conjugates to have a consistent effect in models demonstrating a higher level of heterogeneity and therefore greater homology to what is observed *in vivo*. In the next chapter the effects of such Affimers in more humanised models will be explored.

Chapter 5

Creating a novel 3D cell culture model of HER2+ breast cancer

'Only those who will risk going too far can possibly find out how far one can go.'

-T.S. Eliot

Chapter 5

5 Creating a novel 3D cell culture model for HER2+ breast cancer

5.1 Introduction

Breast cancer is a heterogeneous disease with tumours comprising multiple cell types with varying phenotypes and genotypes. For decades 2D cell culture has been used to study breast cancer with the contribution of multiple immortalised cell lines (168). However, cell lines are a homogeneous population of a single cell type and do not recapitulate the complexity and heterogeneity observed *in vivo*. Following an editorial entitled 'Goodbye Flat Biology' published in Nature in 2003 emerged a new era for tumour modelling (255). Over the last decade scientists have developed many methods to culture breast cancer cells in 3D (187)(discussed in Chapter 1). However, many of these models rely on animal derived matrices and exhibit drawbacks of their own.

5.1.1 Recapitulating the extracellular matrix *in vitro*

5.1.1.1 Biological matrices

The role of the tumour microenvironment has become of increasing interest to scientists. One such component is the basement membrane that comprises type IV collagen, growth factors including FGF, EGF and TGFβ and glycosylated molecules (256). This membrane separates epithelial cells from mesenchymal and is believed to hold particular importance in metastasis (257). Matrigel™ is an animal derived matrix that has the ability to activate signalling pathways in cancer cells that influence drug sensitivity, angiogenesis and cell mortality (258). The components of Matrigel™ itself, however, are not well defined (258) and can lead to variability between batches and thus cannot be used in high throughput drug screens where conditions should be tightly controlled. Another commonly used biological matrix is collagen I, being suitable for breast cancer as collagen makes up a large proportion of the extracellular matrix (176, 259, 260). Biological matrices can reflect cancer cell growth *in vivo* better, however, due to the natural heterogeneity of a

biologically derived substance the matrix composition differs between batches. Results are therefore not always reproducible and do not meet the tight regulation required for preclinical drug screening.

5.1.1.2 Synthetic matrices

Synthetic matrices have also been developed that overcomes variability observed in biologically derived matrices. The use of synthetic hydrogels provides a matrix whose composition is known and can be defined. Hydrogels have been used to study multiple areas of breast cancer including epithelial to mesenchymal transition (259, 261, 262). In early studies the small size of pores in the matrices led to limited and constrained cell growth. The development of hydrogels with macro- sized pores allow for a greater level of tumour outgrowth and nutrient transport (263). That said, it is likely that hydrogel incorporation with other scaffolds could prove to be advantageous.

5.1.1.3 Inert fabricated scaffolds

Non-adherent tissue culture plates are available and commonly used for spheroid outgrowth (176). However, such methods lead to a highly variable population of 3D aggregates that are not compatible for high throughput drug screens (264). To overcome some of the shortcomings physical 3D matrices comprising inert materials have been developed to support consistent and uniform 3D outgrowth. Alvetex® is an inert polystyrene scaffold of 200 μM diameter made from materials commonly used for standard 2D tissue culture that can be used alone or alongside a biological/synthetic matrix (265, 266). Another material utilised is electrospun poly-ε-caprolactone that formed scaffolds capable of harbouring functional neural networks (267). 3D printing of a scaffold using bio- or inert materials to seed cells into also provides the infrastructure to encourage 3D cell outgrowth (268). The use of physical scaffolds boast the advantage of their superior ability for routine cell culture experiments due to ease of handling, long shelf life and affordability.

5.1.2 Growing mammary epithelial cells in 3D cell culture *in vitro*

To fully recapitulate human tumour growth clinical samples should be utilised. Growing human tissue explants outside of the body has provided valuable insight into multiple areas of medicine including brain development and disease modelling (269-271). Such 'organoid' culture systems have also been developed for mammary epithelial cell culture. Primary breast epithelial cells have been successfully grown in both biological and synthetic matrices to form structures resembling *in vivo* breast tissue including morphological and physiological properties (272, 273).

It may be the case that the appropriate model is experiment and cell type dependent. Many models still lack vital components such as stromal cells and appropriate cell culture media to enable longer term culture of primary cells. This is echoed by the lack of translatability of novel oncology therapeutics from preclinical drug models to patients with only 7 % of oncology drugs that enter phase I clinical trials becoming approved therapeutics (166). In part, generating a high-throughput model that provides accurate data translatable to human disease for use in preclinical drug testing would increase the number of successful drugs going through clinical trials.

5.1.3 Aims

The aim of this chapter was to initially investigate differences in the growth of breast cancer cell lines when cultured with and without perfusion. To do this a novel 3D cell culture platform, PerfusionPal was used. Breast cancer cell lines and primary breast derived tumour cells were cultured in the PerfusionPal system. The primary breast tumour cells were previously shown to be unsuccessfully cultured using standardised 2D cell culture techniques. Following this the effect of AfD11M was investigated in the model.

5.2 Results

5.2.1 Using modified FibroLife medium to culture cells in 3D

The HER2 overexpressing cell line BT-474 was grown in modified FibroLife® medium (epiFL) to compare growth to standard media. Cells were sequentially transferred from standard media to epiFL in a method previously described (176). BT-474 cells were grown in standard cell culture flasks and were subjected to successive transfer from RPMI medium to epiFL. The epiFL medium was made up as directed by the manufacturer but omitting FGF and TGFβ (2.13.1). Consistent with previous work (176) cells remained attached to the culture vessel until cells were in 100 % epiFL and were subjected to enzymatic detachment. Cells then began to form loose aggregates before forming more densely packed spheroids that grew up to ~500 μM in diameter (Figure 5.1). It was previously shown that different cell lines have differing abilities to form spheroids in matrix free epiFL culture (176). Repeating this experiment reiterated previously published data that SKBR3 cells formed loose grape-like aggregates and MDA-MB-231 cells formed loose aggregates.

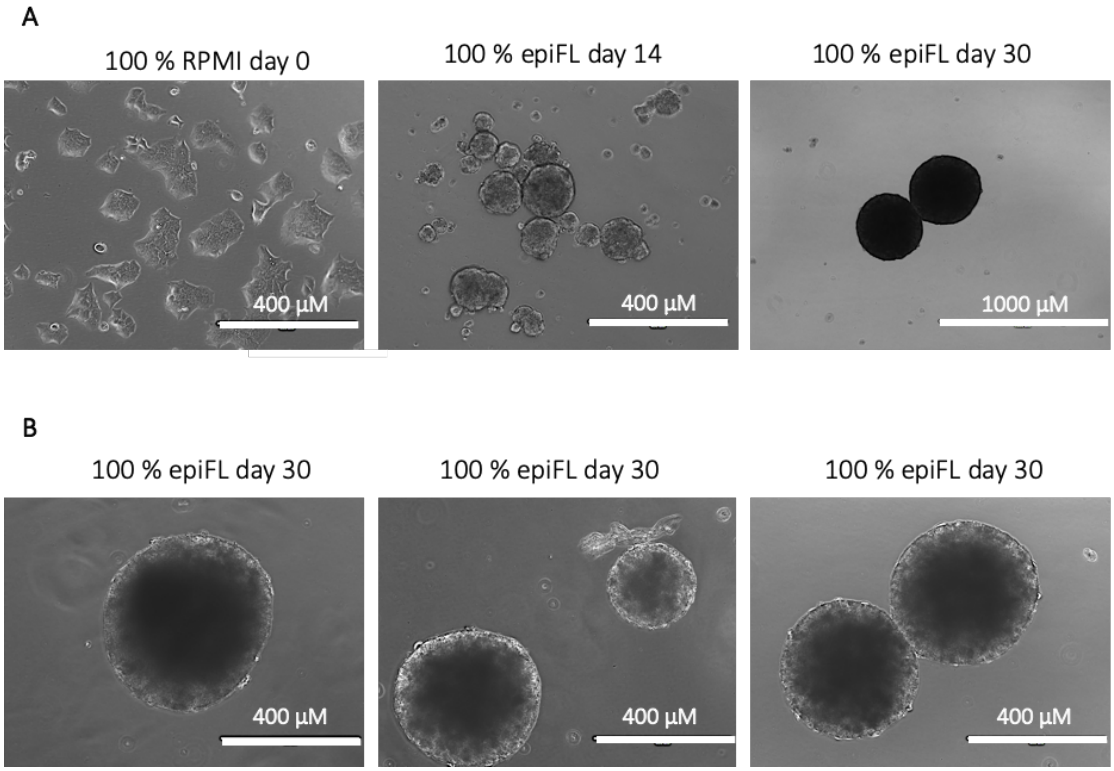


Figure 5.1 BT-474 cells sequentially transferred from RPMI to epiFL media.
BT-474 cells were transferred from 100 % RPMI media to 100 % epiFL media over the course of ~10 days. Cells were cultured in 100 % RPMI, 75 % RPMI, 50 % RPMI, 25 % RPMI and 0 % RPMI with the remainder made up by epiFL. Cells gradually became detached and form aggregates **(A)**, over a longer time period aggregates grew to form large spheroids **(B)**.

5.2.2 Establishment of a novel cell culture system

Whilst spheroid models do recapitulate some of what is observed *in vivo* it is challenging to create uniform spheroids of known cell density so comparable studies can be carried out. To overcome some of the drawbacks of using spheroid models or matrix reliant 3D cell culture we investigated the use of novel 3D cell culture scaffold SeedEZ. The SeedEZ scaffold is composed of multiple randomly arranged inert glass microfibers (Figure 5.2).

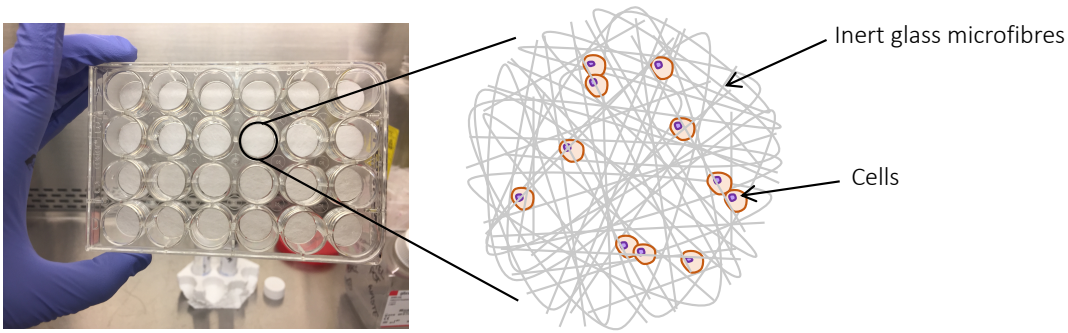


Figure 5.2 SeedEZ scaffold.
The SeedEZ scaffold is composed of randomly arranged inert glass microfibers. Scaffolds are easily transferable to 24 well plate by forceps. When seeded, scaffolds are designed such that cells will integrate through the scaffold in a 3D arrangement.

SeedEZ and PerfusionPal were designed by LenaBioscience, a start-up company based at Georgia Tech in Atlanta, Georgia, U.S.A. The scaffold was designed and optimised by Dr. Jelena Vukasinovik and Dr. JT Shoemaker. PerfusionPal is composed of a reservoir of the high-density liquid perfluorocarbon, 12 open bottom well plate insert that holds the SeedEZ scaffold and a syringe pump (Figure 5.3). Upon optimisation the system was improved to include a plastic 'insert' that was used to push SeedEZ scaffolds to the same distance down all wells.

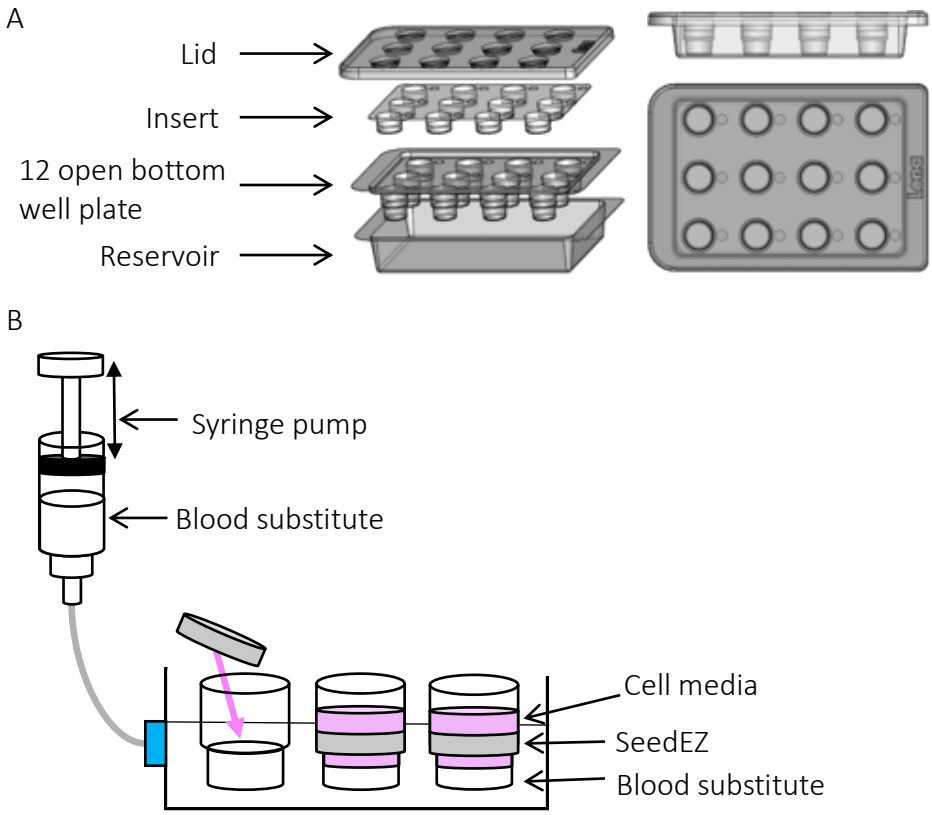


Figure 5.3 3D cell culture system PerfusionPal.
(A) components of the PerfusionPal plate and **(B)** cartoon to show the PerfusionPal plate attached to a syringe pump that is utilised to infuse and withdraw blood substitute that subsequently pushes media through the SeedEZ scaffold recapitulating flow of blood to tissue in the body.

5.2.2.1 Preliminary findings from SeedEZ cell culture

During my time at LenaBioscience preliminary experiments were performed to optimise the culture conditions of the BT-474 cell line in SeedEZ. BT-474 cells were chosen as had previously been identified as a cell line capable of forming spheroids following culture in epiFL. Cells were seeded into the SeedEZ scaffold in either epiFL or RPMI media as either ready formed spheroids or single cell suspension as per section 2.13.2. The effects of coating scaffolds with poly-D-lysine (PDL) prior to cell seeding was also investigated. PDL is an animal free synthetic extracellular matrix that can facilitate cell adhesion to plastic and glass surfaces. As an end point assay cell viability was observed using a LIVE/DEAD viability assay for mammalian cells (2.13.2.2.1). The assay utilises calcein AM, a non-fluorescent cell permeable dye that is converted to highly fluorescent calcein upon exposure to intracellular esterases. Dead cells are identified by Ethidium homodimer-1 that enters cells with compromised membranes, a marker for cell death, and binds to

DNA subsequently leading to a high level of red fluorescence. Together the dyes indicate which cells are live (green) and which are dead (red).

Spheroids that were ready formed in epiFL were unable to integrate into the SeedEZ scaffold (Figure 5.4). This is most likely due to spheroids being too large to enable them to penetrate through the glass fibres into the scaffold. Cells seeded directly in 100 % epiFL were previously cultured in 100 % RPMI. Following detachment by TrypLE™ Express Enzyme (1 x) and centrifugation, cells were resuspended in 100 % epiFL. Cells cultured in epiFL did not show increased cell death compared to culture in 100 % RPMI (Figure 5.4) suggesting that this cell line is able to be transferred directly into 100 % epiFL medium without sequential transfer with no obvious adverse effects. There were no obvious differences between culture in epiFL medium in SeedEZ that had been PDL coated and that had not.

Cells cultured in RPMI media looked to be higher in number but also in cell death, which would be expected (Figure 5.4). Cells cultured in uncoated SeedEZ scaffolds looked to contain aggregates that show evidence of a necrotic core indicated by the red ethidium homodimer-1 stain at the centre of the green calcein (Figure 5.4). At a higher magnification (10x) there appears to be more cells present in uncoated compared to coated scaffolds, however, a larger view would be needed to confirm any significant findings.

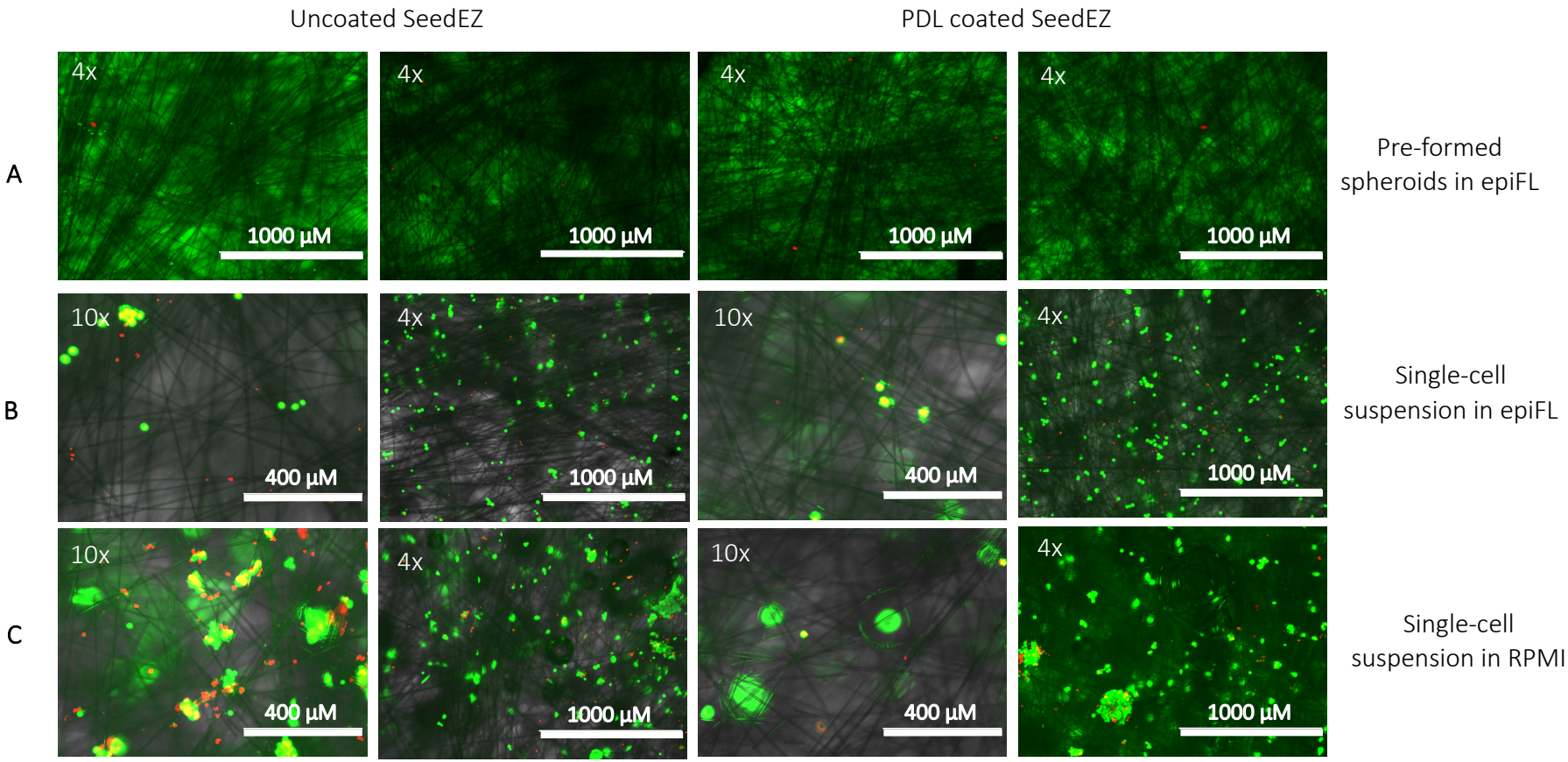


Figure 5.4 Comparing properties of BT-474 cells grown in SeedEZ under different conditions.

BT-474 cells were **(A)** seeded in 6 well plates at a density of 6 x 107 in 50 % RPMI, 50 % modified Fibrolife® media. After 48 hours cells were cultured in 100 % modified Fibrolife® medium. Once spheroids had formed 100 µL was transferred to a SeedEZ scaffold using a wide bore pipette tip **(B)** trypsinised, pelleted and resuspended in either epiFL **(B)** or RPMI **(C)** and made to a concentration of 2 x 107 cells/mL. 100 µL was transferred to SeedEZ. All cells were incubated on the scaffold for ~20 mins prior to the addition of 500 µL culture medium. Cells were cultured for 72 hours prior to analysis of cell life using the Calcein AM live/dead assay. Cells were imaged using an EVOS microscope with magnification stated in the top left corner of images.

5.2.3 Culturing breast cancer cell lines in PerfusionPal and SeedEZ in standard culture media

Whilst the SeedEZ scaffold provides a 3D matrix for cells, the culture itself is static. Solid tumours in the body often have developed their own blood supply through angiogenesis that provide the tumour with the nutrients it needs to grow . To better recapitulate the diffusion of nutrients through the tumour the PerfusionPal system was used alongside the SeedEZ scaffold. The blood substitute used in the reservoir of PerfusionPal is the dense liquid perfluorocarbon. Experiments undertaken by Dr. JT Shoemaker demonstrated that perfluorocarbon is an inert liquid that does not facilitate the transfer of nutrients between wells (data not shown). To test the suitability of the PerfusionPal system for breast cancer disease modelling the breast cancer cell lines BT-474, MDA-MB-231 and AU-565 were seeded in the scaffolds at a range of densities.

5.2.3.1 BT-474

Cells were seeded at a range of densities into the SeedEZ scaffolds and cultured in PerfusionPal for ~5 days (2.13.2). The blood substitute was infused and withdrawn twice every 24 hours going a speed of ~27 μL/min. Half media changes were carried out daily by carefully aspirating 425 μL media from the wells at the point where the syringe pump is fully infused and gently replacing 425 μL down the side of the well. As an end point assay SeedEZ scaffolds were transferred to a clean 24 well plate containing 500 μL media with 10 % AlamarBlue to analyse metabolic activity (2.10.2.2.1). Fluorescence intensity, therefore, directly correlates to metabolic activity.

Initial experiments using the BT-474 cell lines tested different cell seeding densities ranging from 5 x 10^4 to 1 x 10^6 cells/ SeedEZ scaffold (Figure 5.5A). The experiment showed that at higher seeding densitites there was greater metabolic activity of cells with perfusion compared to without. Further experiments were carried out to investigate how higher cell densities responded to perfusion (Figure 5.5B and C). In each experiment there was a trend that perfused scaffolds demonstrated increased metabolic activity compared to unperfused scaffolds. However, difficulties arose when trying to merge the datasets to give representative data, discussed in section 5.2.3.4.

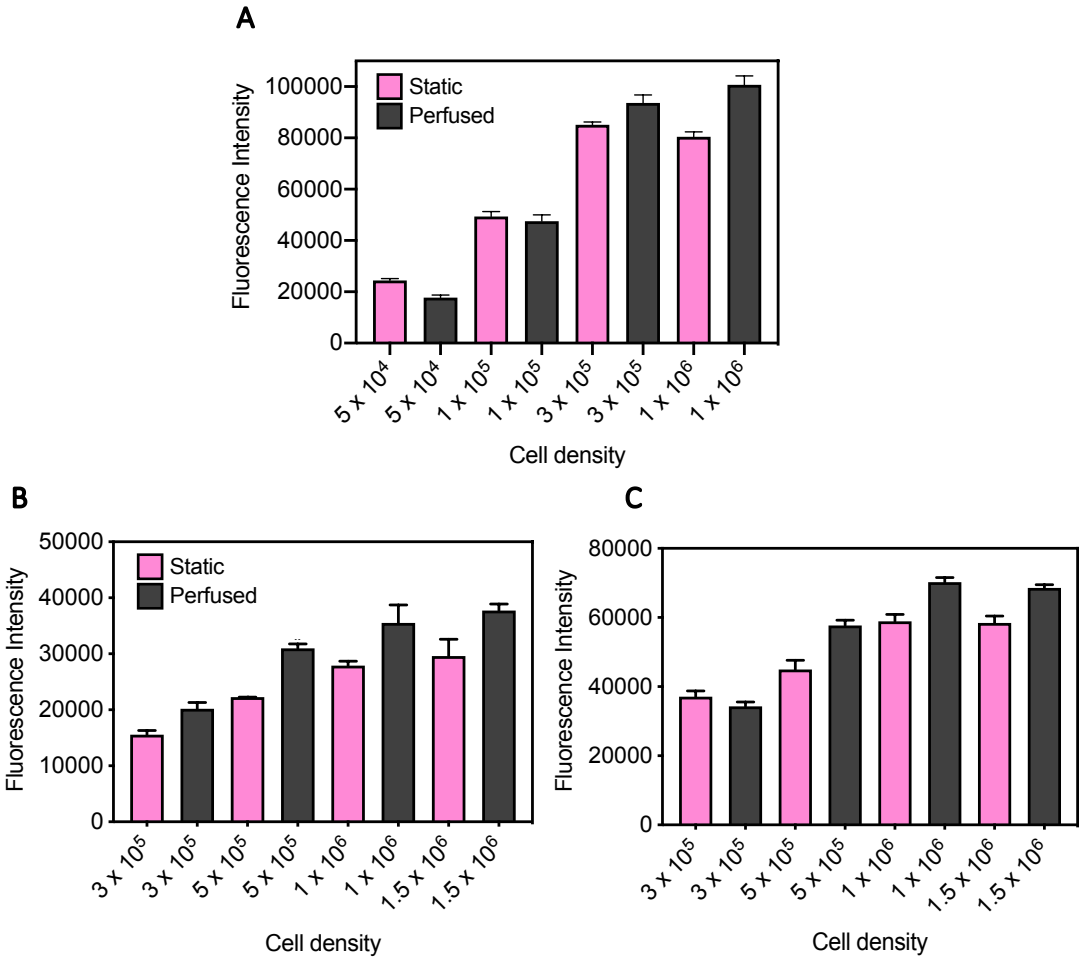


Figure 5.5 BT-474 cells cultured in SeedEZ scaffolds ± PerfusionPal in RPMI media.
Cells were initially cultured in 2D to obtain high enough numbers to seed into SeedEZ scaffolds. Cells were detatched, centrifuged and resuspended in 1 mL cell culture media. Cell counts were performed using a Countess and cells were seeded into SeedEZ scaffolds at specified densitites (X axis). Cells were cultured for 5 days in PerfusionPal with half media changes being undertaken daily. The AlamarBlue assay was used to quantify metabolic activity with fluorescence intensity being read at excitation 570 nm and emission 590 nm using a Tecan Spark microplate reader. **(A)** Initial experiment using low seeding densitites of BT-474 cells **(B and C)** Experiments using higher initial seeding densities. Error bars represent standard error of the mean between three technical repeats. Graphs were generated using GraphPad prism version 8.

To visualise the differences between static and dynamic culture a sample of scaffolds were stained with the live cell dye Calcein AM (2.13.2.2.2). BT-474 cells grown in static culture were visually lower in number and less aggregated than those grown in dynamic culture (Figure 5.6A). In static culture there was a higher level of aggregated cells on the bottom side of SeedEZ compared to smaller aggregates on the top side. When cultured in PerfusionPal the cells observed on the top and bottom side of the SeedEZ scaffold are more uniform suggesting cells distribute evenly throughout the scaffold (Figure 5.6B).

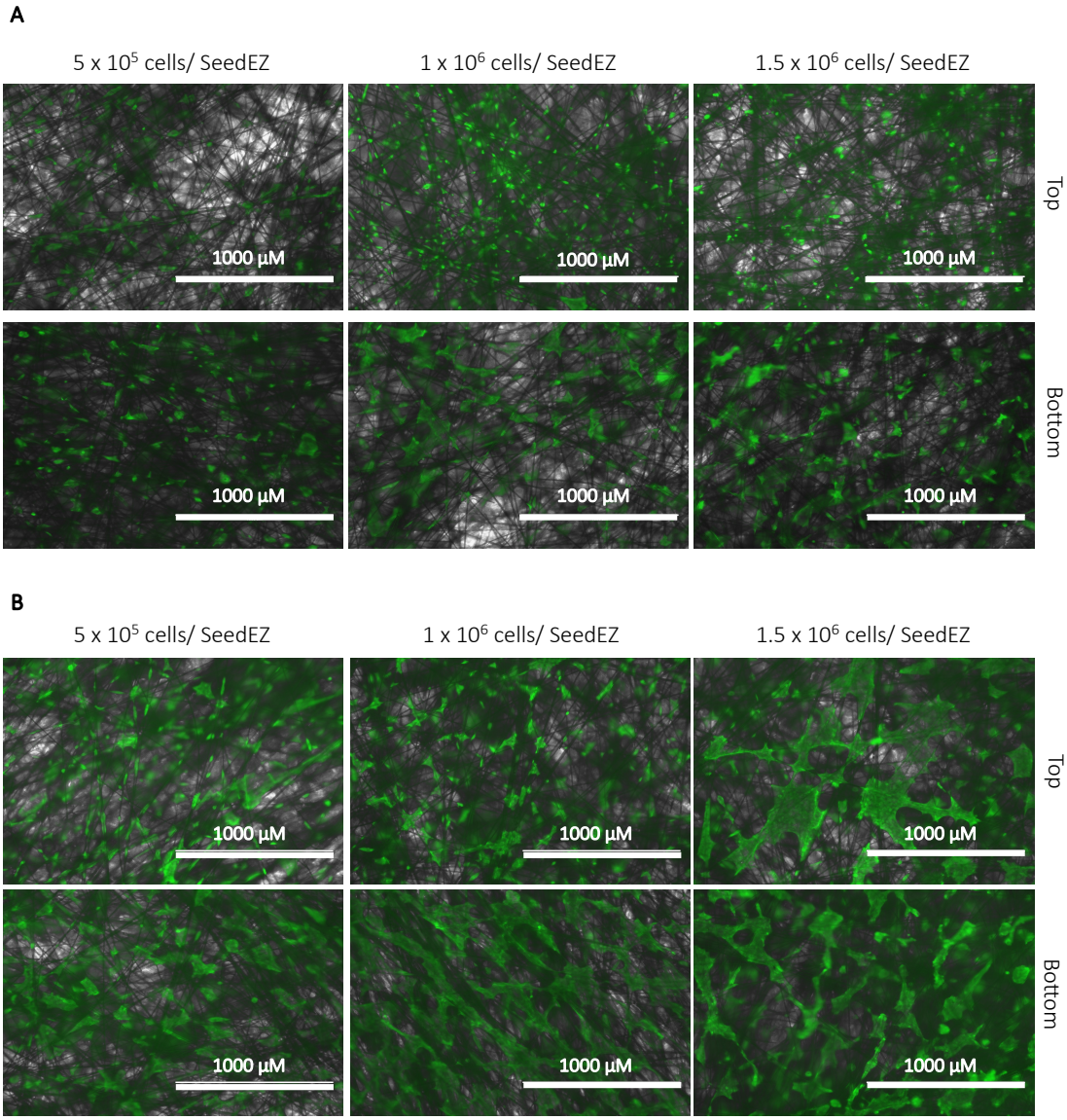


Figure 5.6 BT-474 cells grown in SeedEZ scaffold stained with Calcein AM.
BT-474 cells were seeded in SeedEZ scaffolds at different densities (labelled) on day 0. Scaffolds were cultured in either **(A)** a 24 well culture plate as a static control or **(B)** PerfusionPal. On day 5 scaffolds were incubated with Calcein AM to visualise live cells. Images were taken on an EVOS fluorescent microscope with x4 magnification.

5.2.3.2 MDA-MB-231

Cell lines exhibit morphological differences when observed under the microscope. BT-474 cells tend to grow in clumps whereas MDA-MB-231 cells grow in a consistent monolayer. Therefore, it was interesting to observe differences when grown in 3D culture. Initially MDA-MB-231 cells were seeded at lower densities, as BT-474 were, to observe if a significant increase in metabolic activity could be observed at lower densities in different cell lines. However, again, as with BT-474 the increase in metabolic activity with perfusion compared to static was more evident at higher seeding densities (Figure

5.7A). The MDA-MB-231 cell line were seeded at higher seeding densitites and cultured in SeedEZ scaffolds with and without perfusion for ~5 days (Figure 5.7B, C, D and E). The trend was the same as that observed in BT-474 cells that metabolic activity increased as cell seeding density increased and also with perfusion (Figure 5.7B, C, D and E).

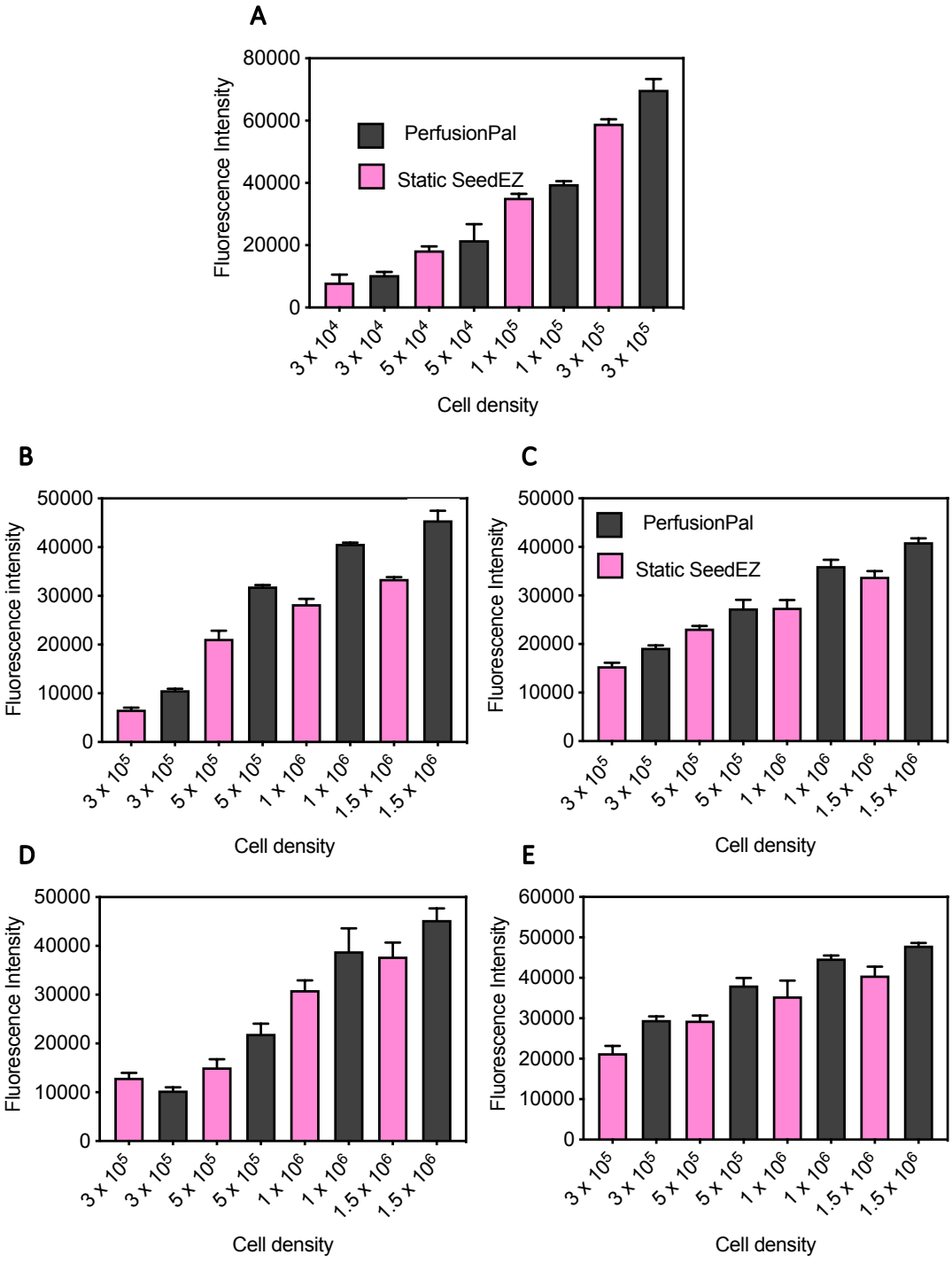


Figure 5.7 Culturing MDA-MB-231 cells in SeedEZ scaffold ± perfusion.

Cells were initially cultured in 2D to obtain high enough numbers to seed into SeedEZ scaffolds. Cells were detatched, centrifuged and resuspended in 1 mL cell culture media. Cell counts were performed using a Countess and cells were seeded into SeedEZ scaffolds at specified densitites. Cells were cultured for 5 days in PerfusionPal with half media changes being undertaken daily. The AlamarBlue assay was used to quantify metabolic activity with fluorescence intensity being read at excitation 570 nm and emission 590 nm using a Tecan Spark microplate reader. **(A)** Initial experiment using low densitites of BT-474 cells **(B, C, D, E)** Repeats of the same experiment using higher seeding densitites. Error bars represent standard error of the mean between three technical repeats. Graphs were generated using GraphPad prism version 8.

5.2.3.3 AU-565

The AU-565 cell line is HER2 overexpressing and proved to be the most susceptible to the Affimer drug conjugates developed (chapter 4). Therefore, it was interesting to observe the growth of this cell line in SeedEZ culture. Upon recommendation of ATCC guidelines AU-565 cells should not be grown beyond 60 % as they begin to differentiate. Therefore, in initial experiments lower densities of AU-565 cells were seeded compared to what had been used with previous cell lines (Figure 5.8A). The trend was again the same as previously observed so AU-565 cells were seeded at higher initial densities in subsequent experiments (Figure 5.8B, C and D). Metabolic activity was greater with increasing cell seeding densitites and with perfusion (Figure 5.8B, C and D). However, the difference between static and perfused culture were inconsistent between biological repeats and so normalising data would again lead to graphs that misrepresent the trend. This problem is discussed in section 5.2.3.4.

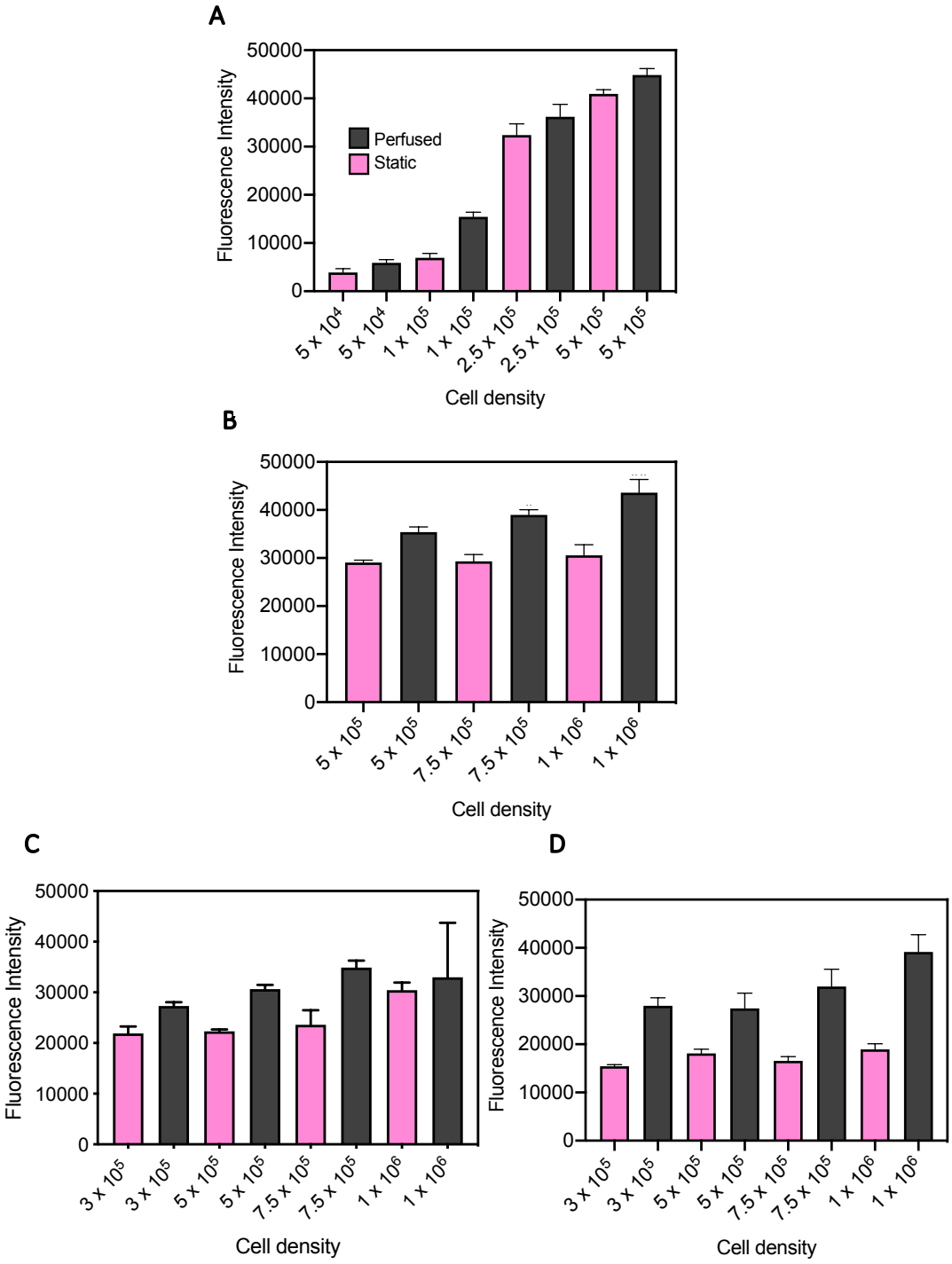


Figure 5.8 Culturing AU-565 cells in RPMI medium in SeedEZ scaffolds with and without PerfusionPal.
Cells were initially cultured in 2D to obtain high enough numbers to seed into SeedEZ scaffolds. Cells were detatched, centrifuged and resuspended in 1 mL cell culture media. Cell counts were performed using a Countess and cells were seeded into SeedEZ scaffolds at specified densitites. Cells were cultured for 5 days in PerfusionPal with half media changes being undertaken daily. The AlamarBlue assay was used to quantify metabolic activity with fluorescence intensity being read at excitation 570 nm and emission 590 nm using a Tecan Spark microplate reader. **(A)** Initial experiment using low densitites of BT-474 cells **(B, C, D)** Repeated experiments using higher initial seeding densities. Error bars represent standard error of the mean. Graphs were generated using GraphPad prism version 8.

5.2.3.4 Normalisation of PerfusionPal experiments between biological repeats

The data presented above for cell lines AU-565, BT-474 and MDA-MB-231 did not show a trend when normalised. This lead to difficulties in combining biological repeats to give an accurate representation of the data collected. Below are graphs showing data used above that has been normalised against the lowest seeding density (Figure 5.9). Individual points plotted is the mean normalised value for each biological repeat (raw data shown in above figures). The data shown in the normalised set does not demomstrate the trend that increased metabolic activity is observed in PerfusionPal compared to static SeedEZ culture as the data has been normalised against its own lowest density. Therefore, for these preliminary experiments of investigating different seeding densities the data was not normalised.

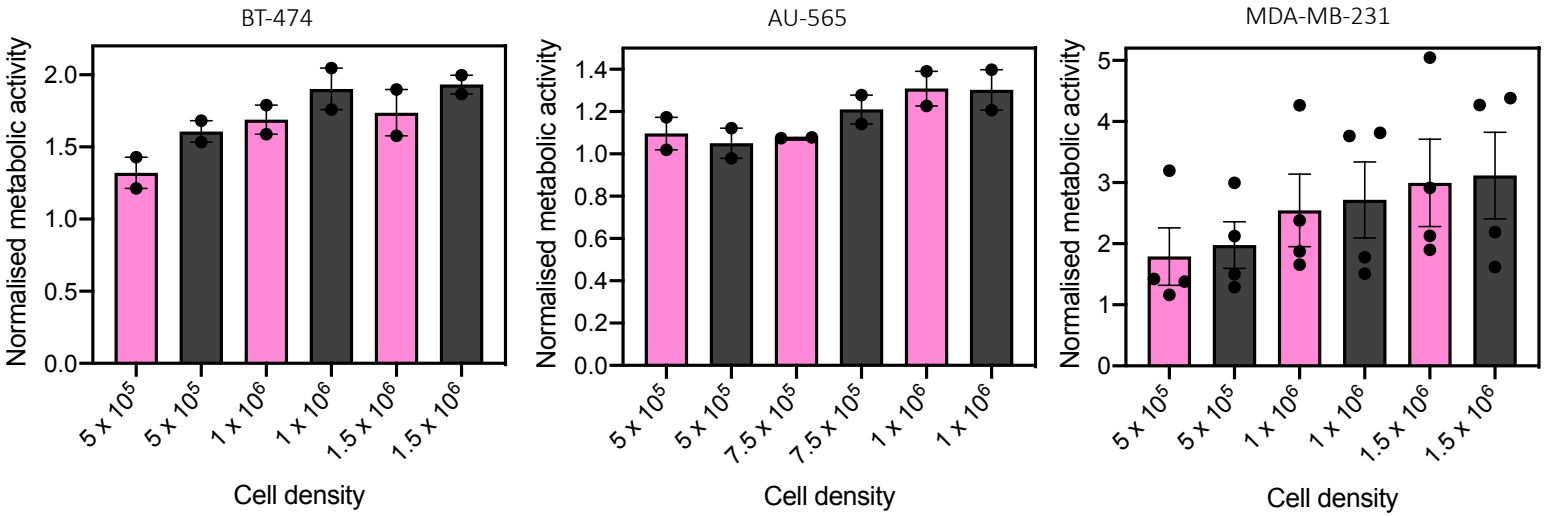


Figure 5.9 Normalisation of PerfusionPal data for AU-565, BT-474 and MDA-MB-231 in standard culture media.
Graphs depict PerfusionPal data for cell lines AU-565, BT-474 and MDA-MB-231, grown in standard tissue culture media (RPMI or DMEM), that has been normalised to the lowest cell density 3 x 10^5 cells/scaffold. Scatter points represent mean values of biological repeats where error bars represent the standard error of the mean between biological repeat mean values. Graphs were created using GraphPad Prism version 8.

5.2.4 Culturing breast cancer cell lines in PerfusionPal with epiFL media

The breast cancer cell lines BT-474, MDA-MB-231 and AU-565 all demonstrated increased metabolic activity when cultured with perfusion compared to without in their standard culture media. We previously demonstrated that BT-474 cells were able to form spheroids in epiFL media with no further additions. To develop PerfusionPal as an animal-free 3D cell culture model the FBS used in standard culture medium needs to be omitted. By using epiFL this aim is fulfilled.

5.2.4.1 BT-474 cultured in PerfusionPal with epiFL

The BT-474 cell line was seeded into SeedEZ scaffold at densities used previously when cultured with RPMI. The cells were cultured in their standard media in 2D before being resuspended into 100 % epiFL for seeding into SeedEZ for culture as a static scaffold or in PerfusionPal (2.13.2). Metabolic activity increased as cell seeding density increased when cultured with perfusion. However, metabolic activity of cells did not increase with seeding density when cultured as static culture.

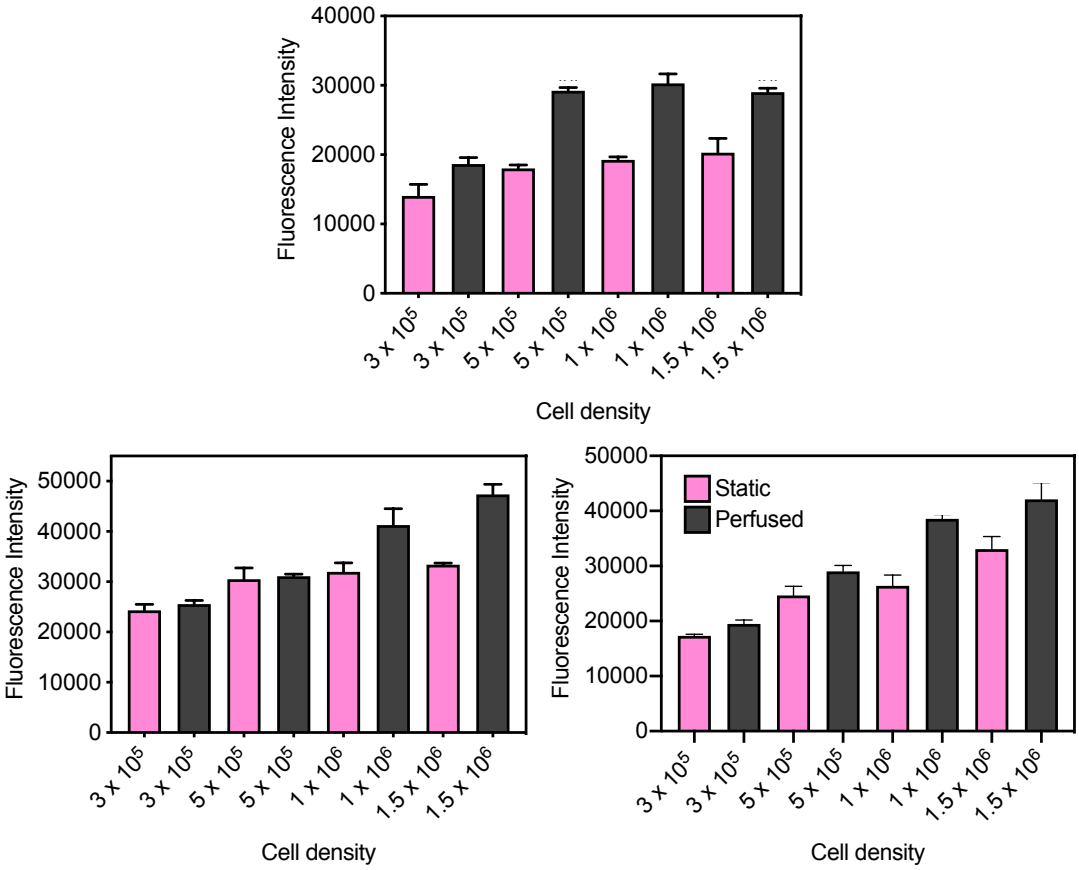


Figure 5.10 BT-474 cells cultured in epiFL media in SeedEZ ± PerfusionPal.
Cells were initially cultured with RPMI in 2D to obtain high enough numbers to seed into SeedEZ scaffolds. Cells were detatched, centrifuged and resuspended in 1 mL epiFL media. Cell counts were performed using a Countess and cells were seeded into SeedEZ scaffolds at specified densitites. Cells were cultured for 5 days in PerfusionPal with half media changes being undertaken daily. The AlamarBlue assay was used to quantify metabolic activity with fluorescence intensity being read at excitation 570 nm and emission 590 nm using a Tecan Spark microplate reader. Each graph is a repeat of the same experiment where error bars represent standard error of the mean between three technical replicates. Graphs were generated using GraphPad prism version 8.

5.2.4.2 MDA-MB-231 cultured in PerfusionPal with epiFL

The MDA-MB-231 cell line were also seeded at the same densities as used for previous PerfusionPal experiments. The trend demonstrated that metabolic activity increased with increasing seeding densities when cultured with PerfusionPal but less so when cultured in static SeedEZ culture (Figure 5.11).

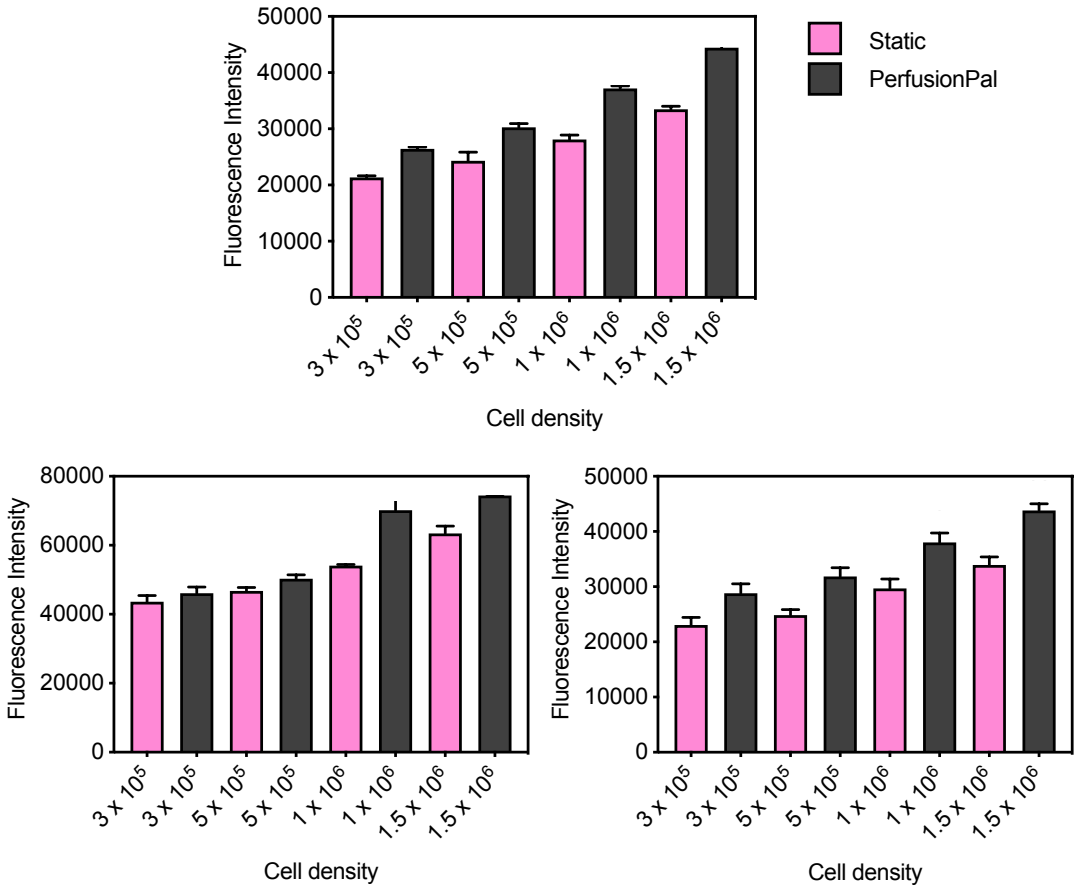


Figure 5.11 Culturing MDA-MB-231 cells in SeedEZ ± PerfusionPal in epiFL media.
Cells were initially cultured with DMEM in 2D to obtain high enough numbers to seed into SeedEZ scaffolds. Cells were detatched, centrifuged and resuspended in 1 mL epiFL media. Cell counts were performed using a Countess and cells were seeded into SeedEZ scaffolds at specified densitites. Cells were cultured for 5 days in PerfusionPal with half media changes being undertaken daily. The AlamarBlue assay was used to quantify metabolic activity with fluorescence intensity being read at excitation 570 nm and emission 590 nm using a Tecan Spark microplate reader. Each graph is a repeat of the same experiment where error bars represent standard error of the mean between three technical repeats. Graphs were generated using GraphPad prism version 8.

5.2.4.3 AU-565 cells cultured in PerfusionPal with epiFL

The cell line AU-565 was again seeded at lower seeding densities due to advice by ATCC. The metabolic activity of cells cultured in PerfusionPal were greater than those cultured in static SeedEZ scaffolds at all cell densitites. The metabolic activity of cells cultured in 100 % epiFL in static SeedEZ scaffolds was low suggesting that AU-565 cells cannot be taken from 100 % RPMI to 100 % epiFL directly. The data suggests that different cell types respond differently to culture in epiFL and PerfusionPal.

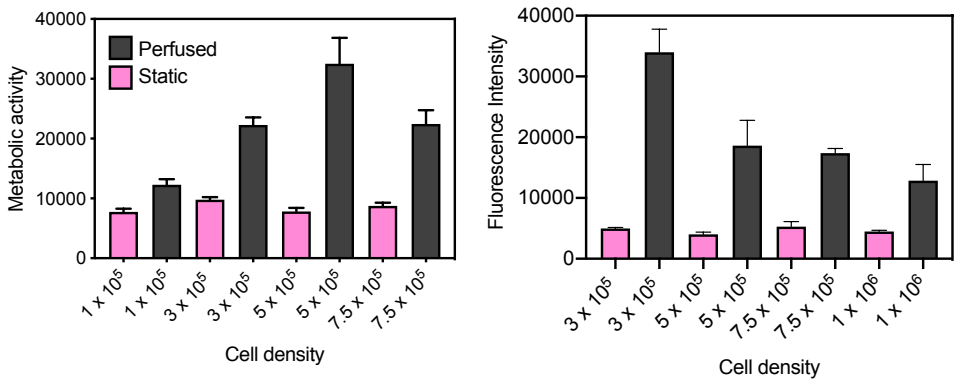


Figure 5.12 AU-565 cells cultured in SeedEZ scaffolds ± PerfusionPal in epiFL media.
Cells were initially cultured with RPMI in 2D to obtain high enough numbers to seed into SeedEZ scaffolds. Cells were detatched, centrifuged and resuspended in 1 mL epiFL media. Cell counts were performed using a Countess and cells were seeded into SeedEZ scaffolds at specified densitites. Cells were cultured for 5 days in PerfusionPal with half media changes being undertaken daily. The AlamarBlue assay was used to quantify metabolic activity with fluorescence intensity being read at excitation 570 nm and emission 590 nm using a Tecan Spark microplate reader. Error bars represent standard error of the mean between three technical repeats. Graphs were generated using GraphPad prism version 8.

5.2.5 Dose response of breast cancer cell lines with Trastuzumab in PerfusionPal

Having shown that breast cancer cell lines can be cultured in standard media and epiFL in PerfusionPal we wanted to investigate the effects of Trastuzumab in the model. Trastuzumab is a monoclonal antibody that targets HER2 overexpression. It is currently the gold standard for treatment of HER2+ breast cancer as previously discussed (1.5.3). In previous chapters it has been demonstrated that Trastuzumab reduces metabolic activity of BT-474 cells to 60 % at concentrations of ~ 6 nM and above. Solid tumours are complex and the ability of a drug to penetrate it can be compromised due to the large size of monoclonal antibodies. We compared the ability of Trastuzumab to penetrate through SeedEZ when cultured under static and dynamic conditions.

The HER2 overexpressing cell line BT-474 and triple negative cell line MDA-MB-231 were seeded at a density of 1 x 10^6 cells/SeedEZ (2.13.2). The following day Trastuzumab was added during a half media change to final concentrations of 0.1, 10 and 1000 μg/mL (~0.69, 69 and 690 nM) diluted in RPMI and DMEM respectively. The Trastuzumab used in these experiments was a kind gift from St. James' University Hospital from Mr. Ikram Ali of the pharmacy department. Trastuzumab was stored at 4 °C and used within one week of obtaining. Scaffolds were then cultured for a further 72 hours before analysis of

metabolic activity by the AlamarBlue assay (2.10.2.2.1). No significant difference in metabolic activity was observed for MDA-MB-231 cells when comparing dynamic to static culture nor with and without drug (Figure 5.13). When normalised to media Trastuzumab was significantly more effective with perfusion compared to without for all concentrations showing activity at concentrations as low as 0.1 μg/mL (~0.69 nM) (Figure 5.13B).

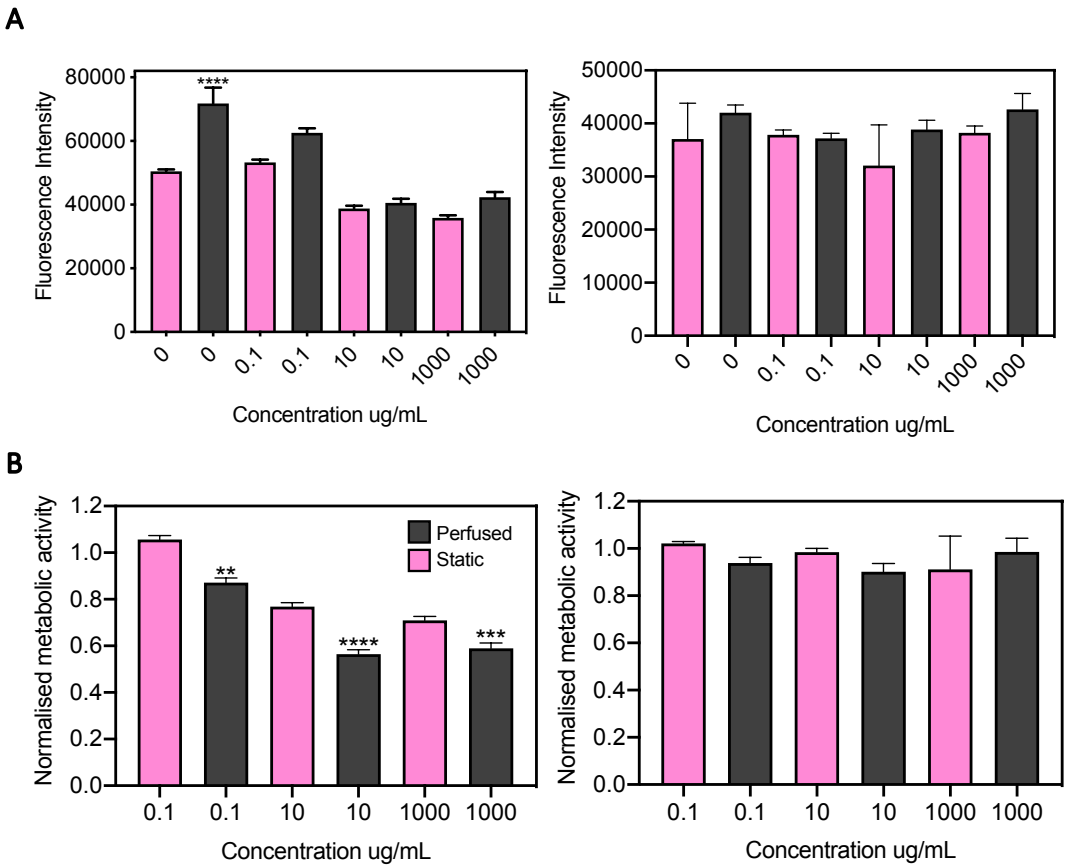


Figure 5.13 BT-474 and MDA-MB-231 dose response with Trastuzumab in PerfusionPal.
BT-474 (left) and MDA-MB-231 (right) cells were cultured in RPMI or DMEM respectively in 2D tissue culture flasks to obtain enough cells for PerfusionPal. Cells were detatched, centrifuged and resuspended in 1 mL epiFL media. Cell counts were performed using a Countess and cells were seeded into SeedEZ scaffolds at a density of 1 x 10^6 cells/SeedEZ. One day later Trastuzumab was diluted in respective media and added as a half media change with final concentrations reflected in graphs. Cells were cultured for a further 72 hours. The AlamarBlue assay was used to quantify metabolic activity with fluorescence intensity being read at excitation 570 nm and emission 590 nm using a Tecan Spark microplate reader. **(A)** Raw data from microplate reader regarding fluorescence intensity, **(B)** dose response normalised to media only. Each graph is representative of n=1 where error bars represent standard error of the mean. Statistical significance was analysed using a one way ANOVE with Tukeys multiple comparison where ** ($P \leq 0.01$), *** ($P \leq 0.001$), **** ($P \leq 0.0001$)Graphs were generated using GraphPad prism version 8.

5.2.6 Growing primary HER2+ cells in PerfusionPal

Having demonstrated that Trastuzumab had a superior effect on BT-474 cells cultured with perfusion compared to without, we wanted to test the effect of AfD11M on primary patient samples in PerfusionPal. Breast cancer tumours are heterogeneous comprising multiple different cell types and extracellular matrix. The contribution of the tumour microenvironment to tumorigenesis has been an evolving field of research over the past decade. Cell lines are homogeneous and do not represent the complexity of *in vivo* breast tumours. Primary patient samples were provided as explants enabling recapitulation of heterogeneity of *in vivo* tumours thus leading to a model that is more translatable from the laboratory to the clinic.

5.2.6.1 AfD11M shows effectiveness in 3D cell culture

Previously, we demonstrated that AfD11M reduced metabolic activity of cells in a dose dependent manner with superior ability compared to AfH7M (Chapter 4). AfD11M was most effective on HER2 overexpressing cell lines AU-565 and SKBR3. At ~20 nM metabolic activity of AU-565 cells incubated with AfD11M was reduced to ~20 % whereas those cultured with AfCM was still ~80 %. To test the efficacy of AfD11M in PerfusionPal compared to static SeedEZ culture a concentration of 20 nM was used. Initially, AU-565 cells were seeded at a density of 2 x 10^5 cells/ SeedEZ as previously described (2.13.2.2). The metabolic activity of all conditions except AfD11M culture was higher with perfusion compared to static culture (Figure 5.14A). When normalised to media control there is insignificant differences between metabolic activity of 2D and 3D culture (Figure 5.14B).

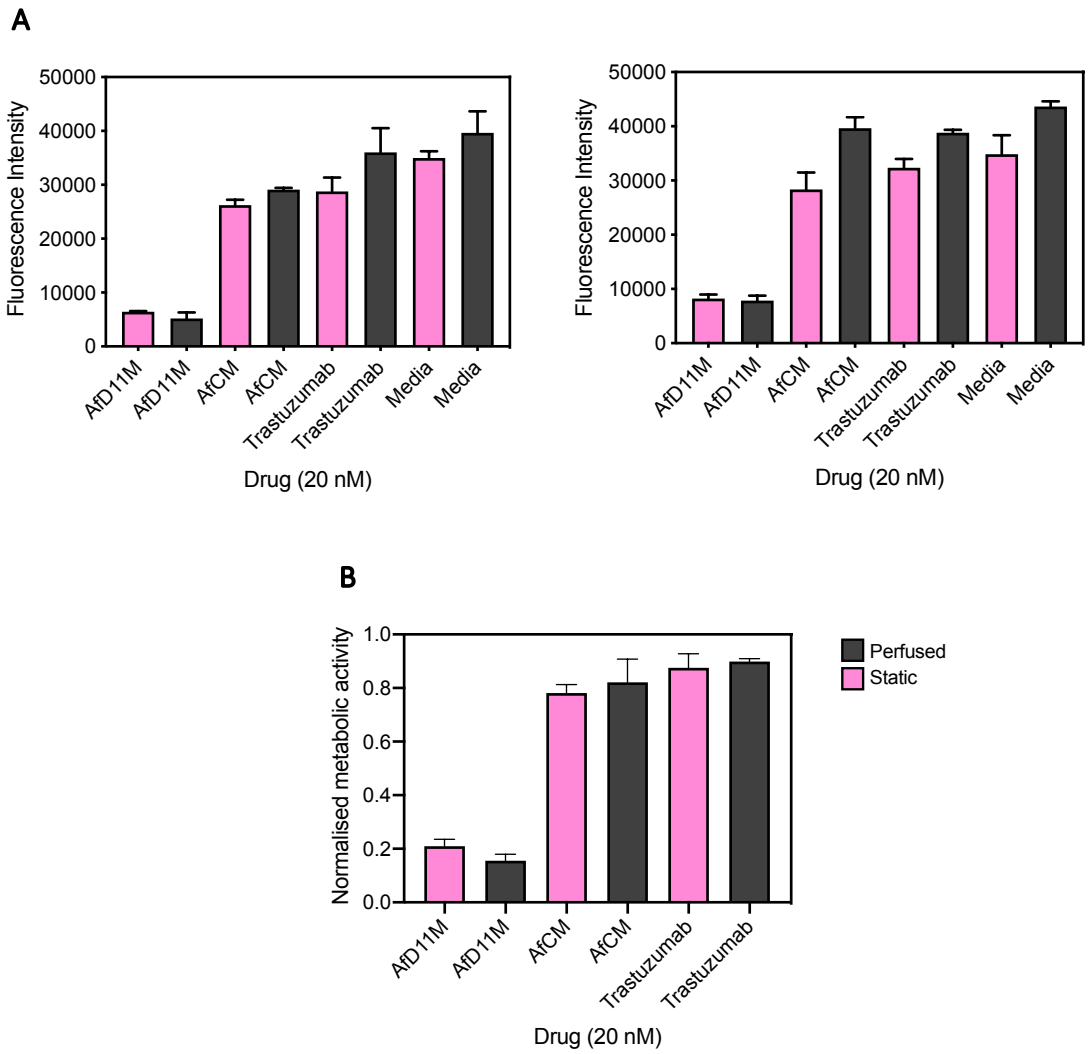


Figure 5.14 AU-565 cells incubation with AfD11M compared to AfCM and Trastuzumab in perfusionPal. AU-565 cells were seeded at a density of 2 x 10^5 cells/SeedEZ. 24 hours later 20 nM AfD11m, AfH7M or Trastuzumab were added as a half media change and incubated for a further 72 hours. Metabolic activity was analysed by the AlamarBlue assay measuring excitation at 570 nm and emission at 590 nm using a Tecan Spark microplate reader. **(A)** Raw data from two biological repeats where error bars represent standard error of the mean between technical repeats. **(B)** Data from **(A)** normalised to media only and combined so error bars represent standard error of the mean between biological replicates. Graphs were generated using GraphPad Prism version 8.

5.2.6.2 Primary breast cancer cells

Primary patient cells were gifted by BCNTB Cell Culture Programme, Barts Cancer Institute. Samples were provided from the tumours of four patients who tested HER2+ and four HER2 negative. Information regarding receptor status, age and trastuzumab response are given in Table 5.1. Patients had not received neoadjuvant therapy with the exception of patient 2400. This patient had previously had cancer 4 years prior in the opposite breast that had been treated with FEC chemotherapy (combination of 5

fluorouracil, epirubicin and cyclophosphamide) followed by one year Trastuzumab. Tamoxifen treatment was suspended due to severe headaches. Epithelial cells isolated from patients were unable to be cultured using standard 2D cell culture techniques by the Breast Cancer Now team.

Patient ID	Age	ER status	HER2 status	HER2 score	Primary or resuccrence	Neoadjuvant therapy	Treatment response
1756	60	+	+	3+	Primary	None	N/A
2400	37	+	+	3+	Recurrence	Docetaxel/carboplatin 3 cycles	Poor
2724	68	+	+	3	Primary	None	N/A
2809	79	-	+	3+	Primary	None	N/A
1681	44	+	-	1+	Primary	None	N/A
2424	98	-	-	0	Primary	None	N/A
2753	74	-	-	1+	Primary	No data	No data
3144	83	-	-	0	Primary	None	N/A

Table 5.1 Table to show characteristics of primary patient tumour cells.
Patient ID were given to ensure samples are anonymous. N/A- not applicable meant that no data was available.

5.2.6.2.1 Primary breast cancer cells cultured in PerfusionPal

Two vials of cells from each patient were provided in vials of ~ 5 x 10^5 live cells at passage 0. Optimal organoid culture used was taken from a previous study by Clevers et al (184) with minor adaptations recommended (2.13.3). Cells were thawed and immediately seeded into SeedEZ scaffolds where they were incubated at 37 °C for 20 mins prior to using forceps to transfer them into the PerfusionPal system as per previously described protocol (2.13.2.2). The following day a half media was carried out either adding media only or AfD11M. Cells were then cultured for a further 72 hours. Metabolic activity was analysed by AlamarBlue assay as previously described (2.10.2.2.1). There were no significant differences between cells cultured in static SeedEZ compared to perfused SeedEZ.

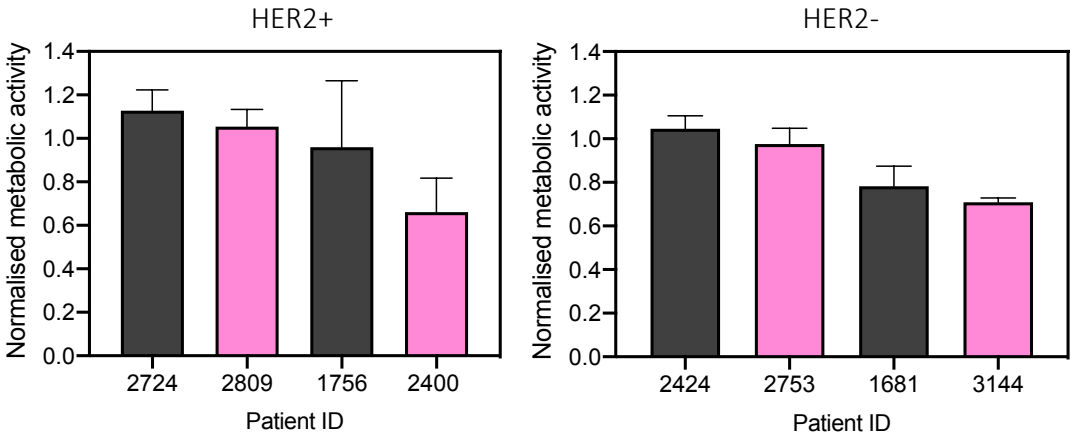
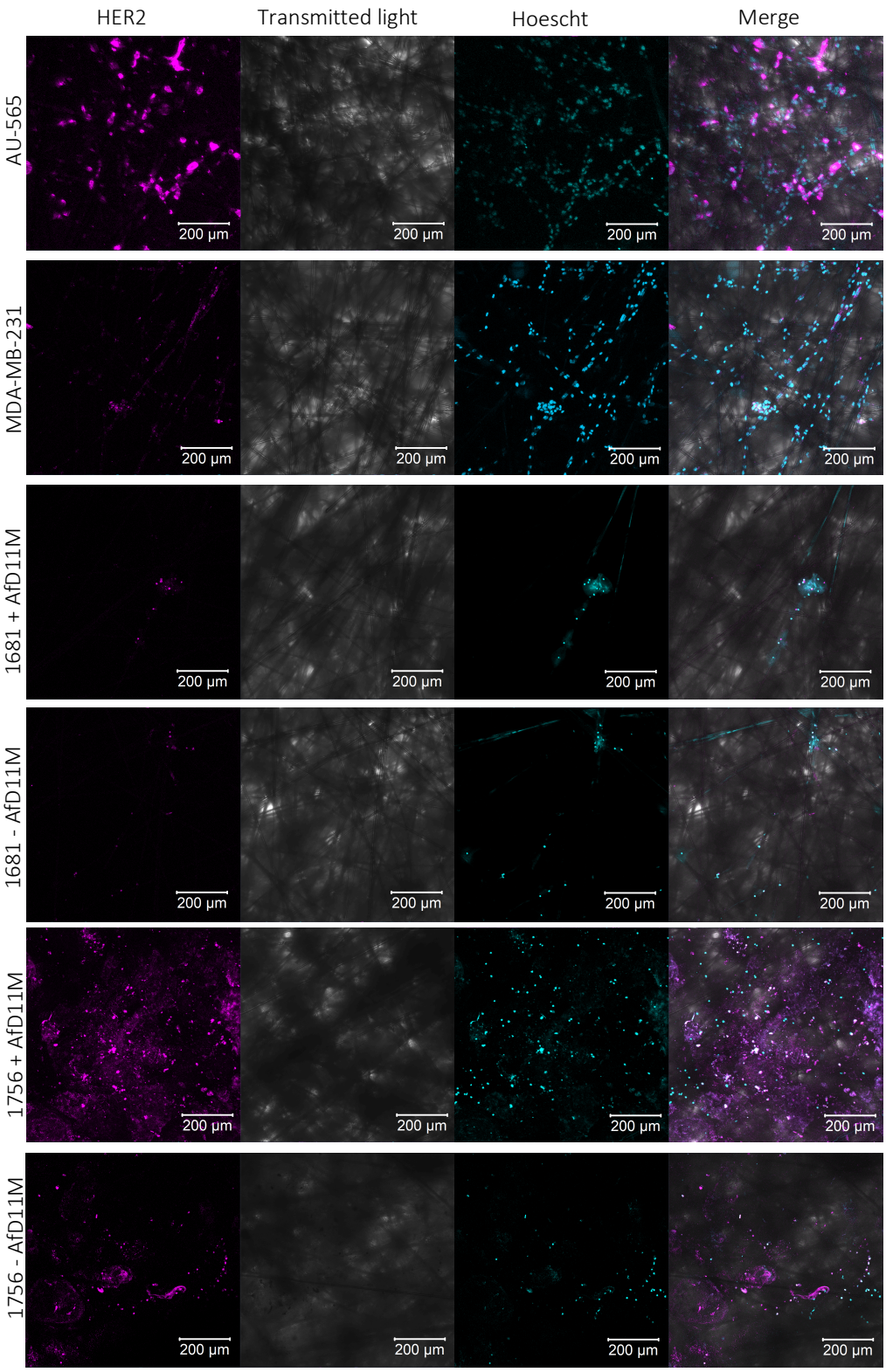
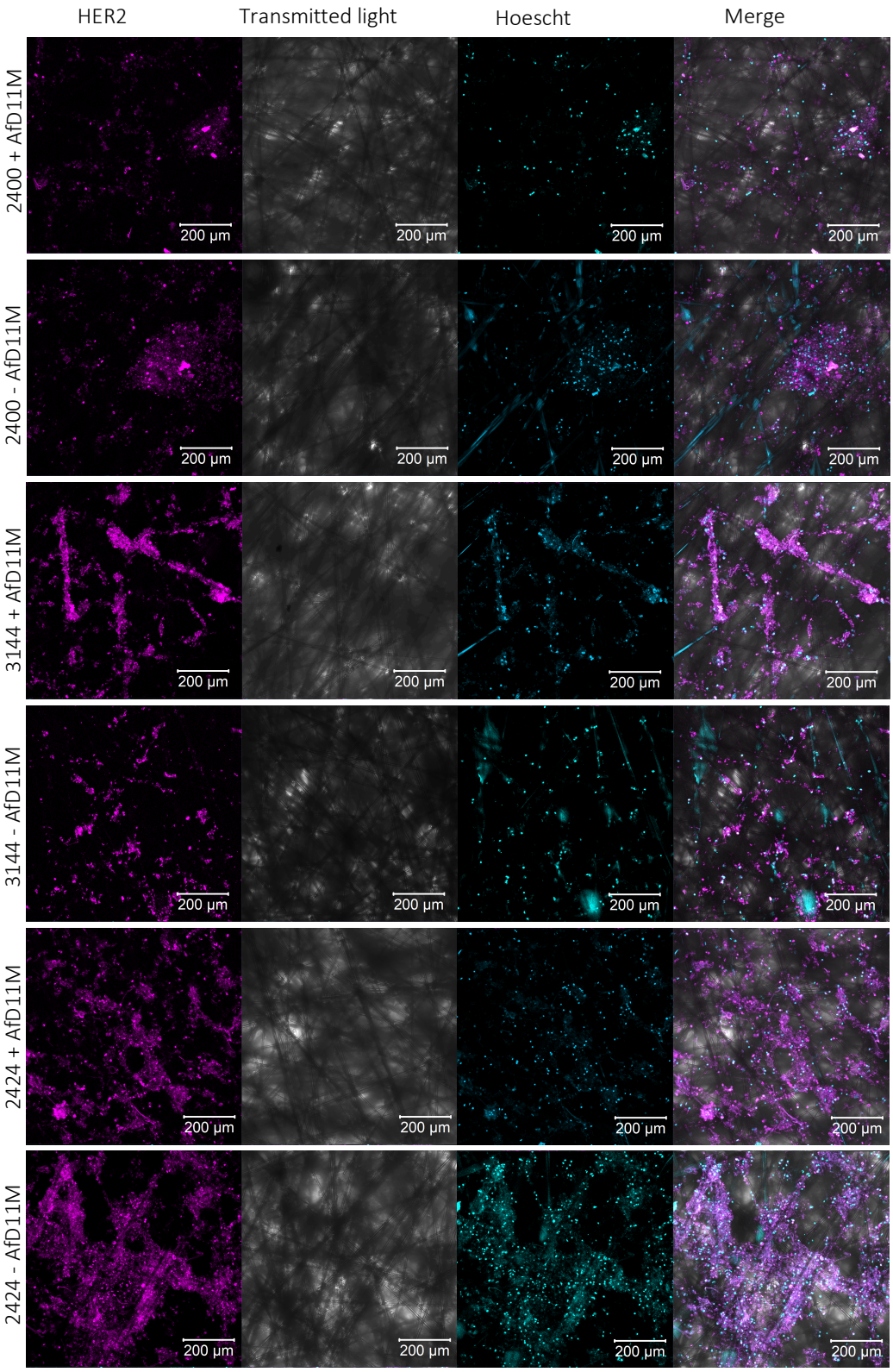


Figure 5.15 Primary breast cancer cell lines cultured in PerfusionPal.
In two separate experiments primary patient samples were seeded into SeedEZ scaffolds and cultured in PerfusionPal for 5 days. One experiment consisted of patient samples 1681, 3144, 1756 and 2400 whilst the other consisted of 2724, 2809, 2424 and 2753. Data was separated to represent HER2+ samples (left) and HER2- samples (right). Metabolic activity was analysed by incubating scaffolds in 500 μL media containing 10 % AlamarBlue. Metabolic activity following AfD11M treatment was normalised to the no treatment control. Fluorescence was measured on a Tecan Spark microplate reader with excitation 570 nm and emission 590 nm. Graphs were generated using GraphPad Prism version 8 where error bars represent standard error of the mean between technical repeats. Data is representative of n=1.

5.2.6.2.2 Analysis of HER2 status post treatment using immunofluorescence

Following analysis by AlamarBlue a sample SeedEZ from each condition was washed 3 x in 1 x PBS and stained with an antibody against HER2 and hoescht nuclear stain. Scaffolds were imaged using a Zeiss upright confocal microscope to obtain maximum intensity projections (Figure 5.16). The HER2 positive cell line AU-565 and HER2 negative cell line MDA-MB-231 were stained as controls. Results from immunofluorescence were ambiguous. Cells seemed to grow in clusters and so the area imaged was the area in which most cells could be visualised. Patient sample 2809 was isolated from a HER2+ tumour and this sample demonstrated higher levels of HER2 staining without AfD11M compared to with. However, high levels of staining could be observed following imaging of HER2 negative sample 3144.


HER2
Transmitted light
Hoescht
Merge
AU-565
MDA-MB-231
1681 + AfD11M
1681 - AfD11M
1756 + AfD11M
1756 - AfD11M
200 µm


HER2
Transmitted light
Hoescht
Merge
2400 + AfD11M
2400 - AfD11M
3144 + AfD11M
3144 - AfD11M
2424 + AfD11M
2424 - AfD11M
200 µm

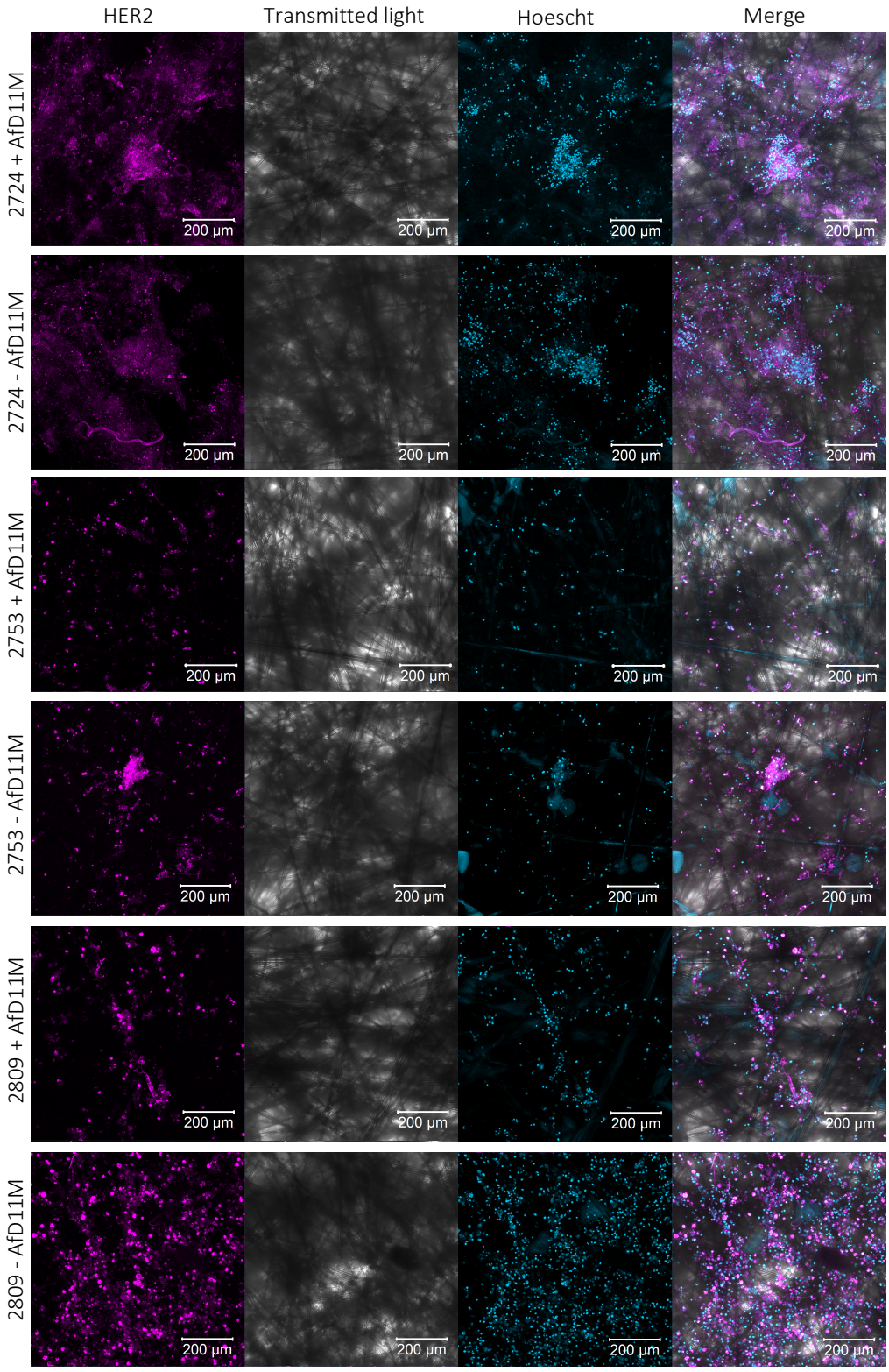


Figure 5.16 Confocal microscopy of HER2 in primary patient samples cultured in PerfusionPal.
Following analysis with AlamarBlue scaffolds were washed 3 x in PBS prior to staining with nuclear stain hoescht (cyan)(1:1000) and anti-HER2 antibody (magenta) (1:2000) with Alexa Fluor™ 488 secondary (1:2000). Scaffolds were imaged using a Zeiss upright confocal microscope with magnification of 10x. Images represent area the of the scaffold in which the highest volume of cells could be viewed. Images were analysed using ZenLite software and maximum intensity projections were made. Data is representative of n=1.

5.3 Discussion and future direction

5.3.1 Using epiFL as a matrix free medium to culture cells in 3D

A previous study has demonstrated the suitability of epiFL as a media to encourage the formation of spheroids from breast cancer cell lines (176). Spheroids were analysed by immunohistochemistry for different markers and were shown to hold characteristics of tumours *in vivo* such as an actively proliferating exterior and apoptotic core (176). When cultured in epiFL the cell lines BT-474 and MDA-MB-231 formed 3D aggregates.

5.3.2 Dynamic perfused culture results in higher metabolic activity compared to static culture

Many 3D cell culture platforms provide a basis for analysing the interaction between multiple cell types and extracellular matrix but overlook biomechanical stimulation. It has been demonstrated that the flow-derived shear stress exerted on cells as a result of constant perfusion can alter growth factors produced in multiple cell types (274, 275). The speed of flow has also been shown to influence drug effects, density and proliferation (274, 276).

Experiments described in this chapter were amongst the first conducted with SeedEZ scaffolds. SeedEZ scaffolds cultured with perfusion generally exhibited greater metabolic activity compared to static SeedEZ culture particularly at higher seeding densities. Cell aggregates have a smaller surface area to volume ratio compared to single cell culture. Large aggregates were more likely at higher seeding densities. At such densities the interstitial flow provides nutrients to cells at the core of the aggregates whilst static culture may only provide nutrients to the periphery. The scaffold, unlike many microfluidic models allows for perfusion to be equally exerted over the whole scaffold so no gradients are observed. This means cells are exposed to uniform biomechanical stress through the whole scaffold.

Differential expression of some genes is observed when cells are cultured in 3D compared to 2D (277). The expression of genes such as apoptotic regulator B-cell lymphoma 2-

related protein A1, (278), integrin β1 expression involved in proliferation (279) and genes involved in the EGFR pathway such as AKT and MAPK (280) have found to be altered in cancer cell lines cultured in 3D. The expression of EGFR and downstream effectors is of particular interest as HER2 activation leads to signalling through the same pathway. The SeedEZ scaffold is easily manipulated allowing cells to easily be removed by enzymatic detatchment for analysis of protein expression by western blot. It may also be that the interstitual fluid pressure exerted in the PerfusionPal model influences further gene expression changes (281, 282). Comparing the expression of genes and subsequent protein product through genome wide microarray analysis and western blot between cells cultured in 2D and 3D and also 3D with and without perfusion would give insight into gene expression changes under perfused conditions.

5.3.3 Primary cell culture in 3D

Having shown that breast cancer cell lines could be cultured in PerfusionPal we then went on to investigate the culture of primary breast cancer cell lines in PerfusionPal. The heterogeneity of breast cancer *in vivo* is not recapitulated by immortilised breast cancer cell lines. It is, therefore, necessary to develop a model that can accurately portray the heterogeneity of breast cancer using primary patient cells. Ideally the model should be robust enough for high-throughput screens to predict drug responses. However, the culture of primary patient cells *ex vivo* is technically challenging (283). Various protocols for the culture of primary patient tumour cells have since been developed (185).

It was hypothesised that the SeedEZ scaffold cultured in PerfusionPal may provide the support network needed to mimic 3D tumour growth *in vivo*. The most successful experimentation model for the culture of primary breast cells at the point of experiment was that of the Clevers laboratory (185). Culture medium components were modified from the Clevers paper upon recommendation of BCNTB Cell Culture Programmr. Whilst the Clevers laboratory demonstrated organoid growth, it was hoped that growing a defined number of patient primary cells in the SeedEZ scaffold experiencing interstitial fluid pressure would recapitulate *in vivo* tumours in a controlled, comparable environment for use in drug screens.

The samples of primary cells provided were a heterogeneous mixture of cells, unlike cell lines. It is likely that the proportion of fibroblast was much higher than that of epithelial cells. The metabolic activity recorded is representative of all cell lines and therefore the potential effect of AfD11M may be masked. As AfD11M targets HER2 that is expressed on the cell surface of epithelial cells the drug should have no effect on fibroblasts. Flow cytometry is a long established technique that would give insight into the primary culture population (284, 285). However, for this type of analysis cells would need to be removed from the scaffold and therefore subject to mechanical strain that could result in a misrepresentation of cell death. It is also unlikely that enough cells could be obtained for such analysis.

In an attempt to analyse HER2 expression and visualise epithelial cells immunofluorescence was used. Results obtained from this analysis were ambiguous. Images of the scaffolds were taken where the greatest number of cells could be viewed. Removing cells from the scaffold prior to immunofluorescent analysis would allow for more detailed cellular images to be obtained potentially giving insight into cell types. However, as primary samples do not show the robustness of cell lines removal from the scaffold may result in a large number of cell death limiting the cells available to observe by immunofluorescence.

5.3.4 Limitations of culturing SeedEZ scaffolds in the PerfusionPal system

Whilst the PerfusionPal system provides advantage over static culture the media flowing through the scaffold is not fresh. Therefore, half-media changes of media were required daily that resulted in pausing experiments. For latter experiments media changes were undertaken without pausing the system but still required taking the system out of the tissue culture incubator leading to a change in external factors, albeit for a short period. Allowing constant flow of media over the scaffold would provide a continuous supply of nutrients to cells without the need for pausing the culture during the experiment. A midi-fluidic model was designed to incorporate the SeedEZ scaffold sandwiched between two pieces of poly-di-methyl-siloxane (PDMS)(Figure 5.17). PDMS has favourable properties for tissue culture such as inert, non-toxic and non-flammable. The design incorporated three inlets and three outlets to allow flow of fresh media over the scaffold throughout

the course of culture, without a need to pause the experiment. However, preliminary tests using the system with media alone resulted in leakage between the two PDMS plates. Discussion led to the idea of using magnets to prevent the need for screws so the force between the two PDMS plates was consistent and not altered by human strength. Using magnets for this purpose would need to be optimised to obtain the right strength to create an airtight seal whilst maintaining scaffold intergrity. This avenue was not persued further in this project but is an idea for future work.

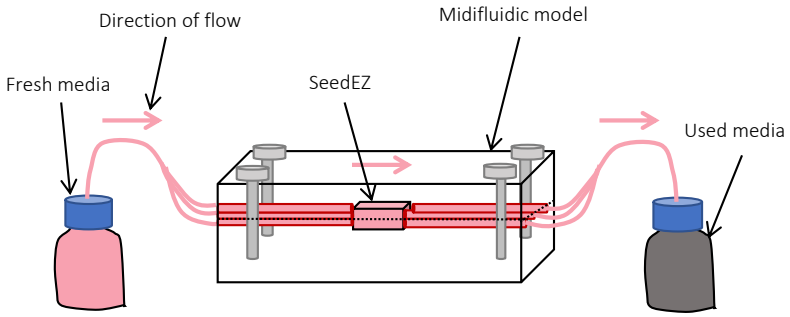


Figure 5.17 Midifluidic model design.
Midifluidic model design incorporating the SeedEZ scaffold sandwiched between two PDMS plates. Flow of media from left to right would be carried out using a peristaltic pump.

5.3.5 Conclusion and future work

The SeedEZ scaffold in PerfusionPal provides a novel matrix-free 3D cell culture system that is easily adaptable for the culture of multiple cell types. The system has also demonstrated potential for the culturing of primary patient samples showing evidence of metabolic activity after 5 days of culture. However, further optimisation and analysis would be needed to validate the PerfusionPal system as a drug discovery platform (discussed in Chapter 7).

Chapter 6

Investigating the interaction between Affimers and the HER2 extracellular domain



'Imagination is more important than knowledge.'

-Albert Einstein

Chapter 6

6 Investigating the interaction between Affimers and HER2 extracellular domain

6.1 Introduction

The drugs predominantly used to treat HER2 overexpressing breast cancer bind to the HER2 receptor in various regions. Lapatinib is a receptor tyrosine kinase inhibitor and binds to the intracellular region of both HER2 and EGFR. The monoclonal antibodies Trastuzumab and Pertuzumab, however, are specific for the HER2 extracellular domain. The antibodies demonstrate synergistic effects due to having alternate binding sites (Figure 6.1). Pertuzumab binds to subdomain II of the HER2 extracellular domain and inhibits receptor dimerization with HER3 (126). Trastuzumab binds to subdomain IV of the HER2 extracellular domain and predominantly has effect through ADCC(75). Binding sites in both cases were deduced by X-ray crystallography.

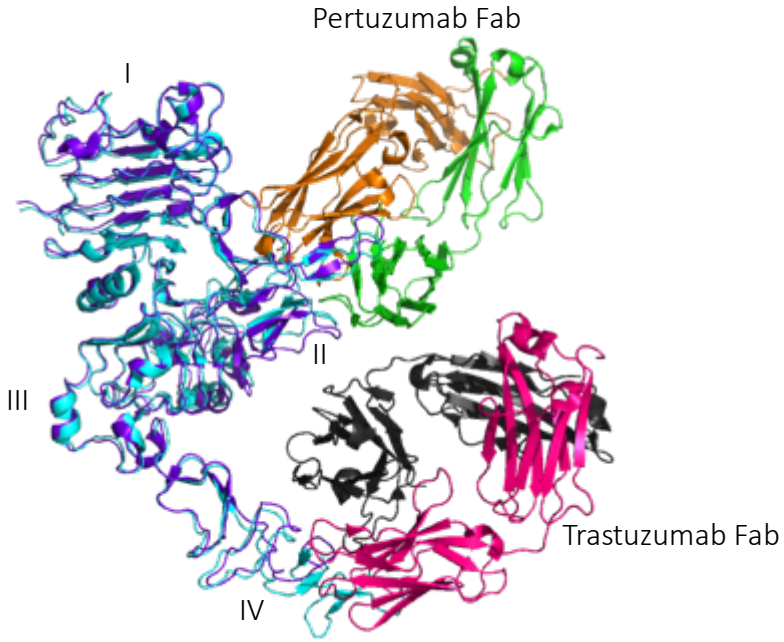


Figure 6.1 Ribbon diagram of the HER2 extracellular domain with Trastuzumab and Pertuzumab Fab regions.
PDB files for HER2 extracellular domain (cyan) with Trastuzumab Fab (heavy chain (grey), light chain (pink)) (1N8Z) and HER2 extracellular domain (pruple) with Pertuzumab Fab (heavy chain (orange), light chain (green)) (1S78) were aligned in MacPyMOL using the 'align' tool to show Trastuzumab binding to subdomain IV and Pertuzumab binding to subdomain II.

6.1.1 X-ray Crystallography

X-ray crystallography is the most favourable way to deduce the atomic and molecular structures of proteins on their own or in complex (286). To achieve crystallisation of a given protein/ protein complex it must be pure and of high enough concentration to reach a level of saturation. Supersaturation occurs above the solubility curve but before precipitation due to disordered aggregation. The relationship between the concentration of the protein and the concentration of precipitating agent is depicted in Figure 6.2. The nucleation zone is where protein excess aggregates to form crystals. The metastable region depicts where crystal growth can occur following nucleation in the nucleation zone (287). To succeed in crystallisation the protein/complex concentration should be high enough for it to come out of solution, but not too high as to aggregate. If a crystal is achieved the next step is to obtain diffraction data. The structure is determined by the way the X-ray beam diffracts away from the crystal onto an electronic detector.

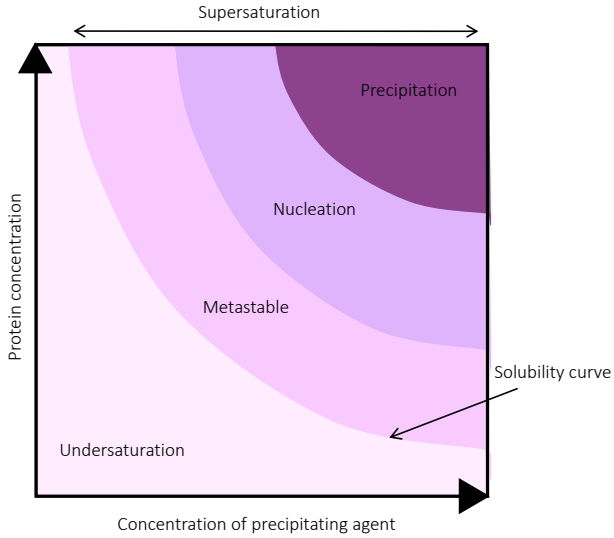


Figure 6.2 Phase diagram for protein crystallisation.
Curve is divided into two main regions; undersaturation zone and supersaturation zone. Within the supersaturation zone the curve is further divided into the precipitation, nucleation and metastable zones.

6.1.2 Aim

In previous chapters AfD11M has demonstrated its ability to have a detrimental effect on HER2 overexpressing breast cancer cell lines specifically. AfD11M was able to bind at nM affinities to the HER2 extracellular domain. For this reason, to elucidate where AfD11M

binds to the HER2 extracellular domain X-ray crystallography was utilised. In this chapter it will be discussed how both HER2 extracellular domain and Affimer D11 were produced and purified as well as a potential binding domain.

6.2 Results

6.2.1 Affimer D11 complex with full length HER2 in mammalian cell culture

The initial experimental design for the production of Affimer D11 in complex with HER2 extracellular domain was to immobilise Affimer D11 on a column that would then capture HER2. For this to be successful the two proteins must display separate tags so binding of HER2 to the column is through Affimer D11 only.

6.2.1.1 Producing Affimer D11 with C-terminal Strep Tag® II

Affimer D11 was sub-cloned into a pET11a vector to contain a tobacco etch virus (TEV) cleavage site and C-terminal Strep Tag® II (Figure 6.3)(2.8.4). Insert DNA of Affimer D11 analysed by DNA gel electrophoresis confirmed insert size to be ~3000 bp (Figure 6.4A). Sequencing by GeneWiz confirmed the correct sequence had been obtained (2.8.4.6). Affimer D11 DNA was transformed into BL21(DE3) Star *E.coli* and two 400 mL cultures were induced by IPTG as described in section 2.7. Cells were pelleted by centrifugation. A small sample of pellet was lysed and samples of the lysate fraction and soluble fraction were analysed by SDS-PAGE to confirm Affimer presence (Figure 6.4B). The remaining pellet was stored at -20 °C until used.



Figure 6.3Components of Affimer D11 Strep Tag II.
Affimer D11 (pink) was subcloned to contain a TEV cleavage site (blue) with the sequence ENLYFQG and Strep Tag II (green) with sequence WSHPQFEK.

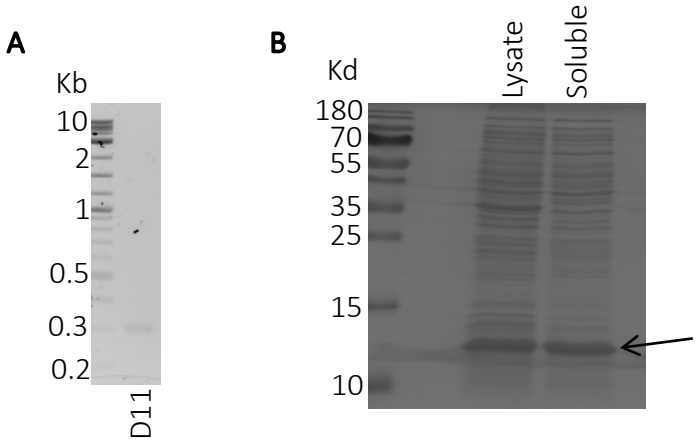


Figure 6.4 Affimer D11 insert DNA and Affimer D11 Strep Tag® II analysis.
(A) Affimer D11 was digested out of pDHis vector and insert DNA was analysed by agarose gel electrophoresis prior to ligation into pET11a Strep tag® II vector. **(B)** Proceeding production, a sample of Affimer D11 Strep Tag® II Affimer pellet was lysed to confirm successful expression. Lysed sample was centrifuged at 16, 000 x g for 20 mins. Samples from whole cell lysate (lysate) and soluble fraction following centrifugation (soluble) were diluted 1:5 in ddH_2O and analysed on a 15 % polyacrylamide gel by SDS-PAGE. Bands were visualised with Coomassie stain, the arrow in **(B)** shows the Affimer protein. Gel images were taken using an Amersham gel imager 600.

6.2.1.2 Growth of HER2 fusion protein in CHO Lec1 cells

HER2 is a highly glycosylated transmembrane protein that contains multiple disulphide bonds. These properties make it desirable to produce in mammalian cells where correct post-translational modifications can take place. The Chinese Hamster Ovary (CHO) Lec1 cell line that was engineered to constitutively express and secrete the HER2 extracellular domain (residues 1-631) as a fusion protein with human growth hormone (hGh) using the pSGHV0 expression vector (288) (Figure 6.5) was a kind gift from Dr. Josef Singer with permission from Prof. Daniel Leahy. The pSGHV0 vector was designed to allow X-ray crystallographic investigation of cysteine-rich glycoproteins such as HER2 (75, 288). Cells were grown to reach 100 % confluency in Alpha MEM, 10 % FBS, 100 nM Methotrexate and 10 μg/mL gentamicin sulphate. Media was then changed to DMEM F12, 10 % FBS, 100 nM Methotrexate and 10 μg/mL gentamicin sulphate and collected as it became more acidic (analysed by colour change of red to yellow/orange) around three times weekly (section 2.14.1). Co-transfection of the pSGHV0 vector with a dihydrofolate reductase gene allowed for increased expression with methotrexate (288). Collected media was stored sterile at 4 °C until a total of 2 litres was collected.

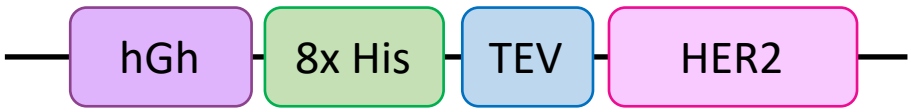


Figure 6.5 Components of HER2 fusion protein.
HER2 extracellular domain (pink) was expressed as a fusion protein with a tobacco etch virus (TEV) cleavage site with the sequence ENLYFQG and 8x histidine tag (green) and human growth hormone (hGh) (purple).

Media collected from CHO Lec1 cells was analysed by western blot for HER2 (section 2.8.3). Western blot analysis was unsuccessful (data not shown). It is hypothesised that the level of FBS in the media caused distortion in the blot. Therefore, instead of optimising the western blot protocol the 2 litres of HER2 conditioned media was purified using an ÄKTA pure as a complex with Affimer D11 to give a more coherent result.

6.2.1.3 Purification of D11 Affimer in complex with HER2 fusion protein

Affimer D11 was used to pull down HER2 from the conditioned media on an ÄKTA pure system (section 2.14.3). The 400 mL Affimer D11 Strep Tag® II pellet was thawed on ice and resuspended in binding buffer prior to lysing using the cell disruptor. The soluble supernatant containing Affimer D11 Strep Tag® II was immobilised on a 1 mL StrepTrap™ High Performance column using the ÄKTA pure system with a flow rate of 1 mL/min. The column was washed with binding buffer until the UV at 280 nM was steady indicating protein eluting from the column had ceased. At this point the HER2 conditioned media was flowed over the column at a flow rate of 1 mL/min. The column was again washed until the UV at 280 nM flatlined. To elute the Affimer D11 Strep Tag® II in complex with HER2 the column was incubated with TEV protease for 12 hours at 4 °C before elution of cleaved products. Anything that remained on the column was eluted with 2.5 mM desthiobiotin in binding buffer. The chromatogram and SDS-PAGE analysis of eluates are shown in figure 3.

No peak was observed on the chromatogram following TEV incubation (Figure 6.6A). This observation was reinforced by SDS-PAGE where no bands could be seen from samples taken from these fractions (Figure 6.6B). Desthiobiotin competes with Strep Tag® II proteins for biotin-binding sites of Strep-Tactin® and so can be used to elute proteins with a Strep Tag® II. Following elution using desthiobiotin protein was eluted from the column and verified by SDS-PAGE (Figure 6.6B). Analysis by SDS-PAGE confirms the presence of

Affimer D11 at ~13 kDa with a further two bands at ~100 kDa and ~120 kDa (Figure 6.6B). The expected molecular weight of the HER2 extracellular domain is ~66 kDa, however, due to glycosylation this increases to ~100 kDa correlating to the lower band following SDS-PAGE. The hGH has an expected mass of ~21 kDa and so the upper band correlates to un-cleaved HER2 hGH fusion protein. The results here suggest that the TEV protease was inefficient in cleaving the tags from the proteins leading to a mixed final population of Affimer D11 in complex with either the HER2 fusion protein, or HER2 alone.

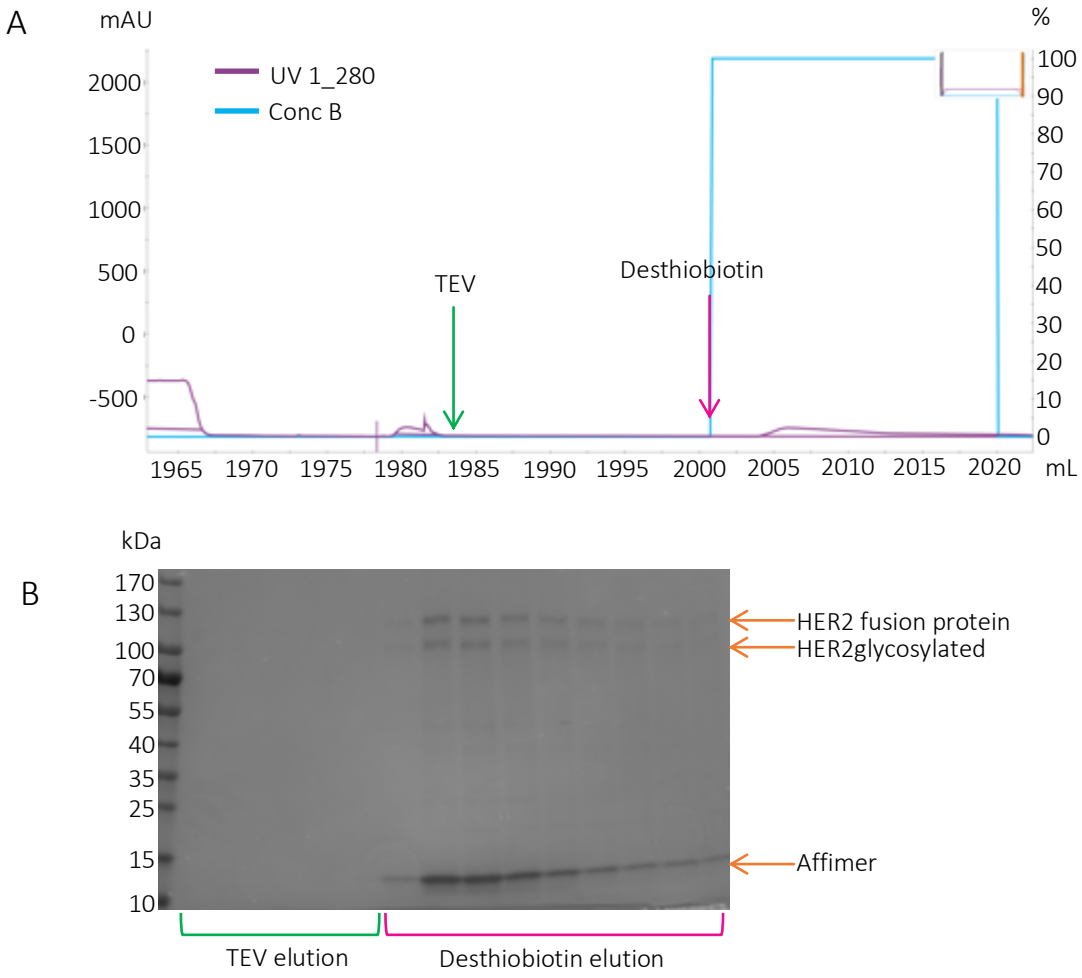


Figure 6.6 Purification of Affimer D11 in complex with HER2 fusion protein.
Affimer D11 with Strep Tag II was immobilised on a 1 mL Strep trap column using an AKTA pure. HER2 was expressed as a fusion protein with human growth hormone (hGh) split by a 6 x His tag and tobacco etch virus (TEV) cleavage site. HER2 fusion protein was flowed over the Strep Trap II column with immobilised Affimer. **A)** chromatogram from the ÄKTA pure showing elution after 12 incubation with TEV protease (green arrow) and elution with desthiobiotin (pink arrow). **B)** TEV elution and desthiobiotin elution fractions were analysed by SDS-PAGE and stained using Coomassie blue and destained to remove background prior to imaging using an Amersham Imager 600.

6.2.1.4 Size exclusion chromatography of Affimer D11 HER2 complex

Following affinity purification the Affimer D11 HER2 extracellular domain was further purified by size exclusion chromatography using a HiLoad Superdex 200 column was equilibrated with 25 mM HEPES, 150 mM NaCl, 1 mM TCEP, pH 7.5 (section 2.14.6). Hypothetically it was predicted that a double peak would occur due to there only being a ~20 kDa difference between expected protein complexes. Eluted fractions were analysed by SDS-PAGE (Figure 6.7). Analysis demonstrated that the protein solution achieved was not pure but contained the previously described mix of cleaved and uncleaved proteins. Further separation techniques would be needed to create a pure product such as ion exchange using a column that allows for separation of proteins similar in size.

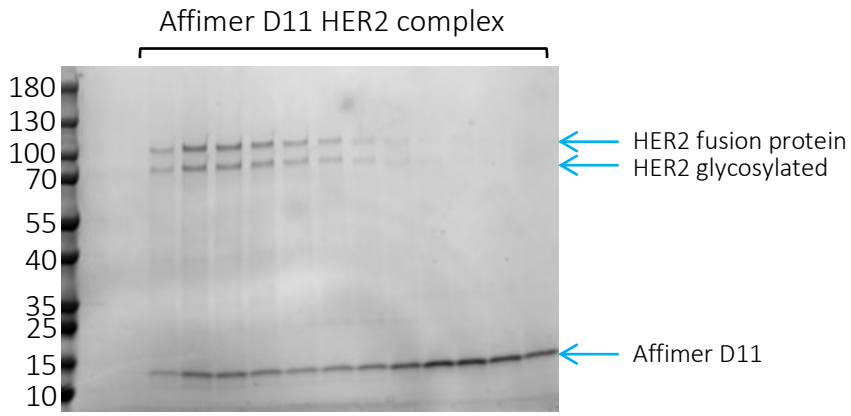


Figure 6.7 SDS-PAGE analysis of Affimer D11 HER2 extracellular domain complex following SEC.
Complex was separated using a HiLoad Superdex 200 clumn prior to analysis by SDS-PAGE. Gels were BioRad precast gels ran at 150 V for ~1 h. Bands were visualised with Instant Blue. Images were taken on an Amersham Imager 600.

6.2.1.5 Crystal trial set up

Despite impurities crystal trials were set up following confirmation of the complex. Complex was dialysed into 10 mM Tris, 50 mM NaCl, pH7.5 and concentrated down to a final concentration of 1.5 mg/mL (section 2.14.7). Crystal trials were set up as sitting drops using the commercially available Morpheous and PACT screens (Molecular Dimensions Ltd, UK) using various protein:buffer ratios (section 2.14.8). Plates were placed into a formulatrix imaging hotel at 22 °C. No crystals formed during a three-month incubation under these conditions.

6.2.2 Production of Peptide: N-glycosidase F (PNGase)

The extracellular domain of HER2 is highly glycosylated. Crystal structures of the HER2 extracellular domain have been obtained following deglycosylation of the protein prior to crystallisation (75). The level of glycosylation on each protein can differ leading to heterogeneity. X-ray crystallography is most successful when a uniform population of pure protein is obtained. Therefore, when upscaling the previous protocol the HER2 protein would be deglycosylated prior to entering crystallisation trials. PNGase F is an enzyme capable of cleaving all sites of glycosylation. Its ability is superior to previously used endodeglycosylase H that cannot deglycosylate mannose containing oligosaccharides (75).

A PNGase F expressing plasmid was purchased from AddGene with thanks to Shaun Lott (289). The protein was expressed in the periplasm of *E. coli.* The plasmid was transformed into BL21 Star™ (DE3) competent *E. coli* cells and expression was induced by IPTG induction as described in section 2.14.4.1. PNGase F was isolated from the periplasm as per the protocol in section 2.14.4.2. The periplasmic fraction was pelleted by centrifuged at 15,000 xg prior to purification using a 5 mL His Trap column on an ÄKTA pure system.

The supernatant was flowed over the column and washed until the UV at 280 nM was constant. PNGase F was eluted from the column with elution buffer (section 2.14.4.2). Samples were taken from the peak labelled 'PNGase F' and analysed by SDS-PAGE (fig. 4A). The purity of eluted PNGase was high with strong bands at 35 kDa (Figure 6.8B). The protein was concentrated to 1.5 mg/mL and flash frozen in elution buffer in liquid nitrogen prior to storing in aliquots at -80 °C until needed.

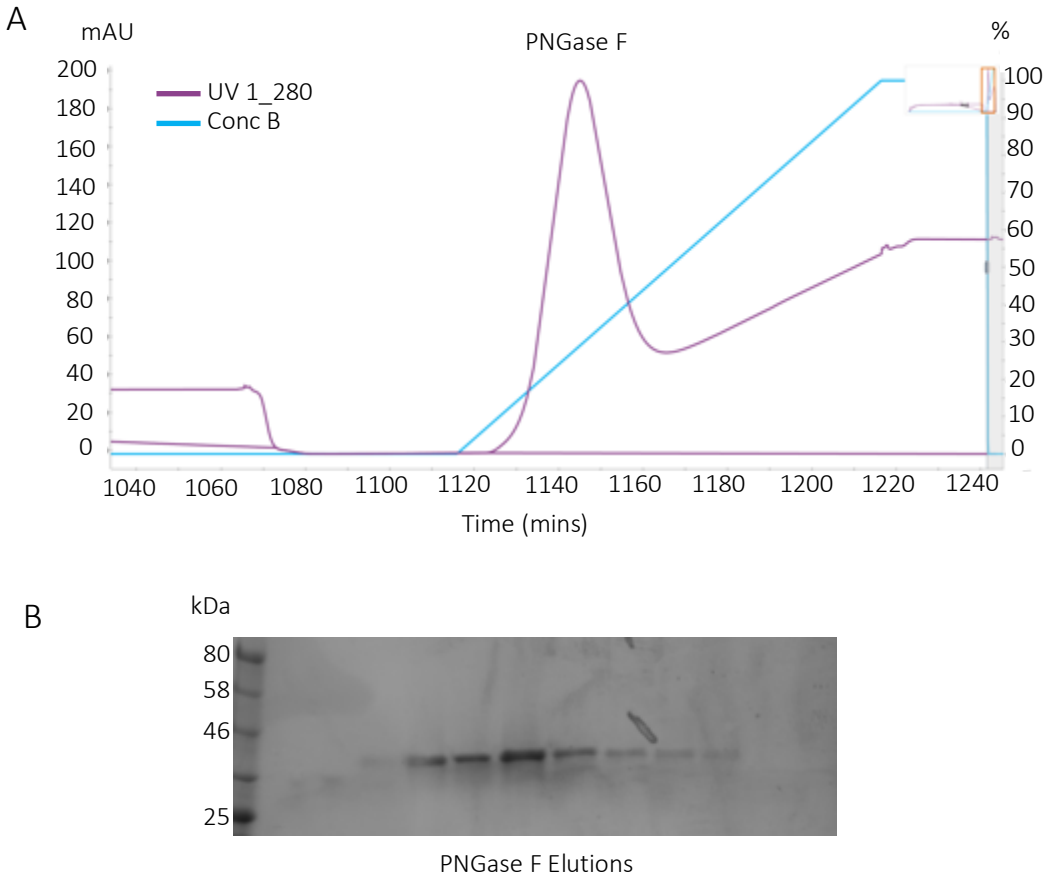


Figure 6.8 PNGase F purification using C-terminal 6x His tag.
PNGase was purified using a 1 mL His Trap column on an ÄKTA pure system. **A)** shows the chromatogram from the ÄKTA pure showing UV at 280 nm (purple) and concentration of B (blue). **B)** Samples of elutions from the peak labelled PNGase F were taken and analysed by SDS-PAGE. Gels were stained with Coomassie blue and destained to remove background. Gels were imaged using the Amersham Imager 600.

6.2.3 Larger scale production of Affimer D11 in complex with full length HER2

Previously, Affimer D11 Strep Tag® II was successfully purified in complex with full length HER2 extracellular domain secreted by CHO Lec1 cells. The protocol was repeated in a larger scale in the hope of producing enough complex to put in a crystal trial. Prior to crystal trials the complex would also be deglycosylated to produce a homogenous protein complex. From 2 litres of conditioned media 60 μL ~1.5 mg/mL complex was produced. Previous crystal trials with HER2 have had protein from ~ 4 mg/mL (75). During the second trial the quantity of HER2 conditioned media was increased, as described below.

6.2.3.1 Production of Affimer D11 Strep Tag® II

Affimer D11 Strep Tag® II was produced in 2 x 400 mL culture as previously described (section 6.2.1.1). The culture was pelleted by centrifugation at 4000 x g. The pellet was resuspended in loading buffer and lysed by sonication. The insoluble fraction was pelleted by centrifugation at 25,000 x g for 45 mins. Affimer D11 Strep Tag® II was immobilised on a 1 mL Strep Trap column.

6.2.3.2 Producing full length HER2 extracellular domain in CHO Lec1 cells

CHO Lec1 cells were grown to 100 % confluency before conditioned media was collected as previously described (section 6.2.1.2). To increase production cells were seeded into a Corning hyperflask to allow a larger volume of media to be collected faster. Media collected was stored sterile at 4 °C. The larger volume of media collected during this upscaling made it unfeasible to use the exact methodology described previously. The 12 L conditioned media was concentrated to 1.4 L using an Amicon® Stirred cell (2.14.1.1). Samples of the media from before and after concentrating were taken and analysed by western blot (Figure 6.9).

The molecular weight of the HER2 glycosylated fusion protein is ~130 kDa. Both unconcentrated and concentrated media has bands at ~60 kDa following SDS-PAGE that are not present in the western blot. This band is most probably albumin, the most

abundant protein in FBS. Western blot analysis shows two main bands in both unconcentrated and concentrated media at ~130 kDa and ~90 kDa. The ~130 kDa band is concurrent with the HER2 hGH fusion protein. It is hypothesised that the ~90 kDa band is a truncated form of the HER2 hGH fusion protein or another protein present in FBS that is abundant with histidine residues. The band is ~95 kDa which is the length of truncated HER2 extracellular domain.

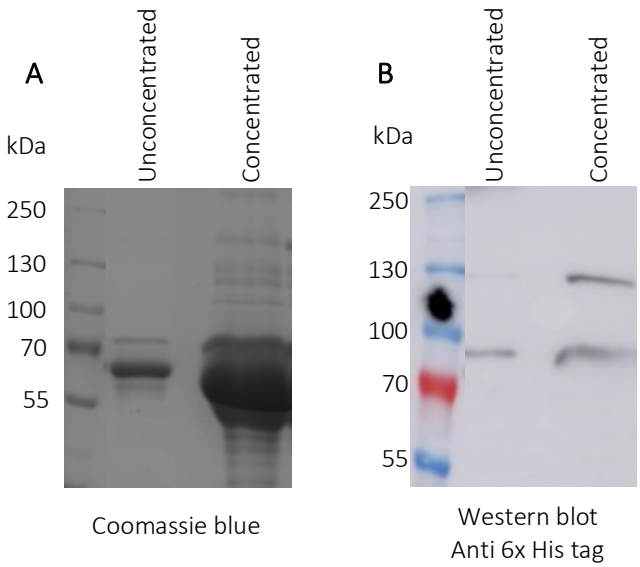


Figure 6.9 Analysis of HER2 fusion protein by SDS-PAGE and western blot.
HER2 fusion protein with 6x His tag and hGh conditioned media was concentrated from 12 L to 1.4 L. Samples were taken before and after concentrating and separated by SDS-PAGE gel electrophoresis before **A)** being stained with Coomassie blue or **B)** transferred onto nitrocellulose membrane prior to detection using anti 6x His (HRP) antibody. Images were taken on the Amersham Imager 600 using the **A)** epiilumination or **B)** chemiluminescence settings.

6.2.3.3 Purification of Affimer D11 Strep Tag® II and full length HER2 extracellular domain complex

Affimer D11 Strep Tag® II was immobilised on a 1 mL Strep Trap column and washed as previously described (section 6.2.3.3). Concentrated HER2 media was passed over the column with a flow rate of 1 mL/min. Due to the increased volume of albumin in concentrated media a wash step was added for every 200 mL media that flowed over the column that would continue until the UV at 280 nM remained steady (Figure 6.10A). This was to minimise unspecific binding of FBS to the column. After all media was added the column was washed prior to elution in 2 mL fractions with desthiobiotin (Figure 6.10B).

Samples were taken from the elution fraction and analysed by SDS-PAGE (Figure 6.10C). There was a band at ~ 13 kDa for the Affimer D11 Strep Tag® II but no band was present at ~130 kDa for full length HER2 extracellular domain. The aim was to saturate the Strep Trap column with Affimer D11 Strep Tag® II and so the final concentration was expected to be higher than that of HER2 extracellular domain.

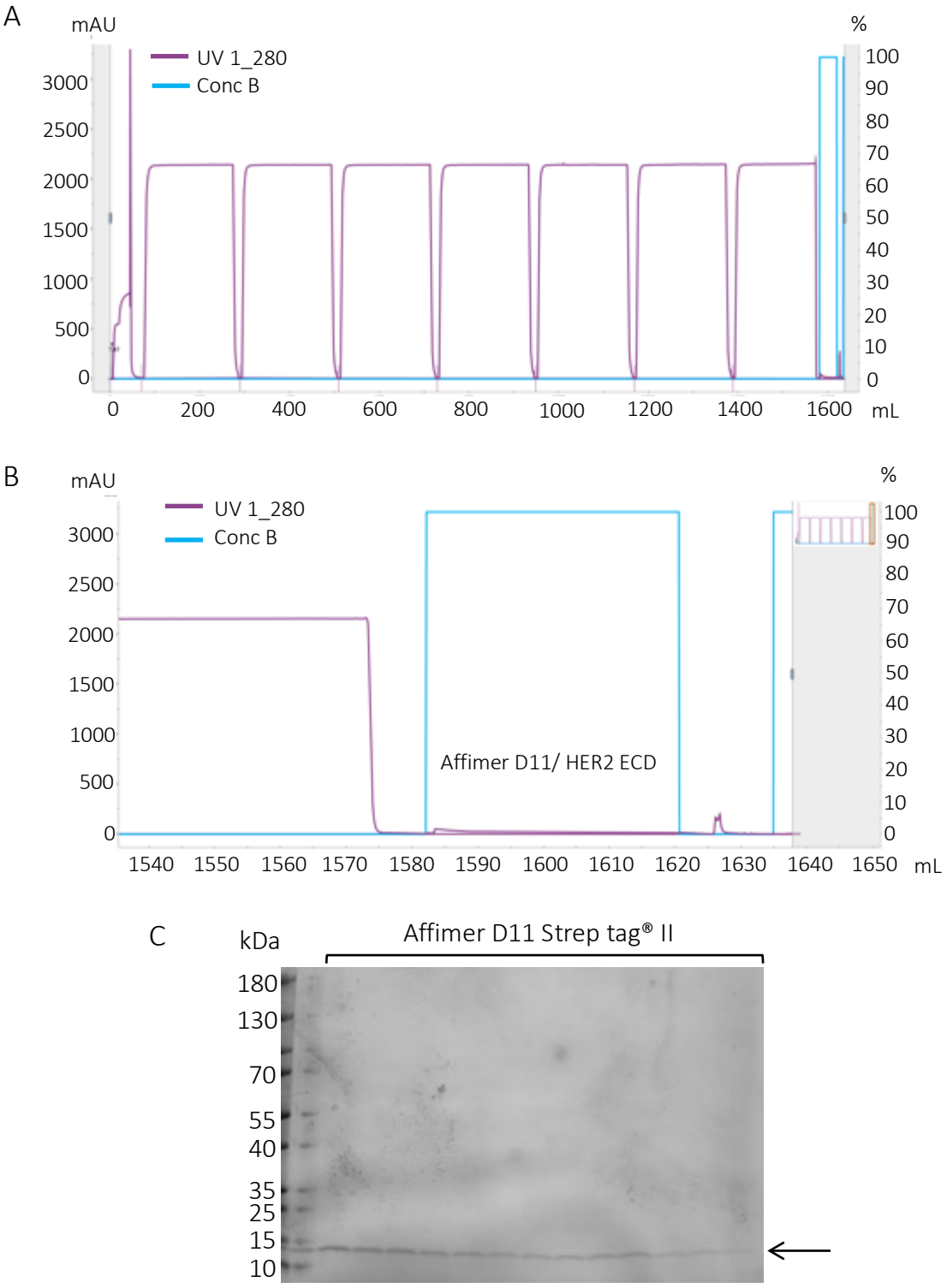


Figure 6.10 Larger scale production of Affimer D11 and HER2 extracellular domain complex.
Affimer D11 containing a TEV cleavage site at the C-terminal Strep II Tag was immobilized on a 1 mL StrepTrap column. HER2 extracellular domain conditioned media was flowed over the column using an AKTA pure system. **A)** Shows the complete AKTA trace displaying washes that occurred every 200 mL media, **B)** AKTA trace zoomed in on the elution fractions **C)** Elution fractions from peak A were analysed by SDS-PAGE to confirm which fraction(s) contained the desired Affimer D11/HER2 ECD protein complex.

6.2.3.4 Tag removal of both Affimer D11 Strep Tag® II and HER2 fusion protein

Affimer D11 Strep Tag® II and HER2 fusion protein were engineered to contain a TEV cleavage site to remove tags and fusion proteins respectively. Following purification the tags were removed by incubation with TEV protease. Fractions from peak A were pooled separately to those from peak B (fig. 6B). Fractions were incubated with 200 μL 1 mg/mL TEV protease and dialysed overnight into 50 mM NaCl, 10 mM Tris, pH 7.5 at 4°C. The following day solutions were mixed with deglycosylating enzyme PNGase F and incubated at 37 °C for 48 h with shaking at 80 r.p.m. Samples were taken at various stages of complex purification and analysed by SDS-PAGE (Figure 6.11). Analysis confirmed that both Affimer D11 Strep Tag® II and HER2 fusion protein were present prior to complex purification. Two bands of suspected sizes were present in peak A at ~13 kDa and ~130 kDa. Once pooled and analysed following TEV and PNGase treatment the HER2 fusion protein band is not visible. However, the sample from peak A was concentrated to ~2 mL for separation by size exclusion chromatography.

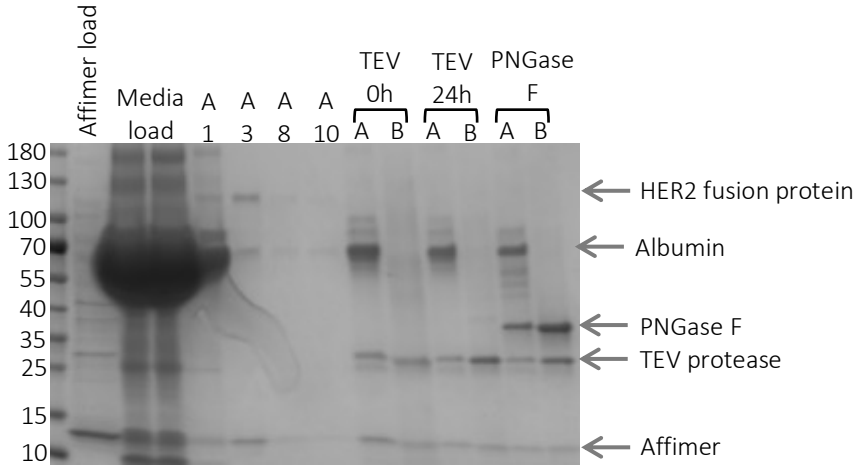


Figure 6.11 SDS-PAGE analysis of various fractions during the purification of Affimer D11/HER2 complex. Samples from various fractions during the purification of Affimer D11 in complex with the HER2 extracellular domain were analysed by SDS-PAGE. Samples were separated on a Bio-Rad 4-16 % gradient gel by gel electrophoresis. The gel demonstrates which proteins were present at various stages of the purification including the glycosylated HER2 fusion protein (~120 kDa), Albumin (66 kDa), PNGase F (35 kDa), TEV protease (26 kDa) and Affimer (13 kDa).

6.2.3.5 Separation of Affimer D11 HER2 complex by gel filtration

The complex was separated by size exclusion chromatography using a HiLoad Superdex 200 column (Figure 6.12). Samples from each peak were analysed by SDS-PAGE. The size

of the Affimer D11 HER2 complex following tag removal and deglycosylation should be ~80 kDa. A peak for PNGase F and TEV protease were expected with corresponding band sizes of ~35.5 kDa and ~27 kDa respectively.

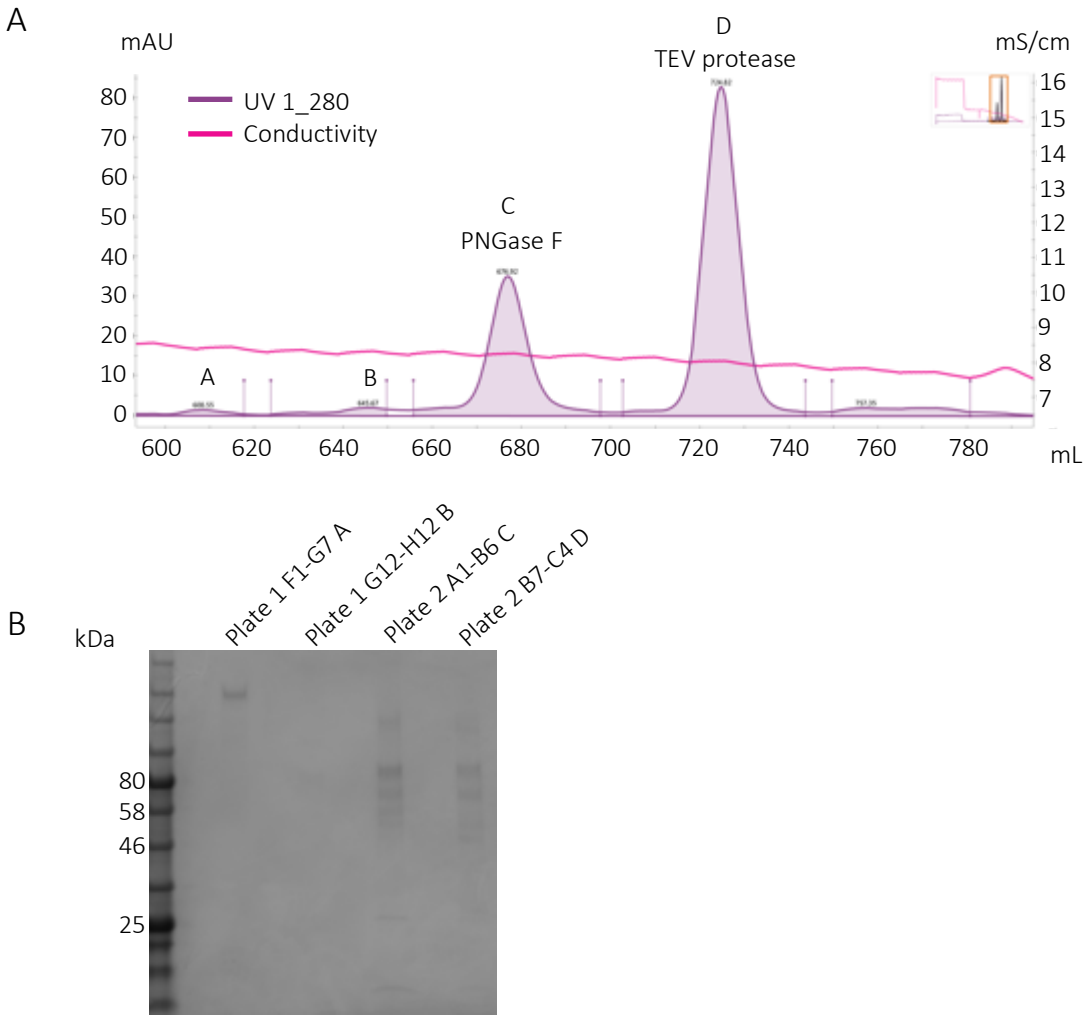


Figure 6.12 Separation of Affimer D11/HER2 complex by SEC and analysis by SDS-PAGE.
Affimer D11 in complex with HER2 extracellular domain was separated by size exclusion chromatography using a HiLoad 26-600 Superdex 200 column on an AKTA pure system. A) shows the chromatogram taken from the AKTA pure during the elution phase of the column. Peaks are labelled A to D. B) shows peaks analysed by SDS-PAGE to confirm protein identity after concentrating.

6.2.3.6 Analysis of unbound HER2 conditioned media

Initial small-scale production produced ~ 1 mg/mL protein complex. Therefore, largescale production should have theoretically produced ~ 6 mg/mL complex. To analyse why this result did not happen unbound HER2 conditioned media was analysed by SDS-PAGE and western blot (Figure 6.13). There were three bands that appeared following SDS-PAGE that could have been HER2 fusion protein (Figure 6.13A). Following western blot analysis

no bands were present at the corresponding sizes (Figure 6.13B). The gel was send for analysis of protein ID.

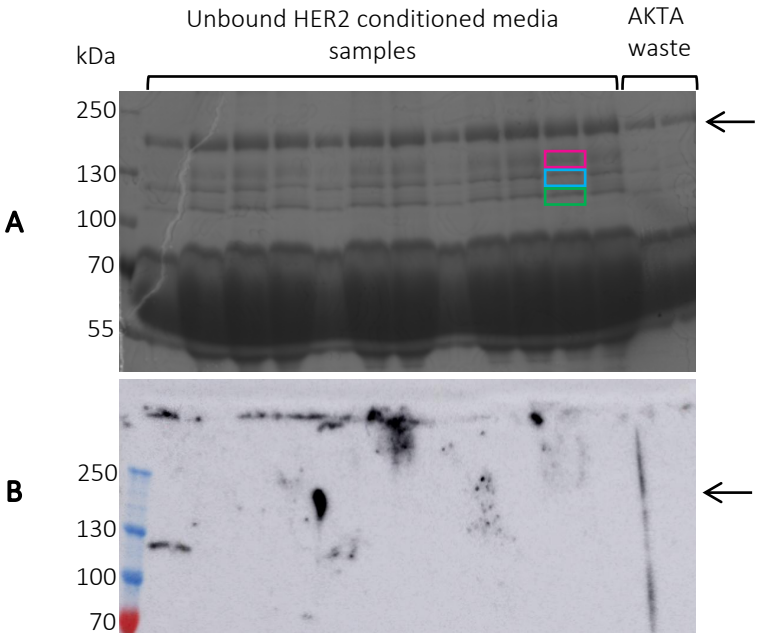


Figure 6.13 Analysis of unbound HER2 conditioned media by SDS-PAGE and western blot.
HER2 extracellular domain was purified by binding of Affimer D11 immobilized on a Strep Trap II column. Samples were taken from various collection tubes containing unbound HER2 conditioned media. Protein samples were separated by SDS-PAGE prior to **(A)** staining with Coomassie blue and destaining to remove background followed by imaging using the epi-illumination setting on an Amersham Imager 600. Bands sent for analysis for protein ID are denoted by coloured boxes (pink, blue, green) or **(B)** being transferred onto a nitrocellulose membrane using a Bio-Rad Turbo blot system followed by staining with a anti-His (HRP) antibody. Luminata substrate was used to detect HRP and images were taken using the chemiluminescence setting on an Amersham Imager 600.

Superseding SDS-PAGE analysis three bands between ~100 and ~130 kDa (pink, blue and green in Figure 6.13) were excised and analysed for protein ID by the mass spectrometry facility at the University of Leeds. Analysis demonstrated that the band circled by the blue box at ~125 kDa contained multiple sequences that correlated to the HER2 extracellular domain sequence (data not shown). HER2 fusion protein presence in the media showed that it did not all bind to Affimer D11 immobilised on the streptactin column. The reason for this is unknown but could be due to oversaturation of the column or too low binding capacity of the column for a high concentration of complex to physically bind.

6.2.4 Expressing the HER2 extracellular subdomains in *E. coli*

Following unsuccessful formation of Affimer D11 and full length HER2 extracellular domain complex by previous methods the potential of producing recombinant HER2 extracellular subdomain fragments in *E. coli* was investigated. There are ten possible

combinations of HER2 subdomain expression (Figure 6.14). All ten possible combinations were screened for expression in three strains of *E. coli* that have properties that are favourable for glycosylated membrane proteins. Lemo21 (DE3) are a BL21(DE3) derived *E. coli* strain optimised for membrane protein overexpression (290). In this strain T7 RNA polymerase activity is controlled by varying levels of its natural inhibitor T7 lysozyme. To control inhibition T7 lysozyme was placed under the influence of an L-rhamnose inducible promoter (290). For this reason expression levels using the Lemo21 system can be altered through the addition of varying levels of L-rhamnose. The SHuffle T7 Express strain are also deficient in proteases Lon and OmpT, in addition to this they promote disulphide bond formation due to the expression of disulphide bond isomerase DsbC leading to an enhanced ability to produce proteins containing multiple disulphide bonds such as HER2 extracellular domain. Rosetta-Gami2(DE3) pLysS enhance disulphide bond formation in the cytoplasm and suppress basal expression of T7 RNA polymerase prior to induction.

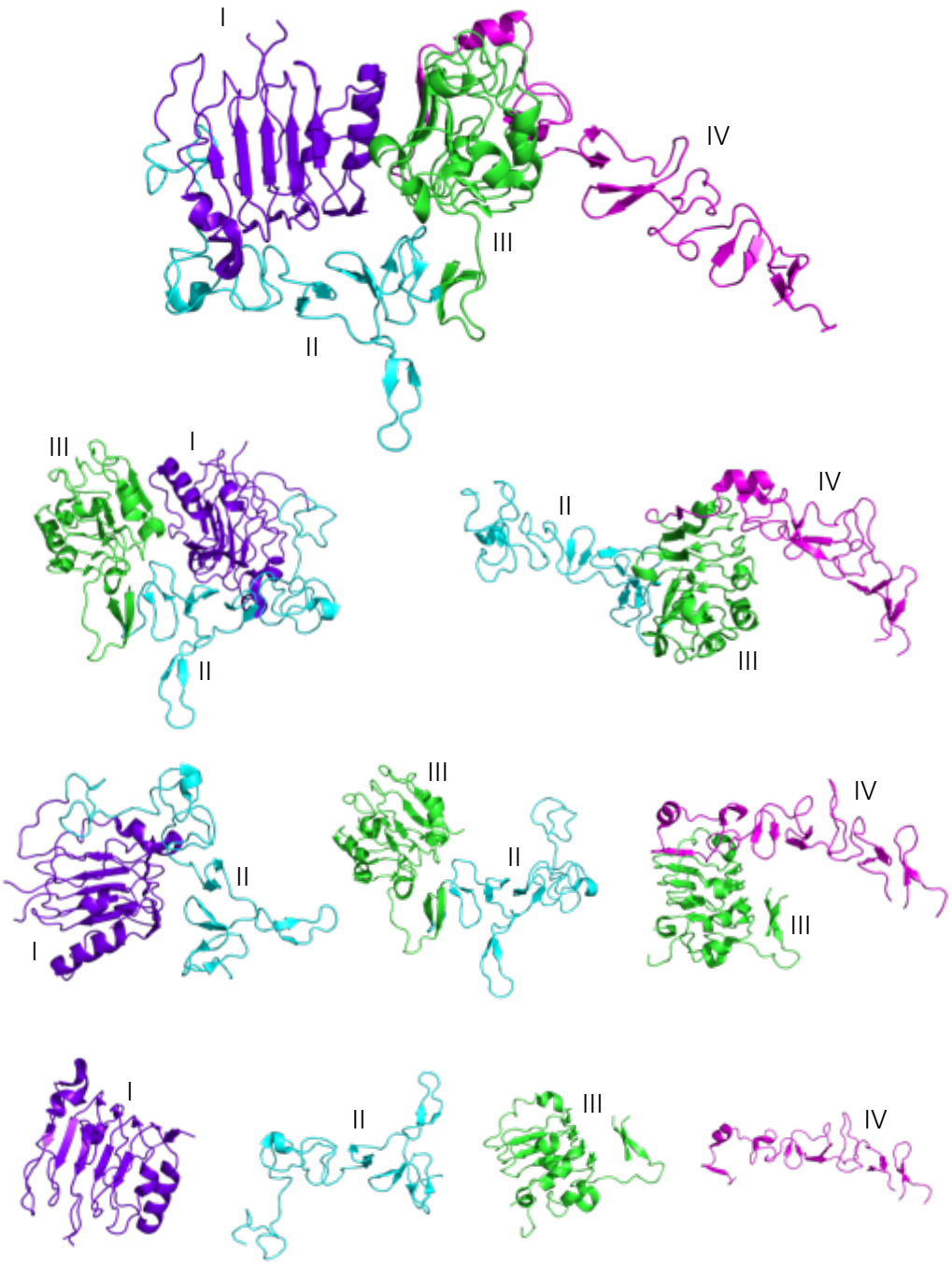


Figure 6.14 Ribbon diagram of ten possible HER2 subdomain structures.
Ten possible combinations of HER2 subdomains I (purple), II (cyan), III (green) and IV (magenta) represented as ribbon diagrams. Images were made using MacPymol images of previously crystallised HER2 extracellular domain (1N8Z).

6.2.4.1 PCR and molecular cloning of HER2 subdomains into pOPIN vectors

HER2 extracellular domain DNA cloned in pSGHV0 plasmid was gifted by Prof. Daniel Leahy. The amino acid sequences of subdomains were predicted to be insoluble. Forward and reverse primers were designed against each HER2 subdomain by Dr. Brian Jackson of the Protein Production Facility at the University of Leeds using the HER2 sequence from PDB file 1N8Z (75). DNA was amplified by PCR using primers to produce DNA encoding the ten possible combinations of HER2 subdomains. PCR products were analysed by agarose gel electrophoresis. All subdomains relying on the forward primer for subdomain 1 were not amplified by PCR (Figure 6.15) indicating unsuccessful annealing of this primer. All other subdomains were successfully amplified and visible following agarose gel electrophoresis (Figure 6.15).

Subdomain	Size (bp)	Subdomain	Size (bp)
SD1234	1893	**SD12**	957
SD1	585	**SD23**	879
SD2	372	**SD34**	936
SD3	507	**SD123**	1464
SD4	429	**SD234**	1308

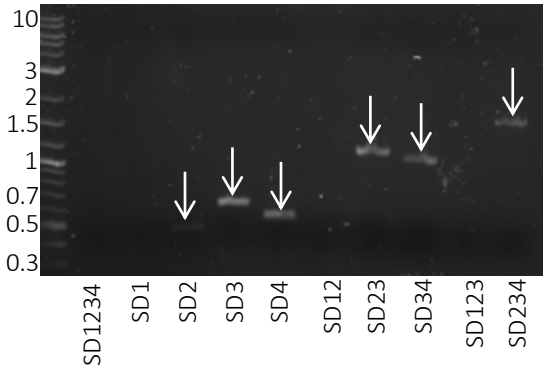


Figure 6.15 PCR amplification of HER2 subdomain analysis by agarose gel electrophoresis.
5 μL sample DNA was mixed with 2 μL 6 x DNA loading dye and separated on a 2 % agarose gel by electrophoresis at 80 V for ~40 minutes. Arrows show successful bands of predicted size of subdomains (SD). Images were taken on a G:Box imaging system.

Following amplification by PCR constructs were cloned into pOPINM and pOPINS vectors incorporating maltose-binding protein (MBP) and small ubiquitin-like modifier (SUMO) as N-terminal fusion proteins respectively (Figure 6.16) following the protocol in section

2.15.1. MBP (pOPINM) (291) and SUMO (pOPINS)(292) were used to increase solubility. Fusion proteins were also engineered to contain a poly-histidine tag for purification by Ni-NTA chromatography and a 3C protease cleavage site to allow for efficient cleavage of pure HER2 subdomain protein prior to crystallisation studies (Figure 6.16).

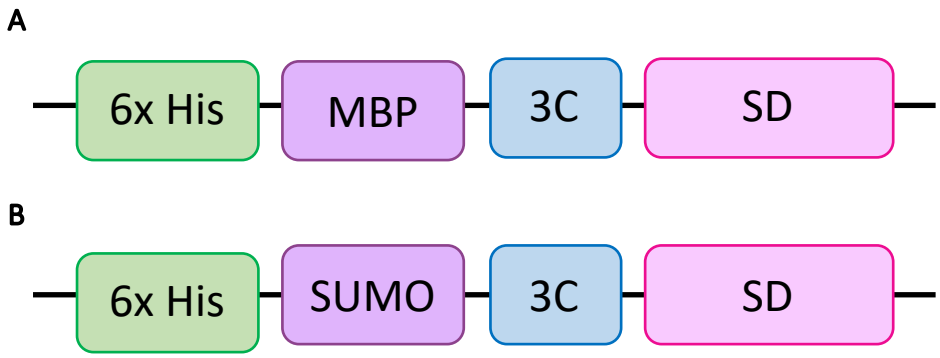


Figure 6.16 Composision of HER2 subdomain fusion proteins.
Subdomains (SD) of HER2 extracellular domain were engineered for expression as fusion proteins with either **(A)** MBP or **(B)** Sumo protein containing a 3D protease cleavage site (3C) and 6 x his tag between.

HiFi assembly reactions (2.15.2) were transformed into DH5 α competent *E. coli* cells (2.15.2.1). Colonies were picked the following day and cultured in 5 mL LB overnight for DNA minipreps the following day. Samples of DNA were sent for sequencing with Eurofins that confirmed the success of ligation reactions incorporating HER2 subdomain DNA into pOPINS and pOPINM vectors (2.15.3.1).

6.2.4.2 Expression trial of HER2 extracellular subdomains

Using *E. coli* as a system for mass producing protein has advantages over mammalian cells with it being cheap, quick and versatile. However, a disadvantage is that bacterial translation machinery is not capable of glycosylation and suboptimal for disulphide bond formation. Therefore when producing HER2 subdomains in *E. coli* not only does protein need to be produced but also correct folding of the protein needs to be achieved.

6.2.4.3 Small scale expression screening using Promega's MagneHis purification system

Aforementioned three *E. coli* strains designed for optimal mammalian protein expression were chosen for use in a small scale expression trial. The expression trial utilised Promega's MagneHis purification system using a Hamilton Star liquid handling robotics platform that enables screening for protein expression and solubility (2.15.4.3). In brief,

DNA of respective subdomains was transformed into each *E. coli* strain respectively (section2.7.1). Colonies were picked into 1 mL LB containing antibiotic in a 2.2 mL 96 deep well plate and incubated overnight at 37 °C 220 rpm. The following day a fresh plate containing 1.8 mL LB was inoculated with 200 μL overnight culture and grown until an OD_{600} of ~0.7 was achieved. For Lemo21(DE3) containing wells varying concentrations of L-rhamnose was added to different wells (0.5, 1, 1.5 and 2 mM). Plates were induced with 8 μL 0.1 M IPTG and grown at 18 °C with shaking at 220 rpm overnight. Following centrifugation the following day the supernatant was discarded and protein was purified following the MagneHis protocol on the Hamilton robot. Purified samples were mixed with 50 μL 2 x loading dye and analysed by SDS-PAGE (2.8.2.1).

Table 1 depicts the expected molecular weights of subdomain fusion proteins with either MBP or SUMO. An initial small scale screen successfully showed faint bands in the Lemo21(DE3) strain with no L-rhamnose added (data not shown). To improve yield of protein from the small scale test, the screen was repeated lysing protein in 2 x lysis buffer, but otherwise identical to above. Analysis by SDS-PAGE showed multiple bands of the correct sizes were produced in the Lemo21(DE3) strain of *E. coli* (Figure 6.17). Strongest bands were from proteins expressed with MBP as a fusion protein so these were taken forward for a large scale expression trial.

Subdomain	Size	+MBP	+Sumo
1	21.7	64.4	34.9
2	13.2	55.9	26.4
3	18.8	61.5	32
4	15.7	58.4	28.9
12	34.9	77.6	48.1
23	32	74.7	45.2
34	34.5	77.2	47.7
123	53.7	96.4	66.9
234	47.7	90.4	60.9

Table 6.1 Molecular weight of HER2 extracellular domain subdomains.
Table shows the molecular weight (kDa) of HER2 extracellular domain alone (size) and with fusion proteins MBP (+MBP) and SUMO (+Sumo).

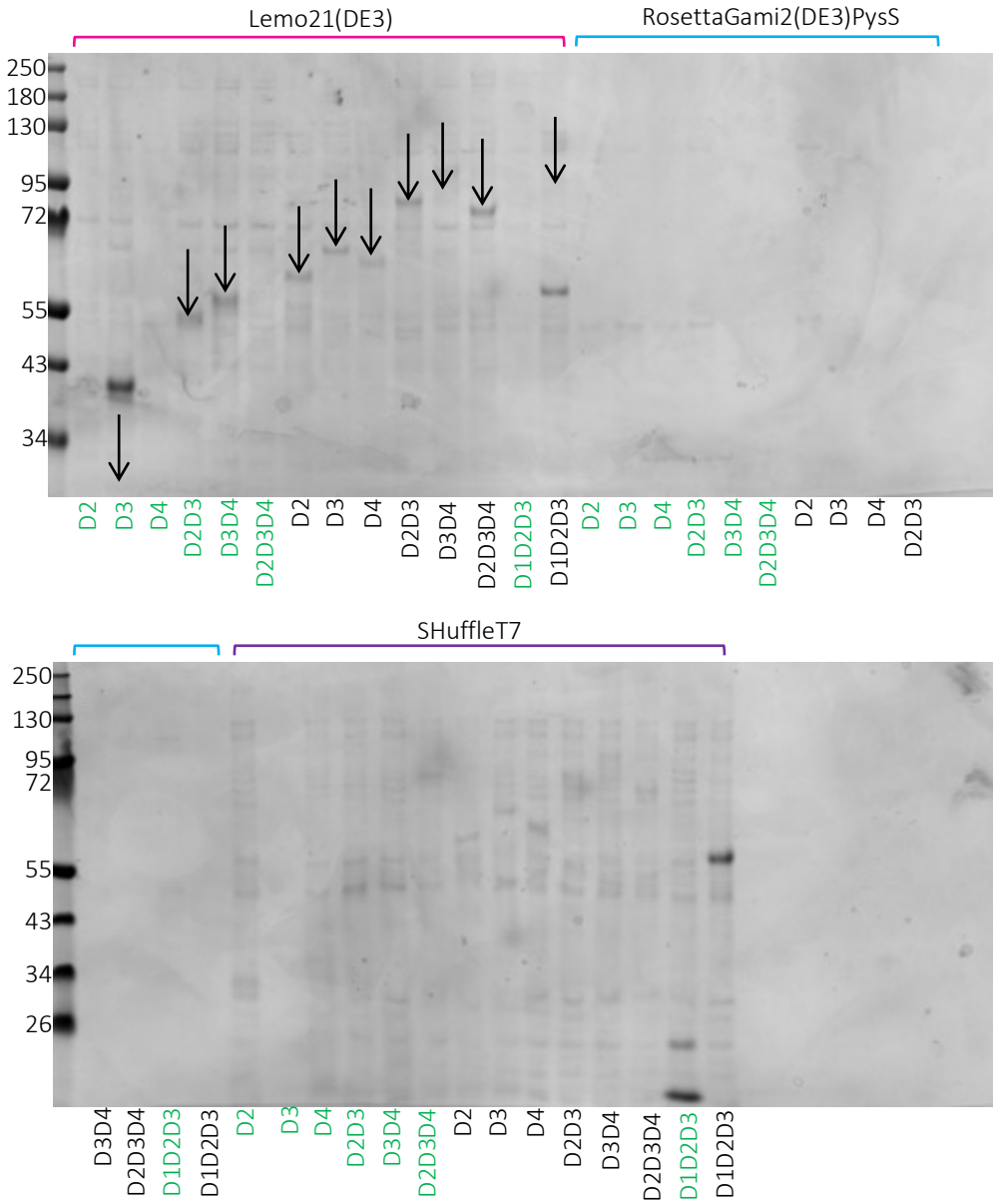


Figure 6.17 Expression trial of HER2 subdomains in different E.coli strains.
HER2 subdomain fusion proteins (SUMO- green, MBP- black) were expressed in Lemo21(DE3), RosettaGami2(DE3)PysS and SHuffleT7 E.coli strains. Proteins purification was carried out by Promega's MagneHis purification system on a Hamilton robot. Purified products were analysed by SDS-PAGE and stained with Instant Blue. Images were taken on a G-Box.

6.2.4.4 Larger scale expression of HER2 subdomain fusion proteins in Lemo21(DE3)

Lemo21(DE3) were confirmed as the optimal *E. coli* strain for the production of HER2 subdomain fusion proteins. Production volume was upscaled to 1 L culture volumes and purified on the bench (2.15.5). Constructs were purified using Ni^{2+} affinity chromatography. First elutions were analysed by SDS-PAGE and western blot (Figure 6.18). Subdomain II and IV MBP fusion proteins seemed to express the best with bands observed following SDS-PAGE and western blot analysis (Figure 6.18). Subdomain III MBP

fusion protein also had a band following SDS-PAGE analysis of lower intensity but western blot analysis for this fusion protein was ambiguous with no clear band (Figure 6.18B).

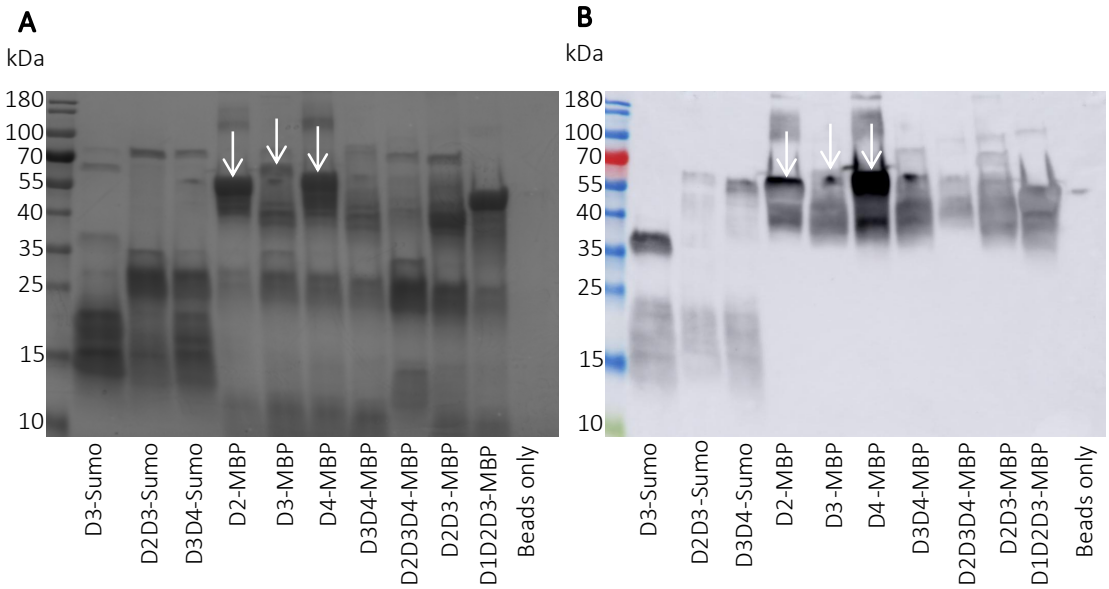


Figure 6.18 Larger scale expression trial of HER2 subdomain fusion proteins in Lemo21(DE3) cells.
HER2 subdomain fusion proteins with either SUMO or MBP were expressed in Lemo21(DE3) E.coli and purified by Ni-NTA chromatography. Samples from elution 1 were analysed by **(A)** SDS-PAGE followed by stain with Coomassie blue and **(B)** western blot to confirm expected molecular weighted. Protein was detected using anti-His HRP antibody and visualised with chemiluminescence. White arrows depict bands that correlate to expected mass. Images were taken on an Amersham Imager 600.

6.2.4.5 Pull down of HER2 subdomain fusion protein by Affimer D11

HER2 subdomain II, III and IV MBP fusion proteins were expressed and produced bands of the correct size. In order for Affimer D11 to bind to HER2 the protein must also be folded correctly. To test the ability of Affimer D11 to bind to any of these subdomains was investigated using a pull-down experiment. In brief, HER2 subdomain II, III and IV MBP fusion proteins were incubated with Affimer D11 Strep Tag II and Strep-Tactin® Sepharose® High Performance resin prior to elution of complex (2.15.6). Elutions were analysed by SDS-PAGE and western blot (Figure 6.19). Analysis by SDS-PAGE showed that detectable levels of Affimer D11 Strep Tag® II were present but no complex. Western blot analysis using an anti-streptactin HRP antibody to detect Strep Tag II proteins showed that Affimer D11 Strep Tag® II was present. Western blot analysis using anti-His HRP antibody to detect polyhistidine tags showed a faint band corresponding to subdomain II following pull down with Affimer D11 Strep Tag II. Following greater exposure this band was more easily visible whilst no band was visible for subdomain II and beads only. In contrast, whilst bands were also visible for HER2 subdomain III and IV MBP fusion proteins

following Affimer D11 Strep Tag II pulldown, these bands were also present in the beads only control suggesting that the bands were due to unspecific binding. The information provided from this experiment gave enough confidence to continue to large scale production of Affimer D11 Strep Tag II and HER2 subdomain II MBP fusion protein for X-ray crystallography.

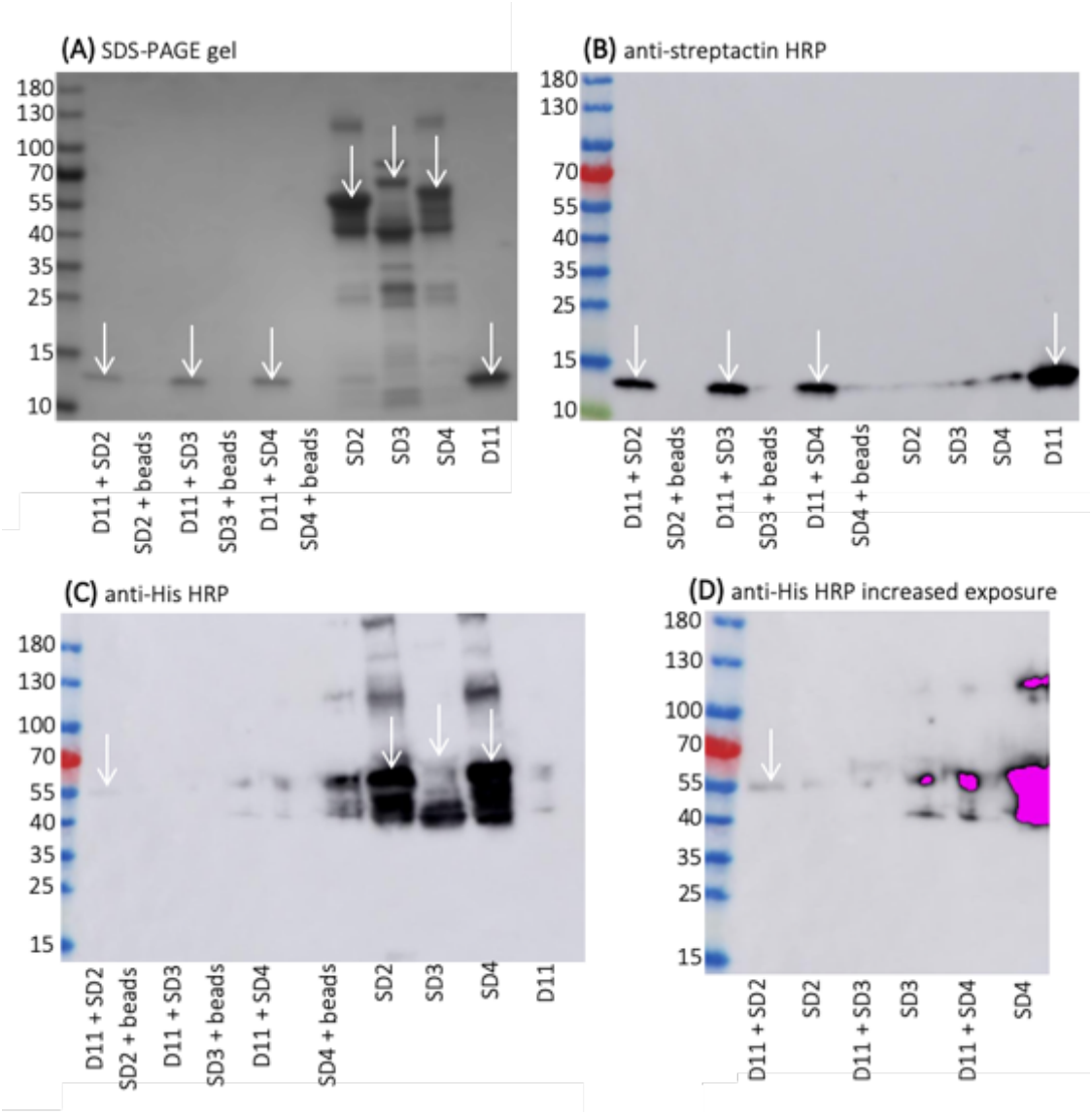


Figure 6.19 Pull-down of Affimer D11/HER2 subdomain complex using streptactin beads. Pull down of Affimer D11 Strep Tag II in complex with subdomain (SD) 2, 3 and 4 of the HER2 extracellular domain using Streptactin beads. Samples were analysed by **(A)** SDS-PAGE and **(B, C, D)** western blot analysis.

6.2.4.6 Production of Affimer D11 Strep-tag® II and HER2 subdomain II MBP fusion protein for X-ray crystallography

For protein structure determination by X-ray crystallography a highly homogeneous, pure and concentrated protein complex is required. Both proteins were produced and purified

separately prior to mixing to form the Affimer D11 Strep-tag® II HER2 subdomain II MBP fusion protein complex.

6.2.4.7 Large scale expression of HER2 subdomain II MBP fusion protein

The HER2 subdomain II MBP fusion protein expressed well in Lemo21(DE3) *E. coli* cells. To achieve a high concentration HER2 subdomain II MBP fusion protein in 10 x 1 L LB cultures were inoculated with 10 mL starter culture (2.15.5). Cultures were pelleted by centrifugation and resuspended in running buffer prior to lysis by the cell disruptor. Following a final high-speed centrifugation step supernatant was purified using a 5 mL His-Trap column on an ÄKTA pure system. The elution peak hypothesised to be HER2 subdomain II MBP fusion protein on the trace (Figure 6.20A) was further analysed by SDS-PAGE (Figure 6.20B). A high level of HER2 protein was achieved shown by large bands at ~56 kDa.

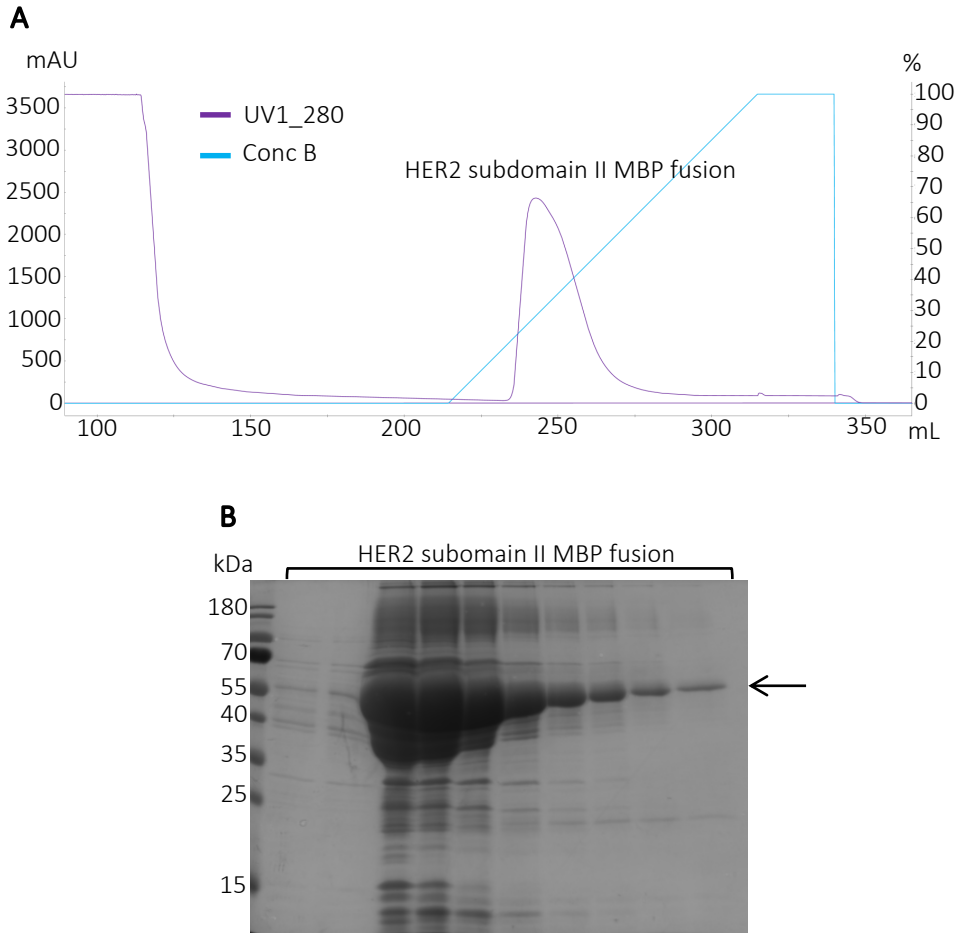


Figure 6.20 Purification of HER2 subdomain II MBP fusion protein.
His-tagged subdomain 2 of the extracellular domain of HER2 was purified as a fusion protein with MBP using two tandem 5 mL Ni-NTA columns on an ÄKTA pure system. **(A)** ÄKTA trace of HER2 subdomain 2 **(B)** SDS-PAGE stained with instant blue of samples from the labelled peak of the AKTA trace with arrow indicating expected ~55.9 kDa mass of subdomain 2 MBP fusion protein. Gels were 10-16 % Bio-RAD pre-cast gels and were ran at 150 V for ~ 1 hour. Gels were incubated with instant blue and destained to remove background prior to imaging using an Amersham imaging system.

6.2.4.8 Production of Affimer D11 Strep Tag II

Affimer D11 Strep-tag® II was cultured in 2 x 400 mL cultures, pelleted and stored at -20 °C until needed. Pellets were resuspended in loading buffer and lysed using a cell disruptor. Following high speed centrifugation to pellet cell debris the supernatant was loaded onto an ÄKTA pure system and purified using a 1 mL Strep Trap HP column. Samples from the elution peak hypothesised to be Affimer D11 Strep-tag® II were analysed by SDS-PAGE (Figure 6.21). SDS-PAGE analysis confirmed the presence of bands at the expected molecular mass of ~13 kDa.

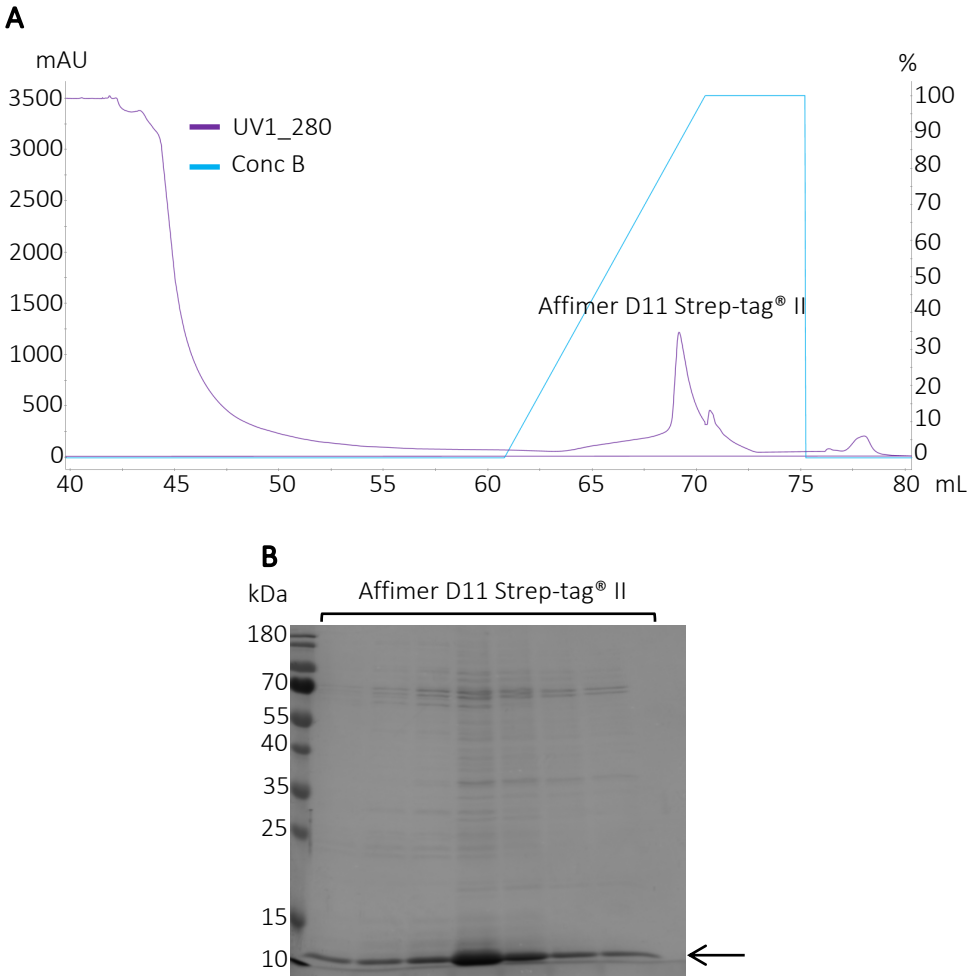


Figure 6.21 Purification of Affimer D11 Strep-Tag® II using Strep Trap HP column on an AKTA.
Strep-tagged Affimer D11 was purified by a 1 mL streptactin column on an AKTA pure system. **(A)** ÄKTA trace of strep tagged Affimer D11 **(B)** samples from peak _ of the ÄKTA trace analysed by SDS-PAGE stained with instant blue, arrow indicating the approximate ~13 kDa mass of Affimer D11. Gels were 10-16 % Bio-RAD pre-cast gels and were ran at 150 V for ~ 1 hour. Gels were incubated with instant blue and destained to remove background prior to imaging using an Amersham imaging system.

6.2.4.9 Tag-removal of Affimer D11 Strep-tag® II and HER2 subdomain II MBP fusion protein

In order to obtain a protein complex with the potential to form crystals the tags of both proteins were removed. The HER2 subdomain II MBP fusion protein contains a 3C protease cleavage site to remove the MBP and hexahistidine tag. Affimer D11 Strep-tag® II contains a TEV cleavage site to remove the Strep-tag® II. Proteins were dialysed with 3C protease or TEV overnight at 4 °C into 1 x PBS (2.15.5.2).

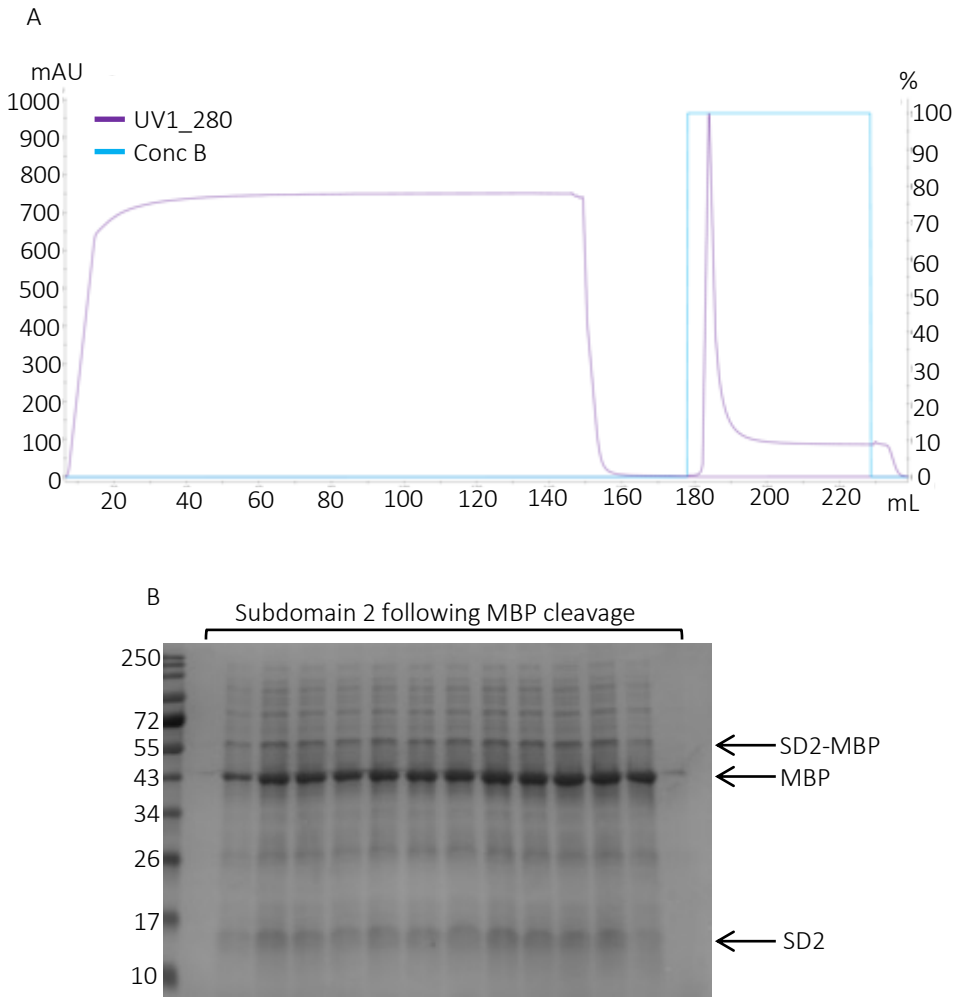


Figure 6.22 Analysis of MBP tag removal by SDS-PAGE.
Subdomain II of HER2 extracellular domain was expressed as a fusion protein with MBP. Following incubation with 3C protease solution was analysed by SDS-PAGE using a 10-16 % Bio-RAD precast gel stained with instant blue. Observed bands confirm the presence of uncleaved subdomain II MBP fusion protein (SD2-MBP) at ~55.9 kDa, cleaved MBP at ~42.5 kDa and untagged subdomain II (SD2) at ~12.9 kDa.

6.2.4.10 Separation of Affimer D11 HER2 subdomain II complex by size exclusion chromatography

Following tag removal a large volume of MBP was still present in the HER2 subdomain II solution. This could be due to MBP saturating the column with a need for a larger column capacity for future experiments. Affimer D11 was mixed with HER2 subdomain II and flowed over a 5 mL His Trap column to remove more MBP. Following this complex was separated by SEC using a HiLoad Superdex 200 column hoping to achieve complex pure enough to enter crystal trials. The MBP is large enough that it should separate from the Affimer D11 HER2 subdomain II complex as larger proteins are eluted from the column first with smaller proteins coming later. Many peaks were visible on the AKTA trace

(Figure 6.23A). Samples of these peaks were taken and analysed by SDS-PAGE (Figure 6.23B and C). Peak A of the AKTA trace (Figure 6.23A) correlated to the 'void' volume. Proteins larger than 70 kDa come off in the void volume possibly due to aggregation. Unfortunately, bands consistent with the size of Affimer D11 and HER2 subdomain II were present in this peak. This suggests that the protein complex had aggregated either together or with other proteins that were present in this peak. Peak E appeared to contain a large volume of MBP, which would be expected. Given the complexities of optimising a purification protocol and crystallography conditions, repeats of this purification will be continued in the future.

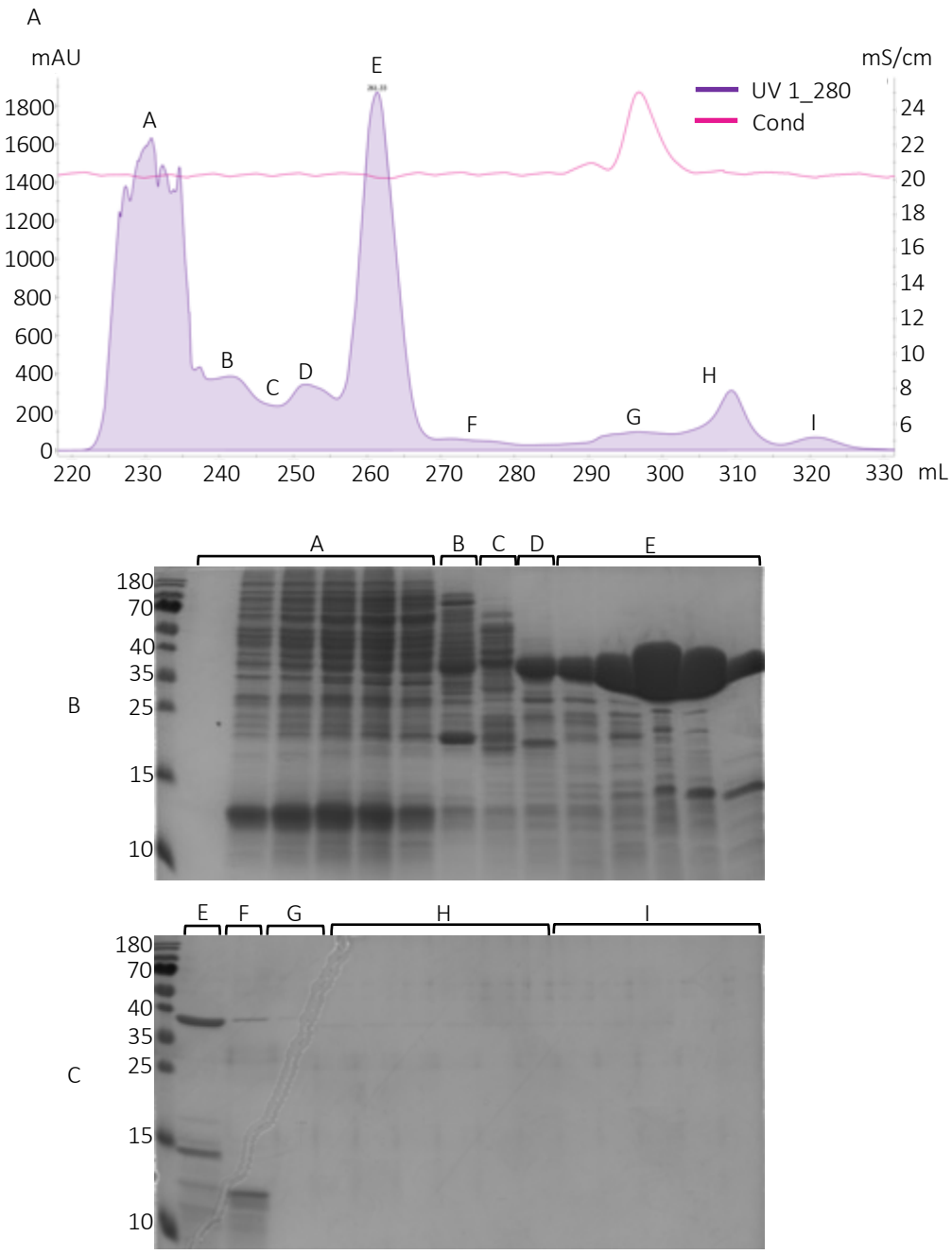


Figure 6.23 SEC of Affimer D11 HER2 subdomain II complex.
Size exclusion chromatography of Affimer D11 and HER2 subdomain II. (A) Trace labelled with peaks that came off of the column (B) SDS-PAGE stained with instant blue. Bands are labelled to correlate to peaks from the trace.

6.3 Chapter summary and future work

Although a complex of Affimer D11 and HER2 subdomain II was not achieved valuable insight was gained into potential binding region and the ability to produce HER2 subdomains in *E. coli*. The original HER2 extracellular domain structure was published in Nature in 2003 (75), since then multiple papers have used the same cell line developed

by Prof. Daniel Leahy and his laboratory to go on to achieve crystal structures (126, 293, 294) whilst others utilised other mammalian cell lines such as HEK293T and CHO cells (157, 295-297). Initially the cell line gifted from the Leahy lab was used to produce HER2 extracellular domain, however, yields were not high enough. Unfortunately, time restraints and lack of reagents prohibited a larger scale trial to grow HER2 extracellular domain by this mean.

6.3.1 Producing HER2 subdomain II in *E.coli*

Structural PDB files could only be found for HER2 extracellular domains produced by mammalian expression. The protein has, however, been produced by bacterial and insect expression for other purposes (298-300). Bacterial expression systems have advantages over mammalian and insect expression such as low costs, high yields and ease of manipulation but disadvantages surrounding the production of highly glycosylated mammalian proteins. The HER2 extracellular domain is rich in N-glycosylation that bacterial translationary machinery is unable to carry out. However, the end aim is to produce a homogeneous complex devoid of glycosylation so, as long as the protein is able to fold properly this could hold an advantage. Previously, bacterially expressed full length HER2 extracellular domain has produced insoluble protein (299, 300). Here, we successfully expressed and purified a high yield of HER2 subdomain II MBP fusion protein from Lemo21(DE3) *E. coli* cells. MBP is a well-defined solubility tag that has improved the solubility of multiple mammalian proteins (301). Results here show that, with optimisation, HER2 subdomains can be expressed in bacterial expression systems to high enough quantities required for X-ray crystallography.

6.3.2 Affimer D11 binding to subdomain II of the HER2 extracellular domain

Although a structure would be needed to fully conclude that correct folding of HER2 subdomain II had been achieved, the ability of Affimer D11 to bind is encouraging. Currently used monoclonal antibodies Trastuzumab and Pertuzumab bind to subdomains IV and II of the HER2 extracellular domain respectively (75, 126). It was hypothesised that Affimer D11 would also bind to one of these regions. Subdomains I and III are highly structured and are primarily involved in the binding of ligands. HER2 is an orphan

receptor so it was hypothesised that an interaction with subdomain I or III would have no therapeutic advantage. The dominant role of subdomain II is to facilitate receptor dimerisation. Pertuzumab prevents receptor dimerization through binding to subdomain II (302). It is unlikely that Affimer D11 binds to the same site as Pertuzumab as the Affimer conjugates are internalised by HER2 overexpressing cells whereas there is no clear evidence that Pertuzumab induces endocytosis of the receptor. Investigating the epitope that Affimer D11 binds to could further elucidate its mechanism of action and could provide a novel binding pocket otherwise unreachable by larger therapeutics such as monoclonal antibodies. Whilst other non-immunoglobulin scaffolds have been raised against HER2 and used to target the delivery of toxic entities no structural data is recorded (223, 236). Comparisons of binding sites between such scaffolds would provide further insight into whether these therapeutics could be used as combination therapy. Treating cells with both drugs in parallel would provide information regarding this if an increased therapeutic effect was observed then drugs would most likely bind to alternate sites.

6.3.3 Chapter conclusion

In this chapter we have identified that Affimer D11 most likely binds to subdomain II or the HER2 extracellular domain in a binding site unique to Pertuzumab. The small size of Affimers allow them to bind to epitopes that would be otherwise unreachable for monoclonal antibodies. The information here suggests that AfD11M could have therapeutic effect in conjunction with currently used monoclonal antibodies Trastuzumab and Pertuzumab against HER2 overexpressing breast cancer cell lines and possibly tumours.

Chapter 7

Discussion and future perspectives

'Promise me you'll always remember: you're braver than you believe, stronger than you seem and smarter thank you think.'

-Piglet

7 Discussion and future perspectives

7.1 Discussion and conclusion

The development of monoclonal antibodies such as Trastuzumab that can target antigens that demonstrate differential expression in tumours saw a new era of stratified cancer therapy. However, drawbacks were soon elucidated and a need for a therapeutic alternative was realised. Research into molecules that target the HER2 antigen rose over the past decade following the development of Trastuzumab. The work in this thesis described the characterisation of Affimers that bind to HER2 and their potential use as a vehicle to deliver a cytotoxic moiety to HER2 overexpressing cancer cells. Isolated Affimers D11 and H7 demonstrated nM binding affinity to the HER2 extracellular domain with no cross-reactivity with HER3, despite high structural homology. Furthermore Affimers reduced metabolic activity of breast cancer cell lines that overexpressed HER2 in a dose dependent manner. Further investigation was carried out to determine the binding site of Affimer D11 on the HER2 extracellular domain. Preliminary results led to the conclusion that subdomain II of the extracellular domain was the likely binding site, however, determination of the crystal structure would provide clarity to this hypothesis. Affimer D11 was tested on cells in both 2D and 3D cell culture. The culture of primary human breast cancer cells in the 3D cell culture system PerfusionPal provided the basis for a fully humanised model that could accurately recapitulate the heterogeneity of breast cancer *in vivo*. Although further optimisation is necessary this investigation provides the basis for a novel 3D cell culture system to culture primary tumour cells and a novel Affimer drug conjugate that specifically targets HER2 expressing cells.

7.2 Affimer D11 and H7 as vehicles for the specific delivery of cytotoxic molecules

The overexpression of HER2 on the cell surface of a subtype of breast cancer is an attractive target for therapeutics. As HER2 is located on the plasma membrane of tumour cells it is easily accessible by drugs and allows for targeted cancer therapy compared to commonly used chemotherapy that leads to off-target, unpleasant, side effects (303). As such Trastuzumab and Pertuzumab that bind to subdomain IV and II of the extracellular

domain were approved for the treatment of HER2 overexpressing breast cancer. Monoclonal antibodies are large molecules that would be unable to bind smaller pockets located deeper in the receptors structure. Therefore, it is likely that there are further novel binding sites to be explored that may be therapeutically benefitial. To date there is no structural information referencing the binding sites of other non-immunoglobulin scaffolds that are being proposed for use in a therapeutic setting, however, the binding site of a non-therapeutic HER2 binding Affibody was novel to the binding sites of Trastuzumab and Pertuzumab (157).

In recent years research into non-immunoglobulin scaffolds has been undertaken to research their potential for overcoming some of the drawbacks of monoclonal antibodies such as their large size and cost to manufacture (304). Whilst there are no approved non-immunoglobulin molecules that have received approval for therapeutic use against HER2, there are examples that target other antigens (233).

A DARPin targeting vascular endothelial growth factor A (abicipar pegol) is in the final stages of FDA approval for the treatment of neovascular age-related macular degeneration (305, 306). The DARPin MP0274 that binds to two unique non-overlapping epitopes on subdomains IV and II of the HER2 extracellular domain is in preclinical development for the inhibition of HER2 signalling in patients who no longer respond to first line treatments (307). An Affibody molecule identified to bind to HER2 by phage display has been successful in phase I/II trials for tumour imaging applications (308). Together, this evidence shows that there is strong potential for non-immunoglobulin scaffolds to be involved in future therapeutics.

7.3 Continuation of the project and future perspective

7.3.1 Further investigation of Affimer drug conjugates

Whilst the small size of Affimers is beneficial for penetration of solid tumours it can also result in enhanced clearing by the kidneys. In order for a non-immunoglobulin scaffold to elicit a therapeutic effect its serum half-life has to be high enough to allow accumulation

at the tumour site opposed to kidneys (309). Multiple methods have been used to increase the half-life of non-immunoglobulin scaffolds intended for therapeutic effect that could be trialled in Affimer reagents. The renal filtration cut-off is ~ 60 kDa, therefore, it is desirable to create an Affimer molecule that is larger than this, but still smaller than monoclonal antibodies to maintain their ability to penetrate solid tumours.

One mechanism to generate larger molecules is to create Affimer dimers that could potentially lead to an increase in half-life as well as an increased affinity. Another method is to generate fusion proteins that incorporate a larger protein such as polyethylene glycol, Fc fragments or human serum albumin (310, 311). Increasing the half-life through increasing the size of the molecule can, however, take away the attributes that make Affimer reagents desirable therapeutics such as their small size and high solubility. Therefore, future work should investigate suitable methods for enhancing the half-life of Affimer drug conjugates whilst maintaining efficacy.

Bispecific non-immunoglobulin scaffolds are another way of functionally improving current therapeutics. Such bispecific protein therapeutics allow duel targeting of a disease associated antigen, such as HER2, and immune cells bringing them in close proximity. It is possible to generate bispecific Affimers, whilst unpublished Avacta Life Sciences have produced a bispecific Fc fusion type I Affimer targeting both programmed cell death-liganed 1 and lymphocyte activation gene 3 demonstrating their potential use in immunotherapy. By producing a bispecific HER2 binding Affimer that can also bind antigens on immune cells this has the potential to elicit an immune response against cells expressing the HER2 antigen specifically.

7.3.2 Determination of the structure of Affimer D11 in complex with the HER2 extracellular domain

Whilst in this investigation the HER2 binding Affimer D11 was able to pull down the HER2 subdomain II preferentially over other domains the result was ambiguous and requires further optimisation. It was shown that the full length HER2 extracellualr domain was successfully produced in the CHO Lec1 cell line previously used to obtain crystal

structures (75). However, this investigation demonstrated that it was also possible to produce individual subdomains of the HER2 extracellular domain in *E. coli*. There is currently no published structural data obtained from HER2 domain protein that has been expressed in *E. coli*. The binding of Affimer D11 to subdomain II of the HER2 extracellular domain insinuates that a protein exhibiting correct folding had been obtained. Obtaining crystal structures of Affimer D11 in complex with both the full length HER2 produced in mammalian cell culture and in complex with subdomain II produced in *E. coli* would give both confidence in the binding site of Affimer D11 and its interaction with other domains and also confidence in the use of *E. coli* for large scale mammalian protein production. The lack of structural data available for the currently isolated HER2 binding non-immunoglobulin scaffolds prevents the identification of a novel therapeutic binding pocket.

7.3.3 Optimisation of PerfusionPal for the culture of primary breast cancer cells

The NCI-60 is a panel of 60 cell lines used for pharmacokinetic and pharmacogenomic analysis of anti-cancer drugs (312). However, whilst correlations in gene networks occur between the NCI-60 panel and clinical samples, differences also occur giving light to limitations in this method (313). The NCI-60 provides a broad panel of multiple cell types but more refined collections have since been generated for breast cancer specifically (194). Whilst unarguably useful, such collections do not consider interstitual pressure, tumour microenvironment or the heterogeneity exhibited by *in vivo* tumours. Therefore more complex preclinical models are needed to better recapitulate *in vivo* tumours.

Culturing primary human cells in a physiologically relevant setting has the potential to enhance drug discovery. In this investigation PerfusionPal was characterised as a potential 3D cell culture candidate for this purpose. The system demonstrated enhanced metabolic activity of cells cultured with perfusion compared to without, this is being attributed to more efficient distribution of media and therefore nutrients throughout the scaffold due to interstitial pressue. However, only preliminary findings were conducted using primary patient samples. Experiments should be repeated using a larger number of samples from both HER2 positive and HER2 negative patients. The development of a high-throughput *ex vivo* model capable of predicting individual patient response to different

anticancer drugs has the potential to improve overall response and subsequent progression free survival (314).

7.3.4 Overcoming resistance to first line therapy in breast cancer cell lines

Acquired and *de novo* resistance are both drawbacks to the use of Trastuzumab and T-DM1 (315). Resistance can arise due to a number of difference mechanisms previously discussed in section 1.5.3.3. A challenge is to develop therapeutics against HER2 that are able to target resistant cells. Resistance has been overcome by targeting HER3 alongside HER2 and/or targeting multiple epitopes on HER2 simultaneously (316). Affimers can be developed against any protein and so potential epitope binding is infinite. In the future Affimers reagents could be screened against the extracellular domain of HER3 to develop Affimer reagents that bind to HER3. Evidence has been shown that resistance can be overcome by co-targeting molecules involved in the downstream signalling pathways such as PI3K (315, 317). Affimer reagents against downstream mediators of cell signalling such as SOS, Grb2 and RAS are currently in development and may prove to have synergistic effects with AfD11M and/ or AfH7M.

7.3.5 Addressing the 3Rs

The work conducted for this thesis had a primary aim to address the ethos of the NC3Rs to reduce, refine and replace the use of animals in research. The primary focus was to reduce the need of animals in preclinical drug testing and development with a longterm potential aim of replacement. These aims were addressed by using Affimers that are an antibody alternative scaffold that do not rely on the use of animals or mammalian cell culture for their production. Also, PerfusionPal that has a longterm aim to incorporate primary patient samples for predictive drug testing. If PerfusionPal could be optimised for the high-throughput culture of primary patient explants it has the potential to reduce the need for animals in preclinical drug development studies.

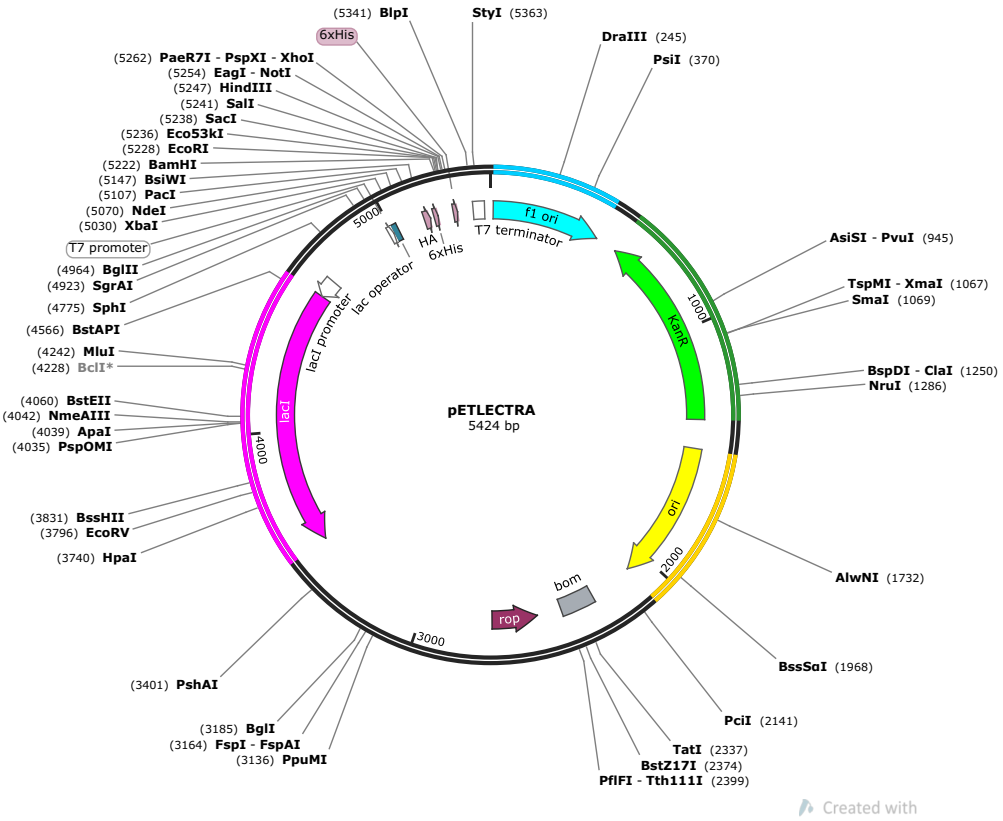
7.4 Conclusion

HER2 binding Affimers demonstrate potential to be investigated for their use as a therapeutic either as an alternative or for use in conjunction with monoclonal antibodies. Affimer D11 and H7 were both isolated with nM affinities for HER2 with high specificity compared to HER3. Both Affimers have demonstrated a reduction in metabolic activity of HER2 overexpressing cell lines in a dose dependent manner.

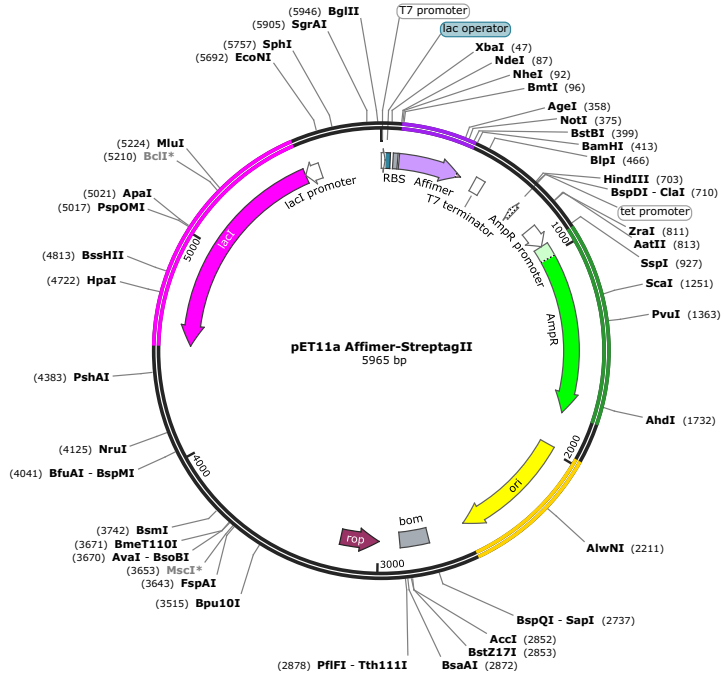
It would be useful if, in the future, the crystal structure of Affimer D11 and H7 in complex with the HER2 extracellular domain was determined. This information would provide valuable insight into the binding site of the Affimers and possible mechanism of action. The information from this study is a basis to demonstrate the potential use of non-immunoglobulin scaffolds, such as Affimers, for use as targeted cancer therapeutics. Also, the investigation highlights the importance of fully humanised 3D cell culture systems and the increasing role they will play in the development of preclinical models for drug testing in the future.

8 Appendix

A



B



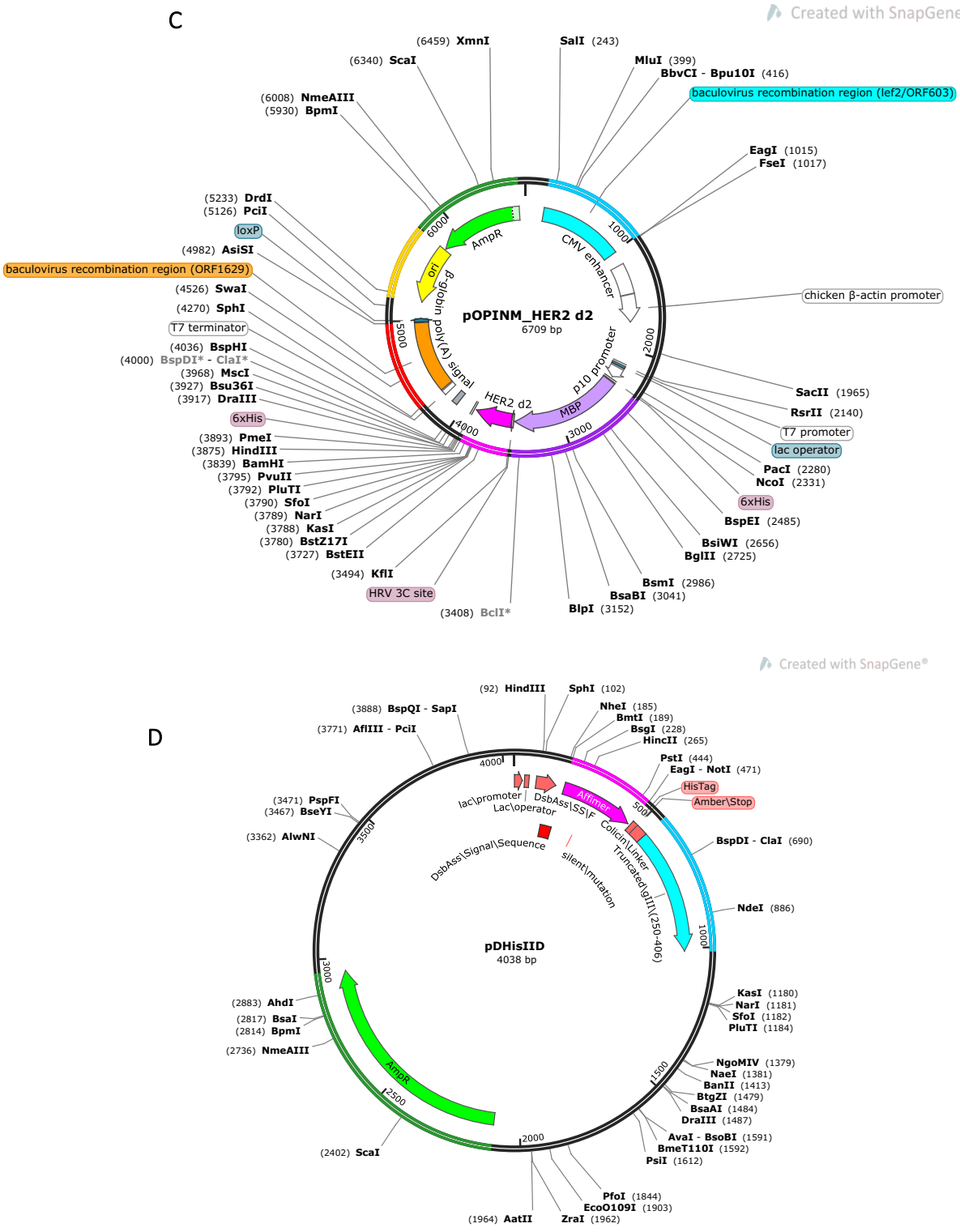


Figure 8.1 Plasmid vector maps.

Plasmid vector maps were generated using SnapGene® Viewer version 4.3.11. Plasmids used were **(A)** pETLECTRA **(B)** pET11a shown with a StrepTag II but was also used with a His tag **(C)** pOPIN vectors, the one demonstrated shows the pOPIN vector with the MBP solubility tag and subdomain II of the HER2 extracellular domain. Variations of this plasmid were used for each of the HER2 extracellular domain constructs and all were made with both MBP and SUMO **(D)** pDHis phagemid.

Bibliography

1. Hanahan D, Weinberg RA. The hallmarks of cancer. Cell. 2000;100(1):57-70.
2. Hanahan D, Weinberg RA. Hallmarks of cancer: the next generation. Cell. 2011;144(5):646-74.
3. Bennett IC, Gattas M, Teh BT. The genetic basis of breast cancer and its clinical implications. Aust N Z J Surg. 1999;69(2):95-105.
4. Narod SA, Salmena L. BRCA1 and BRCA2 mutations and breast cancer. Discov Med. 2011;12(66):445-53.
5. Pereira B, Chin SF, Rueda OM, Vollan HK, Provenzano E, Bardwell HA, et al. The somatic mutation profiles of 2,433 breast cancers refines their genomic and transcriptomic landscapes. Nat Commun. 2016;7:11479.
6. Jesinger RA. Breast anatomy for the interventionalist. Tech Vasc Interv Radiol. 2014;17(1):3-9.
7. Hinck L, Nathke I. Changes in cell and tissue organization in cancer of the breast and colon. Curr Opin Cell Biol. 2014;26:87-95.
8. Perou CM, Sorlie T, Eisen MB, van de Rijn M, Jeffrey SS, Rees CA, et al. Molecular portraits of human breast tumours. Nature. 2000;406(6797):747-52.
9. Cancer Genome Atlas N. Comprehensive molecular portraits of human breast tumours. Nature. 2012;490(7418):61-70.
10. Kunc M, Biernat W, Senkus-Konefka E. Estrogen receptor-negative progesterone receptor-positive breast cancer - "Nobody's land" or just an artifact? Cancer Treat Rev. 2018;67:78-87.
11. Jordan VC. The development of tamoxifen for breast cancer therapy: a tribute to the late Arthur L. Walpole. Breast Cancer Res Treat. 1988;11(3):197-209.
12. Furr BJ, Jordan VC. The pharmacology and clinical uses of tamoxifen. Pharmacol Ther. 1984;25(2):127-205.
13. Leyland-Jones B. Trastuzumab: hopes and realities. Lancet Oncol. 2002;3(3):137-44.
14. Gianni L, Pienkowski T, Im YH, Roman L, Tseng LM, Liu MC, et al. Efficacy and safety of neoadjuvant pertuzumab and trastuzumab in women with locally advanced, inflammatory, or early HER2-positive breast cancer (NeoSphere): a randomised multicentre, open-label, phase 2 trial. Lancet Oncology. 2012;13(1):25-32.
15. Opdam FL, Guchelaar HJ, Beijnen JH, Schellens JH. Lapatinib for advanced or metastatic breast cancer. Oncologist. 2012;17(4):536-42.
16. Aroian RV, Koga M, Mendel JE, Ohshima Y, Sternberg PW. The let-23 gene necessary for Caenorhabditis elegans vulval induction encodes a tyrosine kinase of the EGF receptor subfamily. Nature. 1990;348(6303):693-9.
17. Liu L, Thaker TM, Freed DM, Frazier N, Malhotra K, Lemmon MA, et al. Regulation of Kinase Activity in the Caenorhabditis elegans EGF Receptor, LET-23. Structure. 2018;26(2):270-81 e4.
18. Livneh E, Glazer L, Segal D, Schlessinger J, Shilo BZ. The Drosophila EGF receptor gene homolog: conservation of both hormone binding and kinase domains. Cell. 1985;40(3):599-607.
19. Downward J, Yarden Y, Mayes E, Scrace G, Totty N, Stockwell P, et al. Close similarity of epidermal growth factor receptor and v-erb-B oncogene protein sequences. Nature. 1984;307(5951):521-7.

20. Ullrich A, Coussens L, Hayflick JS, Dull TJ, Gray A, Tam AW, et al. Human epidermal growth factor receptor cDNA sequence and aberrant expression of the amplified gene in A431 epidermoid carcinoma cells. Nature. 1984;309(5967):418-25.
21. Lax I, Mitra AK, Ravera C, Hurwitz DR, Rubinstein M, Ullrich A, et al. Epidermal growth factor (EGF) induces oligomerization of soluble, extracellular, ligand-binding domain of EGF receptor. A low resolution projection structure of the ligand-binding domain. J Biol Chem. 1991;266(21):13828-33.
22. Robinson DR, Wu YM, Lin SF. The protein tyrosine kinase family of the human genome. Oncogene. 2000;19(49):5548-57.
23. Ullrich A, Schlessinger J. Signal transduction by receptors with tyrosine kinase activity. Cell. 1990;61(2):203-12.
24. Sanchez-Soria P, Camenisch TD. ErbB signaling in cardiac development and disease. Semin Cell Dev Biol. 2010;21(9):929-35.
25. Lee KF, Simon H, Chen H, Bates B, Hung MC, Hauser C. Requirement for neuregulin receptor erbB2 in neural and cardiac development. Nature. 1995;378(6555):394-8.
26. Camenisch TD, Schroeder JA, Bradley J, Klewer SE, McDonald JA. Heart-valve mesenchyme formation is dependent on hyaluronan-augmented activation of ErbB2-ErbB3 receptors. Nat Med. 2002;8(8):850-5.
27. Gassmann M, Casagranda F, Orioli D, Simon H, Lai C, Klein R, et al. Aberrant neural and cardiac development in mice lacking the ErbB4 neuregulin receptor. Nature. 1995;378(6555):390-4.
28. Sibilia M, Wagner EF. Strain-dependent epithelial defects in mice lacking the EGF receptor. Science. 1995;269(5221):234-8.
29. Press MF, Cordon-Cardo C, Slamon DJ. Expression of the HER-2/neu proto-oncogene in normal human adult and fetal tissues. Oncogene. 1990;5(7):953-62.
30. Fujio Y, Nguyen T, Wencker D, Kitsis RN, Walsh K. Akt promotes survival of cardiomyocytes in vitro and protects against ischemia-reperfusion injury in mouse heart. Circulation. 2000;101(6):660-7.
31. Matsui T, Rosenzweig A. Convergent signal transduction pathways controlling cardiomyocyte survival and function: the role of PI 3-kinase and Akt. J Mol Cell Cardiol. 2005;38(1):63-71.
32. Suarez Pestana E, Tenev T, Gross S, Stoyanov B, Ogata M, Bohmer FD. The transmembrane protein tyrosine phosphatase RPTPsigma modulates signaling of the epidermal growth factor receptor in A431 cells. Oncogene. 1999;18(28):4069-79.
33. Gensler M, Buschbeck M, Ullrich A. Negative regulation of HER2 signaling by the PEST-type protein-tyrosine phosphatase BDP1. J Biol Chem. 2004;279(13):12110-6.
34. Doherty JK, Bond C, Jardim A, Adelman JP, Clinton GM. The HER-2/neu receptor tyrosine kinase gene encodes a secreted autoinhibitor. Proc Natl Acad Sci U S A. 1999;96(19):10869-74.
35. Song MS, Salmena L, Pandolfi PP. The functions and regulation of the PTEN tumour suppressor. Nat Rev Mol Cell Biol. 2012;13(5):283-96.
36. Wiley HS, Burke PM. Regulation of receptor tyrosine kinase signaling by endocytic trafficking. Traffic. 2001;2(1):12-8.
37. Gur G, Rubin C, Katz M, Amit I, Citri A, Nilsson J, et al. LRIG1 restricts growth factor signaling by enhancing receptor ubiquitylation and degradation. EMBO J. 2004;23(16):3270-81.

38. Baulida J, Kraus MH, Alimandi M, Di Fiore PP, Carpenter G. All ErbB receptors other than the epidermal growth factor receptor are endocytosis impaired. J Biol Chem. 1996;271(9):5251-7.
39. Worthylake R, Opresko LK, Wiley HS. ErbB-2 amplification inhibits down-regulation and induces constitutive activation of both ErbB-2 and epidermal growth factor receptors. J Biol Chem. 1999;274(13):8865-74.
40. Salomon DS, Brandt R, Ciardiello F, Normanno N. Epidermal growth factor-related peptides and their receptors in human malignancies. Crit Rev Oncol Hematol. 1995;19(3):183-232.
41. Normanno N, De Luca A, Bianco C, Strizzi L, Mancino M, Maiello MR, et al. Epidermal growth factor receptor (EGFR) signaling in cancer. Gene. 2006;366(1):2-16.
42. Di Fiore PP, Pierce JH, Kraus MH, Segatto O, King CR, Aaronson SA. erbB-2 is a potent oncogene when overexpressed in NIH/3T3 cells. Science. 1987;237(4811):178-82.
43. Di Fiore PP, Pierce JH, Fleming TP, Hazan R, Ullrich A, King CR, et al. Overexpression of the human EGF receptor confers an EGF-dependent transformed phenotype to NIH 3T3 cells. Cell. 1987;51(6):1063-70.
44. Iqbal N, Iqbal N. Human Epidermal Growth Factor Receptor 2 (HER2) in Cancers: Overexpression and Therapeutic Implications. Mol Biol Int. 2014;2014:852748.
45. Padhy LC, Shih C, Cowing D, Finkelstein R, Weinberg RA. Identification of a phosphoprotein specifically induced by the transforming DNA of rat neuroblastomas. Cell. 1982;28(4):865-71.
46. Schechter AL, Stern DF, Vaidyanathan L, Decker SJ, Drebin JA, Greene MI, et al. The neu oncogene: an erb-B-related gene encoding a 185,000-Mr tumour antigen. Nature. 1984;312(5994):513-6.
47. Muller WJ, Sinn E, Pattengale PK, Wallace R, Leder P. Single-step induction of mammary adenocarcinoma in transgenic mice bearing the activated c-neu oncogene. Cell. 1988;54(1):105-15.
48. Sinn E, Muller W, Pattengale P, Tepler I, Wallace R, Leder P. Coexpression of MMTV/v-Ha-ras and MMTV/c-myc genes in transgenic mice: synergistic action of oncogenes in vivo. Cell. 1987;49(4):465-75.
49. Bargmann CI, Hung MC, Weinberg RA. Multiple independent activations of the neu oncogene by a point mutation altering the transmembrane domain of p185. Cell. 1986;45(5):649-57.
50. Harris RC, Chung E, Coffey RJ. EGF receptor ligands. Exp Cell Res. 2003;284(1):2-13.
51. Blobel CP. ADAMs: key components in EGFR signalling and development. Nat Rev Mol Cell Biol. 2005;6(1):32-43.
52. Wouters MA, Rigoutsos I, Chu CK, Feng LL, Sparrow DB, Dunwoodie SL. Evolution of distinct EGF domains with specific functions. Protein Sci. 2005;14(4):1091-103.
53. Hill RJ, Sternberg PW. The gene lin-3 encodes an inductive signal for vulval development in C. elegans. Nature. 1992;358(6386):470-6.
54. Freeman M. Complexity of EGF receptor signalling revealed in Drosophila. Curr Opin Genet Dev. 1998;8(4):407-11.
55. Butchar JP, Cain D, Manivannan SN, McCue AD, Bonanno L, Halula S, et al. New negative feedback regulators of Egfr signaling in Drosophila. Genetics. 2012;191(4):1213-26.

56. Yarden Y. The EGFR family and its ligands in human cancer. signalling mechanisms and therapeutic opportunities. Eur J Cancer. 2001;37 Suppl 4:S3-8.
57. Barberan S, Martin-Duran JM, Cebria F. Evolution of the EGFR pathway in Metazoa and its diversification in the planarian Schmidtea mediterranea. Sci Rep. 2016;6:28071.
58. Higashiyama S, Abraham JA, Miller J, Fiddes JC, Klagsbrun M. A heparin-binding growth factor secreted by macrophage-like cells that is related to EGF. Science. 1991;251(4996):936-9.
59. Kimura H, Fischer WH, Schubert D. Structure, expression and function of a schwannoma-derived growth factor. Nature. 1990;348(6298):257-60.
60. Cohen S. Purification of a Nerve-Growth Promoting Protein from the Mouse Salivary Gland and Its Neuro-Cytotoxic Antiserum. Proc Natl Acad Sci U S A. 1960;46(3):302-11.
61. Todaro GJ, De Larco JE, Cohen S. Transformation by murine and feline sarcoma viruses specifically blocks binding of epidermal growth factor to cells. Nature. 1976;264(5581):26-31.
62. Shoyab M, McDonald VL, Bradley JG, Todaro GJ. Amphiregulin: a bifunctional growth-modulating glycoprotein produced by the phorbol 12-myristate 13-acetate-treated human breast adenocarcinoma cell line MCF-7. Proc Natl Acad Sci U S A. 1988;85(17):6528-32.
63. Shing Y, Christofori G, Hanahan D, Ono Y, Sasada R, Igarashi K, et al. Betacellulin: a mitogen from pancreatic beta cell tumors. Science. 1993;259(5101):1604-7.
64. Singh B, Carpenter G, Coffey RJ. EGF receptor ligands: recent advances. F1000Res. 2016;5.
65. Wen D, Peles E, Cupples R, Suggs SV, Bacus SS, Luo Y, et al. Neu differentiation factor: a transmembrane glycoprotein containing an EGF domain and an immunoglobulin homology unit. Cell. 1992;69(3):559-72.
66. Carraway KL, 3rd, Weber JL, Unger MJ, Ledesma J, Yu N, Gassmann M, et al. Neuregulin-2, a new ligand of ErbB3/ErbB4-receptor tyrosine kinases. Nature. 1997;387(6632):512-6.
67. Zhang D, Sliwkowski MX, Mark M, Frantz G, Akita R, Sun Y, et al. Neuregulin-3 (NRG3): a novel neural tissue-enriched protein that binds and activates ErbB4. Proc Natl Acad Sci U S A. 1997;94(18):9562-7.
68. Harari D, Tzahar E, Romano J, Shelly M, Pierce JH, Andrews GC, et al. Neuregulin-4: a novel growth factor that acts through the ErbB-4 receptor tyrosine kinase. Oncogene. 1999;18(17):2681-9.
69. Hayes NV, Gullick WJ. The neuregulin family of genes and their multiple splice variants in breast cancer. J Mammary Gland Biol Neoplasia. 2008;13(2):205-14.
70. Ferguson KM, Berger MB, Mendrola JM, Cho HS, Leahy DJ, Lemmon MA. EGF activates its receptor by removing interactions that autoinhibit ectodomain dimerization. Mol Cell. 2003;11(2):507-17.
71. Lax I, Burgess WH, Bellot F, Ullrich A, Schlessinger J, Givol D. Localization of a major receptor-binding domain for epidermal growth factor by affinity labeling. Mol Cell Biol. 1988;8(4):1831-4.
72. Bajaj M, Waterfield MD, Schlessinger J, Taylor WR, Blundell T. On the tertiary structure of the extracellular domains of the epidermal growth factor and insulin receptors. Biochim Biophys Acta. 1987;916(2):220-6.

73. Cho HS, Leahy DJ. Structure of the extracellular region of HER3 reveals an interdomain tether. Science. 2002;297(5585):1330-3.
74. Ogiso H, Ishitani R, Nureki O, Fukai S, Yamanaka M, Kim JH, et al. Crystal structure of the complex of human epidermal growth factor and receptor extracellular domains. Cell. 2002;110(6):775-87.
75. Cho HS, Mason K, Ramyar KX, Stanley AM, Gabelli SB, Denney DW, Jr., et al. Structure of the extracellular region of HER2 alone and in complex with the Herceptin Fab. Nature. 2003;421(6924):756-60.
76. Tzahar E, Waterman H, Chen X, Levkowitz G, Karunagaran D, Lavi S, et al. A hierarchical network of interreceptor interactions determines signal transduction by Neu differentiation factor/neuregulin and epidermal growth factor. Mol Cell Biol. 1996;16(10):5276-87.
77. Graus-Porta D, Beerli RR, Daly JM, Hynes NE. ErbB-2, the preferred heterodimerization partner of all ErbB receptors, is a mediator of lateral signaling. EMBO J. 1997;16(7):1647-55.
78. Sierke SL, Cheng K, Kim HH, Koland JG. Biochemical characterization of the protein tyrosine kinase homology domain of the ErbB3 (HER3) receptor protein. Biochem J. 1997;322 (Pt 3):757-63.
79. Carraway KL, 3rd, Cantley LC. A neu acquaintance for erbB3 and erbB4: a role for receptor heterodimerization in growth signaling. Cell. 1994;78(1):5-8.
80. Siegel PM, Ryan ED, Cardiff RD, Muller WJ. Elevated expression of activated forms of Neu/ErbB-2 and ErbB-3 are involved in the induction of mammary tumors in transgenic mice: implications for human breast cancer. EMBO J. 1999;18(8):2149-64.
81. Carpenter CL, Duckworth BC, Auger KR, Cohen B, Schaffhausen BS, Cantley LC. Purification and characterization of phosphoinositide 3-kinase from rat liver. J Biol Chem. 1990;265(32):19704-11.
82. Otsu M, Hiles I, Gout I, Fry MJ, Ruiz-Larrea F, Panayotou G, et al. Characterization of two 85 kd proteins that associate with receptor tyrosine kinases, middle-T/pp60c-src complexes, and PI3-kinase. Cell. 1991;65(1):91-104.
83. Hiles ID, Otsu M, Volinia S, Fry MJ, Gout I, Dhand R, et al. Phosphatidylinositol 3-kinase: structure and expression of the 110 kd catalytic subunit. Cell. 1992;70(3):419-29.
84. Hellyer NJ, Cheng K, Koland JG. ErbB3 (HER3) interaction with the p85 regulatory subunit of phosphoinositide 3-kinase. Biochem J. 1998;333 (Pt 3):757-63.
85. Songyang Z, Shoelson SE, Chaudhuri M, Gish G, Pawson T, Haser WG, et al. SH2 domains recognize specific phosphopeptide sequences. Cell. 1993;72(5):767-78.
86. Whitman M, Downes CP, Keeler M, Keller T, Cantley L. Type I phosphatidylinositol kinase makes a novel inositol phospholipid, phosphatidylinositol-3-phosphate. Nature. 1988;332(6165):644-6.
87. Auger KR, Serunian LA, Soltoff SP, Libby P, Cantley LC. PDGF-dependent tyrosine phosphorylation stimulates production of novel polyphosphoinositides in intact cells. Cell. 1989;57(1):167-75.
88. Ghosh R, Narasanna A, Wang SE, Liu S, Chakrabarty A, Balko JM, et al. Trastuzumab has preferential activity against breast cancers driven by HER2 homodimers. Cancer Res. 2011;71(5):1871-82.
89. Margolis BL, Lax I, Kris R, Dombalagian M, Honegger AM, Howk R, et al. All autophosphorylation sites of epidermal growth factor (EGF) receptor and HER2/neu are located in their carboxyl-terminal tails. Identification of a novel site in EGF receptor. J Biol Chem. 1989;264(18):10667-71.

90. Kirouac DC, Du J, Lahdenranta J, Onsum MD, Nielsen UB, Schoeberl B, et al. HER2+ Cancer Cell Dependence on PI3K vs. MAPK Signaling Axes Is Determined by Expression of EGFR, ERBB3 and CDKN1B. PLoS Comput Biol. 2016;12(4):e1004827.
91. Ahmad DA, Negm OH, Alabdullah ML, Mirza S, Hamed MR, Band V, et al. Clinicopathological and prognostic significance of mitogen-activated protein kinases (MAPK) in breast cancers. Breast Cancer Res Treat. 2016;159(3):457-67.
92. Dhillon AS, Hagan S, Rath O, Kolch W. MAP kinase signalling pathways in cancer. Oncogene. 2007;26(22):3279-90.
93. Pelicci G, Lanfrancone L, Grignani F, McGlade J, Cavallo F, Forni G, et al. A novel transforming protein (SHC) with an SH2 domain is implicated in mitogenic signal transduction. Cell. 1992;70(1):93-104.
94. Skolnik EY, Lee CH, Batzer A, Vicentini LM, Zhou M, Daly R, et al. The SH2/SH3 domain-containing protein GRB2 interacts with tyrosine-phosphorylated IRS1 and Shc: implications for insulin control of ras signalling. EMBO J. 1993;12(5):1929-36.
95. Egan SE, Giddings BW, Brooks MW, Buday L, Sizeland AM, Weinberg RA. Association of Sos Ras exchange protein with Grb2 is implicated in tyrosine kinase signal transduction and transformation. Nature. 1993;363(6424):45-51.
96. Vojtek AB, Hollenberg SM, Cooper JA. Mammalian Ras interacts directly with the serine/threonine kinase Raf. Cell. 1993;74(1):205-14.
97. Yoon S, Seger R. The extracellular signal-regulated kinase: multiple substrates regulate diverse cellular functions. Growth Factors. 2006;24(1):21-44.
98. Kohler G, Milstein C. Continuous cultures of fused cells secreting antibody of predefined specificity. Nature. 1975;256(5517):495-7.
99. Strohl WR. Current progress in innovative engineered antibodies. Protein Cell. 2018;9(1):86-120.
100. Schroeder HW, Jr., Cavacini L. Structure and function of immunoglobulins. J Allergy Clin Immunol. 2010;125(2 Suppl 2):S41-52.
101. Singh S, Kumar NK, Dwiwedi P, Charan J, Kaur R, Sidhu P, et al. Monoclonal Antibodies: A Review. Curr Clin Pharmacol. 2018;13(2):85-99.
102. Drebin JA, Link VC, Weinberg RA, Greene MI. Inhibition of tumor growth by a monoclonal antibody reactive with an oncogene-encoded tumor antigen. Proc Natl Acad Sci U S A. 1986;83(23):9129-33.
103. Drebin JA, Stern DF, Link VC, Weinberg RA, Greene MI. Monoclonal antibodies identify a cell-surface antigen associated with an activated cellular oncogene. Nature. 1984;312(5994):545-8.
104. Carter P, Presta L, Gorman CM, Ridgway JB, Henner D, Wong WL, et al. Humanization of an anti-p185HER2 antibody for human cancer therapy. Proc Natl Acad Sci U S A. 1992;89(10):4285-9.
105. Denduluri N, Somerfield MR, Eisen A, Holloway JN, Hurria A, King TA, et al. Selection of Optimal Adjuvant Chemotherapy Regimens for Human Epidermal Growth Factor Receptor 2 (HER2) -Negative and Adjuvant Targeted Therapy for HER2-Positive Breast Cancers: An American Society of Clinical Oncology Guideline Adaptation of the Cancer Care Ontario Clinical Practice Guideline. J Clin Oncol. 2016;34(20):2416-27.
106. Vogel CL, Cobleigh MA, Tripathy D, Gutheil JC, Harris LN, Fehrenbacher L, et al. Efficacy and safety of trastuzumab as a single agent in first-line treatment of HER2-overexpressing metastatic breast cancer. J Clin Oncol. 2002;20(3):719-26.
107. Slamon DJ, Leyland-Jones B, Shak S, Fuchs H, Paton V, Bajamonde A, et al. Use of chemotherapy plus a monoclonal antibody against HER2 for metastatic breast cancer that overexpresses HER2. N Engl J Med. 2001;344(11):783-92.

108. Klapper LN, Waterman H, Sela M, Yarden Y. Tumor-inhibitory antibodies to HER-2/ErbB-2 may act by recruiting c-Cbl and enhancing ubiquitination of HER-2. Cancer Res. 2000;60(13):3384-8.
109. Molina MA, Codony-Servat J, Albanell J, Rojo F, Arribas J, Baselga J. Trastuzumab (herceptin), a humanized anti-Her2 receptor monoclonal antibody, inhibits basal and activated Her2 ectodomain cleavage in breast cancer cells. Cancer Res. 2001;61(12):4744-9.
110. Izumi Y, Xu L, di Tomaso E, Fukumura D, Jain RK. Tumour biology: herceptin acts as an anti-angiogenic cocktail. Nature. 2002;416(6878):279-80.
111. Clynes RA, Towers TL, Presta LG, Ravetch JV. Inhibitory Fc receptors modulate in vivo cytotoxicity against tumor targets. Nat Med. 2000;6(4):443-6.
112. Arnould L, Gelly M, Penault-Llorca F, Benoit L, Bonnetain F, Migeon C, et al. Trastuzumab-based treatment of HER2-positive breast cancer: an antibody-dependent cellular cytotoxicity mechanism? Br J Cancer. 2006;94(2):259-67.
113. Lo Nigro C, Macagno M, Sangiolo D, Bertolaccini L, Aglietta M, Merlano MC. NK-mediated antibody-dependent cell-mediated cytotoxicity in solid tumors: biological evidence and clinical perspectives. Ann Transl Med. 2019;7(5):105.
114. Moilanen T, Jokimaki A, Tenhunen O, Koivunen JP. Trastuzumab-induced cardiotoxicity and its risk factors in real-world setting of breast cancer patients. J Cancer Res Clin Oncol. 2018;144(8):1613-21.
115. Yu AF, Yadav NU, Lung BY, Eaton AA, Thaler HT, Hudis CA, et al. Trastuzumab interruption and treatment-induced cardiotoxicity in early HER2-positive breast cancer. Breast Cancer Res Treat. 2015;149(2):489-95.
116. McArthur HL, Hudis CA. Trastuzumab: a picky partner? Clin Cancer Res. 2009;15(20):6311-3.
117. Wilken JA, Maihle NJ. Primary trastuzumab resistance: new tricks for an old drug. Ann N Y Acad Sci. 2010;1210:53-65.
118. Desmedt C, Sperinde J, Piette F, Huang W, Jin X, Tan Y, et al. Quantitation of HER2 expression or HER2:HER2 dimers and differential survival in a cohort of metastatic breast cancer patients carefully selected for trastuzumab treatment primarily by FISH. Diagn Mol Pathol. 2009;18(1):22-9.
119. Scaltriti M, Rojo F, Ocana A, Anido J, Guzman M, Cortes J, et al. Expression of p95HER2, a truncated form of the HER2 receptor, and response to anti-HER2 therapies in breast cancer. J Natl Cancer Inst. 2007;99(8):628-38.
120. Sperinde J, Jin X, Banerjee J, Penuel E, Saha A, Diedrich G, et al. Quantitation of p95HER2 in paraffin sections by using a p95-specific antibody and correlation with outcome in a cohort of trastuzumab-treated breast cancer patients. Clin Cancer Res. 2010;16(16):4226-35.
121. Nagata Y, Lan KH, Zhou X, Tan M, Esteva FJ, Sahin AA, et al. PTEN activation contributes to tumor inhibition by trastuzumab, and loss of PTEN predicts trastuzumab resistance in patients. Cancer Cell. 2004;6(2):117-27.
122. Fujita T, Doihara H, Kawasaki K, Takabatake D, Takahashi H, Washio K, et al. PTEN activity could be a predictive marker of trastuzumab efficacy in the treatment of ErbB2-overexpressing breast cancer. Br J Cancer. 2006;94(2):247-52.
123. Mishra R, Patel H, Alanazi S, Yuan L, Garrett JT. HER3 signaling and targeted therapy in cancer. Oncol Rev. 2018;12(1):355.
124. Park YH, Jung HA, Choi MK, Chang W, Choi YL, Do IG, et al. Role of HER3 expression and PTEN loss in patients with HER2-overexpressing metastatic breast

cancer (MBC) who received taxane plus trastuzumab treatment. Br J Cancer. 2014;110(2):384-91.
125. Howie LJ, Scher NS, Amiri-Kordestani L, Zhang L, King-Kallimanis BL, Choudhry Y, et al. FDA Approval Summary: Pertuzumab for Adjuvant Treatment of HER2-Positive Early Breast Cancer. Clin Cancer Res. 2019;25(10):2949-55.
126. Franklin MC, Carey KD, Vajdos FF, Leahy DJ, de Vos AM, Sliwkowski MX. Insights into ErbB signaling from the structure of the ErbB2-pertuzumab complex. Cancer Cell. 2004;5(4):317-28.
127. Richard S, Selle F, Lotz JP, Khalil A, Gligorov J, Soares DG. Pertuzumab and trastuzumab: the rationale way to synergy. An Acad Bras Cienc. 2016;88 Suppl 1:565-77.
128. Lambert JM, Morris CQ. Antibody-Drug Conjugates (ADCs) for Personalized Treatment of Solid Tumors: A Review. Adv Ther. 2017;34(5):1015-35.
129. Junttila TT, Li G, Parsons K, Phillips GL, Sliwkowski MX. Trastuzumab-DM1 (T-DM1) retains all the mechanisms of action of trastuzumab and efficiently inhibits growth of lapatinib insensitive breast cancer. Breast Cancer Res Treat. 2011;128(2):347-56.
130. Barok M, Tanner M, Koninki K, Isola J. Trastuzumab-DM1 causes tumour growth inhibition by mitotic catastrophe in trastuzumab-resistant breast cancer cells in vivo. Breast Cancer Res. 2011;13(2):R46.
131. Paranjpe R, Basatneh D, Tao G, De Angelis C, Noormohammed S, Ekinci E, et al. Neratinib in HER2-Positive Breast Cancer Patients. Ann Pharmacother. 2019:1060028018824088.
132. Nelson MH, Dolder CR. Lapatinib: a novel dual tyrosine kinase inhibitor with activity in solid tumors. Ann Pharmacother. 2006;40(2):261-9.
133. Nonagase Y, Yonesaka K, Kawakami H, Watanabe S, Haratani K, Takahama T, et al. Heregulin-expressing HER2-positive breast and gastric cancer exhibited heterogeneous susceptibility to the anti-HER2 agents lapatinib, trastuzumab and T-DM1. Oncotarget. 2016;7(51):84860-71.
134. Chames P, Van Regenmortel M, Weiss E, Baty D. Therapeutic antibodies: successes, limitations and hopes for the future. Br J Pharmacol. 2009;157(2):220-33.
135. Hudson PJ, Souriau C. Engineered antibodies. Nat Med. 2003;9(1):129-34.
136. Gaciarz A, Veijola J, Uchida Y, Saaranen MJ, Wang C, Horkko S, et al. Systematic screening of soluble expression of antibody fragments in the cytoplasm of E. coli. Microb Cell Fact. 2016;15:22.
137. Bird RE, Hardman KD, Jacobson JW, Johnson S, Kaufman BM, Lee SM, et al. Single-chain antigen-binding proteins. Science. 1988;242(4877):423-6.
138. Yokota T, Milenic DE, Whitlow M, Schlom J. Rapid tumor penetration of a single-chain Fv and comparison with other immunoglobulin forms. Cancer Res. 1992;52(12):3402-8.
139. Horak E, Heitner T, Robinson MK, Simmons HH, Garrison J, Russeva M, et al. Isolation of scFvs to in vitro produced extracellular domains of EGFR family members. Cancer Biother Radiopharm. 2005;20(6):603-13.
140. Foroumadi S, Rajabibazl M, Rahimpour A, Shahidi S, Ebrahimizadeh W, Yarahmadi M, et al. Production of human single-chain fragment antibody (ScFv) against human epidermal growth factor receptor-2 (HER-2) by phage display technology. In Vitro Cell Dev Biol Anim. 2018;54(2):85-91.

141. Nejatollahi F, Ranjbar R, Younesi V, Asgharpour M. Deregulation of HER2 downstream signaling in breast cancer cells by a cocktail of anti-HER2 scFvs. Oncol Res. 2013;20(8):333-40.
142. Nejatollahi F, Jaberipour M, Asgharpour M. Triple blockade of HER2 by a cocktail of anti-HER2 scFv antibodies induces high antiproliferative effects in breast cancer cells. Tumour Biol. 2014;35(8):7887-95.
143. Chapman AP, Antoniw P, Spitali M, West S, Stephens S, King DJ. Therapeutic antibody fragments with prolonged in vivo half-lives. Nat Biotechnol. 1999;17(8):780-3.
144. Binz HK, Stumpp MT, Forrer P, Amstutz P, Pluckthun A. Designing repeat proteins: well-expressed, soluble and stable proteins from combinatorial libraries of consensus ankyrin repeat proteins. J Mol Biol. 2003;332(2):489-503.
145. Pluckthun A. Designed ankyrin repeat proteins (DARPins): binding proteins for research, diagnostics, and therapy. Annu Rev Pharmacol Toxicol. 2015;55:489-511.
146. Zahnd C, Pecorari F, Straumann N, Wyler E, Pluckthun A. Selection and characterization of Her2 binding-designed ankyrin repeat proteins. J Biol Chem. 2006;281(46):35167-75.
147. Zahnd C, Wyler E, Schwenk JM, Steiner D, Lawrence MC, McKern NM, et al. A designed ankyrin repeat protein evolved to picomolar affinity to Her2. J Mol Biol. 2007;369(4):1015-28.
148. Jost C, Schilling J, Tamaskovic R, Schwill M, Honegger A, Pluckthun A. Structural basis for eliciting a cytotoxic effect in HER2-overexpressing cancer cells via binding to the extracellular domain of HER2. Structure. 2013;21(11):1979-91.
149. Munch RC, Muhlebach MD, Schaser T, Kneissl S, Jost C, Pluckthun A, et al. DARPins: an efficient targeting domain for lentiviral vectors. Mol Ther. 2011;19(4):686-93.
150. Proshkina GM, Shilova ON, Ryabova AV, Stremovskiy OA, Deyev SM. A new anticancer toxin based on HER2/neu-specific DARPin and photoactive flavoprotein miniSOG. Biochimie. 2015;118:116-22.
151. Nord K, Gunneriusson E, Ringdahl J, Stahl S, Uhlen M, Nygren PA. Binding proteins selected from combinatorial libraries of an alpha-helical bacterial receptor domain. Nat Biotechnol. 1997;15(8):772-7.
152. Wikman M, Steffen AC, Gunneriusson E, Tolmachev V, Adams GP, Carlsson J, et al. Selection and characterization of HER2/neu-binding affibody ligands. Protein Eng Des Sel. 2004;17(5):455-62.
153. Alavizadeh SH, Akhtari J, Badiee A, Golmohammadzadeh S, Jaafari MR. Improved therapeutic activity of HER2 Affibody-targeted cisplatin liposomes in HER2-expressing breast tumor models. Expert Opin Drug Deliv. 2016;13(3):325-36.
154. Steffen AC, Orlova A, Wikman M, Nilsson FY, Stahl S, Adams GP, et al. Affibody-mediated tumour targeting of HER-2 expressing xenografts in mice. Eur J Nucl Med Mol Imaging. 2006;33(6):631-8.
155. Steffen AC, Wikman M, Tolmachev V, Adams GP, Nilsson FY, Stahl S, et al. In vitro characterization of a bivalent anti-HER-2 affibody with potential for radionuclide-based diagnostics. Cancer Biother Radiopharm. 2005;20(3):239-48.
156. Ekerljung L, Lindborg M, Gedda L, Frejd FY, Carlsson J, Lennartsson J. Dimeric HER2-specific affibody molecules inhibit proliferation of the SKBR-3 breast cancer cell line. Biochem Biophys Res Commun. 2008;377(2):489-94.

157. Eigenbrot C, Ultsch M, Dubnovitsky A, Abrahmsen L, Hard T. Structural basis for high-affinity HER2 receptor binding by an engineered protein. Proc Natl Acad Sci U S A. 2010;107(34):15039-44.
158. Sochaj-Gregorczyk AM, Serwotka-Suszczak AM, Otlewski J. A Novel Affibody-Auristatin E Conjugate With a Potent and Selective Activity Against HER2+ Cell Lines. J Immunother. 2016;39(6):223-32.
159. Zielinski R, Lyakhov I, Jacobs A, Chertov O, Kramer-Marek G, Francella N, et al. Affitoxin--a novel recombinant, HER2-specific, anticancer agent for targeted therapy of HER2-positive tumors. J Immunother. 2009;32(8):817-25.
160. Tuerk C, Gold L. Systematic evolution of ligands by exponential enrichment: RNA ligands to bacteriophage T4 DNA polymerase. Science. 1990;249(4968):505-10.
161. Schmidt KS, Borkowski S, Kurreck J, Stephens AW, Bald R, Hecht M, et al. Application of locked nucleic acids to improve aptamer in vivo stability and targeting function. Nucleic Acids Res. 2004;32(19):5757-65.
162. Ng EW, Shima DT, Calias P, Cunningham ET, Jr., Guyer DR, Adamis AP. Pegaptanib, a targeted anti-VEGF aptamer for ocular vascular disease. Nat Rev Drug Discov. 2006;5(2):123-32.
163. Gijs M, Penner G, Blackler GB, Impens NR, Baatout S, Luxen A, et al. Improved Aptamers for the Diagnosis and Potential Treatment of HER2-Positive Cancer. Pharmaceuticals (Basel). 2016;9(2).
164. Moosavian SA, Jaafari MR, Taghdisi SM, Mosaffa F, Badiee A, Abnous K. Development of RNA aptamers as molecular probes for HER2(+) breast cancer study using cell-SELEX. Iran J Basic Med Sci. 2015;18(6):576-86.
165. Ohuchi S. Cell-SELEX Technology. Biores Open Access. 2012;1(6):265-72.
166. Hay M, Thomas DW, Craighead JL, Economides C, Rosenthal J. Clinical development success rates for investigational drugs. Nat Biotechnol. 2014;32(1):40-51.
167. Lasfargues EY, Ozzello L. Cultivation of human breast carcinomas. J Natl Cancer Inst. 1958;21(6):1131-47.
168. Holliday DL, Speirs V. Choosing the right cell line for breast cancer research. Breast Cancer Res. 2011;13(4):215.
169. Slamon DJ, Godolphin W, Jones LA, Holt JA, Wong SG, Keith DE, et al. Studies of the HER-2/neu proto-oncogene in human breast and ovarian cancer. Science. 1989;244(4905):707-12.
170. Noel A, Foidart JM. The role of stroma in breast carcinoma growth in vivo. J Mammary Gland Biol Neoplasia. 1998;3(2):215-25.
171. Abbott A. Cell culture: biology's new dimension. Nature. 2003;424(6951):870-2.
172. Bissell MJ. Goodbye flat biology - time for the 3rd and the 4th dimensions. J Cell Sci. 2017;130(1):3-5.
173. Sutherland RM, Inch WR, McCredie JA, Kruuv J. A Multi-component Radiation Survival Curve Using anin VitroTumour Model. International Journal of Radiation Biology and Related Studies in Physics, Chemistry and Medicine. 2009;18(5):491-5.
174. Foty R. A simple hanging drop cell culture protocol for generation of 3D spheroids. J Vis Exp. 2011(51).
175. Jaganathan H, Gage J, Leonard F, Srinivasan S, Souza GR, Dave B, et al. Three-dimensional in vitro co-culture model of breast tumor using magnetic levitation. Sci Rep. 2014;4:6468.
176. Roberts GC, Morris PG, Moss MA, Maltby SL, Palmer CA, Nash CE, et al. An Evaluation of Matrix-Containing and Humanised Matrix-Free 3-Dimensional Cell Culture Systems for Studying Breast Cancer. PLoS One. 2016;11(6):e0157004.

177. Yuhas JM, Li AP, Martinez AO, Ladman AJ. A simplified method for production and growth of multicellular tumor spheroids. Cancer Res. 1977;37(10):3639-43.
178. Debnath J, Muthuswamy SK, Brugge JS. Morphogenesis and oncogenesis of MCF-10A mammary epithelial acini grown in three-dimensional basement membrane cultures. Methods. 2003;30(3):256-68.
179. [Available from: https://www.breastcancertissuebank.org.
180. Carter EP, Gopsill JA, Gomm JJ, Jones JL, Grose RP. A 3D in vitro model of the human breast duct: a method to unravel myoepithelial-luminal interactions in the progression of breast cancer. Breast Cancer Res. 2017;19(1):50.
181. Nash CE, Mavria G, Baxter EW, Holliday DL, Tomlinson DC, Treanor D, et al. Development and characterisation of a 3D multi-cellular in vitro model of normal human breast: a tool for cancer initiation studies. Oncotarget. 2015;6(15):13731-41.
182. Burdall SE, Hanby AM, Lansdown MR, Speirs V. Breast cancer cell lines: friend or foe? Breast Cancer Res. 2003;5(2):89-95.
183. Ellsworth RE, Blackburn HL, Shriver CD, Soon-Shiong P, Ellsworth DL. Molecular heterogeneity in breast cancer: State of the science and implications for patient care. Semin Cell Dev Biol. 2017;64:65-72.
184. Clevers H. Modeling Development and Disease with Organoids. Cell. 2016;165(7):1586-97.
185. Sachs N, de Ligt J, Kopper O, Gogola E, Bounova G, Weeber F, et al. A Living Biobank of Breast Cancer Organoids Captures Disease Heterogeneity. Cell. 2018;172(1-2):373-86 e10.
186. Mazzucchelli S, Piccotti F, Allevi R, Truffi M, Sorrentino L, Russo L, et al. Establishment and Morphological Characterization of Patient-Derived Organoids from Breast Cancer. Biol Proced Online. 2019;21:12.
187. Roberts S, Peyman S, Speirs V. Current and Emerging 3D Models to Study Breast Cancer. Adv Exp Med Biol. 2019;1152:413-27.
188. Sontheimer-Phelps A, Hassell BA, Ingber DE. Modelling cancer in microfluidic human organs-on-chips. Nat Rev Cancer. 2019;19(2):65-81.
189. Kim AA, Nekimken AL, Fechner S, O'Brien LE, Pruitt BL. Microfluidics for mechanobiology of model organisms. Methods Cell Biol. 2018;146:217-59.
190. Montanez-Sauri SI, Sung KE, Berthier E, Beebe DJ. Enabling screening in 3D microenvironments: probing matrix and stromal effects on the morphology and proliferation of T47D breast carcinoma cells. Integr Biol (Camb). 2013;5(3):631-40.
191. Li R, Hebert JD, Lee TA, Xing H, Boussommier-Calleja A, Hynes RO, et al. Macrophage-Secreted TNFalpha and TGFbeta1 Influence Migration Speed and Persistence of Cancer Cells in 3D Tissue Culture via Independent Pathways. Cancer Res. 2017;77(2):279-90.
192. Tang Y, Soroush F, Sheffield JB, Wang B, Prabhakarpandian B, Kiani MF. A Biomimetic Microfluidic Tumor Microenvironment Platform Mimicking the EPR Effect for Rapid Screening of Drug Delivery Systems. Sci Rep. 2017;7(1):9359.
193. Kersten K, de Visser KE, van Miltenburg MH, Jonkers J. Genetically engineered mouse models in oncology research and cancer medicine. EMBO Mol Med. 2017;9(2):137-53.
194. Neve RM, Chin K, Fridlyand J, Yeh J, Baehner FL, Fevr T, et al. A collection of breast cancer cell lines for the study of functionally distinct cancer subtypes. Cancer Cell. 2006;10(6):515-27.
195. Bosma GC, Custer RP, Bosma MJ. A severe combined immunodeficiency mutation in the mouse. Nature. 1983;301(5900):527-30.

196. Flanagan SP. 'Nude', a new hairless gene with pleiotropic effects in the mouse. Genet Res. 1966;8(3):295-309.
197. DeRose YS, Gligorich KM, Wang G, Georgelas A, Bowman P, Courdy SJ, et al. Patient-derived models of human breast cancer: protocols for in vitro and in vivo applications in tumor biology and translational medicine. Curr Protoc Pharmacol. 2013;Chapter 14:Unit14 23.
198. DeRose YS, Wang G, Lin YC, Bernard PS, Buys SS, Ebbert MT, et al. Tumor grafts derived from women with breast cancer authentically reflect tumor pathology, growth, metastasis and disease outcomes. Nat Med. 2011;17(11):1514-20.
199. Marangoni E, Vincent-Salomon A, Auger N, Degeorges A, Assayag F, de Cremoux P, et al. A new model of patient tumor-derived breast cancer xenografts for preclinical assays. Clin Cancer Res. 2007;13(13):3989-98.
200. Dobrolecki LE, Airhart SD, Alferez DG, Aparicio S, Behbod F, Bentires-Alj M, et al. Patient-derived xenograft (PDX) models in basic and translational breast cancer research. Cancer Metastasis Rev. 2016;35(4):547-73.
201. Ledford H. US cancer institute to overhaul tumour cell lines. Nature. 2016;530(7591):391.
202. Eirew P, Steif A, Khattra J, Ha G, Yap D, Farahani H, et al. Dynamics of genomic clones in breast cancer patient xenografts at single-cell resolution. Nature. 2015;518(7539):422-6.
203. Tiede C, Tang AA, Deacon SE, Mandal U, Nettleship JE, Owen RL, et al. Adhiron: a stable and versatile peptide display scaffold for molecular recognition applications. Protein Eng Des Sel. 2014;27(5):145-55.
204. Berrow NS, Alderton D, Sainsbury S, Nettleship J, Assenberg R, Rahman N, et al. A versatile ligation-independent cloning method suitable for high-throughput expression screening applications. Nucleic Acids Res. 2007;35(6):e45.
205. Woodman R, Yeh JT, Laurenson S, Ko Ferrigno P. Design and validation of a neutral protein scaffold for the presentation of peptide aptamers. J Mol Biol. 2005;352(5):1118-33.
206. Turk V, Bode W. The cystatins: protein inhibitors of cysteine proteinases. FEBS Lett. 1991;285(2):213-9.
207. Tiede C, Bedford R, Heseltine SJ, Smith G, Wijetunga I, Ross R, et al. Affimer proteins are versatile and renewable affinity reagents. Elife. 2017;6.
208. Bedford R, Tiede C, Hughes R, Curd A, McPherson MJ, Peckham M, et al. Alternative reagents to antibodies in imaging applications. Biophys Rev. 2017;9(4):299-308.
209. Lopata A, Hughes R, Tiede C, Heissler SM, Sellers JR, Knight PJ, et al. Affimer proteins for F-actin: novel affinity reagents that label F-actin in live and fixed cells. Sci Rep. 2018;8(1):6572.
210. Bandaranayake AD, Almo SC. Recent advances in mammalian protein production. FEBS Lett. 2014;588(2):253-60.
211. Dai X, Cheng H, Bai Z, Li J. Breast Cancer Cell Line Classification and Its Relevance with Breast Tumor Subtyping. J Cancer. 2017;8(16):3131-41.
212. Hendriks BS, Klinz SG, Reynolds JG, Espelin CW, Gaddy DF, Wickham TJ. Impact of tumor HER2/ERBB2 expression level on HER2-targeted liposomal doxorubicin-mediated drug delivery: multiple low-affinity interactions lead to a threshold effect. Mol Cancer Ther. 2013;12(9):1816-28.

213. Vazquez-Lombardi R, Phan TG, Zimmermann C, Lowe D, Jermutus L, Christ D. Challenges and opportunities for non-antibody scaffold drugs. Drug Discov Today. 2015;20(10):1271-83.
214. Bayguinov PO, Oakley DM, Shih CC, Geanon DJ, Joens MS, Fitzpatrick JAJ. Modern Laser Scanning Confocal Microscopy. Curr Protoc Cytom. 2018;85(1):e39.
215. Nagata Y, Burger MM. Wheat germ agglutinin. Molecular characteristics and specificity for sugar binding. J Biol Chem. 1974;249(10):3116-22.
216. Monsigny M, Roche AC, Sene C, Maget-Dana R, Delmotte F. Sugar-lectin interactions: how does wheat-germ agglutinin bind sialoglycoconjugates? Eur J Biochem. 1980;104(1):147-53.
217. Roth J, Binder M, Gerhard UJ. Conjugation of lectins with fluorochromes: an approach to histochemical double labeling of carbohydrate components. Histochemistry. 1978;56(3-4):265-73.
218. Alley SC, Okeley NM, Senter PD. Antibody-drug conjugates: targeted drug delivery for cancer. Curr Opin Chem Biol. 2010;14(4):529-37.
219. Mu FT, Callaghan JM, Steele-Mortimer O, Stenmark H, Parton RG, Campbell PL, et al. EEA1, an early endosome-associated protein. EEA1 is a conserved alpha-helical peripheral membrane protein flanked by cysteine "fingers" and contains a calmodulin-binding IQ motif. J Biol Chem. 1995;270(22):13503-11.
220. Gough NR, Fambrough DM. Different steady state subcellular distributions of the three splice variants of lysosome-associated membrane protein LAMP-2 are determined largely by the COOH-terminal amino acid residue. J Cell Biol. 1997;137(5):1161-9.
221. Maadi H, Nami B, Tong J, Li G, Wang Z. The effects of trastuzumab on HER2-mediated cell signaling in CHO cells expressing human HER2. BMC Cancer. 2018;18(1):238.
222. Zinchuk V, Zinchuk O, Okada T. Quantitative colocalization analysis of multicolor confocal immunofluorescence microscopy images: pushing pixels to explore biological phenomena. Acta Histochem Cytochem. 2007;40(4):101-11.
223. Altai M, Liu H, Ding H, Mitran B, Edqvist PH, Tolmachev V, et al. Affibody-derived drug conjugates: Potent cytotoxic molecules for treatment of HER2 over-expressing tumors. J Control Release. 2018;288:84-95.
224. Sokolova E, Proshkina G, Kutova O, Shilova O, Ryabova A, Schulga A, et al. Recombinant targeted toxin based on HER2-specific DARPin possesses a strong selective cytotoxic effect in vitro and a potent antitumor activity in vivo. J Control Release. 2016;233:48-56.
225. Staudacher AH, Brown MP. Antibody drug conjugates and bystander killing: is antigen-dependent internalisation required? Br J Cancer. 2017;117(12):1736-42.
226. Erickson HK, Widdison WC, Mayo MF, Whiteman K, Audette C, Wilhelm SD, et al. Tumor delivery and in vivo processing of disulfide-linked and thioether-linked antibody-maytansinoid conjugates. Bioconjug Chem. 2010;21(1):84-92.
227. Amiri-Kordestani L, Blumenthal GM, Xu QC, Zhang L, Tang SW, Ha L, et al. FDA approval: ado-trastuzumab emtansine for the treatment of patients with HER2-positive metastatic breast cancer. Clin Cancer Res. 2014;20(17):4436-41.
228. Verma S, Miles D, Gianni L, Krop IE, Welslau M, Baselga J, et al. Trastuzumab emtansine for HER2-positive advanced breast cancer. N Engl J Med. 2012;367(19):1783-91.
229. Montemurro F, Ellis P, Anton A, Wuerstlein R, Delaloge S, Bonneterre J, et al. Safety of trastuzumab emtansine (T-DM1) in patients with HER2-positive advanced

breast cancer: Primary results from the KAMILLA study cohort 1. Eur J Cancer. 2019;109:92-102.
230. Rios-Luci C, Garcia-Alonso S, Diaz-Rodriguez E, Nadal-Serrano M, Arribas J, Ocana A, et al. Resistance to the Antibody-Drug Conjugate T-DM1 Is Based in a Reduction in Lysosomal Proteolytic Activity. Cancer Res. 2017;77(17):4639-51.
231. Sabbaghi M, Gil-Gomez G, Guardia C, Servitja S, Arpi O, Garcia-Alonso S, et al. Defective Cyclin B1 Induction in Trastuzumab-emtansine (T-DM1) Acquired Resistance in HER2-positive Breast Cancer. Clin Cancer Res. 2017;23(22):7006-19.
232. Li G, Guo J, Shen BQ, Yadav DB, Sliwkowski MX, Crocker LM, et al. Mechanisms of Acquired Resistance to Trastuzumab Emtansine in Breast Cancer Cells. Mol Cancer Ther. 2018;17(7):1441-53.
233. Simeon R, Chen Z. In vitro-engineered non-antibody protein therapeutics. Protein Cell. 2018;9(1):3-14.
234. Richards DA. Exploring alternative antibody scaffolds: Antibody fragments and antibody mimics for targeted drug delivery. Drug Discov Today Technol. 2018;30:35-46.
235. Xiang D, Zheng C, Zhou SF, Qiao S, Tran PH, Pu C, et al. Superior Performance of Aptamer in Tumor Penetration over Antibody: Implication of Aptamer-Based Theranostics in Solid Tumors. Theranostics. 2015;5(10):1083-97.
236. Koduvayur SP, Su Y, Kay BK, Lavie A. Targeted Delivery of Deoxycytidine Kinase to Her2-Positive Cells Enhances the Efficacy of the Nucleoside Analog Fludarabine. PLoS One. 2016;11(6):e0157114.
237. Pruszynski M, D'Huyvetter M, Bruchertseifer F, Morgenstern A, Lahoutte T. Evaluation of an Anti-HER2 Nanobody Labeled with (225)Ac for Targeted alpha-Particle Therapy of Cancer. Mol Pharm. 2018;15(4):1457-66.
238. Serwotka-Suszczak AM, Sochaj-Gregorczyk AM, Pieczykolan J, Krowarsch D, Jelen F, Otlewski J. A Conjugate Based on Anti-HER2 Diaffibody and Auristatin E Targets HER2-Positive Cancer Cells. Int J Mol Sci. 2017;18(2).
239. Sochaj-Gregorczyk AM, Ludzia P, Kozdrowska E, Jakimowicz P, Sokolowska-Wedzina A, Otlewski J. Design and In Vitro Evaluation of a Cytotoxic Conjugate Based on the Anti-HER2 Affibody Fused to the Fc Fragment of IgG1. Int J Mol Sci. 2017;18(8).
240. Otto HH, Schirmeister T. Cysteine Proteases and Their Inhibitors. Chem Rev. 1997;97(1):133-72.
241. Jain N, Smith SW, Ghone S, Tomczuk B. Current ADC Linker Chemistry. Pharm Res. 2015;32(11):3526-40.
242. Senter PD, Sievers EL. The discovery and development of brentuximab vedotin for use in relapsed Hodgkin lymphoma and systemic anaplastic large cell lymphoma. Nat Biotechnol. 2012;30(7):631-7.
243. Elgersma RC, Coumans RG, Huijbregts T, Menge WM, Joosten JA, Spijker HJ, et al. Design, Synthesis, and Evaluation of Linker-Duocarmycin Payloads: Toward Selection of HER2-Targeting Antibody-Drug Conjugate SYD985. Mol Pharm. 2015;12(6):1813-35.
244. de Claro RA, McGinn K, Kwitkowski V, Bullock J, Khandelwal A, Habtemariam B, et al. U.S. Food and Drug Administration approval summary: brentuximab vedotin for the treatment of relapsed Hodgkin lymphoma or relapsed systemic anaplastic large-cell lymphoma. Clin Cancer Res. 2012;18(21):5845-9.
245. Yao X, Jiang J, Wang X, Huang C, Li D, Xie K, et al. A novel humanized anti-HER2 antibody conjugated with MMAE exerts potent anti-tumor activity. Breast Cancer Res Treat. 2015;153(1):123-33.

246. Ravasco J, Faustino H, Trindade A, Gois PMP. Bioconjugation with Maleimides: A Useful Tool for Chemical Biology. Chemistry. 2019;25(1):43-59.
247. Kim MT, Chen Y, Marhoul J, Jacobson F. Statistical modeling of the drug load distribution on trastuzumab emtansine (Kadcyla), a lysine-linked antibody drug conjugate. Bioconjug Chem. 2014;25(7):1223-32.
248. Chen L, Wang L, Shion H, Yu C, Yu YQ, Zhu L, et al. In-depth structural characterization of Kadcyla(R) (ado-trastuzumab emtansine) and its biosimilar candidate. MAbs. 2016;8(7):1210-23.
249. Lewis Phillips GD, Li G, Dugger DL, Crocker LM, Parsons KL, Mai E, et al. Targeting HER2-positive breast cancer with trastuzumab-DM1, an antibody-cytotoxic drug conjugate. Cancer Res. 2008;68(22):9280-90.
250. Takagi S, Banno H, Hayashi A, Tamura T, Ishikawa T, Ohta Y. HER2 and HER3 cooperatively regulate cancer cell growth and determine sensitivity to the novel investigational EGFR/HER2 kinase inhibitor TAK-285. Oncoscience. 2014;1(3):196-204.
251. Osada T, Hartman ZC, Wei J, Lei G, Hobeika AC, Gwin WR, et al. Polyfunctional anti-human epidermal growth factor receptor 3 (anti-HER3) antibodies induced by HER3 vaccines have multiple mechanisms of antitumor activity against therapy resistant and triple negative breast cancers. Breast Cancer Res. 2018;20(1):90.
252. Choi BK, Fan X, Deng H, Zhang N, An Z. ERBB3 (HER3) is a key sensor in the regulation of ERBB-mediated signaling in both low and high ERBB2 (HER2) expressing cancer cells. Cancer Med. 2012;1(1):28-38.
253. Qi R, Wang Y, Bruno PM, Xiao H, Yu Y, Li T, et al. Nanoparticle conjugates of a highly potent toxin enhance safety and circumvent platinum resistance in ovarian cancer. Nat Commun. 2017;8(1):2166.
254. Gallery M, Zhang J, Bradley DP, Brauer P, Cvet D, Estevam J, et al. A monomethyl auristatin E-conjugated antibody to guanylyl cyclase C is cytotoxic to target-expressing cells in vitro and in vivo. PLoS One. 2018;13(1):e0191046.
255. Goodbye, flat biology? Nature. 2003;424(6951):861.
256. Kleinman HK, Martin GR. Matrigel: basement membrane matrix with biological activity. Semin Cancer Biol. 2005;15(5):378-86.
257. Albrechtsen R, Nielsen M, Wewer U, Engvall E, Ruoslahti E. Basement membrane changes in breast cancer detected by immunohistochemical staining for laminin. Cancer Res. 1981;41(12 Pt 1):5076-81.
258. Hughes CS, Postovit LM, Lajoie GA. Matrigel: a complex protein mixture required for optimal growth of cell culture. Proteomics. 2010;10(9):1886-90.
259. Wang Y, Mirza S, Wu S, Zeng J, Shi W, Band H, et al. 3D hydrogel breast cancer models for studying the effects of hypoxia on epithelial to mesenchymal transition. Oncotarget. 2018;9(63):32191-203.
260. Velez DO, Tsui B, Goshia T, Chute CL, Han A, Carter H, et al. 3D collagen architecture induces a conserved migratory and transcriptional response linked to vasculogenic mimicry. Nat Commun. 2017;8(1):1651.
261. Suo A, Xu W, Wang Y, Sun T, Ji L, Qian J. Dual-degradable and injectable hyaluronic acid hydrogel mimicking extracellular matrix for 3D culture of breast cancer MCF-7 cells. Carbohydr Polym. 2019;211:336-48.
262. Pradhan S, Slater JH. Tunable hydrogels for controlling phenotypic cancer cell states to model breast cancer dormancy and reactivation. Biomaterials. 2019;215:119177.
263. Fan C, Wang DA. Macroporous Hydrogel Scaffolds for Three-Dimensional Cell Culture and Tissue Engineering. Tissue Eng Part B Rev. 2017;23(5):451-61.

264. Zanoni M, Piccinini F, Arienti C, Zamagni A, Santi S, Polico R, et al. 3D tumor spheroid models for in vitro therapeutic screening: a systematic approach to enhance the biological relevance of data obtained. Sci Rep. 2016;6:19103.
265. Knight E, Murray B, Carnachan R, Przyborski S. Alvetex(R): polystyrene scaffold technology for routine three dimensional cell culture. Methods Mol Biol. 2011;695:323-40.
266. Martinez-Revollar G, Garay E, Martin-Tapia D, Nava P, Huerta M, Lopez-Bayghen E, et al. Heterogeneity between triple negative breast cancer cells due to differential activation of Wnt and PI3K/AKT pathways. Exp Cell Res. 2015;339(1):67-80.
267. Jakobsson A, Ottosson M, Zalis MC, O'Carroll D, Johansson UE, Johansson F. Three-dimensional functional human neuronal networks in uncompressed low-density electrospun fiber scaffolds. Nanomedicine. 2017;13(4):1563-73.
268. Cleversey C, Robinson M, Willerth SM. 3D Printing Breast Tissue Models: A Review of Past Work and Directions for Future Work. Micromachines (Basel). 2019;10(8).
269. Lancaster MA, Renner M, Martin CA, Wenzel D, Bicknell LS, Hurles ME, et al. Cerebral organoids model human brain development and microcephaly. Nature. 2013;501(7467):373-9.
270. Lancaster MA, Huch M. Disease modelling in human organoids. Dis Model Mech. 2019;12(7).
271. Nugraha B, Buono MF, von Boehmer L, Hoerstrup SP, Emmert MY. Human Cardiac Organoids for Disease Modeling. Clin Pharmacol Ther. 2019;105(1):79-85.
272. Sokol ES, Miller DH, Breggia A, Spencer KC, Arendt LM, Gupta PB. Growth of human breast tissues from patient cells in 3D hydrogel scaffolds. Breast Cancer Res. 2016;18(1):19.
273. Linnemann JR, Miura H, Meixner LK, Irmler M, Kloos UJ, Hirschi B, et al. Quantification of regenerative potential in primary human mammary epithelial cells. Development. 2015;142(18):3239-51.
274. Santoro M, Lamhamedi-Cherradi SE, Menegaz BA, Ludwig JA, Mikos AG. Flow perfusion effects on three-dimensional culture and drug sensitivity of Ewing sarcoma. Proc Natl Acad Sci U S A. 2015;112(33):10304-9.
275. Wozniak MA, Chen CS. Mechanotransduction in development: a growing role for contractility. Nat Rev Mol Cell Biol. 2009;10(1):34-43.
276. Goliwas KF, Marshall LE, Ransaw EL, Berry JL, Frost AR. A recapitulative three-dimensional model of breast carcinoma requires perfusion for multi-week growth. J Tissue Eng. 2016;7:2041731416660739.
277. Edmondson R, Broglie JJ, Adcock AF, Yang L. Three-dimensional cell culture systems and their applications in drug discovery and cell-based biosensors. Assay Drug Dev Technol. 2014;12(4):207-18.
278. Zschenker O, Streichert T, Hehlgans S, Cordes N. Genome-wide gene expression analysis in cancer cells reveals 3D growth to affect ECM and processes associated with cell adhesion but not DNA repair. PLoS One. 2012;7(4):e34279.
279. Birgersdotter A, Sandberg R, Ernberg I. Gene expression perturbation in vitro--a growing case for three-dimensional (3D) culture systems. Semin Cancer Biol. 2005;15(5):405-12.
280. Luca AC, Mersch S, Deenen R, Schmidt S, Messner I, Schafer KL, et al. Impact of the 3D microenvironment on phenotype, gene expression, and EGFR inhibition of colorectal cancer cell lines. PLoS One. 2013;8(3):e59689.

281. Hirt C, Papadimitropoulos A, Muraro MG, Mele V, Panopoulos E, Cremonesi E, et al. Bioreactor-engineered cancer tissue-like structures mimic phenotypes, gene expression profiles and drug resistance patterns observed "in vivo". Biomaterials. 2015;62:138-46.
282. Piotrowski-Daspit AS, Tien J, Nelson CM. Interstitial fluid pressure regulates collective invasion in engineered human breast tumors via Snail, vimentin, and E-cadherin. Integr Biol (Camb). 2016;8(3):319-31.
283. Eglen R, Reisine T. Primary cells and stem cells in drug discovery: emerging tools for high-throughput screening. Assay Drug Dev Technol. 2011;9(2):108-24.
284. Ewers SB, Langstrom E, Baldetorp B, Killander D. Flow-cytometric DNA analysis in primary breast carcinomas and clinicopathological correlations. Cytometry. 1984;5(4):408-19.
285. Gedye CA, Hussain A, Paterson J, Smrke A, Saini H, Sirskyj D, et al. Cell surface profiling using high-throughput flow cytometry: a platform for biomarker discovery and analysis of cellular heterogeneity. PLoS One. 2014;9(8):e105602.
286. Smyth MS, Martin JH. x ray crystallography. Mol Pathol. 2000;53(1):8-14.
287. Russo Krauss I, Merlino A, Vergara A, Sica F. An overview of biological macromolecule crystallization. Int J Mol Sci. 2013;14(6):11643-91.
288. Leahy DJ, Dann CE, 3rd, Longo P, Perman B, Ramyar KX. A mammalian expression vector for expression and purification of secreted proteins for structural studies. Protein Expr Purif. 2000;20(3):500-6.
289. Loo T, Patchett ML, Norris GE, Lott JS. Using secretion to solve a solubility problem: high-yield expression in Escherichia coli and purification of the bacterial glycoamidase PNGase F. Protein Expr Purif. 2002;24(1):90-8.
290. Wagner S, Klepsch MM, Schlegel S, Appel A, Draheim R, Tarry M, et al. Tuning Escherichia coli for membrane protein overexpression. Proc Natl Acad Sci U S A. 2008;105(38):14371-6.
291. Sun P, Tropea JE, Waugh DS. Enhancing the solubility of recombinant proteins in Escherichia coli by using hexahistidine-tagged maltose-binding protein as a fusion partner. Methods Mol Biol. 2011;705:259-74.
292. Marblestone JG, Edavettal SC, Lim Y, Lim P, Zuo X, Butt TR. Comparison of SUMO fusion technology with traditional gene fusion systems: enhanced expression and solubility with SUMO. Protein Sci. 2006;15(1):182-9.
293. Lobner E, Humm AS, Goritzer K, Mlynek G, Puchinger MG, Hasenhindl C, et al. Fcab-HER2 Interaction: a Menage a Trois. Lessons from X-Ray and Solution Studies. Structure. 2017;25(6):878-89 e5.
294. Fu W, Wang Y, Zhang Y, Xiong L, Takeda H, Ding L, et al. Insights into HER2 signaling from step-by-step optimization of anti-HER2 antibodies. MAbs. 2014;6(4):978-90.
295. D'Huyvetter M, De Vos J, Xavier C, Pruszynski M, Sterckx YGJ, Massa S, et al. (131)I-labeled Anti-HER2 Camelid sdAb as a Theranostic Tool in Cancer Treatment. Clin Cancer Res. 2017;23(21):6616-28.
296. Wang Z, Cheng L, Guo G, Cheng B, Hu S, Zhang H, et al. Structural insight into a matured humanized monoclonal antibody HuA21 against HER2-overexpressing cancer cells. Acta Crystallogr D Struct Biol. 2019;75(Pt 6):554-63.
297. Geuijen CAW, De Nardis C, Maussang D, Rovers E, Gallenne T, Hendriks LJA, et al. Unbiased Combinatorial Screening Identifies a Bispecific IgG1 that Potently Inhibits HER3 Signaling via HER2-Guided Ligand Blockade. Cancer Cell. 2018;33(5):922-36 e10.

298. Kanthala S, Mill CP, Riese DJ, 2nd, Jaiswal M, Jois S. Expression and purification of HER2 extracellular domain proteins in Schneider2 insect cells. Protein Expr Purif. 2016;125:26-33.
299. Sun Y, Feng X, Qu J, Han W, Liu Z, Li X, et al. Expression and Characterization of the Extracellular Domain of Human HER2 from Escherichia Coli, and Production of Polyclonal Antibodies Against the Recombinant Proteins. Appl Biochem Biotechnol. 2015;176(4):1029-43.
300. Dolgikh VV, Senderskiy IV, Tetz GV, Tetz VV. Optimization of the Protocol for the Isolation and Refolding of the Extracellular Domain of HER2 Expressed in Escherichia coli. Acta Naturae. 2014;6(2):106-9.
301. Dyson MR, Shadbolt SP, Vincent KJ, Perera RL, McCafferty J. Production of soluble mammalian proteins in Escherichia coli: identification of protein features that correlate with successful expression. BMC Biotechnol. 2004;4:32.
302. Agus DB, Akita RW, Fox WD, Lewis GD, Higgins B, Pisacane PI, et al. Targeting ligand-activated ErbB2 signaling inhibits breast and prostate tumor growth. Cancer Cell. 2002;2(2):127-37.
303. Kayl AE, Meyers CA. Side-effects of chemotherapy and quality of life in ovarian and breast cancer patients. Curr Opin Obstet Gynecol. 2006;18(1):24-8.
304. Cruz E, Kayser V. Monoclonal antibody therapy of solid tumors: clinical limitations and novel strategies to enhance treatment efficacy. Biologics. 2019;13:33-51.
305. Kunimoto D, Ohji M, Maturi RK, Sekiryu T, Wang Y, Pan G, et al. Evaluation of Abicipar Pegol (an Anti-VEGF DARPin Therapeutic) in Patients With Neovascular Age-Related Macular Degeneration: Studies in Japan and the United States. Ophthalmic Surg Lasers Imaging Retina. 2019;50(2):e10-e22.
306. Moisseiev E, Loewenstein A. Abicipar pegol-a novel anti-VEGF therapy with a long duration of action. Eye (Lond). 2020;34(4):605-6.
307. Reichert JM, Beck A, Lugovskoy AA, Wurch T, Coats S, Brezski RJ. 9th annual European Antibody Congress, November 11-13, 2013, Geneva, Switzerland. MAbs. 2014;6(2):309-26.
308. Sandstrom M, Lindskog K, Velikyan I, Wennborg A, Feldwisch J, Sandberg D, et al. Biodistribution and Radiation Dosimetry of the Anti-HER2 Affibody Molecule 68Ga-ABY-025 in Breast Cancer Patients. J Nucl Med. 2016;57(6):867-71.
309. Lofblom J, Feldwisch J, Tolmachev V, Carlsson J, Stahl S, Frejd FY. Affibody molecules: engineered proteins for therapeutic, diagnostic and biotechnological applications. FEBS Lett. 2010;584(12):2670-80.
310. AlQahtani AD, O'Connor D, Domling A, Goda SK. Strategies for the production of long-acting therapeutics and efficient drug delivery for cancer treatment. Biomed Pharmacother. 2019;113:108750.
311. Strohl WR. Fusion Proteins for Half-Life Extension of Biologics as a Strategy to Make Biobetters. BioDrugs. 2015;29(4):215-39.
312. Shoemaker RH. The NCI60 human tumour cell line anticancer drug screen. Nat Rev Cancer. 2006;6(10):813-23.
313. Zeeberg BR, Kohn KW, Kahn A, Larionov V, Weinstein JN, Reinhold W, et al. Concordance of gene expression and functional correlation patterns across the NCI-60 cell lines and the Cancer Genome Atlas glioblastoma samples. PLoS One. 2012;7(7):e40062.
314. Niu N, Wang L. In vitro human cell line models to predict clinical response to anticancer drugs. Pharmacogenomics. 2015;16(3):273-85.

315. Piccart M. Circumventing de novo and acquired resistance to trastuzumab: new hope for the care of ErbB2-positive breast cancer. Clin Breast Cancer. 2008;8 Suppl 3:S100-13.
316. Shu M, Yan H, Xu C, Wu Y, Chi Z, Nian W, et al. A novel anti-HER2 antibody GB235 reverses Trastuzumab resistance in HER2-expressing tumor cells in vitro and in vivo. Sci Rep. 2020;10(1):2986.
317. O'Brien NA, McDonald K, Tong L, von Euw E, Kalous O, Conklin D, et al. Targeting PI3K/mTOR overcomes resistance to HER2-targeted therapy independent of feedback activation of AKT. Clin Cancer Res. 2014;20(13):3507-20.